1997

Mass transfer mechanisms in air sparging systems

Washington Jose Braida
Iowa State University

INFORMATION TO USERS

This manuscript has been reproduced from the microfilm master. UMI films the text directly from the original or copy submitted. Thus, some thesis and dissertation copies are in typewriter face, while others may be from any type of computer printer.

The quality of this reproduction is dependent upon the quality of the copy submitted. Broken or indistinct print, colored or poor quality illustrations and photographs, print bleedthrough, substandard margins, and improper alignment can adversely affect reproduction.

In the unlikely event that the author did not send UMI a complete manuscript and there are missing pages, these will be noted. Also, if unauthorized copyright material had to be removed, a note will indicate the deletion.

Oversize materials (e.g., maps, drawings, charts) are reproduced by sectioning the original, beginning at the upper left-hand corner and continuing from left to right in equal sections with small overlaps. Each original is also photographed in one exposure and is included in reduced form at the back of the book.

Photographs included in the original manuscript have been reproduced xerographically in this copy. Higher quality 6" x 9" black and white photographic prints are available for any photographs or illustrations appearing in this copy for an additional charge. Contact UMI directly to order.

UMI

A Bell & Howell Information Company
300 North Zeeb Road, Ann Arbor MI 48106-1346 USA
313/761-4700 800/521-0600

Mass transfer mechanisms in air sparging systems

by

Washington Jose Braida

A dissertation submitted to the graduate faculty
in partial fulfillment of the requirements for the degree of
DOCTOR OF PHILOSOPHY

Major: Civil Engineering (Environmental Engineering)
Major Professor: Say Kee Ong

Iowa State University
Ames, Iowa
1997

Graduate College

Iowa State University

This is to certify that the doctoral dissertation of

Washington Jose Braida

has met the dissertation requirements of Iowa State University

Signature was redacted for privacy.

Committee Member

Signature was redacted for privacy.

Committee Member

Signature was redacted for privacy.

Committee Member

Signature was redacted for privacy.

Committee Member

Signature was redacted for privacy.

Major Professor

Signature was redacted for privacy.

For the Major Program

Signature was redacted for privacy.

For the Graduate College

To

my lovely wife Gaye,

my daughters Maria Eugenia and Constanza

and

my parents

TABLE OF CONTENTS

LIST OF FIGURES

CHAPTER SEVEN

CHAPTER EIGHT

LIST OF TABLES

ACKNOWLEDGMENTS

There were several people who were instrumental in the completion of my dissertation. First and foremost, I would like to express my deep gratitude to Professor Say Kee Ong, for convincing me to attend Iowa State University for my doctorate and for being my dissertation advisor and mentor. He has set high standards that have always helped me learn more and his encouragement was always there along the hills and valleys of this process. I wish to express my appreciation to Professor LaDon Jones for the helpful discussions on the analysis and modeling of my results. I also want to thank Juan Jose Goyeneche, my countrymate and friend, for his invaluable help in the statistical analysis of the data.

I am also grateful to Professor Charles Oulman, Professor L. K. Doraiswamy, and Robert Horton for serving in my doctoral committee.

I gratefully acknowledge my student colleagues, Pak-Hing Lee, Dr. Chul-Sung Kim, Roger Protzman, Steve Van Dyke, Todd Fryzek, and Michael Carr for the great times and encouragement through endless hours of laboratory work. I want to extend special thanks to Dr. Keh-Ping Chao for his valuable input in the early stages of my work.

I would like to express my appreciation to my parents, daughters and relatives for all their love and support. Finally, I would like to express my greatest indebtedness to my wife, Gaye Goker, for her endless support, love, and encouragement.

ABSTRACT

The air-water mass transfer of VOCs during air sparging was investigated using a single-air channel air sparging setup and a 14 cm ($5\frac{1}{2}$ in) diameter soil column. Three different porous media and 10 VOCs were used in the study. Air velocities ranged from 0.2 cm/s to 2.5 cm/s. Experimental results for the single-air channel setup indicated that volatilization of VOCs during air sparging was a diffusion limited process. VOCs, in a thin layer of saturated porous media next to the air channels (identified as the mass transfer zone, *MTZ*), were found to deplete rapidly during air sparging resulting in a steep concentration gradient within this zone while the VOC concentrations outside the zone remained fairly constant. The rapid depletion was associated with faster initial volatilization of VOCs at the air-water interface as compared to the diffusive transport of VOCs to the air-water interface. The size of *MTZ* ranged from 17 to 41 mm or between 70 dp_{50} and 215 dp_{50} (dp_{50} = mean particle size of the porous media) depending on the VOC. A general correlation predicting the size of the *MTZ* was developed. The size of *MTZ* was found to be directly proportional to the aqueous diffusivity of the VOC, the mean particle size, and the uniformity coefficient. The size of *MTZ* was also found to decrease with increasing organic carbon content of the porous media. This effect was larger for VOCs with low solubilities and high partition coefficients.

Air-water mass transfer coefficients (K_G) for the volatilization of VOCs were estimated by fitting experimental data to a one-dimensional diffusion model. The air-water mass transfer coefficients ranged from 1.79×10^{-3} cm/min to 3.85×10^{-2} cm/min for the VOCs tested. Two empirical models were developed for the prediction of mass transfer coefficients by correlating the Damkohler and modified air phase Sherwood numbers with air phase Peclet number, Henry's law constant, and reduced mean particle size of porous media. The estimated lumped mass transfer coefficients ($K_G a$) were found to be directly related to the air diffusivity of the VOC, air velocity, particle size, and inversely related to the Henry's law constant of the VOCs. Based on the two-resistance model, the liquid-side resistance accounted for more than 90% of the total resistance for the air-water interfacial mass transfer.

Experiments with nonaqueous phase liquid (NAPLs) indicated that air sparging may control the spreading of NAPLs and were more effective for NAPLs with higher solubilities

and lower densities. Removal efficiencies of NAPLs and dissolved VOCs were found to be greatly affected by the grain size of the porous media.

The *MTZ* concept and the correlations developed for the single-air channel study were incorporated into a one-dimensional radial diffusion model and were found to successfully predict the air phase concentrations, final aqueous VOC concentrations, and total mass removed for a $5\frac{1}{2}$ in diameter air sparged soil column.

CHAPTER ONE. INTRODUCTION AND OBJECTIVES

Introduction

The U.S. Environmental Protection Agency (EPA) has estimated that about 25% of two million underground storage tank (UST) systems located at 700,000 facilities across the U.S. may be leaking (U.S. EPA, 1988). The improper and illegal disposal of hazardous wastes together with the release of organic chemicals from UST systems have a significant environmental impact on groundwater resources and may be a risk to human health. Volatile organic compounds (VOCs) are generally slightly soluble in water and may volatilize into the air pores of the unsaturated zone. After their release, the VOCs may migrate downward under the influence of gravity, capillary forces, and viscous forces. VOCs commonly found in contaminated groundwater include benzene, creosote mixture, ethylbenzene, xylenes, toluene, and chlorinated hydrocarbons.

Various physical, chemical, and biological treatment methods have been developed to remediate contaminated sites. The most common remedial approach employed in the control and remediation of contaminated aquifers is the pump-and-treat system. The pump-and-treat system uses a series of wells placed downstream of the flow path of the plume to capture the contaminated water. The pumped water is then treated above ground. The effectiveness of the pump-and-treat approach as a remedial technology is uncertain when dealing with contaminants sorbed to the saturated soils or when the site has extensive heterogeneity. A remediation approach frequently used is *in situ* biodegradation in which indigenous microorganisms present in the aquifer are used for the degradation of the organic compounds. The success of bioremediation depends on the enhancement of the degradation capability of the indigenous population through the addition of nutrients and oxygen. As such, bioremediation is sensitive to many physical and chemical variables at a given site. Another remedial approach for contaminated aquifers is the use of physical means such as aeration technologies. One emerging soil aeration technology, air sparging, involves the injection of contaminant-free air, directly below the water table for the stripping/volatilization of volatile

organic compounds (VOCs) and the promotion of biodegradation (Brown et al., 1994). Contaminated air is then removed with extraction wells located in the unsaturated zone.

Even though air sparging has been successfully applied at several contaminated sites, Johnson et al. (1993) pointed out that the mechanism of air flow in saturated porous media and the physical-chemical/biological processes involved during air sparging operations are not yet well understood. Similarly, Reddy et al. (1995) and Chao and Ong (1995) pointed out that the current design and implementation of air sparging systems are based on empirical approaches from field experience.

The physical-chemical processes involved during air sparging is a complex combination of mass transport and transformation processes which include volatilization, dissolution, diffusion, advection, hydrodynamic isolation, and desorption of contaminants. The transformation processes include biodegradation of VOCs from an increase in dissolved oxygen in the contaminated aquifer. The extent of mass transfer during air sparging is dependent on the advective-dispersive characteristics of the air flow, dispersive, and possibly advective characteristics of the groundwater, and the diffusive properties of the VOCs.

Field studies on air sparging are usually not exhaustive and results are not well documented. As a result, it is difficult to thoroughly elucidate the fundamental processes involved in air sparging and the long term performance of this remediation technology. To understand air sparging processes with the eventual goal of designing air sparging systems in an economical and efficient way, it is essential to have a better comprehension of the fundamental contaminant transport and transformation mechanisms involved in the application of this technology.

Objectives

The study will focus on the physical-chemical interactions occurring during air sparging. Biological processes associated with the use of this technology will not be included.

The objectives of this research are divided into three parts as follows:

(i) To investigate and quantify the major and limiting mass transfer processes affecting volatilization of VOCs during air sparging by using a laboratory-scale single-air channel

experimental setup. Different types of VOCs, air flow rates, porous media and the presence of NAPLs were used as variables to provide a better understanding of the mass transfer of VOCs. Mass transfer coefficients for different VOCs were determined for different experimental conditions.

(ii) To correlate the mass transfer coefficients found in objective (i) with macroscopic properties of the system using dimensional analysis. The correlation derived may be used for the prediction of mass transfer for different experimental situations.

(iii) Based on results of objectives (i) and (ii), a model to predict mass transfer was developed and applied to a complex system such as an air sparged soil column.

The approach taken by this dissertation was to investigate the "microscale" effects of air sparging by using an experimental setup with a single-air channel. The results from the single-air channel experiments were then used to predict the results of a more complex system such as air sparged soil columns.

Dissertation Organization

The dissertation is divided into nine chapters. Chapters three, four, six, and seven are in the form of journal papers. Chapter 2 presents a literature review of the different issues related with the operation and application of air sparging as a remediation technology. In Chapter 3, results from well controlled laboratory experiments provided a quantitative insight on the factors influencing the volatilization of VOCs under air sparging conditions. The governing mechanisms for the volatilization of VOCs at the "microscale" level were discussed and based on these observations, a correlation between the mass transfer zone and macroscopic properties of the system was developed. In Chapter 4, an advection-diffusion model was developed and used for the estimation of the air-water mass transfer coefficients for the VOCs under sparging conditions. In this chapter, a dimensionless model for the prediction of mass transfer coefficients was developed. Chapter 5 presents an analysis of the dominant mass transfer resistance affecting the volatilization of VOCs under sparging conditions. In Chapter 6, the effects of air sparging on NAPLs were investigated. The influence of adsorption processes on the performance of air sparging systems is presented in

Chapter 7. Chapter 8 presents the application of a one–dimensional diffusion model to predict the results of air sparged soil columns. Parameters estimated in the earlier chapters were used as inputs for the model. Chapter 9 presents the general conclusions, recommended future work, and closing statement of the study.

References

Brown, R.A., R.J. Hicks, and P.M. Hicks, Use of air sparging for in situ bioremediation, in *Air Sparging for Site Remediation*, edited by R.E. Hinchee, pp. 38-55, Lewis Publishers, Boca Raton, FL, 1994.

Chao, K.P., and S.K. Ong, Air Sparging: effects of VOCs and soil properties on VOC volatilization, in *In Situ Aeration: Air Sparging, Bioventing, and Related Remediation Processes*, R.E. Hinchee, R. Miller, and P. Johnson (eds.), pp. 103-110, Battelle Press, Columbus, OH, 1995.

Johnson, R.L., P.C. Johnson, D.B. McWhorter, R.E. Hinchee, and I. Goodman, An overview of in situ air sparging, *GWMR*, vol. 13(4), pp. 127-135, 1993.

Reddy, K.R., S. Kosgi, and J. Zhou, A review of in-situ sparging for the remediation of VOC-contaminated saturated soils and groundwater, *Hazardous Wastes & Hazardous Materials*, vol. 12(2), pp. 97-117, 1995.

U.S. EPA, *Underground storage tanks: technical requirements*, Federal Register 53:37082, Sept. 23, 1988.

CHAPTER TWO. LITERATURE REVIEW

Air Sparging: Process Description

Contamination of soil and groundwater as a result of accidental spills, leaking underground storage tanks, uncontrolled waste disposal, and leaking landfills is one of the major environmental concerns in the U.S.. Increasingly, innovative strategies are being proposed for the remediation of contaminated soil and groundwater. The direct injection of air into contaminated groundwater was first proposed for the cleanup of contaminated sites as early as 1974 (Raymond, 1974). However, field application of air sparging has only been applied in the last 10 years. The reduction in remediation time and cost by air sparging may be as much as 50% as compared to a pump-and-treat and soil vapor extraction (SVE) system (Control News, 1992).

Air sparging consists of the injection of air into the water saturated zone for the purpose of removing organic contaminants by a combination of volatilization and aerobic biodegradation processes (Johnson et al., 1993). The injection of air under pressure in the saturated zone displaces water from the porous matrix and creates a transient air-filled porosity. The contaminants are transported to the top of the saturated zone and into the unsaturated zone where they are captured by SVE wells. A typical air sparging system has one or more wells where air is injected into the saturated zone (Figure 1).

Different mass transport and transformation processes occur during air sparging operations. The transport processes include volatilization, dissolution, diffusion, advection, hydrodynamic isolation and desorption of contaminants (Reddy et al., 1995). The transformation processes include enhanced biodegradation of VOCs from an increase in dissolved oxygen in the contaminated aquifer. The advective-dispersive characteristic of the air flow plus the dispersive and, possibly, advective characteristics of the groundwater will affect the extent of mass transfer during air sparging. Mass transfer is also affected by the diffusive properties of the VOCs.

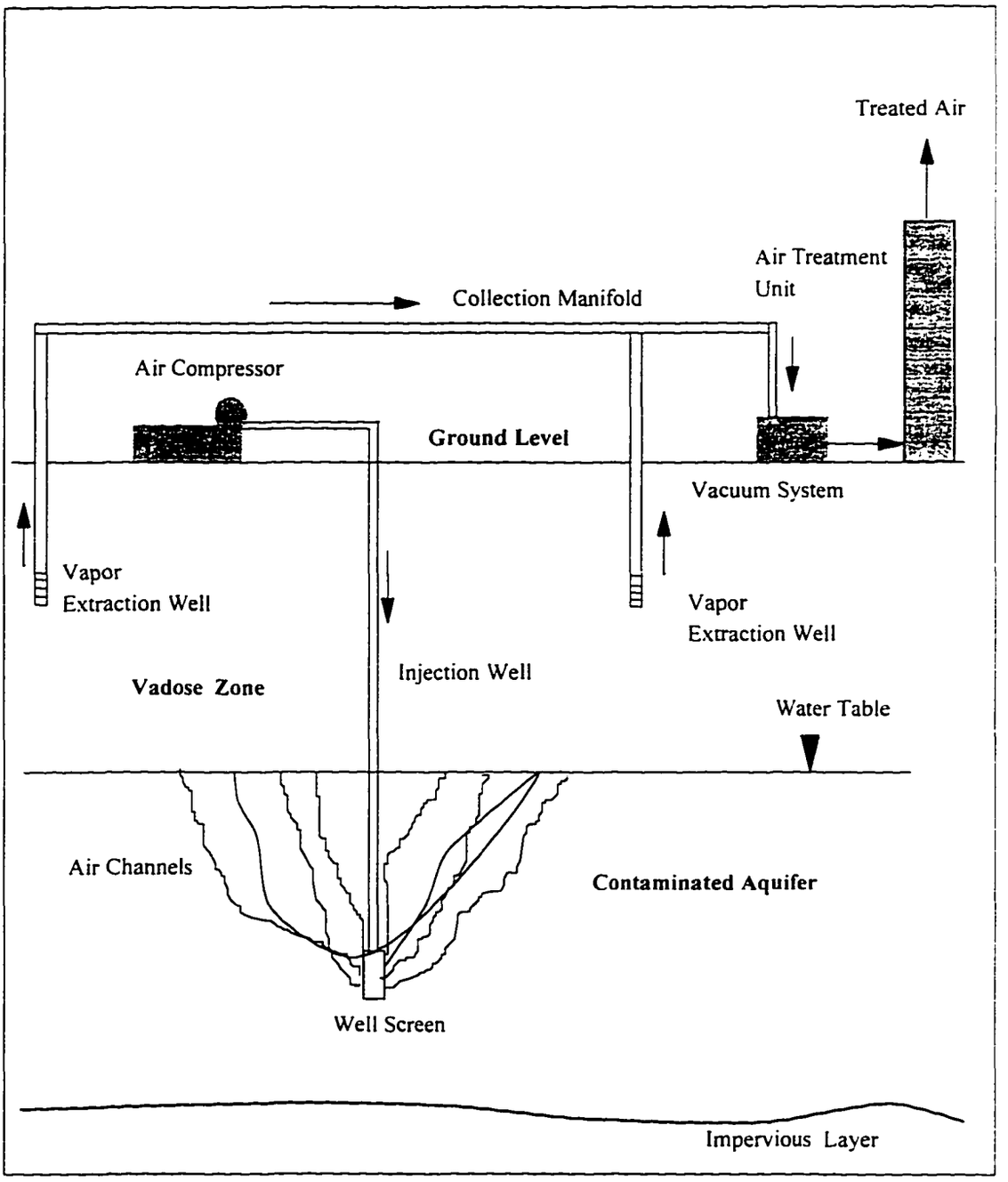

Figure 1. Typical air sparging system

Several treatment technologies which are similar in concept to the conventional air sparging system have been developed. These technologies include the horizontal trench sparging system, in-well air sparging, and biosparging (Suthersan, 1997). Horizontal trench sparging was developed for low permeability conditions and for contamination located less than 30 feet below ground level. Horizontal trench sparging has generated much interest recently as a result of a successful application of the technology at the Savannah River Integrated Demonstration Project (Plummer et al., 1997). In-well air sparging or the vacuum-vaporizer-well technology (UVB) was developed by B. Bernhart (Buermann and Bott-Breuning, 1994). Air is injected into the inner casing of the well containing the contaminated groundwater but the sparged air does not come in contact with the contaminated soil matrix. The injected air produces an air-lift effect which volatilizes the VOC and reoxygenate the groundwater and, at the same time, circulates the groundwater through the well casing and into the aquifer. Biosparging, is a modification of air sparging, where air is injected into the aquifer at very low flow rates (0.5 cfm to less than 2-3 cfm per injection well) to promote biodegradation (Suthersan, 1997).

Despite the successful application of the air sparging technology at several contaminated sites, Chao and Ong (1995) pointed out that the current design and implementation of air sparging systems were based on field experiences only. Some areas where information is lacking and further research are needed to provide a scientific basis for the design of air sparging system include:

(i) field methods and/or empirical correlations for the estimation of air saturation and the size and density of air channels

(ii) the importance of different mass transfer mechanisms during air sparging

(iii) the influence of saturated soil hydrogeology on the mode and behavior of air movement.

Nature of the Injected Air Flow in the Porous Media

Researchers in the field of fluid flow through porous media have used the continuous approach to explain the macroscopic transport processes in porous media. However, fluid

flow and diffusion in porous media may be viewed as taking place within extremely complicated microscopic boundaries that make any rigorous solution of the transport equation in the capillary network of the porous media practically impossible. The continuous approach does not consider the microscopic structure of the porous media channels and fails to explain the behavior of the fluids on the microscopic scale (Dullien, 1979).

The exact nature of air flow in a saturated porous media is not completely understood. Research work in this area is fairly scarce. At the present time, there is no comprehensive study on the pathway and nature of air flow in an aquifer. Several conceptual models on air flow in saturated porous media under air sparging conditions have been proposed. Brown and Fraxendas (1991) proposed that air flow in the saturated zone is in the form of air bubbles which move upwards through the saturated soil column into the unsaturated zone. They suggested that the air movement was analogous to air bubbles formed in an aeration basin and that air sparging in an aquifer may be viewed as a crude air stripping tower in the subsurface with the soil acting as the packing. Other authors such as Middleton and Miller (1990) suggested that the movement of air was through irregular air channels in the saturated soil. The rationale for suggesting a continuous slug of air instead of bubbles was that air tends not to form bubbles in a tightly packed porous medium.

In a laboratory study on air flow in porous media, Ji et al. (1993) found that the most probable air flow behavior in medium to fine grained water saturated porous media was in the form of discrete channels. The authors reported that for grain diameters of 4 mm and larger (medium to coarse gravel), bubbly air flow was observed; for grain sizes of 0.75 mm or less (corresponding to sands, silts, and clays) air flow in channels was prevalent. The transition between these two flow regimes appeared to occur for grain sizes between 4 mm and 0.75 mm. The authors concluded that under natural subsurface conditions, the air channel flow regime would likely occur during air sparging. The asymmetric pattern of air channels formed for a porous media with a mixture of grain sizes suggested that the air channels were sensitive to the medium heterogeneity.

The pathway and nature of air flow in saturated porous media are affected by the air flow rate, air pressure, soil characteristics (particle size and shape), soil permeability, presence of

active surface agents, and the size of well screen or air orifice. The type of soil, soil permeability, and the so-called "air entry pressure" would determine the ease at which air will flow in the porous media. When air is pumped into a well, it must first displace the standing water within the well to the top of the screen opening of the well. The minimum air pressure, P_w, to achieve this is equal to the hydrostatic pressure of the standing water:

$$P_w = \rho_w g h_w \tag{1}$$

where ρ_w (ML^{-3}) is the density of the water, h_w (L) is the water level above the top of the well screen, and g (LT^{-2}) is the acceleration due to gravity. After reaching the top most opening of the well screen, the injected air will penetrate the aquifer only if the air pressure exceeds the head loss through the well screen (P_d) and the capillary pressure of the porous media.

At the interface of a steady state, two-fluid system in porous media, the difference between the pressure of the two fluids is balanced by the surface tension of the interface. This interfacial tension may be quantified by the capillary pressures within the pores of the porous media. The capillary pressure is inversely proportional to the mean radius of curvature of the interface between the two fluids and may be quantified using the Laplace's equation.

$$P_e = P'' - P' = \frac{2\sigma}{r_m} \tag{2}$$

where P_e ($ML^{-1}T^{-2}$) is the capillary pressure, P'' and P' are the pressures of the two different fluids, σ (MT^{-2}) is the surface or interfacial tension, and r_m (L) is the mean radius of curvature at the interface between the two fluids. The fluid with the concave side of the surface must have a pressure P'' which is greater than the pressure P' on the convex side.

In general, the radius of curvature at the interface is a function of the porous media, the particle size, and the contact angle between water and the porous media. A decrease in the mean particle size diameter will correspond to a decrease in the mean radius of curvature.

Capillary entry pressure may be approximated using the following expression (Reddy et al., 1995):

$$P_e = \frac{C\sigma\cos\delta}{dp_{50}\varepsilon} \tag{3}$$

where C (dimensionless) is the shape factor which is a function of the particle shape and distribution, δ is the contact angle, ε (dimensionless) is the void ratio, dp_{50} (L) is the mean particle size, and σ (MT^{-2}) is the interfacial tension previously defined. When the injected air pressure is greater than $P_w+P_e+P_d$, the air displaces part of the pore water and creates a transient air porosity within the media. Air flow will initially be in a horizontal direction but the bouyancy of air will tend to cause the air to flow upwards. Therefore based on the above evaluation, the likely pathway for air flow in an aquifer will be through the pores with the lowest capillary pressure or pathways of least resistance. Changes in the permeability of the soil or in the soil structure will easily cause a change in the path of the air flow. In addition, when air channels hit a less permeable media, lateral dispersion of air may occur resulting in the entrapment or accumulation of a thin continuous air layer under the less permeable media. As a consequence of this phenomenon, some field data seemed to suggest that air flow may be restricted in soils with a hydraulic conductivity of 0.001 cm/sec or less (Middleton and Miller, 1990).

Air injected into the aquifer may travel laterally and vertically depending on the injected air pressures (Brown et al., 1993). The furthest lateral displacement of the air in the saturated zone from the injection wells is defined as the radius of influence (*ROI*). Four common methods are used to determine the *ROI* of the sparging well: (i) pressure changes below the water table, (ii) increase in dissolved oxygen concentrations in the groundwater, (iii) mounding of the water table, and (iv) increase in VOC vapor concentration in the unsaturated zone (McCray and Falta, 1997). None of the four methods mentioned above has been shown to determine the *ROI* definitely. Given the asymmetric nature of the air channel distribution, some researchers have used the zone of influence or areal extent of influence (*AEI*) instead of

the *ROI*. The *AEI* is defined as an inverted cone or paraboloid centered at the sparging well (Reddy et al. 1995, Suthersan, 1997). For effective cleanup, the contaminant zone should be placed within the *ROI* or *AEI*.

Although a knowledge of the nature of air flow in saturated porous media and the ability to predict air flow is central in understanding the physical-chemical processes occurring during air sparging, this work will not investigate the pathway and nature of air flow in saturated porous media. Instead, based on the above discussion and current work done by other researchers, the flow pattern of air will be assumed to occur in the form of discrete air channels.

Mass Transfer and Transport Mechanisms

VOCs in the subsurface may be present as a free phase, adsorbed phase, vapor phase, and dissolved phase. In an air sparged aquifer, the bulk liquid away from the air channel is expected to be quiescent rather than completely mixed. Therefore, mass transfer from the quiescent bulk solution to the air-water interface must be evaluated as a possible limiting mass transfer mechanism. Depending on the air flow rates, it is probable that soil particles adjacent to the air channels have most of their mobile water pushed away except for a thin layer of water attached to the soil particle. Therefore, on the onset of air sparging, the majority of the VOCs volatilized will come from this thin layer of water. Several mass transfer processes (Figure 2) may occur during air sparging:

(i) volatilization of contaminants from groundwater into the sparged air

(ii) desorption of contaminants from soils into groundwater

(iii) advection and diffusion of contaminants in the liquid and gas phases

(iv) dissolution of contaminants from free nonaqueous liquid phase (NAPLs) into groundwater

(v) direct volatilization of NAPLs into the sparged air.

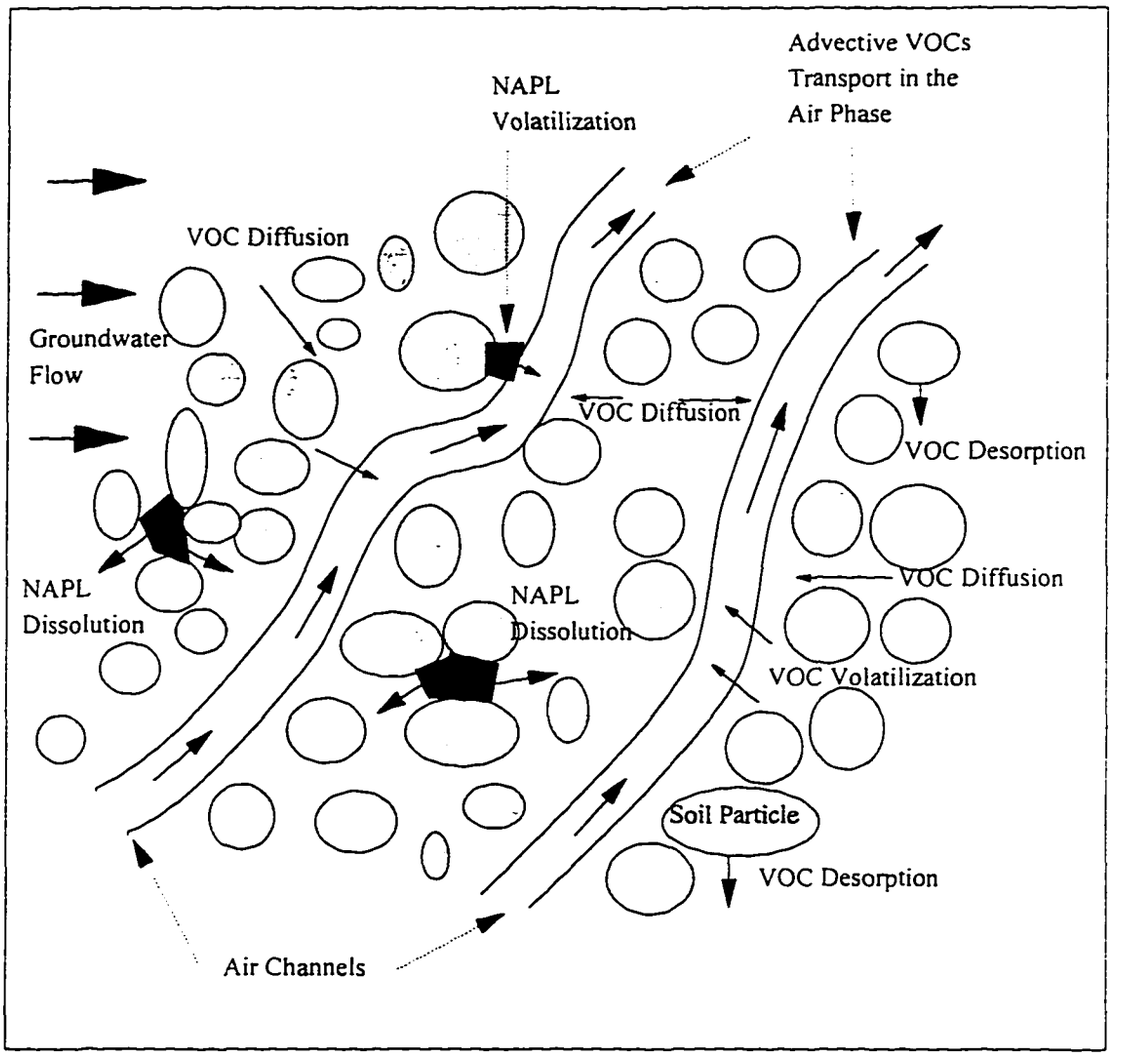

Figure 2. Mass transfer processes occuring during air sparging

Volatilization of VOCs: Air-water mass transfer coefficients

Volatilization of VOCs across the air-water interface for surface waters and in treatment process has been well researched. In these systems, several conceptual theories have been proposed to explain the mass transfer phenomenon. Conceptual theories developed for these systems may be adapted and applied for VOC mass transfer in saturated porous media during air sparging.

The net flux of a chemical in a medium may be described by Fick's first law:

$$F = -D\left(\frac{\partial C}{\partial z}\right) \tag{4}$$

where F is the net flux of chemical per unit surface area ($ML^{-2}T^{-1}$), D is the diffusion coefficient of the chemical in water or air (L^2T^{-1}), C is the concentration of the chemical (ML^{-3}), z is the distance in the medium (L). Under equilibrium conditions, the distribution of VOCs between the water and air phases may be represented by Henry's law:

$$K_H = C_a / C_w \tag{5}$$

where C_a and C_w are concentrations (ML^{-3}) in the air and water phases, respectively, and K_H is the dimensionless Henry's law constant. Henry's law constants are temperature-dependent and their values for a wide variety of compounds are available in the literature (Mackay and Shiu, 1981). Henry's law constant predicts the relative distribution of VOCs in the air and water phases. VOCs with higher Henry's law constant will have a larger fraction of the VOC present in the gas phase.

Several researchers have shown that under advective gas flow conditions such as air sparging, the movement of air across the air-water interface may not provide enough residence time for local equilibrium to be achieved (Mendoza and Frind, 1990). On the other hand, some researchers have found that the assumption of local equilibrium for air-water mass transfer is applicable (Brusseau et al., 1990; Gierke et al., 1992). If the local equilibrium assumption is not applicable, a nonequilibrium mass transfer expression such as

the first order mass transfer relationship used by Sleep and Sykes is usually applied (1989). The nonequilibrium mass transfer expression commonly used is as follows:

$$dC_a / dt = K_L\, a_{wa}[(C_a / K_H) - C_w] \qquad (6)$$

where K_L is the overall mass transfer coefficient (LT^{-1}), and a_{wa} represents the specific interfacial area (L^{-1}). In the above expression, the driving force for the transfer of VOC across the air-water interface is equal to the difference between the equilibrium water concentration (C_a/K_H) and the actual water concentration (C_w).

The physical phenomenon occurring at the air-water interface has been investigated by several researchers. As a result of their research, several conceptual and hydrodynamic models have been proposed. A conceptual model which is presently accepted as describing the diffusive exchange of chemicals between water and air is the two-resistance model. The model was first described by Whitman in 1923 and first applied to environmental situations by Liss and Slater in 1974 (Mackay et al., 1990). The model agrees with the mass flux expressed in equation 4 except that the model assumes the existence of two thin stagnant films on each side of the gas-liquid interface and that a chemical or solute must diffuse in series through the two layers of water and air or viceversa. The rates at which mass are transferred are characterized by the mass transfer coefficients, k, which are essentially mass transfer velocities. Based on this model, the inverse of the overall mass transfer coefficient can be assumed to be the sum of the liquid and gas phase film resistance as given by:

$$\frac{1}{K_L} = \frac{1}{k_L} + \frac{1}{K_H k_A} \qquad (7)$$

where k_L and k_A are the liquid and gas film mass transfer coefficients (LT^{-1}), respectively. For most chemicals with high Henry's law constant, the term $K_H k_A$ is usually larger than k_L, making the liquid film mass transfer, the controlling mass transfer mechanism. According to this model, the concentration gradient would be linear in each film (Figure 3) and the liquid and gas film coefficients may be given by:

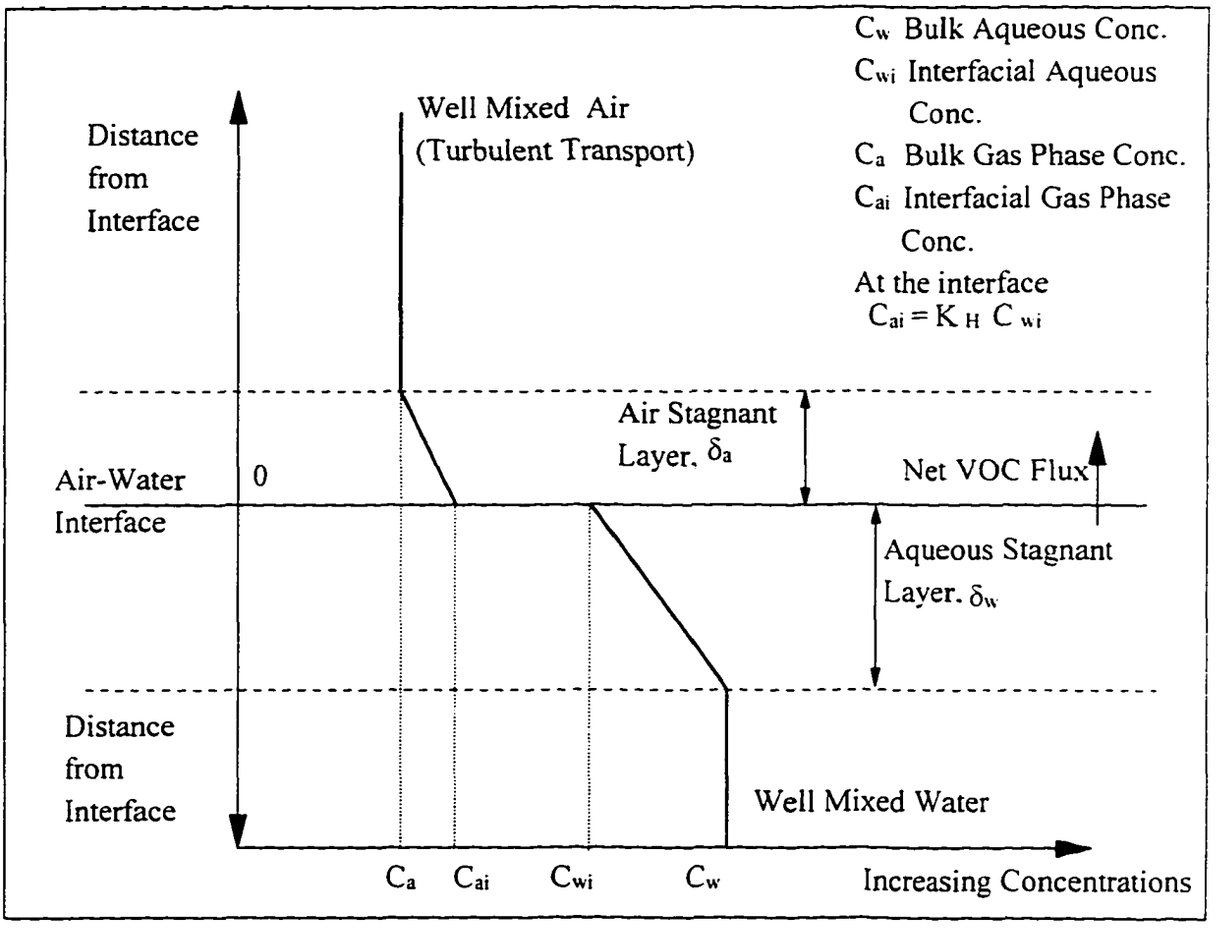

Figure 3. Two-resistance model

$$k_L = D_w / \delta_w \qquad k_A = D_A / \delta_a \tag{8}$$

where D_w and D_A are the diffusivities of the chemical in water and air, respectively, and δ_w (L) and δ_a (L) are the thickness of the stagnant layers or films in the water phase and the air phase, respectively.

In many applications with turbulent flow, mass transport by diffusion is relatively small in comparison with other modes of mass transfer. Consequently, the two-resistance model may not be the best conceptual model to explain the air-water mass transfer under turbulent flow conditions. The concept of a stagnant layer at the air-water interface is probably the weakest assumption in the two-resistance model and to overcome this weakness, Danckwerts (1951) proposed the surface renewal theory. This theory is a conceptual expansion of the penetration theory developed by Higbie in 1935. The main concept is that the fluid at the surface is periodically renewed by turbulent eddies impinging on the air-water interface. Because of the turbulent nature, the thickness of the liquid phase film changes over time and space. When an eddy reaches the air-water interface, the eddy is exposed to the gas phase and nonsteady state diffusion of the compound into and out of the liquid phase occurs.

Higbie proposed that the exposure time of the eddy, θ, is short enough that diffusion into the liquid is slow and the dissolving compound is never able to reach the full depth of the eddy. Under these conditions, the average liquid film mass transfer coefficient may be expressed as:

$$k_L = 2(D_w / \theta\pi)^{0.5} \tag{9}$$

Experience shows that the exponent on D_w may range from near zero to 0.9 (Treybal, 1968). Unlike the two-resistance model where mass transfer is dependent on the film thickness, mass transfer using the surface renewal theory is dependent on the frequency of renewal by the eddies. Dankwerts assumed that the renewal of the surface elements has a Gaussian distribution and found that the liquid and gas transfer coefficients may be expressed as a

function of the diffusivity (D) of the chemical in the liquid and air phase, respectively, as given below:

$$k_L = \sqrt{D_w r_w} \qquad k_A = \sqrt{D_A r_a} \tag{10}$$

where r_w and r_a are the mean renewal rates on the water and air side, respectively.

Several other conceptual theories have been proposed since the surface renewal theory was put forth by Danckwerts. O'Connor and Dobbins (1956) proposed the film renewal model which combines the two-resistance model and Danckwerts' renewal model. Arguing that the liquid content of the liquid film at the interface is continuously replaced in a random manner by liquid from the bulk region, O'Connor and Dobbins proposed that the liquid transfer coefficient may be given by:

$$k_L = (D_w\, r_w)^{0.5}\, coth\, [(r_w \cdot \delta_w^2)/D_w] \tag{11}$$

Equation 11 becomes equations 9 or 10 when the renewal velocity r_w approaches infinity or zero, respectively.

Other models include the random eddy model of Harriot (1962) and the surface divergence model of Brumley and Jirka (1988). Brumley and Jirka model uses the divergence of the horizontal liquid velocity at the surface plane to interpret the mechanism of gas transfer at the near surface region.

Several models which combine convective fluid flow in the interfacial region and measurable turbulence properties in the bulk region have been proposed. These models include the large-eddy model postulated by Fortescue and Pearson (1967), the small-eddy model of Lamont and Scott (1970) and the model suggested by Theofanous et al. (1976). The last model combines the large-eddy model for low turbulent Reynolds number (<500) with the small-eddy model for high Reynolds number (>500). Theofanous et al. found that the liquid film coefficient may be correlated with various dimensionless parameters as follows:

$$k_L = f_n (Sc^{-0.5}, Re^{-0.5}) \qquad for\ Re < 500 \tag{12}$$

$$k_L = f_n (Sc^{-0.5}, Re^{-0.25}) \qquad for\ Re > 500 \tag{13}$$

where Sc is the Schmidt number ($\mu_w / \rho_w D_w$) and Re is the turbulent Reynolds number.

Considerable amount of research has been devoted in determining the limiting mass transfer layer and estimating the mass transfer coefficients for gases and organic chemicals in wastewater and in natural bodies of water. In the field of wastewater, various types of aeration and air stripping equipment have been evaluated to assess the transfer of oxygen from air to water phase and the removal efficiency of VOCs from wastewater. Matter-Muller et al. (1981) concluded that the transfer of volatile substances from water to the air phase was strongly dependent on the type of gas-liquid contacting operation (bubble aeration, surface aeration, stripping towers, etc.). The authors also found that the mass transfer coefficients and the degree of saturation of the exit gas with respect to the VOC were important parameters in determining the transfer of the VOC from water to air. This conclusion supports the use of equation 6 to describe the mass transfer rate across the two phases. Munz and Roberts (1989) showed using a laboratory-scale mechanical surface aeration unit that the mass transfer coefficient for a volatile organic compound may be related to that of oxygen by a proportionality factor ψ:

$$\psi = (k_{L,i} / k_{LO2}) = (D_{L,i} / D_{LO2})^n \cong (K_{L,i} / K_{LO2}) \tag{14}$$

where the $K_{L,i}$ and K_{LO2} are the overall mass transfer coefficients for the VOC and oxygen, respectively, and $D_{L,i}$ and D_{LO2} are the aqueous molecular diffusion coefficients for the VOC and oxygen, respectively. Equation 14 is extremely useful and has become increasingly popular because it can be used to predict the mass transfer coefficients of different VOCs based on their diffusivities. However, it must be emphasized that the proportionality factor ψ is a constant only when the transport mechanism for both compounds, i.e., VOC and oxygen, is controlled by the liquid phase resistance of the mass transfer. If the gas phase resistance would in fact contribute to the overall mass transfer resistance in a significant way, the ψ

values will be smaller, and the potential of volatilization of a given compound will be overestimated accordingly. Munz and Roberts found significant deviations in the values of ψ for the least volatile compounds and concluded that the gas phase mass transfer resistance is more important than previously assumed. As a consequence of these findings, the authors concluded that mass transfer for compounds with dimensionless Henry's law constant ≥ 0.55 was probably completely liquid phase controlled. The value of the constant n was found to vary between 0.5 and 1.0. The lower value of n, 0.5, is for turbulent conditions closely representing the surface renewal theory while the higher value, 1.0, represents the stagnant films as in the two-resistance model. In their study, the liquid mass transfer coefficient k_L was found to be proportional to the square root of the diffusivity of the VOC in accordance with the surface renewal theory.

The diffusivity or diffusion coefficient D, is a property of the chemical compound and is dependent on temperature, pressure and the physical-chemical nature of the components of the system such as the type of media. In the absence of experimental data, gas phase diffusivities can be estimated based on the kinetic theory of gases using the Hirschfelder-Bird-Spotz correlation (Perry and Chilton, 1978). Estimation of the diffusivity in liquids in the absence of experimental data cannot be made with the same accuracy as for gases due to a lack of an adequate theory for the liquid structure. However, for dilute solutions of nonelectrolytes, the empirical correlation of Wilke and Chang may be used (Treybal, 1968):

$$D_{AB} = 7.4 \times 10^{-8} (\phi M_B)^{0.5} T/\mu v_A^{0.6} \qquad (15)$$

where D_{AB} is the diffusivity of A (L^2T^{-1}, cm^2s^{-1}) in dilute solution in solvent B, M_B is the molecular weight (M, g) of the solvent B, T is the absolute temperature (K), μ is the solution viscosity in centipoise ($ML^{-1}T^{-1}$), v_A is the solute molal volume (cm^3g^{-1}) at the normal boiling point (L^3M^{-1}), and ϕ is the association factor for the solvent (2.6 for water as a solvent). The value of v_A may be estimated from tables based on the individual atomic and molecular contributions to the molal volume. Due the changes in viscosity with concentration and the

changes in the degree of ideality of the solution, equation 15 cannot be applied for concentrated solutions.

In natural bodies of water, wind speed along with the presence of wave fields and water currents have been shown to be important parameters controlling mass transfer at the air-water interface (Janhe et al., 1984). Studies by Mackay and Yuen (1983) have shown that the mass transfer coefficients for various VOCs were strongly dependent on the wind speed. Volatilization rates were measured using a 6 meters wind-wave tank for 11 VOCs. Experimental data confirmed the validity of the two-resistance model for high wind speeds and showed that there were no interaction amongst the VOCs when the VOCs were volatilized simultaneously. The authors also found that the mass transfer coefficient was a function of the wind friction velocity (the hydrodynamic parameter) and the Schmidt number which characterized the solute diffusion properties and temperature effect.

As previously stated, an air sparged aquifer may be visualized as an array of air channels with the volatilization of VOCs occurring at the air-water interface located at the wall of each air channel. The effectiveness of air sparging as a remediation technology is related to the ability of the system to provide maximum contact between the contaminated aquifer materials and the air flow. So far, information on mass transfer coefficients for the volatilization of VOCs under sparging conditions is fairly scarce (Szatkowski et al., 1995). In a later section of this chapter, correlations for mass transfer coefficients of VOCs under different experimental conditions will be presented.

Sorption-desorption of VOCs onto porous media

Much of the information obtained for the volatilization of VOCs from bulk water may be applicable for air sparging systems. However, the presence of the porous media introduces new factors which may affect the volatilization of VOCs. These factors include the increase in the distance that VOCs must travel to reach the air-water interface and sorption of the VOCs onto the soil matrix. For soil media with a high affinity for VOCs, desorption of VOCs from the soil to the groundwater may play a role in mass transfer. VOCs with high

partition coefficients are less likely to volatilize even when the VOC has a high Henry's law constant.

Adsorption of the VOCs is defined as the accumulation of VOCs at the water-solid interface while absorption is defined as the partition of VOCs between two phases. The term sorption is used when both adsorption and absorption are occurring and cannot be distinguished from one another. Partitioning between the dissolved and sorbed solutes for a given temperature may be modeled using linear or nonlinear isotherms as presented below:

$$C_S = K_d C_w \tag{16}$$

$$C_S = K_f C_W^n \tag{17}$$

where C_S represents the concentration of the VOCs sorbed onto the soil matrix (MM^{-1}), C_w is the concentration of VOC in the liquid phase (ML^{-3}), K_d is the linear partition coefficient (L^3M^{-1}), and K_f represents the Freundlich partition coefficient ($L^{3n}M^{-n}$).

Due to the nonpolar nature of most VOCs, sorption of VOCs onto soils may be correlated with the organic matter content in the porous media. While the linear partition coefficient, K_d, of a chemical varies significantly from soil to soil, the ratio between K_d and the mass fraction of organic carbon in the soil (f_{oc}) is less variable. This ratio results in a proportionality constant for each organic compound known as the organic carbon partition coefficient (K_{oc}). This relationship can be represented as (Karickhoff et al., 1979; Karickhoff, 1984):

$$K_d = f_{oc} K_{oc} \tag{18}$$

The above relationship is considered to be valid for organic carbon contents greater than 0.1%. When contaminants are in contact with low organic carbon aquifer material ($f_{oc} < 0.001$), adsorption of contaminants may play a significant role. Sorption of organic products may be two to four times higher than the values predicted by equation 18 (Piwoni and Banerje, 1989). Most organic contaminants are rapidly sorbed onto soils but desorption

can be very slow. This phenomenon tends to reduce the efficiency of remediation technologies such as air sparging (Suthersan, 1997).

The linear isotherm (equation 16) has been widely used to describe the transport of VOCs in the subsurface (Gierke et al., 1990, Ong and Lion, 1991). Karickhoff (1984) suggested that use of linear isotherm is a reasonable assumption if the contaminant concentrations were lower than 10^{-5} M or less than half the water solubility of the organic contaminant. Based on experimental results, Karickhoff (1979) derived an empirical correlation between the organic carbon partition coefficient and the octanol-water partition coefficient (K_{ow}):

$$log\ K_{oc} = log\ K_{ow} - 0.21 \qquad (19)$$

The above equation is useful for estimating the organic carbon partition coefficient of an organic compound from the chemical properties of the compound.

As presented in the previous paragraph, sorption of VOCs to soil particles may play an important role in the distribution of the VOCs in the solid-liquid-gas phase system such as air sparging. Ong and Lion (1991) showed that the sorption of TCE in different soils and under different moisture conditions may be accounted for by: (a) dissolution of TCE in the water bound to the soil particle as governed by Henry's law (this contribution can constitute a large fraction of the total mass of VOC for soils with low organic carbon content), and (b) sorption of TCE at the solid-liquid interface as governed by the saturated partition coefficient. VOCs with high partition coefficients are less likely to volatilize even when the VOCs have high Henry's law constants. Under a dynamic air flow situation, removal of VOCs at the air-water interface may occur so fast that the desorption of the VOCs could become the rate limiting step in the transfer of VOCs into the gas phase.

Pavlostathis and Mathavan (1992) conducted batch desorption experiments with field-contaminated soils and found that a substantial portion of the sorbed contaminant resisted desorption. The desorption pattern showed an initial fast desorption phase followed by a slow desorption phase. The authors also found that the rate and extent of desorption were independent of the soil and VOC properties such as organic carbon content, cation exchange

capacity, specific surface area, and water solubility. Several researchers have modeled the sorption-desorption phenomenon as a first order kinetic process (Brusseau and Rao, 1989: Armstrong et al., 1994). The rate limited sorption-desorption model may be expressed as:

$$\frac{dC_S}{dt} = k_S\left(C_w - C_w^*\right) \tag{20}$$

where C_S is the concentration of VOC sorbed onto the soil particles (MM^{-1}), C_w is the actual aqueous concentration of the VOC (ML^{-3}), C^*_w is the equilibrium aqueous concentration of the VOC in contact with the soil surface (ML^{-3}), and k_S is the first order sorption-desorption coefficient ($L^3M^{-1}T^{-1}$). Using the linear isotherm described by equation 16, equation 20 can be rearranged as follows:

$$\frac{dC_S}{dt} = k_S\left(K_d C_w - C_S\right) \tag{21}$$

where the dimension of k_S is T^{-1}.

Weber et al. (1991) studied conceptually the sorption phenomenon in subsurface systems and their effects on contaminant fate and transport. The emphasis of this study was the development of concepts involved in the sorption-desorption phenomenon and the translation of these concepts into functional models for characterizing sorption-desorption rates and equilibrium. Several conceptual mass transfer models applicable to situations such as the volatilization of volatile compounds from solids and liquids, the dissolution of nonaqueous phase liquid into water and treatment process were presented in this study. The authors stated that under the typical fluid flow conditions found in subsurface systems, molecular diffusion generally dominates the microscopic mass transfer. This molecular diffusion has two main components: (a) random or Fickian diffusion, and (b) Knudsen diffusion or "constrained diffusion". Knudsen diffusion occurs when molecular velocities and ratios of longitudinal to radial pore lengths are high, such as in the gas phase. However, according to

the authors, Fickian motion as described by equation 4 is the dominant diffusion mechanism in liquid phase.

Finally, Nadim and coworkers (1997) studied the mass transfer limitations for the desorption of VOCs and the liquid phase diffusion of organic molecules in unsaturated soils during soil vapor extraction operations. The authors concluded that the gas phase effluent concentrations were a result of: (i) removal of compounds initially dissolved in the liquid layer which was responsible for the rapid exponential decrease of the VOCs concentration in the effluent air, and (ii) slow desorption for the VOCs from the solid phase which was the reason for the long tailing in the effluent concentration observed during soil vapor extraction.

Dissolution and volatilization of nonaqueous phase liquids (NAPLs) in the subsurface

In general, mass transfer limitations observed in the field have been attributed to the slow diffusion of the dissolved pollutants from low permeability porous media to the mobile groundwater or to the gas phase of the vadose zone. Releases of organic products from hazardous waste sites may also result in the migration of contaminants as a separate organic phase. The behavior of these organic phases is controlled by three major forces: capillary forces, viscous forces, and buoyancy forces. In a typical aquifer, organic liquid is trapped in saturated porous media as a result of capillary forces. Depending of their densities, NAPLs are classified as light nonaqueous phase liquids (LNAPLs) and dense nonaqueous phase liquids (DNAPLs).

LNAPLs are less dense than water and are vertically transported through soil until they reach the capillary fringe where they spread horizontally forming floating pools. DNAPLs, which are more dense than water, are vertically transported through soil by gravity and capillary forces until they reach an impermeable layer. Conrad et al. (1992) in a visualization study of residual organic liquid trapped in aquifers found that large amounts of organic contaminants were trapped as isolated microscopic blobs. The size, shape, and spatial distribution of these blobs of residual organic liquid affected the dissolution of the organic contaminants into the groundwater. For an air sparged NAPL-contaminated aquifers, Baker et al. (1996) proposed that the rate of mass removal was time dependent and depended on the

degree of contact between the air and the NAPL ganglia. A fast removal rate is achieved initially as contaminant closest to the air channels are volatilized. Subsequent mass removal is slower because contaminants must diffuse to the air channels before being removed.

Wilkins et. al (1995) studied the volatilization of NAPLs in unsaturated sandy porous media and found that the effluent concentration of the contaminant in vapor phase deviated from local equilibrium values by 10-40 % for pore velocities ranging from 0.25 to 1.5 cm/s. In addition the mass transfer rates were found to decrease with decreasing soil mean grain size.

Powers et al. (1992) investigated the steady state dissolution of NAPLs in saturated subsurface systems and found that the dissolution rate of NAPLs was dependent on the distribution pattern of the NAPLs and the aqueous phase velocity. In addition, Powers et al. (1994) found that the length of time required to dissolve NAPLs was substantially longer than the times predicted by equilibrium calculations. The dissolution of NAPLs may be modeled using a first order kinetic expression:

$$\theta_w \frac{\partial C_w}{\partial t} = \alpha(S - C_w) \tag{22}$$

where θ_w is the water filled porosity (dimensionless), S represents the aqueous solubility of the organic chemical (ML^{-3}), C_w represents the actual concentration of the organic chemical in the liquid phase (ML^{-3}), and α represents the mass transfer coefficient (T^{-1}). Powers et al. (1994) reported that longer cleanup times were associated with coarse or graded media and speculated that this was due to the larger and more amorphous NAPL blobs present in the media. Miller et al. (1990) successfully used a local equilibrium assumption to compute mass transfer rates between a toluene NAPL and flowing water in a laboratory study using glass beads as a porous media. The findings of this study were in agreement with the work by Powers and her coworkers, except that mass transfer rate was not significantly related with the mean particle size.

In a series of modeling studies on the application of horizontal SVE systems, Gomez-Lahoz et al. (1994a, and 1994b) and Rodriguez Maroto et al. (1994) showed that remediation by SVE may be diffusion controlled, limited by the dissolution of the NAPL into the aqueous phase and/or desorption controlled. Their modeling studies showed that the remediation time was dependent on the length of the clay lenses which the organic contaminants have to cross before reaching into the gas phase. In addition, remediation time was dependent on the diameter of the NAPLs and the initial concentration of the contaminants. These authors found that at the start of the extraction, the VOC concentration in the soil gas was very high but dropped rapidly to a fairly low constant tailing concentration. The time of the tailing was observed to increase with an increase in the diffusion layer thickness. The information presented above, suggested that the presence of NAPLs may introduce new limitations in the transport and removal of VOCs during air sparging operations.

Modeling Mass Transfer

Due to the complexity associated with air flow through saturated porous media, a fundamental approach in predicting the mass transfer rates of VOCs for air sparging is currently not available in the literature. Several empirical air-water mass transfer correlations derived in the field of chemical engineering and for soil vapor extraction systems will be presented to provide a quantitative idea of mass transfer coefficients for air sparging systems.

Mass transfer coefficients for the volatilization of organic solutes from water were estimated by many researchers. Among them, Mackay and Yuen (1983) studied the volatilization of 11 different organic compounds from aqueous phase and concluded that the two-resistance model may be applied to model mass transfer. They also found that the Schmidt number, *Sc* (dimensionless ratio between viscosity and the product of density times molecular diffusivity) correlated well with the mass transfer coefficients.

Linton and Sherwood (1950) developed a dimensionless correlation that may be applied for the estimation of the overall liquid side mass transfer coefficient for air flowing through porous media in the form of discrete air channels. The correlation was developed using data from Sherwood and Gilliland for wetted-wall towers and their own mass transfer studies for

water flow through pipes with soluble walls. The correlation developed by Linton and Sherwood is presented below. The Reynolds number for the correlation ranged from 2,000 to 35,000 while the Schmidt number ranged from 0.6 to 3000.

$$Sh = 0.023\, Re^{0.83}\, Sc^{1/3} \tag{23}$$

where *Sh* represents the Sherwood number (dimensionless mass transfer coefficient), and *Re* and *Sc* represents the Reynolds and Schmidt numbers, respectively. Mathematical description of these dimensionless parameters are presented in Appendix A.

Using soil columns packed with Ottawa sand and other aggregate porous media, Gierke and coworkers (1992) showed that the vapor transport of toluene in the unsaturated soil columns was a nonequilibrium transport process. With the aid of mathematical models, mass transfer was shown to be impacted by the dispersion, film transfer, and intraaggregate diffusion. The mass transfer coefficient used in the model was derived from that of Crittenden and coworkers (1986) and is given as follows:

$$K_L a = \frac{15 D_p S}{(1-S) K_H R_a^2} \tag{24}$$

where $K_L a$ is the overall liquid side lumped mass transfer coefficient (T^{-1}), D_p represents the intraaggregate diffusion coefficient (L^2T^{-1}), S is the degree of saturation (dimensionless), K_H is the dimensionless Henry's law constant, and R_a is the aggregate radius (L).

Work done by Cho and Jaffe (1990) showed that during infiltration into a soil column, equilibrium conditions for the volatilization of VOCs between the dissolved and gas phase cannot always be used. Szatkowski et al. (1995) used an experimental setup with a constant interfacial area between phases to investigate the resistance to aqueous-vapor mass transfer at the air-water phase boundary. Using dimensional analysis, Szatkowski and coworkers found that the modified Sherwood number correlated to several macroscopic properties of the system. The correlation obtained by Szatkowski et al. was as follows:

$$Sh_w' = a_{aw}\, d_p \left(0.023 Sc_w^{0.5} + 0.849\, \mathrm{Re}_w^{0.861}\, Sc_w^{0.5}\right) \qquad \text{for } 0.001 \le Re_w \le 0.1 \tag{25}$$

The modified Sherwood number for the aqueous phase (Sh_w') was defined as:

$$Sh_w' = \frac{K_L\, a_{aw}\, d_p^{\,2}}{D_w} = \frac{k_{aw}\, d_p^{\,2}}{D_w} \tag{26}$$

Definition of the variables may be found in Appendix A.

Szatkowski et al. reported that predictions from the correlation described in equation 25 were in good agreement with work done by other researchers (Cho et al., 1994; and Turek and Lange, 1981). A shortcoming of this study was that only one VOC and one type of porous media was used. Because of this shortcoming, the mass transfer coefficients were correlated with the hydrodynamic conditions (air and water velocities) of the experiment only, but not with the chemical properties of the VOCs and physical properties of the porous media.

Based on experimental and computational simulations of TCE extraction in sandy soils, Armstrong et al. (1993) concluded that the mass transfer processes may not be represented by a simple first order rate constant but rather by a time dependent mass transfer coefficient. They used a decreasing power law relationship for the mass transfer coefficient and studied the influence of the Damkohler number on mass transfer. The Damkohler number is the ratio between mass partitioning and mass removal by advection. A shortcoming of this study and probably a reason why a time dependent mass transfer coefficients was considered, was that diffusion effects were not included in the transport equation for the dissolved phase.

Mohr (1995) assessed the influence of groundwater flow on air-water mass transfer rate by using an empirical correlation. The correlation was developed for water flowing around a sphere of air and is given by:

$$Nu = 2 + 0.6\, Re^{1/2} Sc^{1/3} \tag{27}$$

where *Nu* is the Nusselt number representing the ratio of mass transfer with and without convection, *Re* and *Sc* are the Reynolds and Schmidt numbers, respectively. Definition of these dimensionless numbers may be found in Appendix A. For typical groundwater conditions of $Sc = 1000$ and a groundwater flow of 0.3 m/day, Mohr showed that the *Nu* number, which may be viewed as dimensionless mass transfer coefficient, increased by less than 35% in comparison to the stagnant water solution. This implies that groundwater flow has minimum impact on mass transfer at the air-water interface.

Chao (1997) derived a correlation for the dimensionless Sherwood number (which includes the mass transfer coefficient) with the air phase Peclet number (*Pe*), the dimensionless mean particle size (d_o), and the Henry's law constant (K_H). The correlation was statistically obtained from a series of nonequilibrium air-water mass transfer experiments using a bench scale air sparging system. The correlation was:

$$Sh = 10^{-4.71} Pe^{0.84} d_o^{1.71} K_H^{-0.61} \tag{28}$$

Miller and coworkers (1990) studied the dissolution of NAPLs in glass beads with toluene as a contaminant. The experiments were conducted using packed columns and at various NAPLs fluid saturation levels. The authors found that the interfacial mass transfer rate was directly related to the aqueous phase velocity and nonaqueous phase fluid saturation while no significant dependence on the mean particle size was found.

Powers et al. (1992), investigating the steady-state dissolution of NAPLs trapped within saturated porous media, developed a phenomenological model correlating the modified Sherwood number with the grain size (d_{50}), uniformity coefficient (*UC*), and water phase Reynolds number. The correlation is given by:

$$Sh' = 57.7 Re^{0.61} d_{50}^{0.64} UC^{0.41} \tag{29}$$

where Sh' is the modified Sherwood number as defined in Appendix A. In a later study Powers and coworkers (1994) extended the correlation model (equation 29) by incorporating changes in the interfacial area as a result of NAPL dissolution. The new model can be represented as:

$$Sh' = 4.13\, Re^{0.598}\, d_o^{0.673}\, UC^{0.369} \left(\frac{\theta_n}{\theta_o}\right)^{\beta_t} \tag{30}$$

where the ratio (θ_n/θ_o) is the ratio between the actual and initial NAPL volumetric fraction. The exponent β_t varied between 0.75 and 0.96 depending on the porous media. The authors were able to correlate the value of the exponent β_t with the dimensionless mean grain size and the uniformity coefficient of the porous media.

Wilkins et al. (1995) correlated the volatilization of NAPLs with several physical properties of the porous media. The mass transfer coefficient is given by:

$$k_{aw} = 10^{-0.42} D_w^{0.38} v_w^{0.62} d_{50}^{0.44} \tag{31}$$

where k_{aw} is the lumped mass transfer coefficient (T^{-1}). Other variables in equation 31 are defined in Appendix A. Wilkins and coworkers compared the results of their studies for the volatilization of NAPLs in unsaturated porous media with that of Powers et al. (1992) for the dissolution of NAPLs in saturated porous media. Wilkins and coworkers pointed that for saturated systems, the rate of NAPLs dissolution was inversely correlated to the soil mean size while in unsaturated porous media, volatilization of NAPLs was positively correlated with soil mean grain size. In addition, the dissolution rate was strongly correlated with the uniformity coefficient for unsaturated porous media while the uniformity coefficient had no effect in saturated porous media. Wilkins and coworkers attributed the differences to the differences in NAPL configuration and the differences in the flowing phase in saturated and unsaturated porous media.

VOCs transport in porous media

Several models explaining the mass transfer of oxygen and VOCs at the air-water interface may be found in the literature. These models are greatly simplified and do not exactly represent the conditions for a wide range of air flow rates during air sparging. Among them are the simple steady-state and nonsteady-state models developed by Wilson and coworkers (Clark et al., 1996). A more elaborate model was developed by Marley et al. (1992) which described the distribution of air pressure and air velocity during the air sparging operation. The model assumed that: (i) stagnant conditions for water, (ii) steady state mass transfer conditions, (iii) no biodegradation, and (iv) air wells acted as line sources with air flow obeying Darcy's law. Sellers and Scherber (1992) derived an exponential equation describing the change in groundwater concentration when air sparging was used. They assumed that the rate of pollutant diffusing into the sparging bubbles was balanced by the loss of dissolved phase contaminant from the groundwater. A model developed by Sleep and Sykes (1993a, 1993b) included three-phase flow and interfacial mass transfer due to volatilization and dissolution but assumed equilibrium conditions between the phases. Other attempts to model air sparging systems included the model by Gvirtzman and Gorelik (1992) and the work of Ostendorf et al. (1993). In a review paper on air sparging, Reddy et al. (1995) presented a model from the work of Abriola and Pinder (1985) on multiphase transport of organic compounds in porous. The modified model included microscale volatilization and biodegradation processes, macroscale advection and dispersion processes, and interfacial mass transfer processes such as adsorption, desorption, dissolution, and volatilization.

A more refined model which incorporated the diffusion of the VOCs from the porous matrix to the air channels was proposed by Hein et al. (1994). The model showed that the mass transfer was dominated by gaseous dispersion and advection, and liquid diffusion. The model equations are as follows:

$$\frac{\partial C_w(z,r,t)}{\partial t} = \left(\frac{Ed}{r}\right)\frac{\partial}{\partial r}\left(r\frac{\partial C_w(z,r,t)}{\partial r}\right) \tag{32}$$

$$\frac{\partial C(z,t)}{\partial t} = \left(\frac{1}{Pe}\right)\frac{\partial^2 C(z,t)}{\partial z^2} - \frac{\partial C(z,t)}{\partial z} + 2St[C_w(z,r,t) - C(z,t)] \tag{33}$$

where C_w and C are the dimensionless water and air concentrations of the pollutant, respectively; z and r are the dimensionless axial and radial coordinates, respectively; t is the time elapsed; Ed is the pore diffusion modulus (rate of transport by radial diffusion/rate of transport by advection); Pe is the air phase Peclet number (rate of transport by advection/rate of transport by axial dispersion); and St is the Stanton number (rate of transport by air/water mass transfer/rate of transport by advection). The description of all these dimensionless parameters may be found in Appendix A. The numerical model was shown to be more sensitive to changes in the air phase Peclet number and pore diffusion modulus. Changes in the Stanton number did not affect the model output and this was in accordance with the previous work done by Gierke et al. (1992) for SVE systems. The work done by Hein et al. supported the hypothesis that the mass transfer was controlled by molecular diffusion. Hein et al. model was developed by assuming a vertical air channel and that VOCs diffused from the porous media to the air channel. Under these assumptions, the term representing the interfacial mass transfer between the liquid phase and the gas phase as presented in equation 33 should be stated as a boundary condition linking the transport between the two phases rather than as defined in the model.

Drucker and Di Julio (1996) developed a diffusion limited model which is similar to that of Wilson et al. (1994). Predictions of the model seemed to agree with results from a soil column experiment using TCE as the contaminant. No adsorption effects were considered in the development of the model and its validity for other VOCs was not proven. Sensitivity analysis with the model indicated that the diffusion coefficient and the air channel radius had the biggest impact on remediation rate. The influence of Henry's law constant was limited to values between 0.01 and 0.35. For values smaller than 0.01, the rate of volatilization is the controlling factor in the remediation while for values larger than 0.35 diffusion of VOC in the

liquid phase controlled the process. The analysis showed that beyond a certain air flow rate, no further improvement in the removal rate was achieved.

In general, current models addressed the removal of VOC by air sparging on a macroscale. The influence of microscale processes such as the diffusion of VOCs through the porous media to the air channels has not been fully addressed yet. This research will study the influence of "microscale" processes governing the volatilization of VOCs and the results from a single-air channel system will be incorporated into a model with the aim of explaining the behavior of mass transfer in more complex systems.

References

Abriola, L.M., and G.F. Pinder, A multiphase approach to the modeling of porous media contamination by organic compounds. I. Equation Development, *Water Resources Research*, vol. 21(1), pp. 11-18, 1985.

Armstrong, J.E., J. Croise, and V. Kaleris, Simulation of rate-limiting processes controlling the vapour extraction of trichloroethylene in sandy soils, in *Proceedings of the International Conference on the Environment and Geotechnics*, Paris, France, pp. 327-334, April 6-8, 1993.

Baker, D.M., and C.H. Benson, Review of factors affecting in situ air sparging, in *Proceedings of the Non-Aqueous Phase Liquid (NAPLs) in Subsurface Environment: Assessment and Remediation*, edited by L.N. Reddi, Washington, D.C., pp. 292-310, November 12-14, 1996.

Brown, R.A., and R. Fraxendas, Air sparging extending volatilization to contaminated aquifers, Prepublication draft presented at the Symposium on Soil Venting, Robert S. Kerr Environmental Research Laboratory, Houston, TX, April 29-May 1, 1991.

Brown, R.A., R.J. Hicks, and P.M. Hicks, Use of air sparging for in situ bioremediation in *Air Sparging for Site Remediation*, edited by R.E. Hinchee, pp. 38-55, Lewis Publishers, Boca Raton, FL, 1994.

Brumley, H.B., and G.H. Jirka, Air-water transfer of slightly soluble gases: turbulence, interfacial processes and conceptual models, *J. Physico-Chemical Hydro.*, vol. 10(3), pp. 295-319, 1988.

Brusseau, M.L., and P.S.C. Rao, Sorption nonideality during organic contaminant transport in porous media, *CRC Critical Reviews in Environmental Control*, vol. 19(1), pp. 33-99, 1989.

Brusseau, M.L., Transport of organic chemicals by gas advection in structured or heterogeneous porous media: development of a model and application to column experiments, *Water Resources Research*, vol. 27(12), pp. 3189-3199, 1991.

Brusseau, M.L., R.E. Jessup, and P.S.C. Rao, Sorption kinetics of organic chemicals: evaluation of gas purge and miscible-displacement techniques, *Environ. Sci. Technol.*, vol. 24(5), pp. 727-735, 1990.

Buermann, W., and G. Bott-Breuning, Bioremediation by groundwater circulation using the vacuum-vaporizer-well (UVB) technology: basics and case study, in *Air Sparging for Site Remediation*, edited by R.E. Hinchee, pp. 97-107, Lewis Publishers, Boca Raton, FL, 1994.

Chao, K. P., Aqueous-vapor mass transfer of VOCs in saturated porous media under air sparging conditions, Ph.D. Dissertation, 176 pp., Polytechnic University, Brooklyn, NY, 1997.

Chao, K.P., and S.K. Ong, Air Sparging: effects of VOCs and soil properties on VOC volatilization, in *In Situ Aeration: Air Sparging, Bioventing, and Related Remediation Processes*, R. Hinchee, R. Miller, and P. Johnson (eds.), pp. 103-110, Battelle Press, Columbus, OH, 1995.

Cho, H.J., and P.R. Jaffe, The volatilization of organic compounds in unsaturated porous media during infiltration, *Journal of Contaminant Hydrology*, vol. 6, pp. 387-410, 1990.

Cho, H.J., P.R. Jaffe, and J.A. Smith, Simulating the volatilization of solvents in unsaturated soils during laboratory and field experiments, *Water Resources Research*, vol. 29(10), pp. 3329-3342, 1994.

Clark, A.N., D.J. Wilson, and R.D. Norris, Using models for improving in-situ cleanup of groundwater, *Environmental Technology*, July/August, pp. 34-41, 1996.

Conrad, S.H., J.L. Wilson, W.R. Mason, and W.J. Peplinski, Visualization of residual organic liquid trapped in aquifers, *Water Resources Research*, vol. 28(2), pp. 467-478, 1992.

Control Technology News, VOC remediation costs, time frames reduced up to 50% with air sparging, *J. Air Waste Management Assoc.*, vol. 42(5), p. 729, 1992.

Crittenden, J.C., N.J. Hutzler, D.G. Geyer, J.L. Oravitz, and G. Friedman, Transport of organic compounds with saturated groundwater flow: model development and parameter sensitivity, *Water Resources Research*, vol. 22(3), pp. 271-284, 1986.

Danckwerts, P.V., Significance of liquid-film coefficients in gas adsorption, *Ind. Eng. Chem.*, vol. 43(6), pp. 1460-1467, 1951.

Drucker, A.S., and S.S. Di Julio, Groundwater clean up by *In Situ* air sparging: development of a model and application to saturated soil column experiments, in *Proceedings of the Water Environmental Federation 69 th. Annual Conference & Exposition.* Dallas, Texas, October 5-9, 1996.

Dullien, F.A.L., *Porous Media. Fluid Transport and Pore Structure*, Academic Press, Inc.. NY, 1979.

Fortescue, G.E., and F.R.E. Pearson, On gas absorption into a turbulent liquid, *Chem. Eng. Sci.*, vol. 22, p.1163, 1967.

Gierke, J.S., N.J. Hutzler, and J.C. Crittenden, Modeling the movement of volatile organic chemicals in columns of unsaturated soil, *Water Resources Research*, vol. 26(7), pp. 1529-1547, 1990,

Gierke, J.S., N.J. Hutzler, and D.B. McKenzie, Vapor transport in columns of unsaturated soil and implications for vapor extraction, *Water Resources Research.*, vol. 28(2), pp. 323-335, 1992.

Gomez-Lahoz, C., J.M. Rodriguez-Maroto, and D.J. Wilson, Soil cleanup by in-situ aeration. XVII. Field scale model with distributed diffusion, *Separation Science and Technology*, vol. 29(10), pp. 1251-1274, 1994a.

Gomez-Lahoz, C., J.J. Rodriguez, J.M. Rodriguez-Maroto, and D.J. Wilson, Biodegradation phenomena during soil vapor extraction. III. Sensitivity studies for two substrates, *Separation Science and Technology*, vol. 29(10), pp. 1275-1291, 1994b.

Gvirtzman, H., and S. Gorelik, The concept of in situ vapor stripping for removing VOCs from groundwater, *Transport in Porous Media*, vol. 8, pp. 71-92, 1992.

Harriott, P., A random eddy modification of the penetration theory, *Chem. Eng. Sci.*, vol. 17, pp. 149-154, 1962.

Hein, G.L., N.J. Hutzler, and J.S. Gierke, Quantification of the mechanisms controlling the removal rate of volatile contaminants by air sparging, in *Proc. of the 1994 National Conference on Environmental Engineering*, J.N. Ryan and M. Edwards (eds), pp. 556-563, ASCE, NY, NY, 1994.

Jahne, B., K.H. Fisher, J. Ilmberger, P. Libner, W.Weis, D. Imboden, U. Lemin, and J.M. Jaquet, Parameterization of air/lake exchange, in *Gas Transfer at Water Surfaces*, W. Brutsaert and G.H. Jirka (eds.), D. Reidel, Boston, pp. 459-466, 1984.

Ji, W., A. Dahmani, D.P. Ahlfeld, J.D. Lin, and E. Hill, Laboratory study of air sparging: Air flow visualization, *GWMR*, vol. 13(4), pp. 115-126, 1993.

Johnson, R.L., P.C. Johnson, D.B. McWhorter, R.E. Hinchee, and I. Goodman, An overview of in situ air sparging, *GWMR*, vol. 13(4), pp. 127-135, 1993.

Karickhoff, S.W., D.S. Brown, and T.A. Scott, Sorption of hydrophobic pollutants on natural sediments, *Water Research*, vol. 13, pp. 241-248, 1979.

Karickhoff, S.W., Organic pollutant sorption in aquatic systems, *J. Hydraulic Eng.*, ASCE, vol. 110, pp. 707-735, 1984.

Lamont, J.C. and D.S. Scott, An eddy-cell model of mass transfer in the surface of a turbulent liquid, *AIChE J.*, vol. 16, p. 513, 1970.

Linton, W.H. and T.K. Sherwood, Mass transfer from solid shapes to water in stream line and turbulent flow, *Chemical Eng. Progress*, vol. 46(5), pp. 258-264, 1950.

Lyman, W.J., W.F. Reehl, and D. H. Rosemblatt, *Handbook of Chemical Properties Estimation Methods*, American Chemical Society, Washington D.C., 1990.

McCray, J.E., and R.W. Falta. Numerical simulation of air sparging for remediation of NAPL contamination, *Ground Water*, vol. 35(1), pp. 99-110,1997.

Mackay, D., and W.Y. Shiu, A critical review of Henry's law constant for chemicals of environmental interest, *J. Phys. Chem. Ref. Data*, vol. 10(4), pp. 1175-1199, 1981.

Mackay, D., W.Y. Shiu, K.T. Valsaraj, and L.J. Thibodeaux, Air-water transfer: the role of partitioning, in *Air Water Mass Transfer. Selected Papers from the Second International Symposium on Gas Transfer at Water Surfaces*, S.C Wilhelms and J.S. Gulliver (eds.), ASCE, NY, NY, 1990.

Mackay, D., and A.T.K. Yuen, Mass transfer coefficients correlations for volatilization of organic solutes from water, *Environ. Sci. and Technol.*, vol. 17(4), pp. 211-233, 1983.

Marley, M.C., F. Li, and S. Magee, The application of a 3-D model in the design of air sparging systems, in *Proc. of the 1992 Conference on Petroleum Hydrocarbons and Organic Chemicals in Groundwater: Prevention, Detection and Restoration*, NWWA, Houston, Texas, pp. 377-392, 1992.

Matter-Muller, C., W. Guer, and W. Giger, Transfer of volatile substances from water to the atmosphere, *Water Research*, vol. 15, pp. 1271-1279, 1981.

Mendoza, C., and E.O. Frind, Advective-dispersive transport of dense organic vapors in the unsaturated zone: I. Model development, *Water Research*, vol. 23(3), pp. 379-387, 1992.

Middleton, A.C., and D. Miller, In situ aeration of groundwater - a technology overview, in *Proceedings of the Conference on Prevention and Treatment of Soil and Groundwater Contamination in the Petroleum Refining and Distribution Industry*, Montreal, Canada, October 16-17, 1990.

Miller, C.T., M.M. Poirier-McNeill, and A.S. Mayer, Dissolution of trapped nonaqueous phase liquids: mass transfer characteristics, *Water Resources Research*, vol. 26(11), pp. 2783-2796, 1990.

Mohr, D.H., Mass transfer concepts applied to in situ air sparging, Paper presented at the *In Situ and On-Site Bioremediation Third International Symposium*, San Diego, California, April 24-27, 1995.

Munz, C., and P.V. Roberts, Gas-liquid phase mass transfer resistances of organic compounds during mechanical aeration, *Water Research*, vol. 23(5), pp. 589-601, 1989.

Nadim, F., A. Nadim, G.E. Hoag, and A.M. Dahmani, Desorption rate limitation in the extraction of organic molecules from unsaturated soils during soil venting operations, *Journal of Contaminant Hydrology*, vol. 25, pp. 21-37, 1997.

O'Connor, D.L., and W.E. Dobbins, The mechanism of reaeration in natural streams. *J. Sanit. Engrg.* Div., ASCE, vol. 82(6), Paper No. 215, 1956.

Ong, S.K., and L.W. Lion, Effects of soil properties and moisture on the sorption of TCE vapor, *Water Research*, vol. 25(1), pp. 29-36, 1991.

Ostendorf, D.W., E.E. Moyer, and E.S. Hinlein, Petroleum hydrocarbon sparging from intact core sleeve samples, in *Proc. of the 1993 Conference on Petroleum Hydrocarbons and Organic Chemicals in Groundwater: Prevention, Detection and Restoration*, NWWA, Houston, Texas, pp. 415-427, 1993.

Pavlostathis, S.G., and G.M. Mathavan, Desorption kinetics of selected organic compounds from field contaminated soils, *Environ. Sci. and Tech.*, vol. 26(3), pp. 532-538, 1992.

Perry, R. H. and C. H. Chilton, *Chemical Engineer's Handbook*, 5th Edition, pp. 3.231-3.234, McGraw-Hill, NY, NY, 1978.

Piwoni, M.D., and P. Banerjee, Sorption of volatile organic solvents from aqueous solution onto subsurface solids, *Journal of Contaminant Hydrology*, vol. 4, pp. 169-173, 1989.

Powers, S.E., L.M. Abriola, and W.J. Weber Jr., An experimental investigation of nonaqueous phase liquid dissolution in saturated subsurface systems: steady state mass transfer rates, *Water Resources Research*, vol. 28(10), pp. 2691-2705, 1992.

Powers, S.E., L.M. Abriola, and W.J. Weber Jr., An experimental investigation of nonaqueous phase liquid dissolution in saturated subsurface systems: transient mass transfer rates, *Water Resources Research*, vol. 30(2), pp. 321-332, 1994.

Plummer, C. R., J.D. Nelson, and G.S. Zumwalt, Horizontal and vertical well comparison for in situ air sparging, *GWMR*, vol. 17(1), pp. 91-96, 1997.

Raymond, R.L, *Reclamation of Hydrocarbon Contaminated Waters*, U.S. Patent Office 3,846,290, 1974.

Reddy, K.R., S. Kosgi, and J. Zhou, A review of in-situ sparging for the remediation of VOC-contaminated saturated soils and groundwater, *Hazardous Wastes & Hazardous Materials*, vol. 12(2), pp. 97-117, 1995.

Rodriguez-Maroto, J.M., C. Gomez-Lahoz, and D.J. Wilson, Soil cleanup by in-situ aeration. XVIII. Field-scale models with diffusion from clay structures, *Separation Science and Technology*, vol. 29(11), pp. 1367-1399, 1994.

Sellers, K., and R. Schreiber, Air sparging model for predicting groundwater cleanup rate, in *Proc. of the 1992 Conference on Petroleum Hydrocarbons and Organic Chemicals in Groundwater: Prevention, Detection and Restoration*, NWWA, Houston, Texas, pp. 365-376, 1992.

Sleep, B.E., and J.F. Sykes, Modeling the transport of volatile organics in variable saturated media, *Water Resources Research*, vol. 25(1), pp. 81-92, 1989.

Sleep, B.E., and J.F. Sykes, Compositional simulation of groundwater contamination by organic compounds. 1. Model development and verification, *Water Resources Research*, vol. 29(6), pp. 1697-1708, 1993a.

Sleep, B.E., and J.F. Sykes, Compositional simulation of groundwater contamination by organic compounds. 2. Model applications, *Water Resources Research*, vol. 29(6), pp. 1709-1718, 1993b.

Suthersan, S.S., *Remediation Engineering: Design Concepts*, pp. 91-121, CRC Press, Inc., Boca Raton, FL, 1997.

Szatkowski, A., P.T. Imhoff, and C.T. Miller, Development of a correlation for aqueous-vapor phase mass transfer in porous media, *Journal of Contaminant Hydrology*, vol. 18, pp. 85-106, 1995.

Theofanous, T.G., R.N. Houze, and L.K. Brumfield, Turbulent mass transfer at free, gas-liquid interface, with applications to open-channel, bubble and jet flows, *Int. J. of Heat and Mass Transfer*, vol. 19, pp. 613-624, 1976.

Treybal, R.E., *Mass Transfer Operations*, pp. 29-31. McGraw-Hill Kogakusha Ltd., 2nd Edition, Tokyo, Japan, 1968.

Turek, F., and R. Lange, Mass transfer in trickle-bed reactors at low Reynolds number. *Chem. Eng.*, vol. 36, pp. 569-579, 1981.

U.S. EPA, *Underground storage tanks: technical requirements*, Federal Register 53:37082, Sept. 23, 1988.

Weber, W.J. Jr., P.M. McGinley, and L.E. Katz. Sorption phenomena in subsurface systems: concepts, models and effects on contaminant fate and transport, *Water Research*, vol. 25(5), pp. 499-528, 1991.

Wilkins, M.D., L.M. Abriola, and K.D. Pennel, An experimental investigation of rate-limited nonaqueous phase liquid volatilization in unsaturated porous media: steady state mass transfer, *Water Resources Research*, vol. 31(9), pp. 2159-2172, 1995.

CHAPTER THREE. AIR SPARGING EFFECTIVENESS: THE AIR CHANNEL MASS TRANSFER ZONE

A paper submitted to Water Resources Research

Washington J. Braida and Say Kee Ong

Abstract

Air sparging is one of the many innovative technologies being developed for the remediation of contaminated groundwater. Using a single air channel apparatus, mass transfer of VOC were found to occur within a thin layer of saturated porous media next to the air channel. In this zone, the VOCs were found to rapidly deplete during air sparging resulting in a steep concentration gradient while the VOC concentration outside the zone remained fairly constant. The size of this mass transfer zone was between 17 mm and 41 mm or 70 dp_{50} and 215 dp_{50} (dp_{50} = mean particle size). The size of the mass transfer zone was found to be proportional to the aqueous diffusivity of the VOC, the mean particle size, and the uniformity coefficient. A general correlation predicting the size of the mass transfer zone was developed. The correlation incorporated the properties of the porous media, the air phase Peclet number, and the Pore Diffusion Modulus. The model was developed using data from eight different VOCs. The tailing effect of the air phase concentration and the rebound in the VOC concentration after the sparging system is turned off are some of the consequences of the existence of this mass transfer zone.

Introduction

The U.S. Environmental Protection Agency (EPA) has estimated that about 25% of the two million underground storage tank (UST) systems located at 700,000 facilities may be leaking (U.S. EPA, 1988). The release of volatile organic compounds (VOCs) from UST systems has a significant environmental impact on groundwater resources and may pose a risk to human health. VOCs commonly found in contaminated aquifers include aromatic

hydrocarbons such as benzene and xylenes, and chlorinated hydrocarbons such as trichloroethylene.

A remedial approach for VOC-contaminated aquifer is the in situ air sparging technology. Air sparging involves the injection of contaminant-free air below the water table. The air flow through the aquifer results in the volatilization of VOCs from the aqueous phase. At the same time, oxygen is transferred from air to the contaminated groundwater which in turn may promote the biodegradation of VOCs (Brown et al., 1994). Contaminated air is then removed by an extraction well in the unsaturated zone.

Even though air sparging has been successfully applied at several contaminated sites, Johnson et al. (1993) pointed out that the mechanism of air flow in saturated porous media and the physical-chemical processes involved during air sparging operations are not well understood. The injection of air into the aquifer creates complex transient physical-chemical conditions within the subsurface environment. The exact nature of air flow in a saturated porous media is not completely understood and research work in this area is fairly limited. In an air flow visualization study using glass beads as a porous media, Ji et al. (1993) found that in medium to fine grained water saturated porous media, air flows in discrete pore-scale channels. With a vertical air sparging well, the network of air channels formed may be visualized as the roots of a tree (Drucker and Di Julio, 1996). Based on this pattern of air channels network, many remedial engineers/scientists have used the radius of influence (ROI) of the sparging well in the design of air sparging systems despite the lack of agreement among researchers and engineers on the definition and field estimation of the ROI (McCray and Falta, 1997). Even if the ROI is an important design parameter, the ROI basically provides a macroscopic estimate of the volume of the aquifer impacted by the well. However, the contaminated water impacted by the air channels is that which are nearest to the air-water interface. Volatilization of VOCs at the air-water interface will result in a VOC concentration gradient in the aqueous phase causing VOCs in the bulk water to diffuse to the interface (see Figure 1). If the rate of transport by liquid diffusion is slower than the volatilization rate of the VOCs at the interface a situation would arise in which the actual volume of the contaminated aquifer impacted by the sparging well would be less than the

total volume defined by the ROI. Therefore, within the volume as defined by the ROI, it is probable that a portion of this volume would be directly impacted by the air channels while a portion of the volume would not be impacted by the air channels.

Ji (1994) proposed in a theoretical study that volatilization occurred by the diffusion of VOCs through saturated porous media to a cylindrical air channel. In his modeling efforts, he showed that a steep aqueous concentration profile was formed close to the air-water interface. To model mass transfer of VOCs during air sparging, Hein et al. (1994) proposed an arbitrarily defined cylindrical boundary away from the air channel where the VOC aqueous concentration remained constant. Based on this selected boundary condition, Hein and coworkers showed that the air flow rate and the aqueous diffusion rate were the main parameters controlling VOC volatilization. To model air sparging in soil columns, Drucker and Di Julio (1996) assumed that the air channels in the soil column can be represented by a composite of evenly spaced cylindrical air channels. Each of the air channels was surrounded by a nonadvective aqueous region. Sensitivity analysis of the proposed model showed that the time needed to achieve 90% removal of the initial mass of VOC was inversely proportional to the diameter of the air channels but was directly proportional to the aqueous diffusivity of the VOCs. Using a one-dimensional model and results from soil column experiments, Chao (1997) estimated that the volume impacted by the air channels (called the "mass transfer zone") was as low as 15% to as much as 40% of the total air sparged volume depending on the air flow rate and porous media used.

The work of the researchers cited above showed that aqueous diffusion is an important controlling mechanism during air sparging and the differences in the volatilization of various VOCs may be due to the distinctive "mass transfer zone" which may be a limiting factor for the proper operation of air sparging systems. If the size of the mass transfer zone is small compared to the distance between two air channels, remediation times will increase dramatically due to diffusion transport limitations.

The objective of this work was to experimentally confirm, for dissolved contaminant plumes, the existence of a mass transfer zone surrounding the air channels and to study the influence of air sparging conditions and the physical-chemical properties of VOCs and

porous media on the size of the mass transfer zone. Experiments were conducted using a single air-channel experimental setup. An estimate of the size of the air channel mass transfer zone will provide further insights into the physical-chemical phenomena controlling the VOCs volatilization during air sparging.

Materials and Methods

To investigate and quantify the mass transfer zone associated with air channels during air sparging, an experimental apparatus as shown in Figure 2 was built. The experimental setup consisted of an air channel of approximately 1.58 mm above the saturated porous media. The size of the air channel was within the range of the sizes of air channels observed by others (Ji, 1994). The single-air channel apparatus removed some of the complexities associated with using a typical air sparging system such as a soil column and may be used to assess the major mass transfer processes limiting the volatilization of VOCs under controlled conditions. The apparatus was made of thick acrylic sheets with dimensions 17.5 cm long, 5 cm wide, and 11 cm depth. The apparatus was covered with a flat acrylic piece which provided a gap of approximately 1.58 mm (1/16") for the circulation of humidified air.

In-house compressed air was used as the air source. The air was filtered to remove particulates and oil droplets, and humidified before being introduced into the experimental apparatus. Air flow was measured with a Gilmont model 11 flowmeter (Barrington, IL). Fifteen sample points as shown in Figure 2 were included to allow water samples to be collected throughout the porous media profile. A sample point to measure the VOC concentration in the effluent gas was included. Since the air flow rates under air sparging conditions are much higher than the water flow rate in an aquifer, stagnant water conditions were used for the experimental runs. The experimental runs were conducted at room temperature ($21^{\circ}C \pm 2^{\circ}C$).

Three different types of sand, graded Ottawa sand, sand 30/50, and sand 70/100 from U.S. Silica Company (Ottawa, IL), were used in the study. The properties of the porous media are summarized in Table 1. Specific surface areas were measured using the ethylene glycol monoethyl ether (EGME) procedure (Chihacek and Bremmer, 1979) and organic carbon

content was determined using the Walkley-Black procedure (Nelson and Sommers, 1982). Eleven VOCs with saturated solubilities ranging from 30 mg/L to 1800 mg/L and Henry's law constants ranging from 0.07 to 0.37 were studied. A summary of the physical-chemical properties of the VOCs is shown in Table 2. The aqueous solutions of various VOC concentrations were prepared from HPLC grade chemicals purchased from Sigma-Aldrich Chemical Company, Inc. (Milwaukee, WI). Concentrations of the VOCs used in the experiments ranged from 8 mg/L to 150 mg/L. A slurry was made by carefully mixing the porous media with the aqueous solution of the VOCs. The reactor was then packed layer by layer with the slurry to avoid entrapment of air bubbles and immediately sealed to minimize loss of VOCs. For each type of porous medium, four different air velocities: 0.2, 0.5, 1.1, and 2.5 cm/s were used. Values of the velocity of air in the air channels during air sparging operations have not been reported in the literature. The measurement of this value requires the knowledge of the injected air flow, the *ROI*, and the air saturation. The last two values are very difficult to determine in the field and may be the reason of the lack of information about air velocities in field applications. The range of air velocities selected for this study is consistent with typical field vapor extraction rates in which air pore velocities are generally expected to be less than 2 cm/s (Baehr et al., 1989)

The VOC concentration in the air phase and in the liquid phase were measured with a Hewlett-Packard 5890 Series II gas chromatograph (Avondale, PA) equipped with a HP-5 capillary column and a flame ionization detector. Air phase concentration was determined by direct injection of 1 ml sample while liquid phase concentration was measured using the head-space technique. For the head space technique, 25 µl of an aqueous sample was placed in a 1.8 ml aluminum crimp cap vial and the aqueous concentration was estimated from the measured head space concentration after equilibrium was reached.

Results and Discussion

Mass Transfer Zone

A typical set of results showing the change in the VOC concentrations in the exhaust air over time is presented in Figure 3. The corresponding changes in the aqueous concentrations

for various distances away from the air-water interface are shown in Figures 4 and 5. The results presented are for the center row of sampling points on the experimental setup. The air velocity for Figures 3, 4, and 5 was 2.5 cm/s. The change in the concentration of VOCs in the exhaust air, presented in Figure 3, typically represents the behavior of the effluent air concentration for field-scale air sparging systems with an initial rapid decrease in the VOC concentration followed by a slower change in the VOC concentration and a finally with the VOC concentration remaining fairly constant. The asymptotic VOC concentration in the exhaust air was reached between 2 and 3 hours after the start of the sparging, implying that a quasi-steady condition for the volatilization of the VOCs was reached for all the experimental runs. Discussion on the relative volatility of each individual VOC will not be presented since our main focus is on the existence of the mass transfer zone and the effects of physical-chemical properties of the soil and VOC on the mass transfer zone.

Measurement of aqueous VOC concentrations indicated that there was a concentration gradient at the start of the experiments as a result of losses of VOCs during the packing of the reactor (Figure 4 and 5). Separate experiments indicated that when the apparatus was left alone for 18 hours, VOC losses, other than losses due by the initial packing, were less than 2%. Experimental data showed that during air sparging the VOC aqueous concentration was rapidly depleted within a thin layer of porous media next to the air channel. The rapid depletion is the result of a faster volatilization of VOCs at the air-water interface than the diffusive transport of the VOCs to the air-water interface (Figures 4 and 5). After 4 hours of sparging the concentration gradient for each VOC became fairly constant suggesting that a quasi-steady state condition for the diffusion of the VOC through the porous media was reached. After quasi-steady state conditions were reached, a distinctive zone with a steep concentration gradient was found in the porous media. In all experiments, the 8-hour concentration profiles of the aqueous phase corresponded to the fairly constant VOC concentration in the air phase. Therefore, the aqueous concentration profiles strongly suggest that the volatilization of VOCs during air sparging may be controlled by the aqueous diffusion of VOCs through the porous media to the air channels. The aqueous concentration

profile showed that the air channels have a mass transfer zone beyond which the effects of the air flow were strongly reduced.

The size of the mass transfer zone appeared to be somewhat dependent on the type of VOC (see Figures 4 and 5), and the porous media (Figure 6) but marginally dependent on the air velocity (Figure 7). For convenience, the size of the mass transfer zone was assumed to be the distance from the air-water interface to where the VOC concentration was 90% of the bulk VOC concentration. The size of the zone for the various experimental conditions was estimated to be between 17 mm and 41 mm. For the experiments using Ottawa sand, which has the largest uniformity coefficient, the size of the mass transfer zone was between 22 mm (115 dp_{50}) and 40 mm (210 dp_{50}) depending on the contaminant and the air flow rate. For sand 30/50, with an average grain size of 0.305 mm and an uniformity coefficient of 1.41, the size of the mass transfer zone ranged between 22 mm (70 dp_{50}) and 41 mm (130 dp_{50}). For sand 70/100, the size of the mass transfer zone was between 17 mm (100 dp_{50}) to 36 mm (215 dp_{50}). Unfortunately, examination of these values cannot directly show the influence of the mean particle size and uniformity coefficient of the porous media on the size of the mass transfer zone. Other parameters which may have a potential influence on the size of the mass transfer zone included the aqueous and air diffusivities of the VOCs, the porosity of the porous media, and the Henry's law constant of the VOCs. A tool which may be used to assess the influence of the various physical-chemical factors on the size of the mass transfer zone is the dimensionless number modeling approach.

Model Correlation of Mass Transfer Zone

To characterize the influence of different physical-chemical parameters on the size of the mass transfer zone, a regression analysis of various dimensionless numbers which incorporated the size of the mass transfer zone and the various physical-chemical parameters of the VOCs and the porous media was conducted. The regression analysis had two objectives: (a) to determine which parameters most strongly affect the size of the air channel mass transfer zone, and (b) to generate a model which may predict the size of the mass transfer zone for different conditions.

The dimensionless numbers used in the regression analysis are presented in Table 3 and they were selected because they included most of physical-chemical parameters which potentially have an effect on the size of the mass transfer zone. The dimensionless numbers to be modeled included the air phase Peclet number (*Pe*), which is the ratio of the rate of transport by advection and the rate of transport by diffusion in the air phase, the Pore Diffusion Modulus (*Ed*), which is the ratio between the mass transport by radial diffusion in the aqueous phase and the mass transport by advection in the gas phase, and the Henry's law constant (K_H). The *Pe* numbers used in the determination of this correlation ranged from 0.052 to 1.523. The width of the mass transfer zone (*MTZ*) was included in the Pore Diffusion Modulus (*Ed*). Properties of the porous media used in the dimensionless analysis included the porosity (ε), the uniformity coefficient (*UC*), and the dimensionless average particle size $d_o = dp_{50}/d_m$ as used by Wilkins et al. (1995). The term d_m is the mean grain size of a "medium" sand as defined by the USDA and is equal to 0.05 cm (Driscoll, 1986).

A multiple, stepwise regression analysis was conducted to determine the best fit for *Ed* with the other dimensionless numbers using a log linearized correlation as shown below. The regression analysis was conducted for 8 of the 10 VOCs. The 1,2 dichlorobenzene and 1,2,4 trichlorobenzene were reserved for verification.

$$log(Ed) = \beta_o + \beta_1 log(Pe) + \beta_2 log(UC) + \beta_3 log(\varepsilon) + \beta_4 log(K_H) + \beta_5 log(d_o) \qquad (1)$$

The stepwise regression procedure evaluated the least square residual (r^2) and the F statistical parameter of each predictor to determine the most appropriate model parameters. The regression analysis was performed using the statistical software SAS 6.10 (SAS Institute Inc., 1993). The variables in the model which were found to be significant at the F = 0.15 level are presented in equation (2).

$$Ed = 10^{-7.70}\, Pe^{-1.10}\, UC^{-1.74}\, d_0^{0.65} \qquad r^2 = 0.9032 \qquad (2)$$

Both the porosity of the media and the Henry's law constant for the VOCs were not selected to be included in the empirical model. A summary of the stepwise analysis is shown in Table 4. The Peclet number (*Pe*) explained most of the variation of the Pore Diffusion Modulus (*Ed*) followed by the uniformity coefficient (*UC*) and the dimensionless mean particle size (d_o). The lack of correlation of the Henry's law constant with the *Ed* ($F < 0.15$) in the empirical model seemed to suggest that the size of the *MTZ* does not depend of the volatility of the VOC and this strongly implies that air sparging is a diffusion controlled process.

The experimental and predicted Pore Diffusion Modulus are plotted as shown in Figure 8 along with the 95% confidence intervals. To test the validity of the model, the correlation (equation 2) was used to predict the *Ed* values of 1,2 dichlorobenzene and 1,2,4 trichlorobenzene which were not included in the regression analysis. Results of the predicted values are shown in Figure 9. Despite the differences in solubility and Henry's law constant values especially for 1,2,4 trichlorobenzene, the correlation was found to predict the size of the mass transfer zone for these two organic compounds.

A direct comparison of the effects of the physical-chemical parameters of the system on the size of the mass transfer zone can be made by expressing equation (2) in terms of each individual physical-chemical property:

$$MTZ = 10^{3.43} \frac{D_w^{0.5} dp_{50}^{0.72} UC^{0.87} v_{air}^{0.05}}{D_a^{0.55}} \qquad (3)$$

Examination of equation (3) revealed that the size of the mass transfer zone was directly proportional to the square root of the aqueous diffusivity of the VOC but was inversely related with the air diffusivity of the VOC. The mean particle size and the uniformity coefficient of the porous media have a direct impact on the size of the mass transfer zone. Intuitively, equation (3) is correct since the size of the mass transfer zone will be affected by the aqueous phase diffusivity, the size of the particle present, and how well distributed was the porous media. The velocity of the sparged air was included in the Pore Diffusion

Modulus and in the air phase Peclet number but its influence on the size of the mass transfer zone was marginal as indicated by the low value of its exponent. A one order of magnitude change in the air velocity (0.2 to 2.5 cm/s) for the experiments conducted resulted in only a 14% change of the size of the mass transfer zone.

The existence of a mass transfer zone surrounding the air channels during air sparging operations implies that VOC removal by volatilization during air sparging is a diffusion limited process. An important observation which can be drawn from this study is that if the distance between two air channels is larger than twice the size of the mass transfer zone then portions of the aquifer within the ROI would not be affected by the air flow, i.e. portions of the air sparged volume would not be remediated. This conclusion is in agreement with the results reported by Ahlfeld et al. (1994). These authors, using a simple diffusion model, showed that decreasing the average channel spacing from 480 to 20 mm resulted in a three order of magnitude reduction in the cleanup time. The existence of this mass transfer zone explains the long tailing effect in the VOC concentration in the gas phase typically seen after the aquifer is sparged for sometime and the rebound in aqueous VOC concentration after the sparging system is turned off. In addition, work done by Bass and Brown (1997) indicated that even when the VOCs were shown to be removed in the gas stream, measurements of VOC concentrations in the soil core seemed to be statistically unchanged. By quantifying and assessing the various physical-chemical parameters affecting the size of the mass transfer zone along with an understanding of distribution of air channels in the aquifer, more accurate air sparging models may be developed to predict the performance of air sparging systems under various operation conditions.

Conclusions

A mass transfer zone was shown to be associated with air channels during air sparging operations. In the mass transfer zone, a steep VOC concentration gradient was found to form after several hours of air sparging. The size of this zone ranged between 17 mm and 41 mm or between 70 and 215 dp_{50}. The presence of the mass transfer zone strongly suggests that the volatilization of VOCs by air sparging is a diffusion limited process.

An empirical model using the Pore Diffusion Modulus (*Ed*) which included the size of the mass transfer zone was found to correlate well with the air phase Peclet number (*Pe*), the uniformity coefficient (*UC*), and the dimensionless mean particle size (d_o). Based on the correlation, the size of the mass transfer zone was found to be proportional to the aqueous diffusivity of the VOC, the uniformity coefficient, and the mean particle size of the porous media. Air velocity had a marginal effect on the size of the mass transfer zone under the experimental conditions tested.

The existence of the mass transfer zone under air sparging conditions implies that for remediation to be successful, the air channels during air sparging must be as close as possible with the mass transfer zones of the two adjacent air channels overlapping each other. In other words, the larger the mass transfer zone, the higher are the chances that air sparging will be effective. For small mass transfer zones associated for example with tight aquifer materials, a larger volume of contaminated soil within the radius of influence of the well will remain unaffected by the air flow and remediation will take a longer time.

Notation

C_{air} C_{water}	VOC concentration in the air and aqueous phases, ML^{-3}
D_w	VOC aqueous diffusivity, L^2T^{-1}
D_a	VOC air diffusivity, L^2T^{-1}
d_o	dimensionless mean particle size
dp_{50}	mean particle size, L
Ed	Pore Diffusion Modulus, dimensionless
ε	porous media porosity, dimensionless
K_H	Henry's law constant, dimensionless
K_{ow}	octanol-water partition coefficient, dimensionless
MTZ	width of the mass transfer zone, L
Pe	air phase Peclet number, dimensionless
UC	uniformity coefficient, dimensionless
v_{air}	air velocity (air flow rate/air channel cross sectional area), LT^{-1}

Acknowledgments

The authors would like to thank Juan Jose Goyeneche for his technical assistance in the statistical analysis of the data.

References

Ahfeld, D., A. Dahamani, and W. Ji, A conceptual model for field behavior of air sparging and its implications for application, *GWMR*, vol 14(4), pp. 132-139, 1994.

Baehr, A.L., G.E. Hoag, and C. Marley, Removing volatile contaminants from the unsaturated zone by inducing advective air phase transport, *Journal of Contaminant Hydrology.*, vol. 4, pp. 1-26, 1989.

Bass, H.D., and R.A. Brown, Performance of air sparging systems a review of case studies, in *In Situ and On-Site Bioremediation: Volume 1*, edited by B. C. Alleman and A. Leeson, pp. 117-122, Battelle Press, Columbus, OH, 1997.

Brown, R.A., R.J. Hicks, and P.M. Hicks, Use of air sparging for in situ bioremediation, in *Air Sparging for Site Remediation*, edited by R.E. Hinchee, pp. 38-55, Lewis Publishers, Boca Raton, FL, 1994.

Chao K.P., Aqueous-vapor mass transfer of VOCs in saturated porous media under air sparging conditions, Ph.D. Dissertation, 176 pp., Polytechnic University, Brooklyn, NY, 1997.

Chihacek L.J., and J.M. Bremmer, A simplified ethylene glycol monoethyl ether procedure for assessment of soil surface area, *Soil Sci. Soc. Am. J.*, vol. 43, pp. 821-822, 1979.

Driscoll, F.G., *Groundwater and Wells*, 2nd Edition, Johnson Filtration Systems, St. Paul, Minn., 1986.

Drucker A.S., and S.S. Di Julio, Groundwater clean up by *In Situ* air sparging: development of a model and application to saturated soil column experiments, in *Proceedings of the Water Environmental Federation 69 Th. Annual Conference & Exposition*, Dallas, TX, October 5-9, 1996.

Hein, G.L., N.J. Hutzler, and J.S. Gierke, Quantification of the mechanisms controlling the removal rate of volatile contaminants by air sparging, in *Proc. of the 1994 National conference on Environmental Engineering*, edited by J.N. Ryan and M. Edwards, pp. 556-563, ASCE, NY, NY, 1994.

Ji, W., A. Dahamani, D.P. Ahlfeld, J. D. Lin, and E. Hill, Laboratory study of air sparging: Air flow visualization, *GWMR*, vol. 13(4), pp. 115-126, 1993.

Ji, W., Air sparging: Experimental and theoretical analysis of flow and numerical modeling of mass transfer, Ph.D. Dissertation, 154 pp., The University of Connecticut, Storrs, CT, 1994.

Johnson, R.L., P.C. Johnson, D.B. McWorther, R.E. Hinchee, and I. Goodman, An overview of in situ air sparging, *GWMR*, vol. 13(4), pp. 127-135, 1993.

Lyman, W.J., W.F. Reehl, and D.H. Rosemblatt, *Handbook of Chemical Properties Estimation Methods*, American Chemical Society, Washington D.C., 1990.

McCray, J.E. and R.W. Falta. Numerical simulation of air sparging for remediation of NAPL contamination, *Ground Water*, vol. 35(1), pp. 99-110, 1997.

Nelson, D.W., and L.E. Sommers, Total carbon, organic carbon, and organic matter, in *Methods of Soil Analysis, Part 2, Chemical and Microbiological Properties*, Second Edition, edited by A.L. Page, pp. 570-571, American Society of Agronomy, Inc., Soil Science Society of America, Inc., Madison, WI, 1982.

Perry, R.H. and C.H. Chilton, *Chemical Engineer's Handbook*, 5th Edition, pp. 3-231-3.234, McGraw-Hill, NY, NY, 1978.

Treybal, R.E., *Mass Transfer Operations*, 2nd Edition, pp. 29-31, McGraw-Hill Kogakusha Ltd., Tokyo, Japan, 1968.

SAS Institute Inc., *SAS® Software: Changes and Enhancements. Release 6.10*, Carey, NC, 1993.

U.S. EPA, *Underground storage tanks: technical requirements*, Federal Register 53:37082, Sept., 1988.

Wilkins, M.D., L.M. Abriola, and K.D. Pennel, An experimental investigation of rate-limited nonaqueous volatilization in unsaturated porous media: steady state mass transfer, *Water Resources Research*, vol. 31(9), pp. 2159-2172, 1995.

Table 1. Physical-chemical properties of porous media

Type of Sand	Mean Particle Size (cm)	Uniformity Coefficient	Specific Surface Area (m^2/g)	Porosity	Organic Carbon (%)
Ottawa Sand	0.0190	2.16	1.99	0.377	0.0066
Sand 30/50	0.0305	1.41	1.17	0.370	0.0062
Sand 70/100	0.0168	1.64	2.73	0.400	0.0063

Table 2. Physical-chemical properties of VOCs at 20°C (Lyman et al., 1990)

compound	Molecular Weight	K_H	Solubility (mg/l)	D_a (cm^2/s) *	$D_w \times 10^6$ (cm^2/s) **	log K_{ow}
Benzene	78.12	0.195	1780	0.0923	9.59	2.12
Toluene	92.15	0.233	515	0.0830	8.46	2.73
Ethylbenzene	106.18	0.291	152	0.0732	7.63	3.15
o-Xylene	106.18	0.178	130	0.0759	7.63	2.95
m-Xylene	106.18	0.247	175	0.0759	7.63	1.38
p-Xylene	106.18	0.256	198	0.0759	7.63	3.26
Chlorobenzene	112.56	0.137	500	0.0725	8.52	2.84
n Propylbenzene	120.21	0.369	60	0.0544	6.99	3.87
1,2 Dichlorobenzene	147.00	0.118	145+	0.0829	7.97	3.60
1,2,4 Trichlorobenzene	181.44	0.069	30+	0.0686	7.09	4.30
Styrene	104.16	0.0967	300	0.0746	7.89	2.95

* Estimated from Hirschfelder, Bird, and Spotz

** Estimated from Wilke and Chang correlation (Treybal,1968)

\+ at 25°C

Table 3. Dimensionless numbers used for modeling

Dimensionless Number	Equation	Comments
Pore Diffusion Modulus (Ed)	$\frac{D_w dp_{50}}{v_{air}(MTZ)^2}$	Mass transport by radial aqueous diffusion / Mass transport by gas advection
Air Phase Peclet Number (Pe)	$\frac{v_{air} dp_{50}}{D_a}$	Rate of transport by gas advection / Rate of transport by molecular gas diffusion
Dimensionless Mean Grain Size (d_o)	$\frac{dp_{50}}{d_m}$	d_m= 0.05 cm is the mean grain size of a "medium" size sand
Porosity (ε)	$\frac{V_{Total} - V_{solid}}{V_{Total}}$	Void volume/total volume
Henry's Law Constant K_H	$\frac{C_{air}}{C_{water}}$	Ratio of air phase concentration to aqueous phase concentration
Uniformity Coefficient (UC)	$\frac{d_{60}}{d_{10}}$	Measured of the grain size distribution

Table 4. Summary of stepwise regression analysis

Variable	Parameter Estimate	Standard Error	Partial r^2	Model r^2
Intercept	-7.6972	0.0572		
Pe	-1.1014	0.0388	0.7526	0.7526
UC	-1.7335	0.2573	0.1396	0.8895
d_o	0.6549	0.1814	0.0137	0.9032

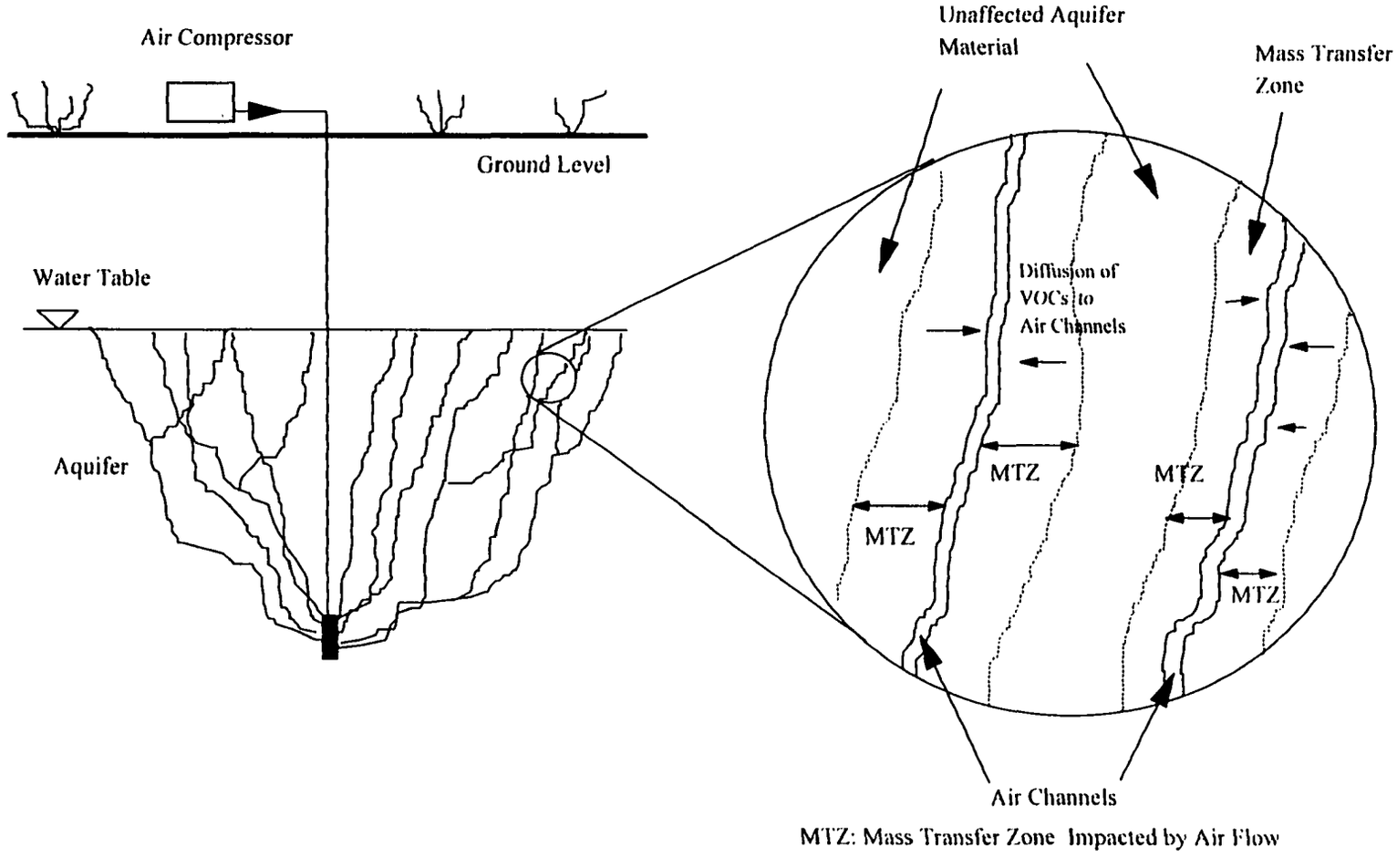

Figure 1. Conceptual sketch of air channels and mass transfer zone

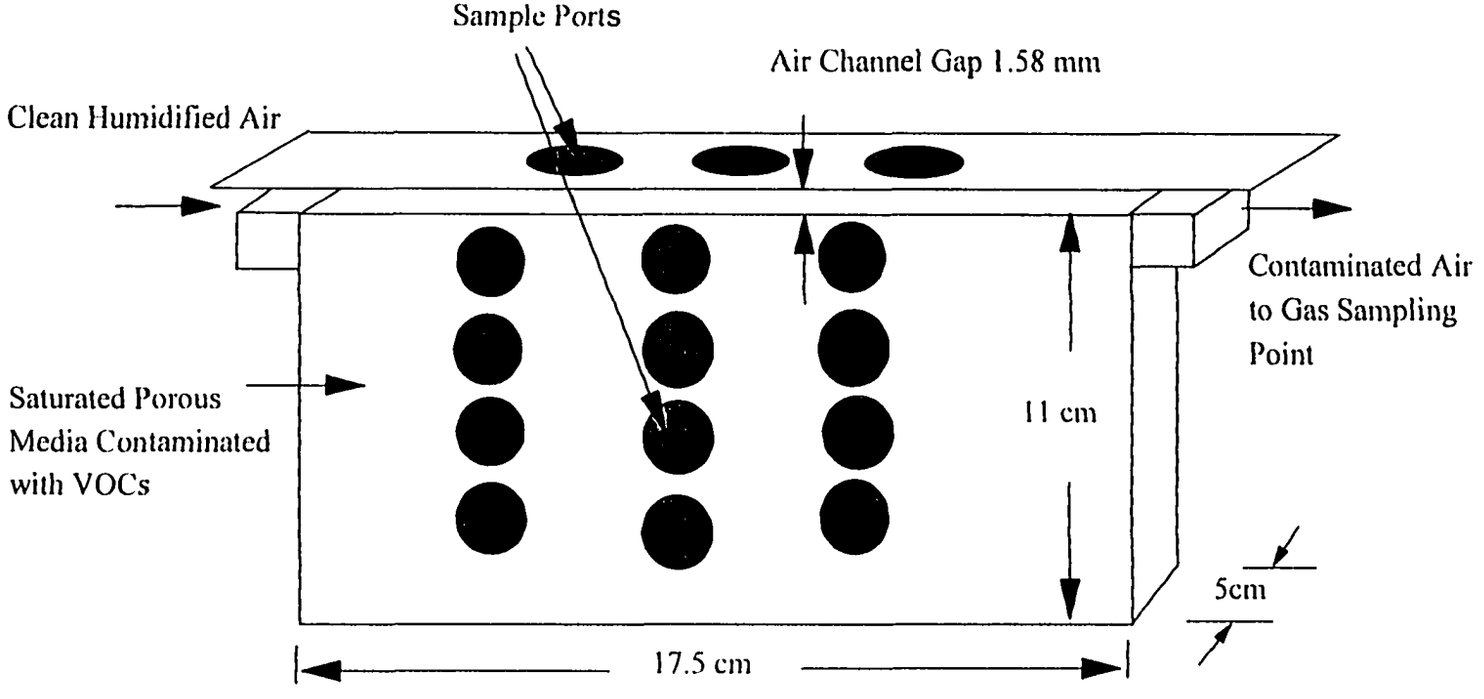

Figure 2. Single-air channel apparatus

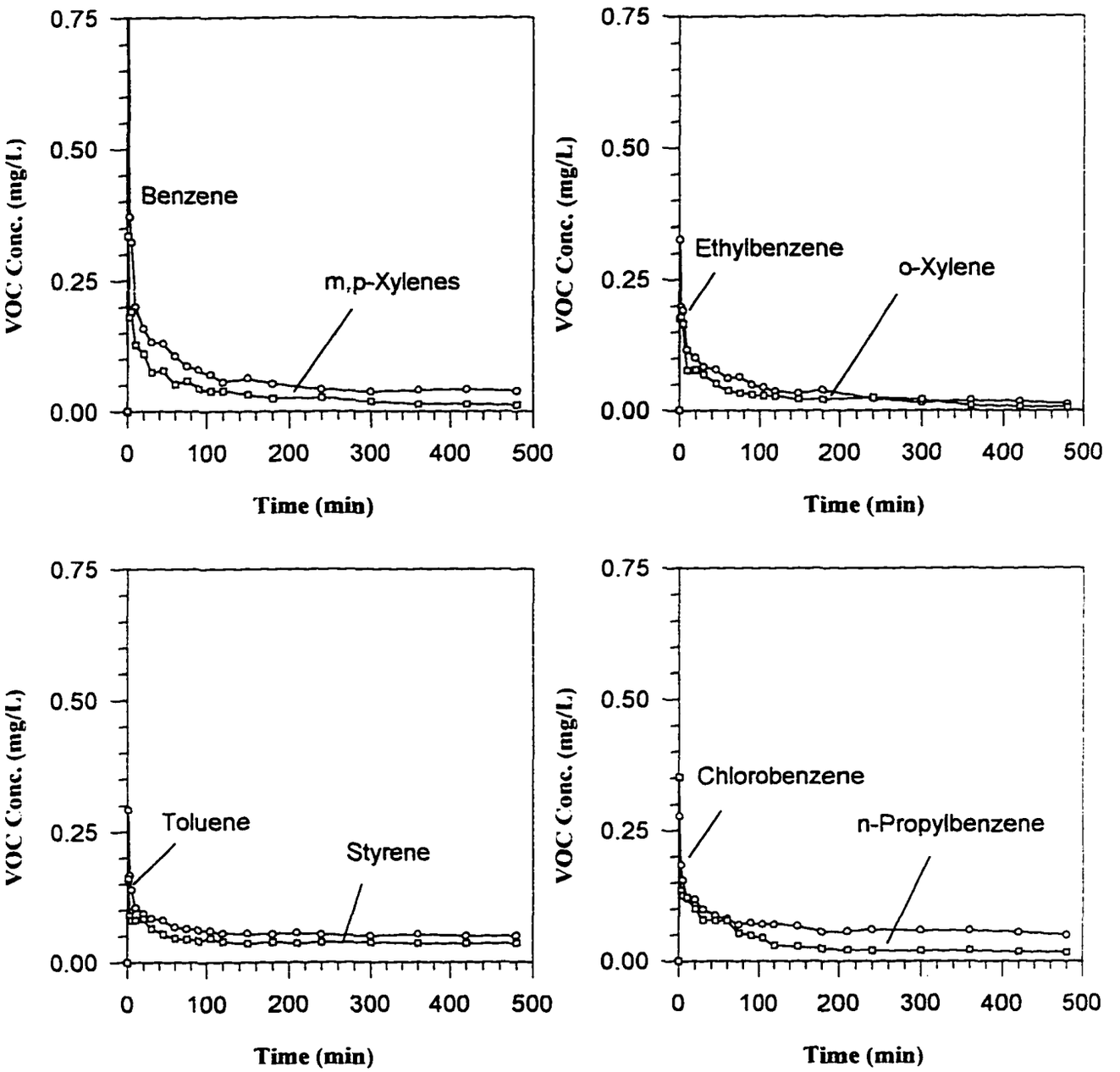

Figure 3. VOC concentrations in the air phase for Ottawa sand at an air flow rate of 2.5 cm/s

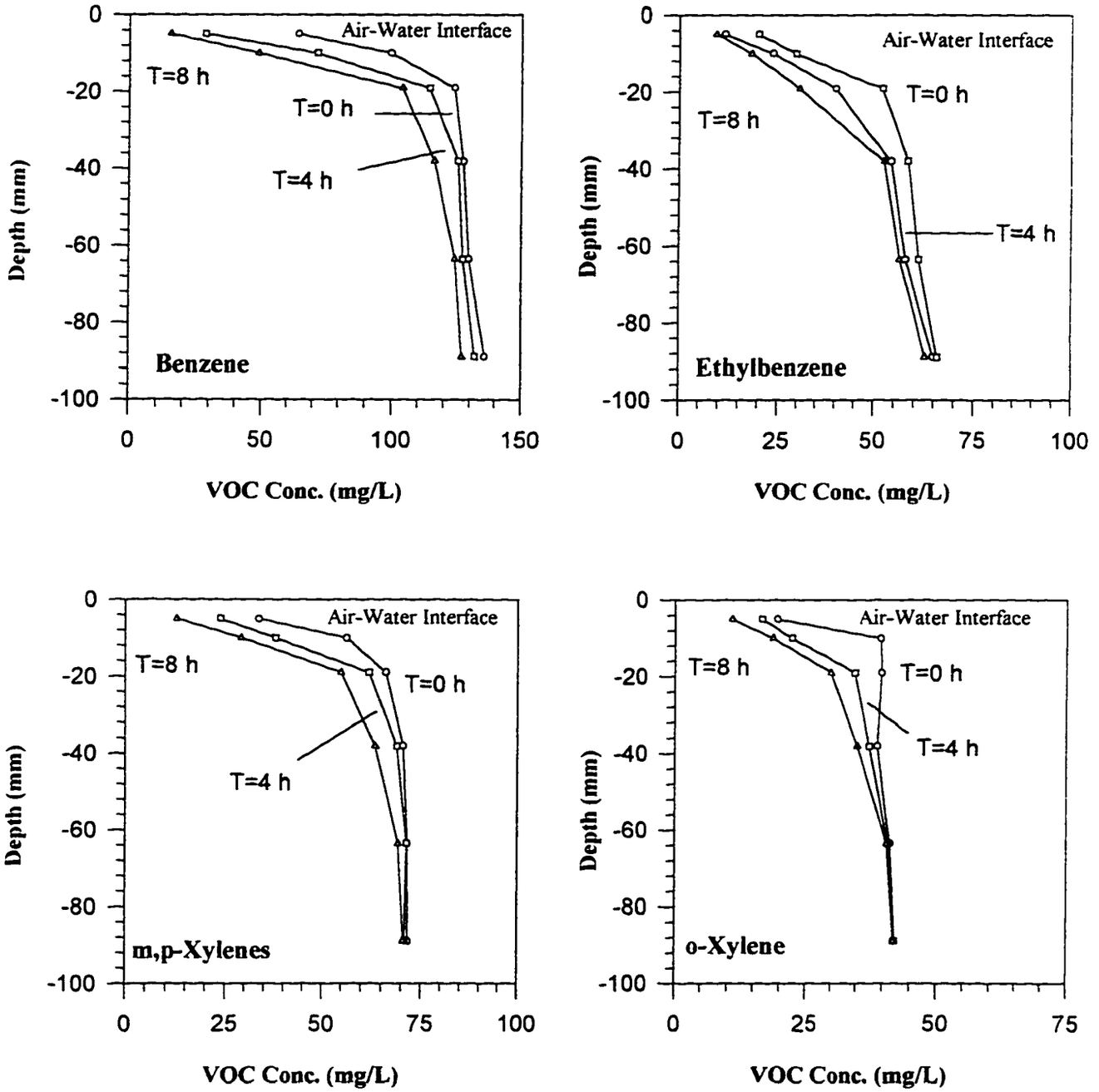

Figure 4. VOC concentration profiles for various times during air sparging (Ottawa sand, air flow rate 2.5 cm/s)

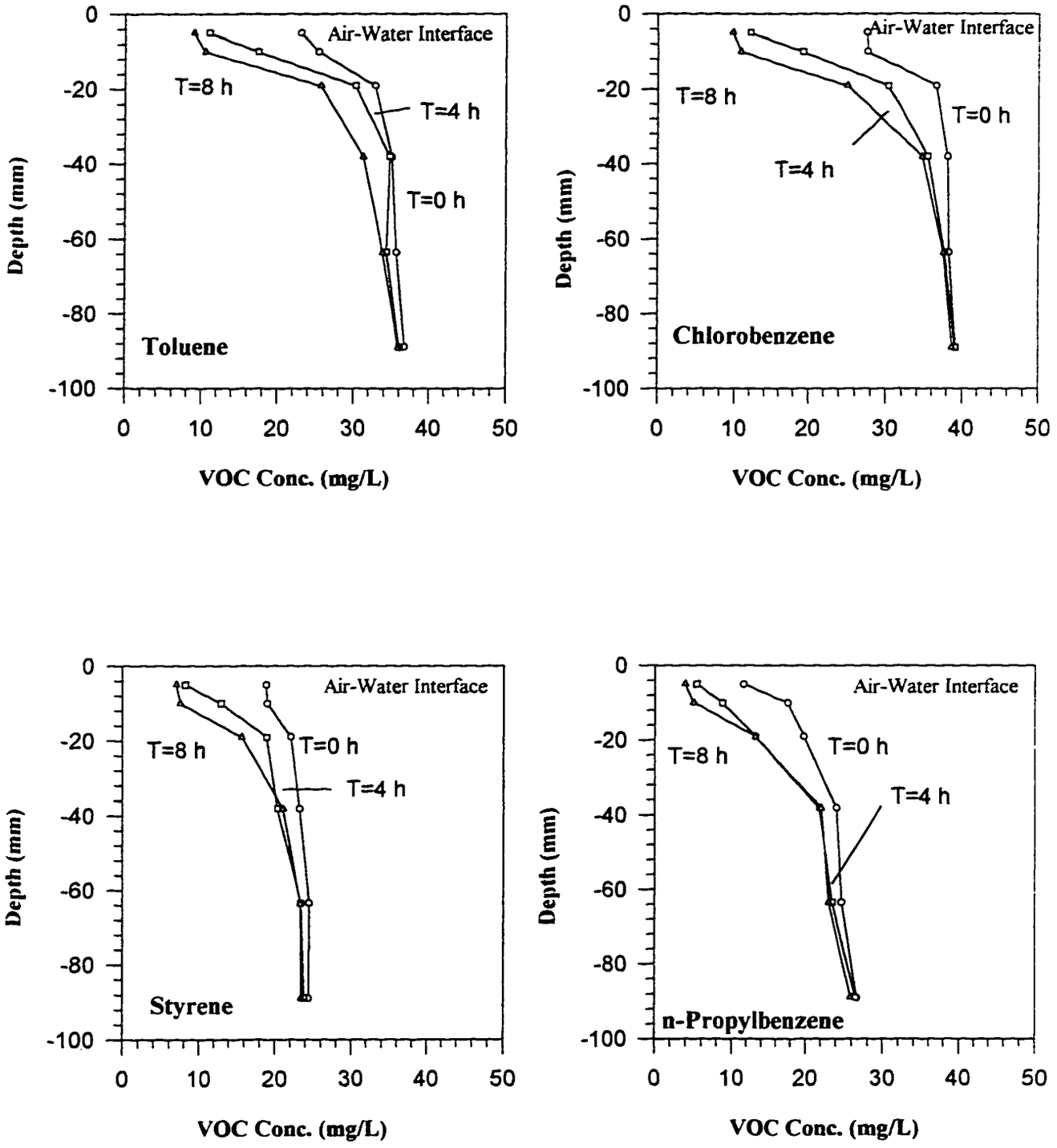

Figure 5. VOC concentration profiles for various times during air sparging (Ottawa sand, air flow rate 2.5 cm/s)

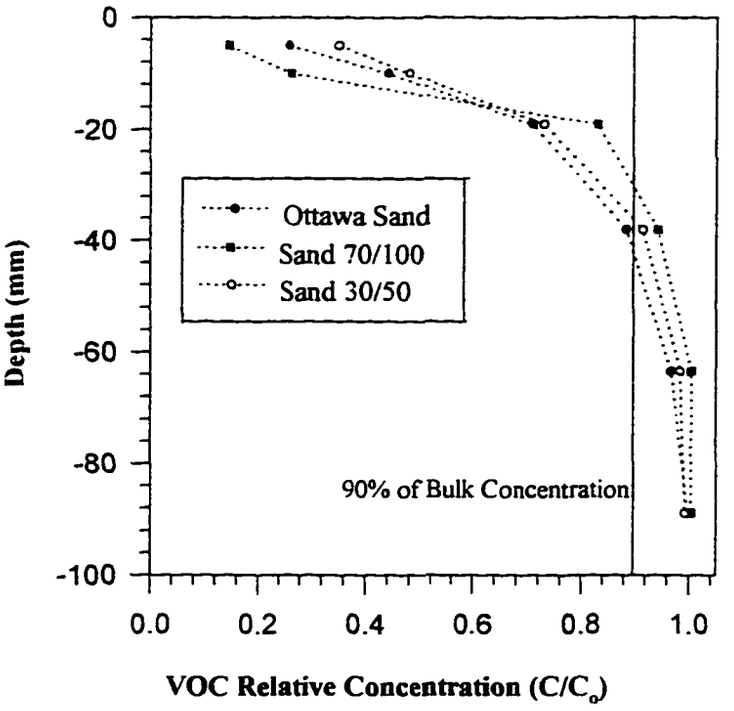

Figure 6. o-Xylene concentration profiles for different porous media (air flow rate 2.5 cm/s)

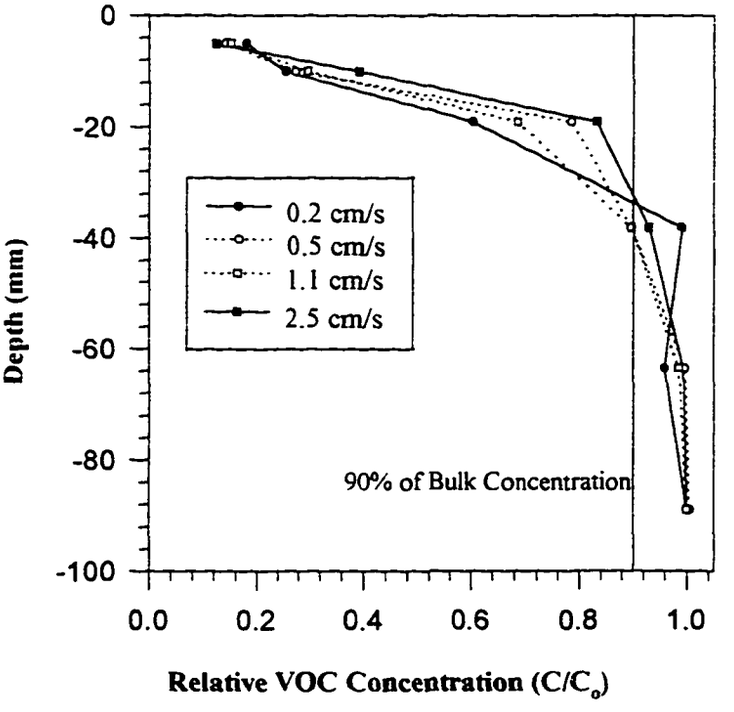

Figure 7. Benzene concentration profiles for different air flow rates (Ottawa sand)

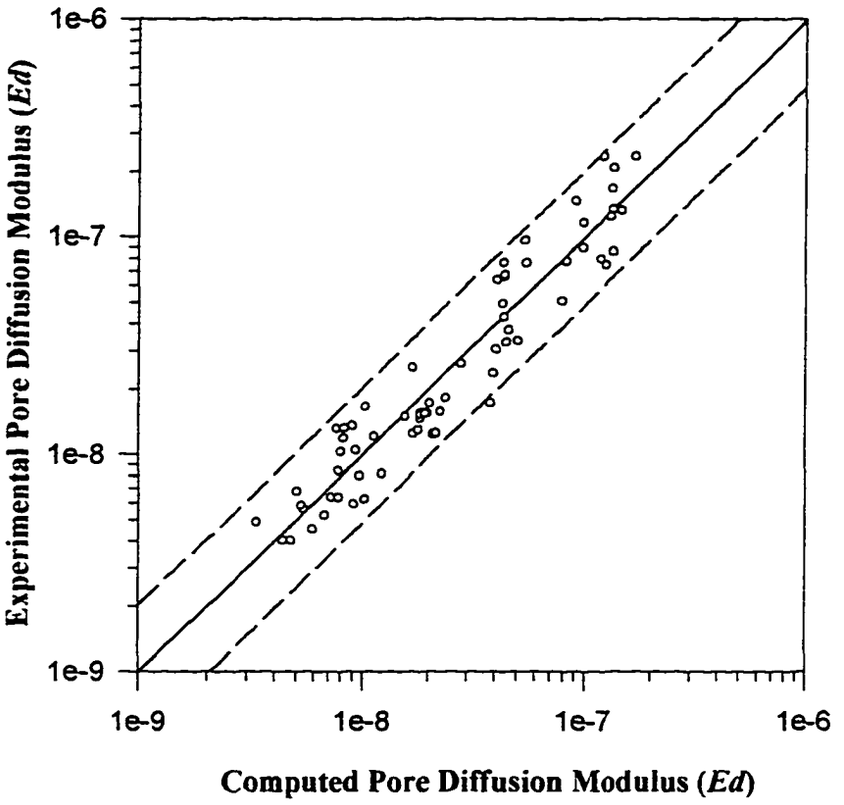

Figure 8. Pore Diffusion Modulus: experimental vs. computed values with 95% confidence interval plots

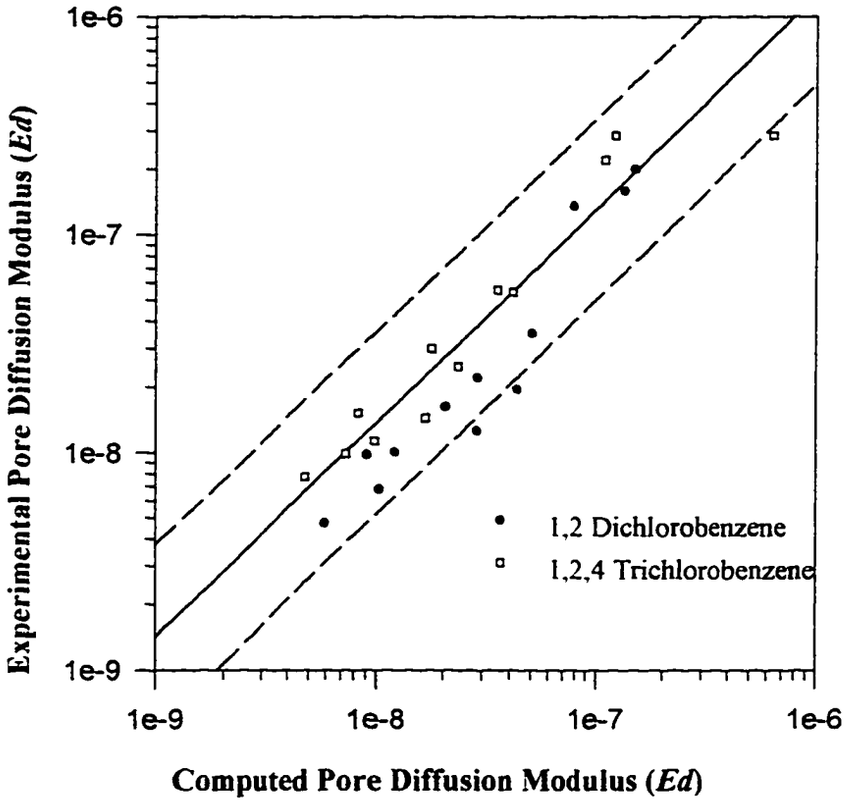

Figure 9. Comparison of experimental and computed Pore Diffusion Modulus for 1,2 Dichlorobenzene and 1,2,4 Trichlorobenzene with 95% confidence interval plots

CHAPTER FOUR. AIR-WATER MASS TRANSFER COEFFICIENTS

A paper submitted to Water Resources Research

Washington J. Braida and Say Kee Ong

Abstract

Experiments investigating the mass transfer of several volatile organic compounds (VOCs) across the air-water interface were conducted using a single-air channel air sparging system. Three different porous media were used in the study. Air velocities ranged from 0.2 cm/s to 2.5 cm/s. The tortuosity factor for each porous media and the air-water mass transfer coefficients were estimated by fitting experimental data to a one-dimensional diffusion model. Tortuosity factors found were 0.52 for Ottawa sand, 0.51 for sand 30/50, and 0.47 for sand 70/100. The estimated mass transfer coefficients (K_G) ranged from 1.79 x 10^{-3} cm/min to 3.85 x 10^{-2} cm/min. The estimated lumped mass transfer coefficients ($K_G a$) were found to be directly related to the air diffusivity of the VOC, air velocity, particle size, and inversely related to the Henry's law constant of the VOCs. Of the four parameters, the parameter which controlled or had a dominant effect on the lumped mass transfer coefficient was the air diffusivity of the VOC. Two empirical models were developed by correlating the Damkohler and the modified air phase Sherwood numbers with the air phase Peclet number, Henry's law constant, and the reduced mean particle size of the porous media. The correlation developed in this study may be used to obtain better predictions of mass transfer fluxes for field conditions.

Introduction

In situ air sparging has been used for more than 10 years with varying success for the remediation of aquifers contaminated with dissolved volatile organic compounds (VOCs) and nonaqueous phase liquids (NAPLs). In a typical air sparging system, clean air is injected below the water table to strip or volatilize VOCs from the aqueous phase. In addition, aerobic biodegradation is enhanced through the transfer of oxygen from air to the

contaminated groundwater (Brown et al., 1994). Air sparging is usually used in combination with a vacuum extraction system located in the unsaturated zone.

Despite the widespread use of air sparging as a remedial technology, an understanding of the different operative processes present during air sparging has lagged behind the practical application of the technology. Injection of air into the aquifer creates complex transient physical conditions within the subsurface environment. Laboratory air flow visualization studies showed that the prevalent air flow in fine to medium grained saturated porous media was in the form of discrete air channels (Ji et al., 1993). Under air sparging conditions, VOCs in the aqueous phase must travel by diffusion through the porous media to the air channels before being volatilized at the air-water interface. Several researchers have shown that for advective gas flow conditions such as air sparging and soil vapor extraction, the movement of air across the air-water interface may not provide enough residence time for local equilibrium to be achieved between the VOCs in the water and air phases (Mendoza and Friend, 1992; Armstrong et al., 1993). Nonequilibrium mass transfer relationships such as the first order mass transfer equation have been used to describe the mass transfer of VOCs in porous media (Sleep and Sykes, 1989; Szatkowski et al., 1995; Brusseau, 1991; Gierke et al., 1992; Armstrong et al., 1993; and Hein et al., 1994). The first order mass transfer equation is represented by:

$$J = K_G\left(K_H C_w - C_a\right) = K_L\left(C_w - \frac{C_a}{K_H}\right) \tag{1}$$

where J represents the mass transfer flux across the air-water interface ($ML^{-2}T^{-1}$), C_a and C_w are the gas and liquid phase concentrations (ML^{-3}), respectively at the air-water interface, K_H is the Henry's law constant (dimensionless), and K_G and K_L are the gas phase and liquid phase overall mass transfer coefficients (LT^{-1}), respectively. Volatilization of VOCs across the air-water interface is a two-phase phenomenon driven by the difference in the chemical potential of the species in both phases. In equation 1, the driving force for the transfer of VOC across the air-water interface is given by the difference between the equilibrium air or water concentration ($K_H C_w$ or C_a/K_H) and the actual air or liquid phase concentration (C_a or

C_w). Careful examination of equation 1 indicates that the value of the mass transfer coefficient will be determined by the liquid and gas phase concentrations selected to define the potential gradient. For a given mass flux, J, a different mass transfer coefficient value will be needed if the bulk concentration of the VOC in each phase is used instead of the VOC concentrations at the air-water interface. Even though the VOC concentrations at the air-water interface may more accurately represent the physics of the system, measurement of the VOC concentrations at the air-water interface is not possible. Therefore, the standing issue in the estimation of the mass transfer coefficients between gas and liquid phases during air sparging is to define in a practical way, the driving force (i.e., concentration gradient) for the volatilization of VOCs. Since an air sparged porous media is not a completely mixed system, the task of defining the concentration gradient is more challenging.

The objective of this work was to investigate the air-water mass transfer process for a wide range of system parameters using an experimental setup where the interfacial area between the air and liquid phases was held constant. Mass transfer coefficients determined in the study were then correlated with various dimensionless numbers. The correlations developed in this study may be used to predict the mass transfer coefficients for different operating conditions.

Materials and Methods

The approach taken was to use an experimental setup which would simulate air flow in a single discrete air channel in saturated porous media. Figure 1 shows the experimental apparatus used for the investigation of air-water mass transfer processes during air sparging. The apparatus consisted of a single air channel of approximately 1.58 mm located above the saturated porous media. Using a single air channel would provide "microscopic" information such as changes in the aqueous phase concentrations as a function of distance from the air-water interface with time. The size of the air channel used was within the range of the sizes of air channels observed by others (10 to 20 pore size diameters) during air sparging (Ji, 1994). The apparatus was made of 6.35 mm (1/4") thick acrylic sheets and was 17.5 cm long, 5 cm wide, and 11 cm deep. The apparatus was covered with a flat acrylic piece which provided a gap of approximately 1.58 mm (1/16") for the circulation of humidified air.

Three columns of five sample points each, as shown in Figure 1, were included to allow water samples to be collected throughout the porous media profile. A glass T connector in the exhaust line was used as a gas sampling point to measure the VOC concentration in the effluent gas.

In-house compressed air was used as the air source. Prior to its introduction into the experimental setup, air was filtered to remove particulates and oil drops and then humidified. Air flow was measured with a Gilmont Model 11 flowmeter (Barrington, IL). Stagnant water conditions were used for all the experimental runs. Since the air flow rates under typical sparging conditions are much higher than the flow rates of water in an aquifer, use of a stagnant flow condition was reasonable within the experimental test period. The experimental runs were conducted at room temperature ($21^{\circ}C \pm 2^{\circ}C$).

To assess the influence of the physical-chemical properties of VOCs and the porous media on the rate of volatilization of VOCs, three different porous media, eleven VOCs, and four air flow rates were used. The three different types of sand used in the study were: (a) graded Ottawa sand, (b) sand 30/50, and (c) sand 70/100. All three sands were obtained from U.S. Silica Company (Ottawa, IL). The properties of the porous media are summarized in Table 1. Specific surface areas were measured using the ethylene glycol monoethyl ether (EGME) procedure (Chihacek and Bremmer, 1979) and organic carbon content was determined using the Walkley-Black procedure (Nelson and Sommers, 1982). The VOCs used had saturated solubilities ranging from 30 mg/L to 1800 mg/L and Henry's law constants ranging from 0.07 to 0.37. A summary of the physical-chemical properties of the VOCs is presented in Table 2. Partition coefficients of the VOCs for the three porous media were determined using the head space technique described by Garbarini and Lion (1985). Linear partition coefficients were found to range between 0.025 mL/g and 0.082 mL/g. Aqueous solutions of the different VOCs with concentrations ranging from 8 mg/L to 150 mg/L were prepared using HPLC grade chemicals. All chemicals were purchased from Sigma-Aldrich Chemical Company Inc. (Milwaukee, WI). A slurry was made by carefully mixing the porous media with the aqueous solution of the VOCs. The reactor was then rapidly packed layer by layer with the slurry to avoid entrapment of air bubbles and immediately sealed to minimize VOCs losses. Aqueous samples were then taken from the various sampling points to determine the

initial aqueous phase concentration in the porous media. Air was then circulated through the air channel. For each type of porous medium, four different air velocities, 0.2, 0.5, 1.1, and 2.5 cm/s, were used. There are not reported values of air velocity during field scale air sparging operations. This lack of information may be due to the difficulties associated with the determination of the *ROI* and air saturation in the field. These two values together with the air injection rate are needed to estimate the air pore velocity. The range of air velocities selected for this study was within the range of air velocities typically found for field applications of soil vapor extraction in which air pore velocities are expected to be less than 2 cm/s (Baehr, 1989).

To check for possible losses through adsorption of VOCs onto the reactor walls or leaks in the experimental setup, an 18-hour long experiment without air flow was conducted. The reactor was filled as described above and the VOC concentrations across the porous media were measured at the start and end of the 18-hour experiment. VOC losses were found to be less than 2%.

The VOC concentrations in the air phase and liquid phase were measured with a Hewlett-Packard 5890 Series II gas chromatograph (Avondale, PA) equipped with a HP-5 capillary column and a flame ionization detector. Air phase concentration was determined by direct injection of 1 mL sample into the gas chromatograph. The liquid phase concentration was determined using the head-space technique where 25 μL of an aqueous sample was placed in a 1.8 mL aluminum crimp cap vial. After equilibrium was reached, the head space concentration was measured by direct injection of a head space sample into the gas chromatograph. The aqueous concentration was then estimated from the measured head space concentration.

Results and Discussion

VOC Concentration Profiles and Mass Transfer Zone (MTZ)

A typical set of results showing the change in benzene concentrations over time in the exhaust air and in the water phase is presented in Figure 2. Air flow rate was 1.1 cm/s. Concentration profiles for other VOCs were similar to that of Figure 2 and are not presented here. The results presented are for the center column of sampling points on the experimental

setup. Experimental measurements showed that liquid phase concentrations at 5 and 10 mm below the air-water interface were slightly lower in the first column of sampling points but slightly higher in the last column of sampling points. The aqueous phase concentration at larger depths, i.e., greater than 10 mm below the air-water interface were similar for all the sampling rows. Therefore, concentration profiles of center column generally represented the average value of the VOC aqueous concentration at any given depth. The change in the benzene concentration of the exhaust air is shown in Figure 2a. The results of Figure 2a typically represents the behavior of the exhaust air concentration for field-scale air sparging systems where the VOC concentrations in the exhaust air was characterized by a rapid decrease in VOC concentration followed by a fairly constant low VOC concentration. The asymptotic concentration in the exhaust air for the experimental apparatus was reached after 2 to 3.5 hours of sparging. This implies that a quasi-steady state condition was reached for the volatilization of the VOCs. A steep aqueous concentration gradient with very low benzene concentration at the air-water interface was evident as shown in Figure 2b. However, a short distance away from the interface, the benzene concentrations were fairly constant and did not change even after 8 hours of sparging. Braida and Ong (1997) have defined this concentration gradient zone as the mass transfer zone (*MTZ*). At the onset of air sparging, the majority of the VOC volatilized came from the *MTZ* adjacent to the air channel while the VOC in the bulk liquid several centimeters away from the air channel remained almost unaffected by the air flow. The development of the *MTZ* may be the result of a faster rate of VOC volatilization at the air-water interface as compared to the diffusive transport of VOCs through the porous media to the air-water interface. For all the experiments, the *MTZ* (i.e., the concentration gradient zone) for each VOC became fairly constant after four hours of sparging suggesting that a quasi-steady state condition was reached whereby the mass transfer to the air phase was controlled by the diffusion of the VOCs through the *MTZ*. The presence of a concentration gradient at the start of the experiments was due to VOC losses during the packing of the material into the reactor.

Estimation of Mass Transfer Coefficients

To describe the transport of VOCs throughout the porous media and their volatilization across the air-water interface, a one-dimensional diffusion model was used. Because of the very low organic carbon content and low partition coefficients of the porous media, sorption of VOCs was not considered in the model for the estimation of mass transfer coefficients. Assuming stagnant conditions for the aqueous phase, the equation describing diffusive transport of VOCs through the porous media can be stated as follows:

$$\varepsilon \frac{\partial C_w}{\partial t} = \tau D_w \frac{\partial^2 C_w}{\partial z^2} \tag{2}$$

where z (L) is the depth of the porous media with the air-water interface located at $z = 0$ and the bottom of the reactor at $z = L$, C_w is the aqueous concentration of the VOC (ML^{-3}), D_w is the aqueous diffusivity of the VOC (L^2T^{-1}), ε is the porosity of the porous media (dimensionless), and τ is the tortuosity factor (dimensionless) which accounts for the change in the length of the diffusion path of the VOCs in the porous media.

The initial and boundary conditions (IC and BC) for the experimental setup were:

IC C_w is known for all z at time zero (experimental data)

BC $$\tau D_w \frac{\partial C_w}{\partial z} = -K_G\left(K_H C_w - C_a\right) \quad \text{at } z = 0 \text{ for all t} \tag{3}$$

$$\frac{\partial C_w}{\partial z} = 0 \quad \text{at } z = \text{L for all t} \tag{4}$$

Based on equation 3, the driving force for the volatilization of VOCs was the difference in the chemical potential between the VOCs in the two phases. Since the VOC concentrations C_w and C_a at the interface were not known, estimating the mass transfer coefficients based on the VOC concentration at the interface would not be useful for field applications. According to the two-resistance model of Lewis and Whitman (1924) for mass transfer, two laminar sublayers exist at each side of the air-water interface where molecular diffusion controls the

transport of compounds. Beyond these thin laminar regions, turbulent conditions for the transport of chemical compounds were assumed to be prevalent. Using the two-resistance model, the concentration gradient will be based on the bulk concentrations of the chemicals in each phase. However, for air channels in porous media, the assumption of turbulent conditions in the aqueous phase for the transport of contaminants is not a valid assumption. The difference between the assumptions of the two-resistance model and the situation found in saturated porous media during air sparging operations is shown in Figure 3. Because of the concentration gradient in the vicinity of the air channels, bulk concentration in the aqueous phase cannot be used to define the driving force for the mass transfer. To overcome this difficulty, a volumetric weighted average concentration, $\overline{C}_w$, of the mass transfer zone (*MTZ*) was proposed and used for the aqueous concentration term on the right hand side of equation 3. The volumetric average concentration, $\overline{C}_w$, was computed as follows:

$$\overline{C}_w = \frac{\sum V_n C_{wn}}{\sum V_n} \tag{5}$$

where V_n is the volume of the n layer (L^3), C_{wn}(ML^{-3}) is the aqueous concentration of VOC in the n layer, and the summation extends to all the layers included in the *MTZ*. The reason for selecting this concentration was that the *MTZ* was the region directly impacted by the air channel but beyond the *MTZ*, air flow had negligible impact on the dissolved contaminants. Movement of contaminants from the bulk phase into the *MTZ* was by diffusion only as described by equation 2.

To simplify the estimation of the mass transfer flux, VOCs volatilized from the air-water interface were assumed to be rapidly swept away from the air-water interface. Therefore, the air concentration, C_a, at the air water interface may be assumed to be negligible. With these assumptions, the first boundary condition (equation 3) can be rewritten as:

$$\tau D_w \frac{\partial C_w}{\partial z} = -K_G K_H \overline{C}_w \tag{6}$$

The VOC concentration in the effluent air was computed using the transport equation for the VOCs in the air phase:

$$V_a \frac{d\overline{C}_a}{dt} = -Q_a \overline{C}_a + K_G A K_H \overline{C}_w \qquad (7)$$

where $\overline{C}_a$ is the measured VOC concentration in the effluent air (ML^{-3}), V_a represents the air volume (L^3) in the experimental setup, Q_a represents the air flow (L^3T^{-1}), A is the air-water interfacial area (L^2) of the experimental setup (87.5 cm^2).

The objective of the modeling approach was to estimate the gas side overall mass transfer coefficient (K_G) by numerically solving equation 2 with boundary conditions defined by equations 4 and 6. Equation 2 was solved numerically using the Continuous System Modeling Program (CSMP) software (IBM, 1972). The value of K_G determines the flux of VOCs at the air-water interface while τ determines the final shape of the VOC concentration profile in the porous media. The VOC concentration profile was divided into 26 horizontal layers of variable thickness (thinner layers were used closer to the air-water interface to compute more accurately the VOC concentrations in this region). τ is a property of the porous media and was estimated by fitting the computed VOC concentration profile to the experimentally determined aqueous concentration profile. With an initial value of τ, a K_G value was estimated by matching the actual mass volatilized with the computer's estimate of the total mass volatilized. The value of τ was then adjusted to recompute the aqueous phase concentration profile and the K_G was estimated again by matching the computed mass volatilized with the actual mass of VOC volatilized. The iteration was completed when the two successive sets of estimated values and the actual values for the VOC aqueous phase concentration profile, air phase concentration, and the total mass of VOC volatilized differed by less than 2%. The τ value determined for a given porous media was then used to estimate the K_G values for all the other experimental runs involving the same porous media. Figure 4 shows the experimental and the estimated results for air phase and aqueous phase concentration profile for benzene after eight hours of sparging. The approach taken for this

study is different from other studies. For this study, both air phase and liquid phase VOC concentrations were used to estimate the mass transfer coefficients allowing for a more accurate estimation of the mass transfer coefficients. Other studies used only the air phase VOC concentration to estimate the mass transfer coefficient. As such, simplifications to the mathematical models had to be made in other studies and usually a lumped model is used.

As expected, the tortuosity factor was found to be dependent on the porous media. The values estimated were: 0.52 for Ottawa sand, 0.51 for sand 30/50 and 0.47 for sand 70/100. The values estimated were in general agreement with the values reported elsewhere (Schaefer et al., 1995). Estimated mass transfer coefficients values (K_G) are shown in Table 4 and they ranged from 1.79 x 10^{-3} cm/min for n-propylbenzene in sand 70/100 with an air velocity of 0.2 cm/s to 3.85 x 10^{-2} cm/min for 1,2,4 trichlorobenzene in Ottawa sand with an air velocity of 2.5 cm/s. The overall mass transfer coefficients (cm/min) may be transformed to lumped mass transfer coefficients (s^{-1}) by multiplying with the specific interfacial area (0.09 cm^{-1}) of the air-water interface of the experimental setup. For the experimental conditions, the lumped mass transfer coefficients ranged from 2.7 x 10^{-6} s^{-1} to 5.8 x 10^{-5} s^{-1}. These values compared favorably well with the values of 2 to 6 x 10^{-6} s^{-1} reported by Fisher et al. (1996) for the soil vapor extraction of four chlorinated VOCs in a sand box and the values (2 x 10^{-6} s^{-1} to 2 x 10^{-3} s^{-1}) reported by Cho and Jaffe (1990) for the volatilization of TCE in soil columns during infiltration. The last two studies used experimental setups that were very different from the single-air channel reactor used in this study and were designed to depict the unsaturated zone. The similarities in the range of values for the air phase lumped mass transfer coefficients may suggest that not all the volume subjected to air sparging or soil vapor extraction was affected by the advecting air.

Model Correlation of Lumped Mass Transfer Coefficients

A visual inspection of the mass transfer coefficients (K_G) showed that the coefficients were inversely dependent on the Henry's law constant of the VOC but directly dependent on air velocity and some of the physical-chemical properties of the porous media. Other parameters which may correlate with the mass transfer were the concentration of the VOC present in the reactor and the aqueous and air diffusivities of the VOCs. To assess the impact

of the physical-chemical properties of the VOCs and porous media on the mass transfer coefficients, a regression analysis of various dimensionless numbers which incorporated the physical-chemical properties of the VOCs and the porous media were conducted. The regression analysis had two objectives: (a) to determine the parameters which may be correlated with the lumped mass transfer coefficient, and (b) to generate a model which may predict the lumped mass transfer coefficient for different conditions.

Four dimensionless expressions for the mass transfer coefficient were used in the regression analysis. They were: (a) Sherwood number (Sh_w) for the aqueous phase, (b) Sherwood number (Sh_a) for the air phase, (c) modified Sherwood number ($Sh_a^{'}$) for the air phase (Szatkowski et al., 1995), and (d) Damkohler number (ϖ) as described by Armstrong et al. (1993). The independent variables used were the Peclet number (Pe) for the air phase, uniformity coefficient (UC), dimensionless particle size (d_o), and porosity (ε) for the porous media, Henry's law constant (K_H) for the VOCs and the dimensionless VOC concentration (X = VOC bulk concentration/VOC aqueous solubility). A description of all the dimensionless parameters used is presented in Table 3. The Peclet number based on the experimental conditions ranged from 0.052 to 1.523.

Multiple stepwise regression analysis was conducted to determine the best fit for the four expressions of the dimensionless mass transfer coefficient with the other dimensionless numbers as shown below:

$$log(Y) = \beta_0+\beta_1 log(Pe)+\beta_2 log(UC)+\beta_3 log(\varepsilon)+\beta_4 log(K_H)+\beta_5 log(d_o)+\beta_6 log(X) \qquad (8)$$

where Y represents any of the four mass transfer dimensionless numbers cited previously and β_i are coefficients determined by the regression analysis.

The stepwise regression procedure evaluated the least square residual (r^2) and the F statistical parameter of each predictor to determine the most appropriate model parameters. To be included in the model, variables must be significant at the F=0.15 level. The regression analysis was performed using the statistical software SAS 6.10 (SAS Institute, 1993). A summary of the stepwise analysis is shown in Table 4. The aqueous phase

Sherwood number correlated very poorly with the independent variables (r^2 = 0.48), but the correlation improved when the air phase Sherwood number (Sh_a) was used (r^2 = 0.6948). The modified air phase Sherwood number correlated well with the reduced mean particle size, the Henry's law constant for the VOC, the air phase Peclet number and the porosity of the porous media. Since the standard error for the estimated exponent for porosity was greater than 50% and the total improvement for the correlation was almost negligible (r^2 changed from 0.794 to 0.799), porosity was dropped from the correlation. Both the uniformity coefficient and the reduced concentration were not selected by the regression analysis. The correlation was as follows:

$$Sh_a^{'} = 10^{-7.14}\, Pe^{0.16}\, d_o^{1.66}\, K_H^{-0.83} \qquad r^2 = 0.7940 \qquad (9)$$

Likewise, porosity did not improve the overall correlation for the Damkohler model and was dropped from the correlation. In addition to porosity, the reduced particle size was excluded from the correlation for the same reasons and neither uniformity coefficient nor the reduced concentration was selected by the regression analysis. The correlation was as follows:

$$\varpi = 10^{-4.81}\, Pe^{-0.79}\, K_H^{-0.83} \qquad r^2 = 0.8535 \qquad (10)$$

Uniformity coefficient may be considered as a surrogate parameter for the particle size distribution of the porous media. The lack of influence of the uniformity coefficient on the mass transfer coefficients was in agreement with the work conducted by Wilkins et al. (1995) on the volatilization of NAPLs in unsaturated porous media. These authors found that mass transfer rate for the volatilization of NAPLs in unsaturated porous media was positively correlated with the soil grain size but was negligibly impacted by variations in grain size distribution. For the correlation described in equation 9, the reduced mean particle size and the Henry's law constant explained most of the variation of the modified Sherwood number. For the correlation shown in equation 10, Pe and K_H explained all the variation of the Damkohler number. The experimental and predicted modified Sherwood and Damkohler numbers are shown in Figure 5 and Figure 6, respectively. Equations 9 and 10 may be

expressed in terms of $K_G a$ and the other variables as shown in equations 11 and 12, respectively:

$$K_G a = 10^{-4.98} D_a^{0.84} v_{air}^{0.16} dp_{50}^{-0.18} K_H^{-0.83} \quad (11)$$

$$K_G a = 10^{-6.05} D_a^{0.79} v_{air}^{0.21} dp_{50}^{-0.79} K_H^{-0.83} \quad (12)$$

Equations 11 and 12 showed that the air phase lumped mass transfer coefficient was dependent on gas diffusivity of the VOC but was inversely related to the Henry's law constant of the VOC and the mean particle size of the porous media. Both equations showed similar exponents for all the independent variables except for the constant term and the mean particle size. The lumped mass transfer coefficient values predicted by equation 11 were plotted against the values predicted by equation 12 as shown in Figure 7. Figure 7 shows that both correlations were equivalent and gave similar predictions of the gas side lumped mass transfer coefficients.

The low value of the exponent for the air velocity indicated that air velocity have limited impact on the lumped mass transfer coefficients although the creation of more turbulent conditions in the air channel may enhance mass transfer. Likewise, VOCs with higher air diffusivities will be more favorably volatilized into the air phase. The inverse relationship of the air phase lumped mass transfer coefficient to the Henry's law constant of the VOC is correct since the air phase mass transfer coefficient is related to the liquid phase mass transfer coefficient by the following:

$$K_G = \frac{K_L}{K_H} \quad (13)$$

By substituting equation 13 into equations 11 and 12, the liquid side lumped mass transfer coefficient was directly dependent on the 0.17 power of the Henry's law constant. The small positive exponent for the Henry's law constant suggests that even though the volatility of VOC may influence the transfer of VOCs from the liquid phase to the air phase, other physical-chemical properties such as the diffusion of the VOCs have control or have a more

dominant effect on the mass transfer process.

Conclusions

A one-dimensional diffusion model was used to estimate tortuosity factors and mass transfer coefficients for the volatilization of VOCs under controlled conditions. Tortuosity factors were 0.52 for Ottawa sand, 0.51 for sand 30/50, and 0.47 for sand 70/100. The overall gas phase mass transfer coefficients (K_G) were estimated from experimental data to range from 1.79 x 10^{-3} cm/min to 3.85 x 10^{-2} cm/min.

Two empirical models for the quantification of the lumped mass transfer coefficients of VOCs under sparging conditions were developed. The modified Sherwood number (Sh'_a) and the Damkohler number (ϖ) were found to correlate well with the air phase Peclet number, the Henry's law constant, and the dimensionless particle size of the porous media. Based on the correlations, the lumped mass transfer coefficient for the air phase was found to be proportional to the gas diffusivity of the VOC but was inversely proportional to the VOC Henry's law constant. Lumped air phase mass transfer coefficients did not correlate well with the particle size distribution (uniformity coefficient) and dimensionless VOC concentration. The dominant and controlling parameter in the correlations for the prediction of the mass transfer coefficients was the gas diffusivity of the VOC. Results of this study provided direct experimental evidence that air sparging is a diffusion controlled process. It is expected that the correlation developed in this study for the air phase mass transfer coefficient and the physical-chemical properties of the system will provide a basis for better predictions of mass transfer fluxes in field applications.

Notation

C_a, C_w	VOC concentration in the air and aqueous phases, ML^{-3}
$\overline{C}_w$	VOC weighted concentration average in the MTZ, ML^{-3}
$\overline{C}_a$	measured VOC concentration in the exhaust air phase, ML^{-3}
D_w	VOC aqueous diffusivity, L^2T^{-1}
D_a	VOC air diffusivity, L^2T^{-1}

d_o	dimensionless mean particle size
dp_{50}	mean particle size, L
ϖ	Damkohler number, dimensionless
ε	porous media porosity, dimensionless
τ	tortuosity coefficient, dimensionless
K_H	Henry's law constant, dimensionless
K_{ow}	octanol-water partition coefficient, dimensionless
MTZ	width of the mass transfer zone, L
Pe	air phase Peclet number, dimensionless
UC	uniformity coefficient, dimensionless
v_{air}	air velocity, LT^{-1}
Sh_a	air phase Sherwood number, dimensionless
Sh_w	water phase Sherwood number, dimensionless
Sh'_a	air phase modified Sherwood number, dimensionless
X	reduced VOC concentration, dimensionless.
a	specific interfacial area, L^{-1}
K_G	overall air side mass transfer coefficient, LT^{-1}
$K_G a$	lumped air side mass transfer coefficient, T^{-1}
K_L	overall aqueous side mass transfer coefficient, LT^{-1}
$K_L a$	lumped aqueous side mass transfer coefficient, T^{-1}

References

Armstrong, J.E., J. Croise, and V. Kaleris, Simulation of rate-limiting processes controlling the vapour extraction of trichloroethylene in sandy soils, in *Proceedings of the International Conference on the Environment and Geotechnics*, Paris, France, pp. 327-334, April 6-8, 1993.

Baehr, A.L., G.E. Hoag, and C. Marley, removing volatile contaminants from the unsaturated zone by inducing advective air phase transport, *Journal of Contaminant Hydrology*, vol 4. pp 1-26, 1989.

Braida, W.J., and S.K. Ong, Air sparging effectiveness: the air channel mass transfer zone. submitted to *Water Resources Research*, 1997.

Brown, R.A., R.J. Hicks, and P.M. Hicks, Use of air sparging for in situ bioremediation, in *Air Sparging for Site Remediation*, edited by R. E. Hinchee, pp. 38-55, Lewis Publishers, Boca Raton, FL, 1994.

Brusseau, M.L., Transport of organic chemicals by gas advection in structured or heterogeneous porous media: development of a model and application to column experiments, *Water Resources Research*, vol. 27(12), pp. 3189-3199, 1991.

Chihacek L.J., and J.M. Bremmer, A simplified ethylene glycol monoethyl ether procedure for assessment of soil surface area, *Soil Sci. Soc. Am. J.*, vol. 43, pp. 821-822, 1979.

Cho, H.J., and P. Jaffe, The volatilization of organic compounds in unsaturated porous media during infiltration, *Journal of Contaminant Hydrology*, vol. 6, pp. 387-410, 1990.

Driscoll, F.G., *Groundwater and Wells*, 2nd Edition, Johnson Filtration System, St. Paul, Minn., 1986.

Fisher, U., R. Schulin, M. Keller, and F. Stauffer, Experimental and numerical investigation of soil vapor extraction, *Water Resources Research*, vol. 32(12), pp. 3413-3427, 1996.

Garbarini, D.G., and L.W. Lion, Evaluation of sorptive partitioning of nonionic pollutants in closed systems by headspace analysis, *Environ. Sci. Technol.*, vol. 19(1), pp. 1122-1129, 1985.

Gierke, J.S., N.J. Hutzler, and D.B. McKenzie, Vapor transport in columns of unsaturated soil and implications for vapor extraction, *Water Resources Research*, vol. 28(2), pp. 323-335, 1992.

Hein, G.L., N.J. Hutzler, and J.S. Gierke, Quantification of the mechanisms controlling the removal rate of volatile contaminants by air sparging, in *Proc. of the 1994 National conference on Environmental Engineering*, edited by J.N. Ryan and M. Edwards, pp. 556-563, ASCE, NY, NY, 1994.

IBM, System/360 Continuous System Modeling Program user's manual, Program Number 360A-CX, 5th ed., IBM Corp., Technical Publ. Dept., White Plains, New York, 1972.

Ji, W., A. Dahamani, D.P. Ahlfeld, J.D. Lin, and E. Hill, Laboratory study of air sparging: Air flow visualization, *GWMR*, vol. 13(4), pp. 115-126, 1993.

Ji, W., Air sparging: Experimental and theoretical analysis of flow and numerical modeling of mass transfer, Ph.D. Dissertation, 154 pp., The University of Connecticut, Storrs, CT, 1994.

Lewis, W.K., and W.G. Whitman, Principles of gas adsorption, *Industrial and engineering Chemistry*, 16, pp. 1215-1220, 1924.

Lyman, W.J., W.F. Reehl, and D.H. Rosemblatt, *Handbook of Chemical Properties Estimation Methods*, American Chemical Society, Washington D.C., 1990.

Mendoza, C., and E.O. Frind, Advective-dispersive transport of dense organic vapors in the unsaturated zone: I. Model development, *Water Resources*, vol. 23(3), pp. 379-387, 1992.

Nelson, D.W., and L.E. Sommers, Total carbon, organic carbon, and organic matter, in *Methods of Soil Analysis, Part 2, Chemical and Microbiological Properties*, Second Edition, edited by A.L. Page, pp. 570-571, American Society of Agronomy, Inc., Soil Science Society of America, Inc., Madison, WI, 1982.

Perry, R.H., and C.H. Chilton, *Chemical Engineer's Handbook*, 5th Edition, pp. 3-231-3.234, McGraw-Hill, NY, NY, 1978.

Treybal, R.E., *Mass Transfer Operations*, 2nd Edition, pp. 29-31, McGraw-Hill Kogakusha Ltd., Tokyo, Japan, 1968.

Schaefer, C.E., R.R. Arands, H.A. van der Sloot, and D.S. Kosson, Prediction and experimental validation of liquid-phase diffusion resistance in unsaturated soils, *Journal of Contaminant Hydrology*, vol. 20, pp. 145-166, 1995.

Sleep, B.E., and J.F. Sykes, Modeling the transport of volatile organics in variable saturated media, *Water Resources Research*, vol. 25(1), pp. 81-92, 1989.

SAS Institute Inc., *SAS® Software: Changes and Enhancements. Release 6.10*, Carey, NC, 1993.

Szatkowski, A., P.T. Imhoff, and C.T. Miller, Development of a correlation for aqueous-vapor phase mass transfer in porous media, *Journal of Contaminant Hydrology*, vol. 18, pp. 85-106, 1995.

Wilkins, M.D., L.M. Abriola, and K.D. Pennel, An experimental investigation of rate-limited nonaqueous volatilization in unsaturated porous media: steady state mass transfer, *Water Resources Research,* vol. 31(9), pp. 2159-2172, 1995.

Table 1. Physical-chemical properties of porous media

Type of Sand	Mean Particle Size (cm)	Uniformity Coefficient	Specific Surface Area (m^2/g)	Porosity	Organic Carbon (%)
Ottawa Sand	0.0190	2.16	1.99	0.377	0.0066
Sand 30/50	0.0305	1.41	1.17	0.370	0.0062
Sand 70/100	0.0168	1.64	2.73	0.400	0.0063

Table 2. Physical-chemical properties of VOCs at 20°C (Lyman et al., 1990)

Compound	Molecular Weight	K_H	Solubility (mg/L)	D_a (cm^2/s)*	$D_w \times 10^6$ (cm^2/s)**	log K_{ow}
Benzene	78.12	0.195	1780	0.0923	9.59	2.12
Toluene	92.15	0.233	515	0.0830	8.46	2.73
Ethylbenzene	106.18	0.291	152	0.0732	7.63	3.15
o-Xylene	106.18	0.178	130	0.0759	7.63	2.95
m-Xylene	106.18	0.247	175	0.0759	7.63	1.38
p-Xylene	106.18	0.256	198	0.0759	7.63	3.26
Chlorobenzene	112.56	0.137	500	0.0725	8.52	2.84
n Propylbenzene	120.21	0.369	60	0.0544	6.99	3.87
1,2 Dichlorobenzene	147.00	0.118	145+	0.0829	7.97	3.60
1,2,4 Trichlorobenzene	181.44	0.069	30+	0.0686	7.09	4.30
Styrene	104.16	0.0967	300	0.0746	7.89	2.95

* Estimated from Hirschfelder, Bird, and Spotz (Perry and Chilton, 1978)
** Estimated from Wilke and Chang correlation (Treybal,1968)
\+ at 25°C

Table 3. Estimated air phase mass transfer coefficients for various compounds, porous media, and air velocities (cm/min).

Media	Air Velocity (cm/s)	Benzene	Ethyl-benzene	m,p-Xylene	o-Xylene	Toluene	Chloro-benzene	Styrene	n-Propyl-benzene	1,2 Dichloro-benzene	1,2,4 Trichloro-benzene
ottawa	0.2	0.00648	0.00338	0.00361	0.00563	0.00379	0.00589	0.00597	0.00329	0.00597	0.01377
ottawa	0.5	0.00410	0.00298	0.00385	0.00528	0.00879	0.01328	0.01599	0.00504	0.01019	0.00965
ottawa	1.1	0.00486	0.00436	0.00467	0.00436	0.00637	0.01156	0.01707	0.00463	0.00923	0.02487
ottawa	2.5	0.00594	0.00464	0.00394	0.00595	0.00721	0.01243	0.01956	0.00487	0.01253	0.03854
30/50	0.2	0.00668	0.00483	0.00465	0.00527	0.00376	0.00707	0.00996	0.00280	0.00393	0.01361
30/50	0.5	0.00635	0.00406	0.00432	0.00717	0.00524	0.00897	0.01180	0.00209	0.00245	0.01016
30/50	1.1	0.00391	0.00336	0.00319	0.00534	0.00467	0.00784	0.01105	0.00466	0.01283	0.01913
30/50	2.5	0.00510	0.00439	0.00444	0.00598	0.00526	0.00797	0.01087	0.00412	0.00736	0.00913
70/100	0.2	0.00558	0.00361	0.00339	0.00434	0.00417	0.00511	0.00743	0.00179	0.00629	0.00671
70/100	0.5	0.00876	0.00633	0.00594	0.01097	0.00537	0.00782	0.00967	0.00257	0.00672	0.01445
70/100	1.1	0.00517	0.00398	0.00605	0.00746	0.00637	0.00802	0.01435	0.00221	0.00766	0.00822
70/100	2.5	0.00689	0.00514	0.00510	0.01034	0.00551	0.00787	0.01781	0.00232	0.00781	0.01995

Table 4. Dimensionless numbers used for modeling

Dimensionless Number	Equation	Comments
Damkohler Number (ϖ)	$\frac{K_G a L_o}{v_{air}}$	Mass transport by water-air partition / Mass transport by gas advection
Aqueous Phase Sherwood Number (Sh_w)	$\frac{K_L dp_{50}}{D_w}$	Mass transport by water-air partition / Mass transport by liquid diffusion
Air Phase Sherwood Number (Sh_a)	$\frac{K_G dp_{50}}{D_a}$	Mass transport by water-air partition / Mass transport by gas diffusion
Modified Air Phase Sherwood Number (Sh'_a)	$\frac{K_G a dp_{50}^2}{D_a}$	Mass transport by water-air partition / Mass transport by gas diffusion
Dimensionless Concentration	$\frac{C_w}{Sol.}$	Actual VOC bulk concentration / VOC aqueous solubility
Air Phase Peclet Number (Pe)	$\frac{v_{air} dp_{50}}{D_a}$	Rate of transport by gas advection / Rate of transport by molecular gas diffusion
Dimensionless Mean Grain Size (d_o)	$\frac{dp_{50}}{d_m}$	d_m= 0.05 cm is the mean grain size of a "medium" size sand (Driscoll, 1986)
Porosity (ε)	$\frac{V_{Total} - V_{Solid}}{V_{Total}}$	Void volume / Total volume
Henry's Law Constant K_H	$\frac{C_a}{C_w}$	Ratio of air phase concentration to aqueous phase concentration
Uniformity Coefficient (UC)	$\frac{d_{60}}{d_{10}}$	Measure of the grain size distribution

Table 5. Summary of stepwise regression analysis

Modified air phase Sherwood number

Variable	Parameter Estimate	Standard Error	Partial r^2	Model r^2
Intercept	-7.1387	0.0646		
d_o	1.6598	0.1217	0.4329	0.4329
K_H	-0.8264	0.0603	0.3186	0.7515
Pe	-0.1626	0.0332	0.0425	0.7940

Damkohler number

Variable	Parameter Estimate	Standard Error	Partial r^2	Model r^2
Intercept	-4.8104	0.0568		
Pe	-0.7875	0.0356	0.6614	0.6614
K_H	-0.8332	0.0672	0.1921	0.8535

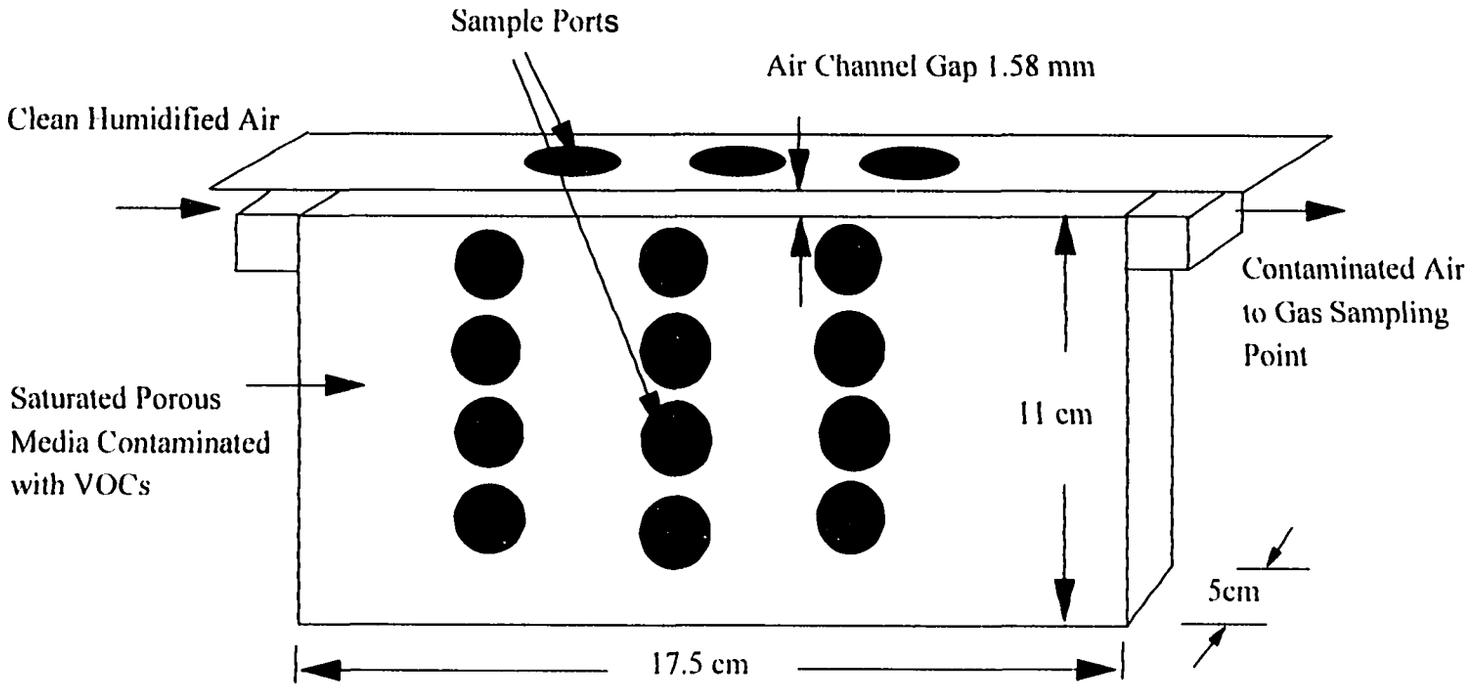

Figure 1. Single-air channel apparatus

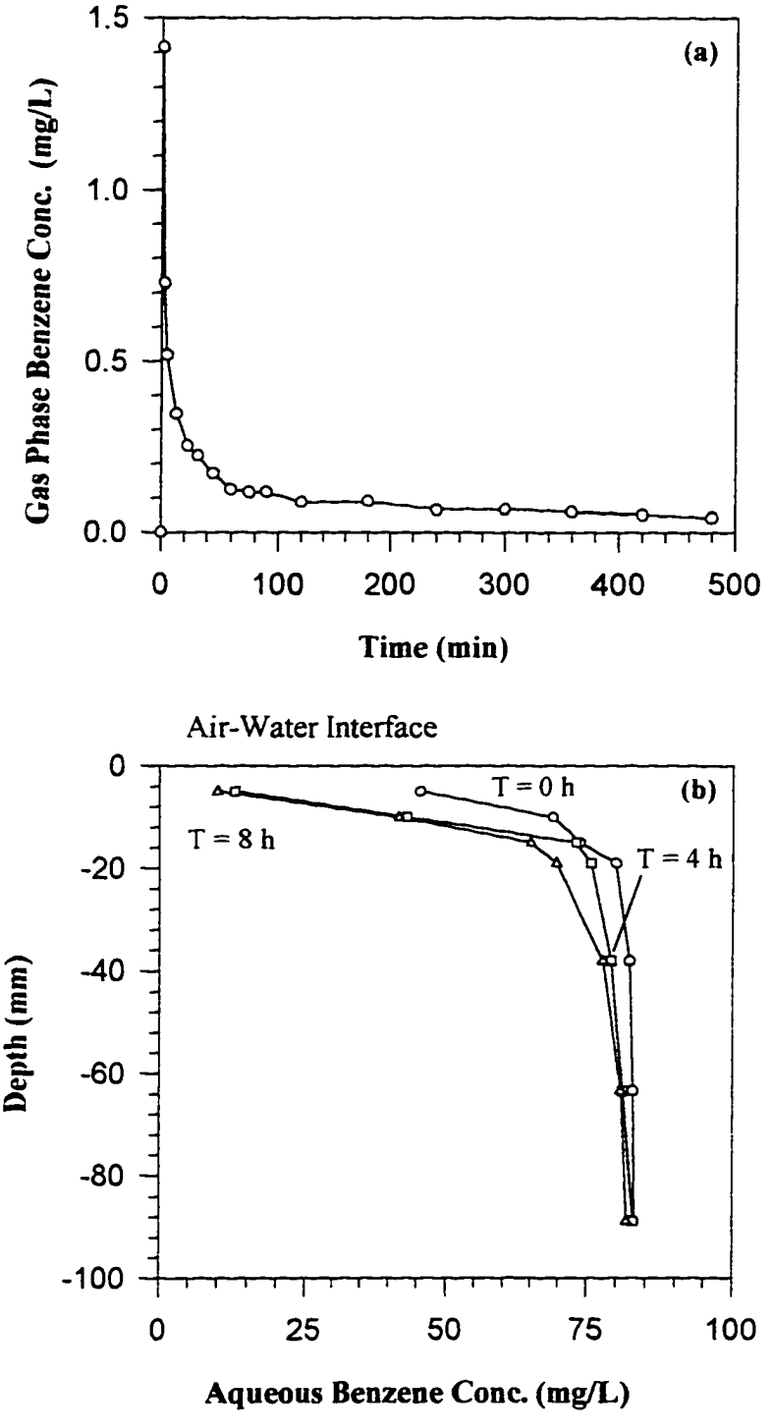

Figure 2. (a) Benzene concentration (mg/L) in the exhaust air
(b) Benzene concentration (mg/L) in aqueous phase
for sand 70/100 and air velocity of 1.1 cm/s

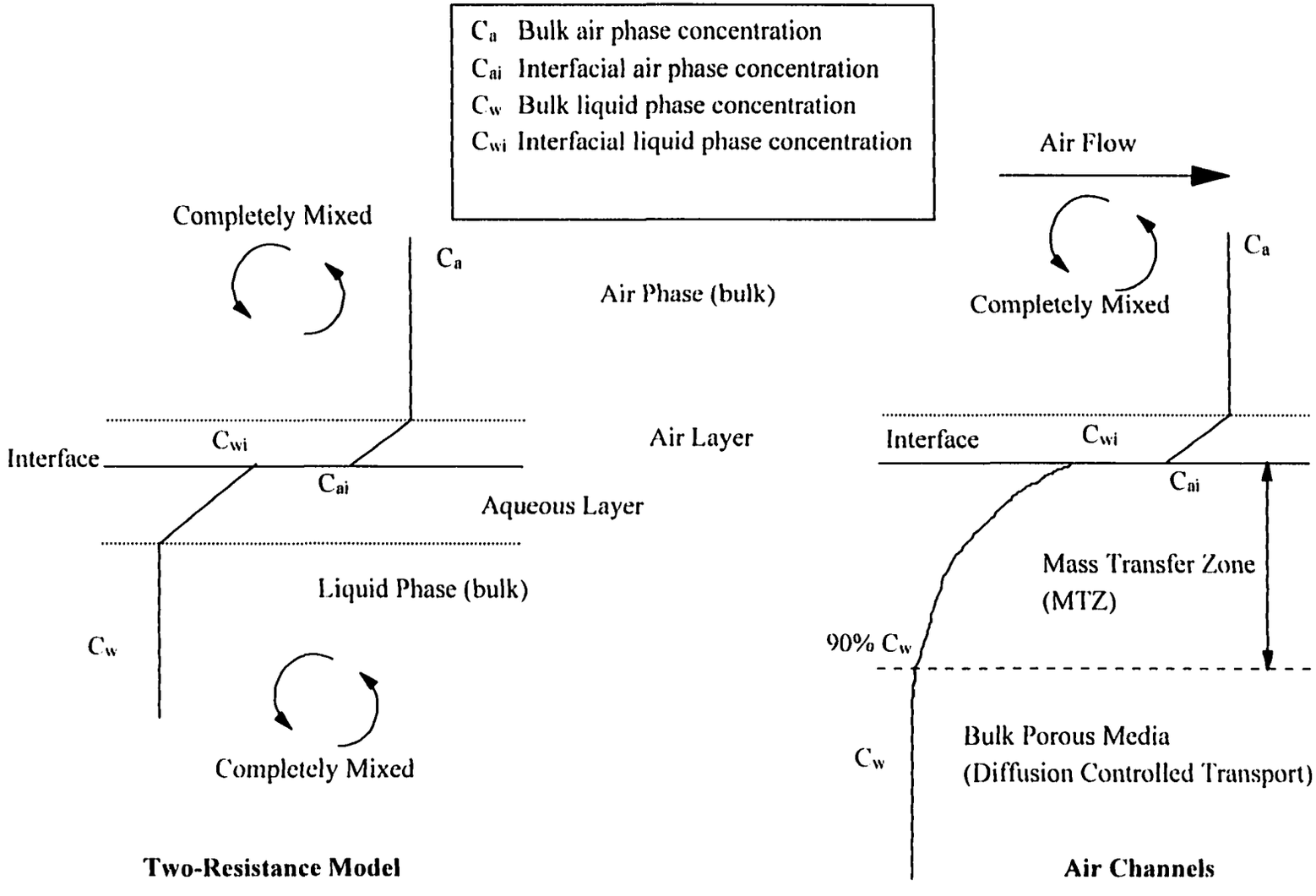

Figure 3. Air-water interface mass transfer, two-resistance model and air channel conditions

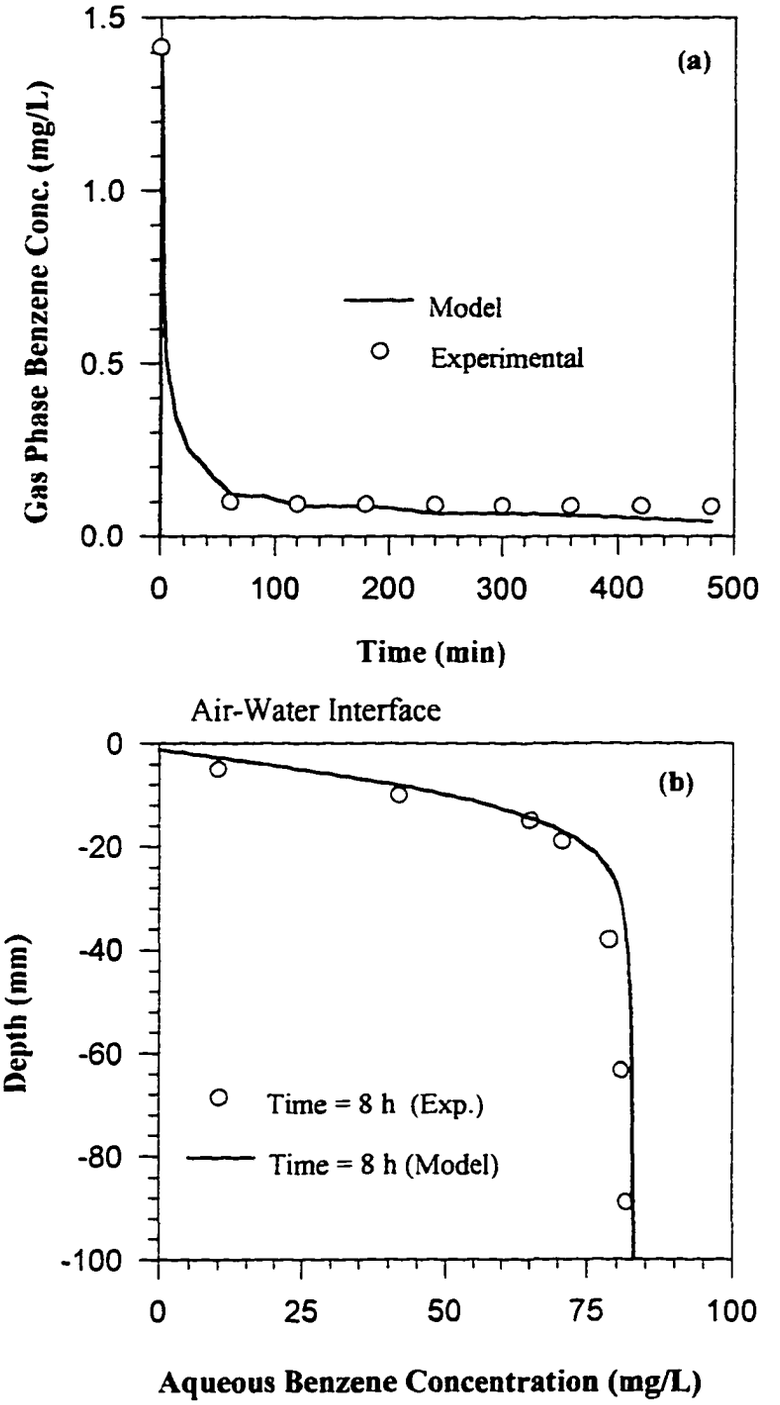

Figure 4. Experimental and predicted benzene concentration for sand 70/100 and air velocity of 1.1 cm/s: (a) exhaust air, (b) aqueous concentration

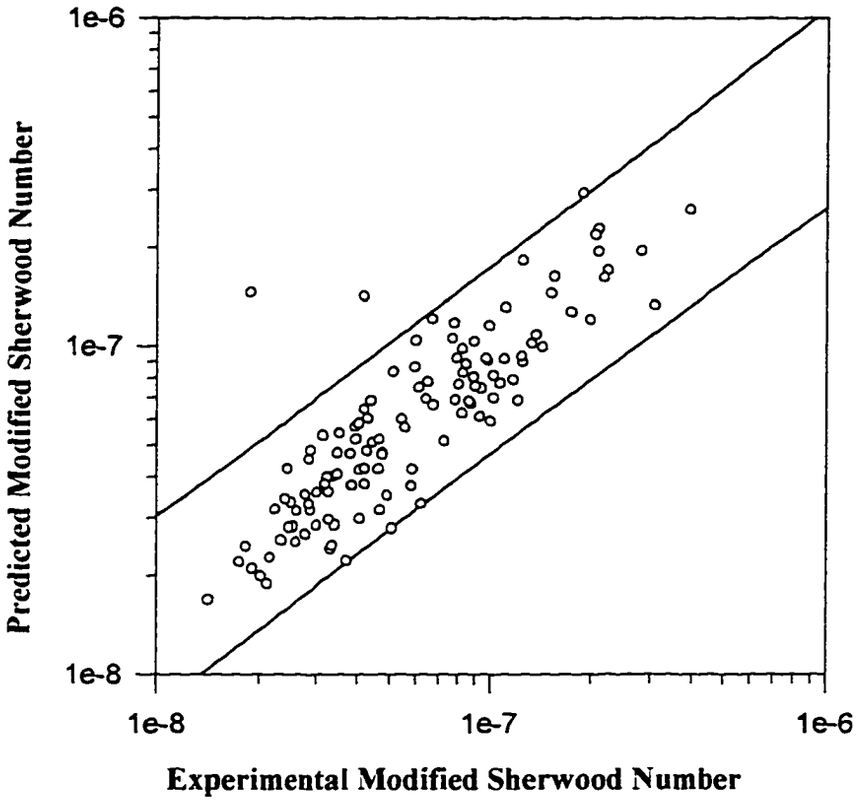

Figure 5. Experimental vs. predicted modified Sherwood number and 95% confidence interval for the population

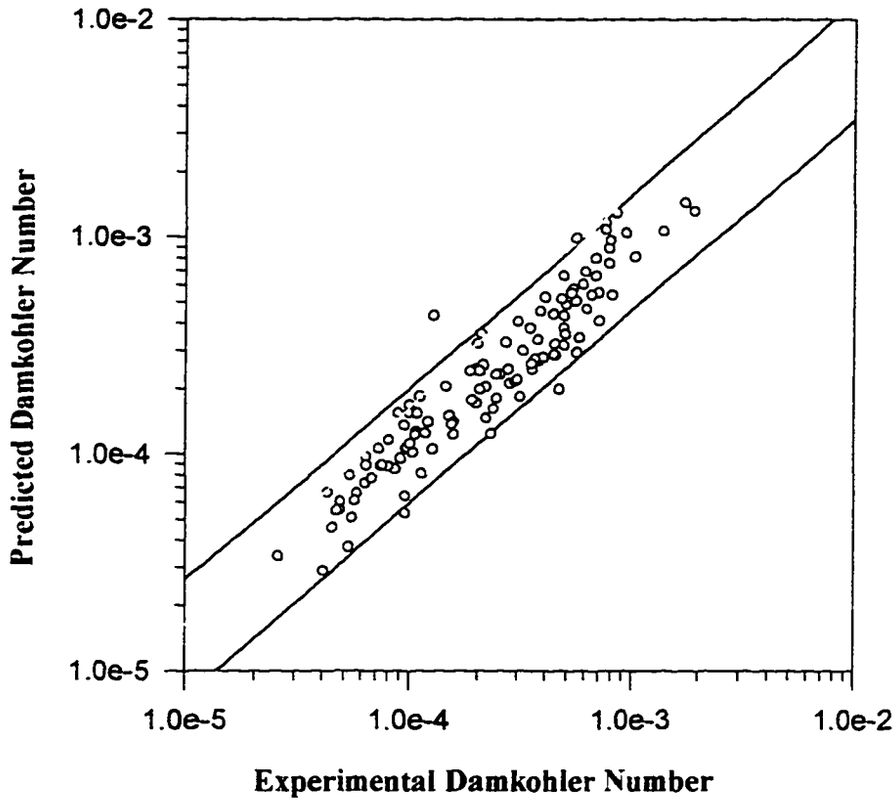

Figure 6. Experimental vs. predicted Damkohler number and 95% confidence interval for the population

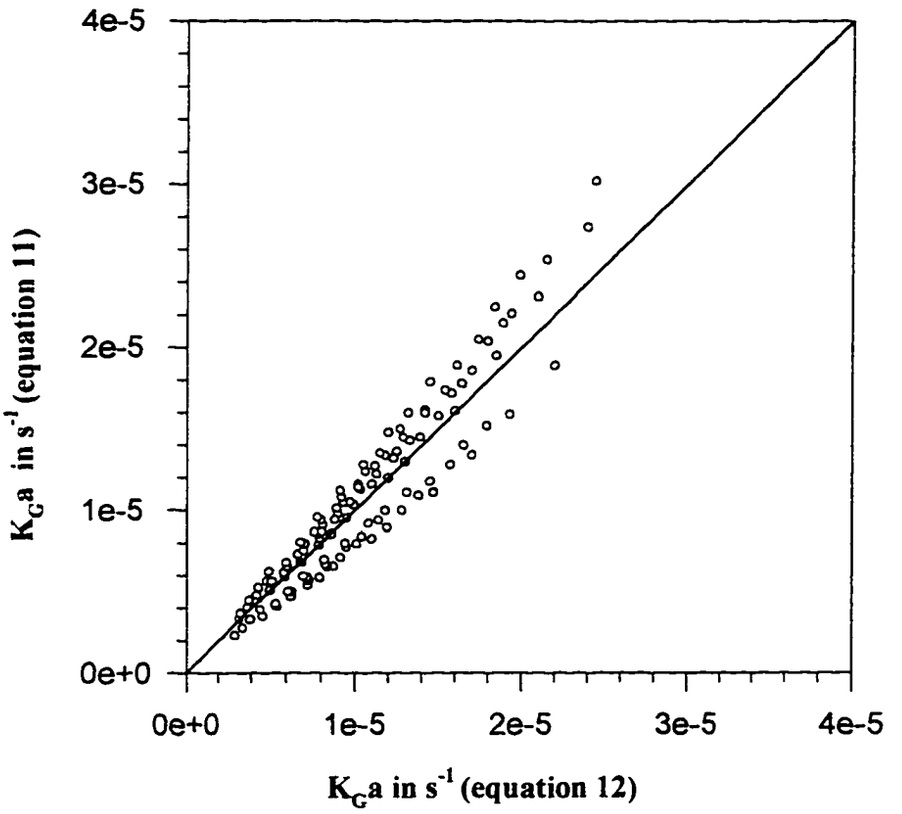

Figure 7. Estimated gas side lumped mass transfer coefficient using eq. 11 vs. estimated lumped gas side mass transfer coefficient using eq. 12

CHAPTER FIVE. VOLATILIZATION OF VOCs UNDER AIR SPARGING CONDITIONS: MASS TRANSFER ANALYSIS

Introduction

Nonequilibrium mass transfer between air and water and vice versa has been extensively studied and many models have been proposed to explain the transport mechanisms governing the transfer of molecules across the interface. Chapter 2 presented a summary of the different conceptual and hydrodynamic models which have been developed to explain the volatilization and adsorption of chemicals at the air-water interface. Although a fair amount of research has been done in this area, studies on the controlling mechanisms in the volatilization of VOCs in saturated porous media during air sparging is fairly scarce.

In previous chapters, diffusion was identified as the controlling mechanism in the nonequilibrium mass transfer of VOCs from groundwater to the air-water interface during air sparging operations. Although the overall mass transfer of VOCs seemed to be controlled by their diffusion through the porous media to the air channels, the mechanisms controlling the interfacial phenomenon of volatilization have not been elucidated yet.

The objective of this chapter is to study the controlling mechanism for the volatilization of VOCs at the air-water interface during air sparging operations. This objective was achieved by using the estimated mass transfer coefficients in Chapter 4 to test the applicability of the two-resistance model of Whitman (1923). The contributions of the liquid and air phase resistances to the overall mass transfer resistance were estimated and the influence of parameters such as air velocity and mean particle size on the relative resistance to the mass transfer was assessed.

Materials and Methods

A description of the single-air channel experimental setup, experimental procedures, and computational methods used for the determination of mass transfer coefficients was presented in Chapter 4. Appendix C includes a sample of the CSMP computer program developed for the estimation of the mass transfer coefficients.

Results and Discussion

A conceptual model, describing the diffusive exchange of chemicals between water and air is the two-resistance model. The model was first described by Whitman in 1923 and first applied to environmental transfer by Liss and Slater (1974). The model agrees with the mass flux expressions (equation 1) used in Chapter 4 for the estimation of mass transfer coefficients except that the model assumes the existence of two stagnant thin films on each side of the air-water interface. Transfer of chemicals or solutes from one phase to the other must diffuse through the two thin layers in series. The rate at which mass is transferred in each layer is characterized by the mass transfer coefficients k which is essentially the transfer velocities. Based on the two-resistance model, the inverse of the overall mass transfer coefficient is equal to the sum of the liquid and gas phase film resistance:

$$\frac{1}{K_G} = \frac{K_H}{k_L} + \frac{1}{k_A} \qquad (1)$$

where k_L and k_A are the liquid and gas film coefficients (LT^{-1}), respectively. For most chemicals with high Henry's law constant, the term K_H/k_L is usually larger than $1/k_A$, making the liquid film mass transfer the controlling mass transfer mechanism.

Overall gas side mass transfer resistances were computed by taking the reciprocal of the overall gas side mass transfer coefficients estimated in Chapter 4. For each experimental condition (i.e., porous media type and air velocity), the values of the overall gas side mass transfer coefficients (K_G^{-1}) were plotted against the Henry's law constant of the VOCs. As seen in equation 1, this plot should result in a straight line with slope equal to $1/k_L$ and intercept of $1/k_A$. Figures 1 to 3 show plots of the estimated overall gas side mass transfer resistances against the Henry's law constant and the regression lines with their 95% confidence intervals. Ten different VOCs were initially used in each plot with Henry's law constants ranging from 0.069 to 0.369. However, to obtain a good linear relationship, outliers were not included in the regression analysis. The good linear relationships in Figures 1 to 3 suggest that the two-resistance model of Whitman may be applied to the volatilization of VOCs under air sparging conditions. The surface renewal model postulated by

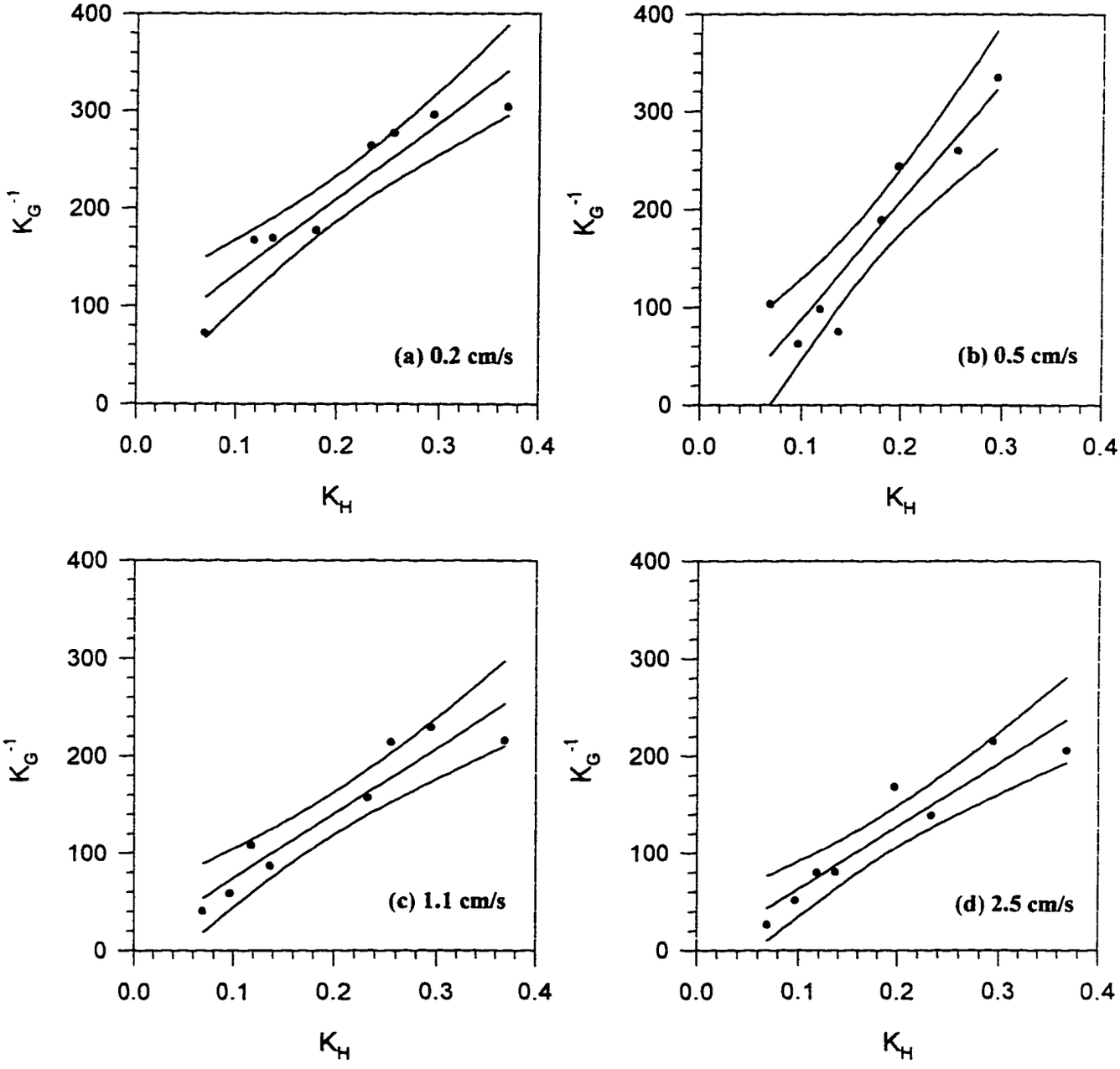

Figure 1. Interfacial mass transfer resistance vs. Henry's Law constant for Ottawa sand and 95% confidence limits

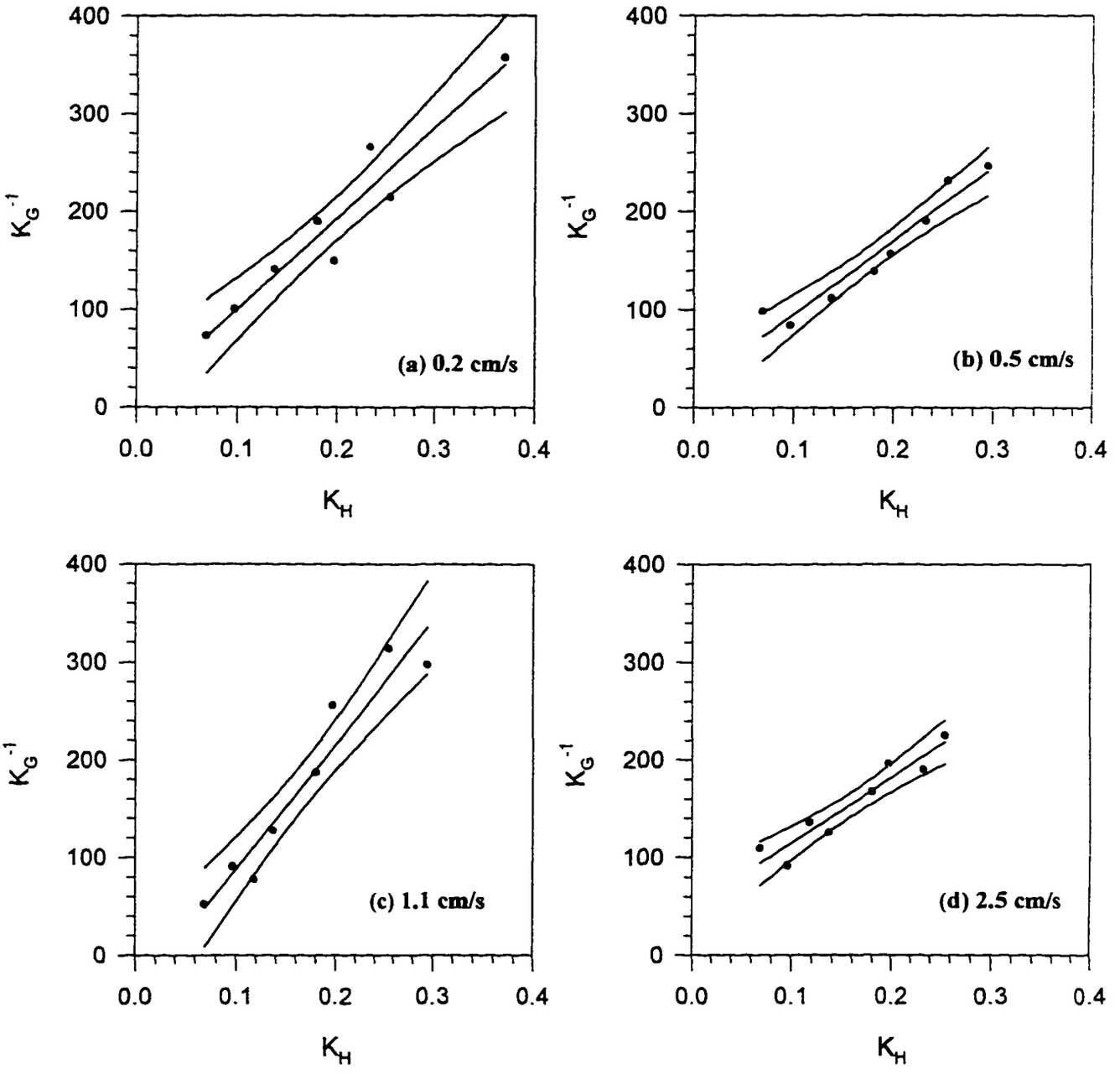

Figure 2. Interfacial mass transfer resistance vs. Henry's law constant for sand 30/50 and 95% confidence limits

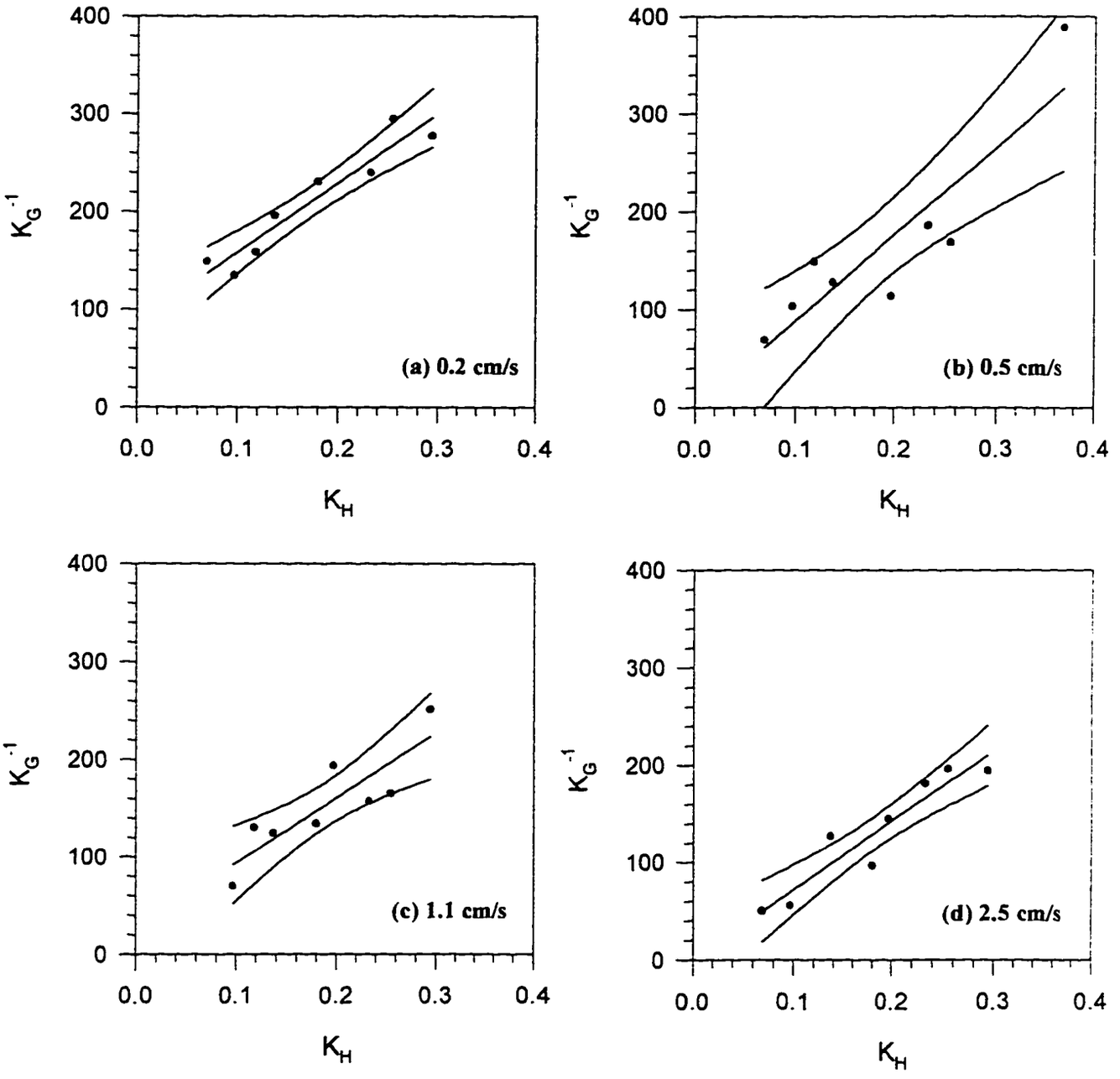

Figure 3. Interfacial mass transfer resistance vs. Henry's law constant for sand 70-100 and 95% confidence interval

Danckwerts (1951) may show a similar behavior if the overall resistance was plotted against the Henry's law constant (Schwarzenbach et al., 1993).

The Danckwerts model assumed a continuous turnover of bulk fluid at the interface as a consequence of the level of turbulence in the fluid. Although this situation may be acceptable for the highly turbulent air phase in the air channels during air sparging, the aqueous phase surrounding the air channels is rather quiescent. Therefore, the turbulence effects may be assumed to be marginal as compared to the diffusional transport of the VOCs.

Assuming that the liquid side ($1/k_L$) and gas side ($1/k_A$) contributions to the overall resistance were only dependent on the porous media and air velocity, ($1/k_L$) and ($1/k_A$) may be estimated. The estimated values for ($1/k_L$) and ($1/k_A$) along with their standard deviations are presented in Table 1. The correlation coefficients for all the plots except for two were close to one.

Table 1. Liquid and gas side mass transfer resistance. Regression analysis results.

Porous Media	Air Velocity (cm/s)	k_A^{-1} (min/cm)	k_L^{-1} (min/cm)	r^2
Ottawa	0.2	88 ± 26	653 ± 108	0.90
Ottawa	0.5	-75 ± 32	1401 ± 165	0.94
Ottawa	1.1	17 ± 27	634 ± 117	0.86
Ottawa	2.5	-17 ± 20	770 ± 97	0.93
Sand 30-50	0.2	8 ± 32	928 ± 140	0.90
Sand 30-50	0.5	-7 ± 13	870 ± 61	0.98
Sand 30-50	1.1	-42 ± 36	1280 ± 184	0.91
Sand 30-50	2.5	31 ± 18	750 ± 99	0.92
Sand 70-100	0.2	78 ± 22	748 ± 142	0.90
Sand 70-100	0.5	-5 ± 49	904 ± 223	0.77
Sand 70-100	1.1	50 ± 39	573 ± 187	0.65
Sand 70-100	2.5	1 ± 29	712 ± 139	0.84

Examination of the values for the gas side mass transfer resistances showed a larger variation in the data with five negative values. Since is not possible to have a negative resistance, for these cases, a value equal to zero, i.e., no gas side resistance, was assumed for comparative purposes. The large variation in the data was expected considering the accumulation of uncertainties after two transformation of the experimental data (i.e., concentration to mass transfer coefficients to mass transfer resistances). Table 1 showed that

the liquid side mass transfer rates (k_L) were smaller than the corresponding gas side mass transfer rates (k_A). This result is in agreement with the findings reported in Chapter 3 and Chapter 4 whereby liquid diffusion controls the volatilization of VOCs under air sparging operations.

The liquid mass transfer resistance is given by the product of the Henry's law constant (K_H) and the reciprocal of the liquid side mass transfer rate (k_L). Its relative influence in the overall resistance is dependent on the type of chemical. Table 2 shows the relative influence of the gas and liquid side mass transfer resistance on the overall gas side mass transfer resistance for 1,2,4 trichlorobenzene ($K_H = 0.069$), and n-propylbenzene ($K_H = 0.369$). 1.2.4 trichlorobenzene and n-propylbenzene were the least volatile and most volatile VOCs used in the study, respectively.

Table 2. Relative liquid side and gas side mass transfer resistance for selected VOCs.

Porous Media	Air Velocity (cm/s)	1,2 . Trichlorobenzene		n-Propylbenzene	
		Gas Side Resistance (%)	Liquid Side Resistance (%)	Gas Side Resistance (%)	Liquid Side Resistance (%)
Ottawa	0.2	58 - 72	28 - 42	20 - 32	68 - 80
Ottawa	0.5	0	100	0	100
Ottawa	1.1	0 - 50	50 - 100	0 - 12	88 - 100
Ottawa	2.5	0 - 5	95 - 100	0 - 1	99 -100
Sand 30/50	0.2	0 - 38	62 - 100	0 - 10	90 - 100
Sand 30/50	0.5	0 - 9	91 - 100	0 - 2	98 - 100
Sand 30/50	1.1	0	100	0	100
Sand 30/50	2.5	20 - 49	51 - 80	4 - 15	85 - 96
Sand 70/100	0.2	51 - 66	34 - 49	17 - 27	73 - 87
Sand 70/100	0.5	0 - 42	58 - 100	0 - 11	89 - 100
Sand 70/100	1.1	18 - 64	36 - 82	5 - 30	70 - 95
Sand 70/100	2.5	0 - 40	60 - 100	0 - 10	90 - 100

The relative resistance included in Table 2 show that for VOCs with high values of Henry's law constant, most of the resistance to the mass transfer was located in the liquid phase. In general, liquid side resistance accounted for more than 90% of the total resistance to the mass transfer. For VOCs with low volatility such as 1,2,4 trichlorobenzene, a higher

portion of the overall resistance was in the gas phase for low air velocity. The air velocity and porous media characteristics seemed to have an impact on the relative magnitude of the two resistance. For example, the gas side mass transfer resistance for Ottawa sand seemed to decrease from 60% to 5% when the air speed increased from 0.2 cm/s to 2.5 cm/s. Sand 30-50 showed a similar general trend for 1,2,4 trichlorobenzene. No consistent trends were observed to quantify the influence of porous media in the relative distribution of the mass transfer resistance.

According to the Whitman (1923) model, the liquid and gas phase mass transfer rates may be related to the diffusivity of the VOCs as follows:

$$k_L = D_w / \delta_w \qquad k_A = D_A / \delta_a \qquad (2)$$

where D_w and D_A are the diffusivities of the chemical in bulk water and air, respectively, and δ_w (L) and δ_a (L) are the thicknesses of the stagnant layers in the water phase and the air phase, respectively. Schwarzenbach et al. (1993) reported values of $5x10^{-3}$ to $5x10^{-2}$ cm for δ_w and 0.1 to 1 cm for δ_a for the transport of chemicals in water reservoirs to the atmosphere. In saturated porous media under stagnant conditions and with minimum mixing, the size of the stagnant liquid side film, δ_w, may be assumed to be larger than the values reported by Schwarzenbach and coworkers. Using equation 2, the thickness of the water phase stagnant layer may be computed as presented in Table 3.

The estimated thicknesses of the liquid phase stagnant film were one to two orders of magnitude larger than the corresponding values for water reservoirs. The results imply that turbulent eddy diffusion was either not present or was very small in the liquid side of the interface. This suggests that the air flow in the air channels did not introduce any significant mixing effect on the surrounding saturated porous media. Table 3 shows that δ_w in general decreased with increasing air velocities. Because of the errors involved in the analysis, a 10% to 20% difference in the values of δ_w for a 10 fold increase in the air velocity, would not indicate that there were some air mixing effects. To further clarify this point, Figure 4 presents a plot of the liquid side mass transfer coefficient as a function of the air velocity for the three porous media used. Figure 4 suggests that the k_L were fairly constant if the

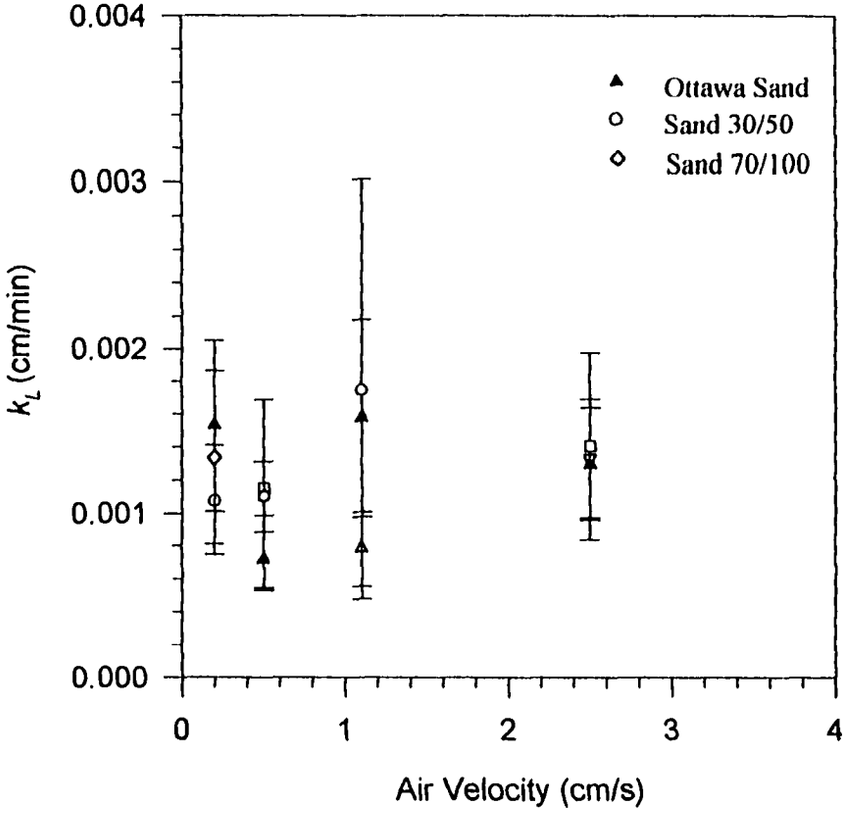

Figure 4. Liquid side mass transfer coefficients as a function of air velocity for different porous media

experimental errors were considered. Another way of visualizing the size of the liquid side film thickness was to compare the δ_w with the grain size of the media. Values presented in Table 3 inferred that δ_w's were approximately 15 to 50 times the grain size of Ottawa sand. Data in Table 3 shows that the liquid phase layer did not penetrate more than 0.9 cm into the porous media. As a result of this lack of mixing, the movement of the VOCs towards the air-water interface will be controlled by the liquid diffusion. In comparison to the *MTZ* as reported in Chapter 3, the thickness of the stagnant liquid layer was between 20% to one order of magnitude smaller than the size of the *MTZ*.

Table 3. Estimated values for δ_w (cm) for Ottawa sand at different flow rates

VOC	0.2 cm/s	0.5 cm/s	1.1 cm/s	2.5 cm/s
Benzene	0.38 ± 0.06	0.81 ± 0.09	0.36 ± 0.07	0.44 ± 0.06
Ethylbenzene	0.30 ± 0.05	0.64 ± 0.08	0.29 ± 0.05	0.36 ± 0.05
m,p-Xylene	0.30 ± 0.05	0.64 ± 0.08	0.29 ± 0.05	0.36 ± 0.05
o-Xylene	0.30 ± 0.05	0.64 ± 0.08	0.29 ± 0.05	0.36 ± 0.05
Toluene	0.33 ± 0.05	0.72 ± 0.08	0.32 ± 0.06	0.39 ± 0.05
Styrene	0.31 ± 0.04	0.66 ± 0.08	0.30 ± 0.05	0.37 + 0.05
n-Propylbenzene	0.29 ± 0.04	0.59 ± 0.07	0.28 ± 0.05	0.32 ± 0.04
Chlorobenzene	0.34 ± 0.06	0.72 ± 0.08	0.27 ± 0.05	0.39 ± 0.05
1,2 DCB	0.31 ± 0.05	0.66 ±0.08	0.30 ± 0.05	0.37 ± 0.06
1,2,4 TCB	0.28 ± 0.05	0.59 ± 0.07	0.27 ± 0.05	0.33 ± 0.04

Conclusions

The controlling mechanisms in the volatilization of VOCs at the air-water interface during air sparging operations were analyzed using the nonequilibrium mass transfer coefficients determined by using a single-air channel setup. Regression analysis of the data showed that the two-resistance model of Whitman may be used to describe the volatilization of VOCs. Unlike the bulk water in reservoirs and rivers, the presence of porous media resulted in the lack of mixing in the liquid phase. This may favor the use of the two-resistance model for the description of liquid phase mass transfer. For VOCs with large Henry's law constants (such as n-propylbenzene), the liquid side film controlled the volatilization at the interface

and may account for more than 90% of the total resistance. For VOCs with low Henry's law constants (such as 1,2,4 trichlorobenzene), air velocity and the mean particle size of the porous media have some impact on the relative magnitude of the gas side film resistance to mass transfer. The air phase resistance may range from 0% to 72% of the total resistance for a compound such as 1,2,4 trichlorobenzene with a low Henry's law constant. Even though gas phase resistance seemed to decrease with higher air velocities, no consistent trends were observed to assess the influence of porous media characteristics on the relative magnitude of the gas side resistance to mass transfer.

Experimental data implies that there was a lack of mixing effect on the liquid side of the air channel. As a result of this, any technological modification of air sparging that would improve the mixing in the liquid phase would likely improve the efficiency of air sparging as a remediation technology. For example, intermittent air injection may result in improvements in VOC removal.

References

Danckwerts, P.V., Significance of liquid-film coefficients in gas adsorption, *Ind. Eng. Chem.*, vol. 43(6), pp. 1460-1467, 1951.

Liss, P.S. and P.G. Slater, Flux gases across the air-sea interface, *Nature*, vol. 247, pp. 181-184, 1974.

Schwarzenbach, R.P., P.M. Gschwend, and D.M. Imboden, *Environmental Organic Chemistry*, p. 218, John Wiley & Sons, Inc., New York, 1993.

Whitman, W.G., The two-film theory of gas absorption, *Chem. Metal Eng.*, vol. 29, pp. 146-150, 1923.

CHAPTER SIX. FATE OF NONAQUEOUS PHASE LIQUIDS UNDER AIR SPARGING CONDITIONS

A paper to be submitted to Journal of Contaminant Hydrology

Washington J. Braida and Say Kee Ong

Abstract

Nonequilibrium air-water mass transfer experiments using a single-air channel setup were conducted to investigate the fate of nonaqueous phase liquids (NAPLs) under air sparging conditions. Chlorobenzene was used as a dense NAPL (DNAPL) while benzene was used as a light NAPL (LNAPL), respectively. Two dimensional isoconcentration profiles drawn from experimental results showed that air sparging may effectively control the spreading of NAPLs plumes and may be used as a remediation technology. The control of the spreading and remediation of the contaminant plume seemed to be more effective for NAPLs with higher solubilities and diffusivities. Removal efficiency for the VOCs was affected by the grain size of the porous media. More than 50% reduction in the removal rate of benzene was found when a porous medium of mean particle size of 0.168 mm was used instead of a porous medium with a mean particle size of 0.305 mm. Experimental results suggest that diffusion of VOC from the NAPL to the air-water interface controlled the mass transfer. Removal efficiencies were independent of air flow rate. According to the results of this study, air sparging may be an effective remedial tool for controlling the contaminant plume. Effective remediation of NAPLs can only be realized if the advective air flow can interact with the NAPL and diffusion limitations can be overcome.

Introduction

In the past few years, the growth of innovative technologies such as air sparging for the remediation of contaminated soil and groundwater has created the need for a deeper understanding of the physical/chemical/biological processes involved during remediation. Organic contaminants may be found dissolved in the groundwater, adsorbed onto the soil

matrix, or present as a separate phase. Free product of organic compounds in the form of nonaqueous phase liquids (NAPLs) may be present in contaminated groundwater close to the source of contamination. NAPLs may be categorized as: dense nonaqueous phase liquid (DNAPLs) which are denser than water and light nonaqueous phase liquid (LNAPLs) which are less dense than water. Organic compounds forming DNAPLs include chlorinated hydrocarbons while petroleum products and low molecular weight hydrocarbons tend to form LNAPLs. As a result of gravity and capillary forces NAPLs move through the unsaturated zone downward and laterally. Once they reach the water table, LNAPLs will spread on the freatic surface while DNAPLs may continue to migrate below the water table and into the aquifer.

Pump-and-treat technology has been shown to be ineffective in the remediation of NAPLs. Thus, alternative remedial technologies such as in situ air sparging has been the focus of much research recently for the remediation of NAPLs. Although air sparging has been used as a remedial technology for sites containing NAPLs, not much is known about the effect of air sparging on the fate and spreading of NAPLs in the saturated porous media.

Using a laboratory-scale air sparging system, Johnson et al. (1997) reported that the removal efficiency of NAPLs increased with pulsed air injection and for compounds with high solubilities but was not affected by an increase in air velocities. As expected, the authors observed low removal rates for chemicals located away from the air channels. McCray and Falta (1997) searching for more accurate means to define the radius of influence of sparging wells, reported that the effective zone for NAPL remediation would overlap the regions of high air saturations. Wilkins et al. (1995) reported that the rate of volatilization of NAPLs in unsaturated porous media was dependent on the air velocity, the diffusivity of the organic compound in air, and the porous media mean particle size.

The physical-chemical behavior of NAPLs in an aquifer is expected to be different from the behavior of the dissolved product. For example, under air sparging conditions, partitioning of organic compounds between NAPLs and the advective air stream is expected to be governed by Raoult's law rather than Henry's law. Besides the direct volatilization of NAPLs, the fate and distribution of NAPLs in porous media is also dependent on the dissolution of the NAPL. Several researchers have conducted simple visualization

experiments to study the distribution of NAPLs in porous media (Kennedy and Lennox, 1997; Schroth et al., 1995; Zhou and Blunt, 1997; Conrad et al., 1992), while others have investigated the dissolution of NAPLs in saturated porous media. Miller et al. (1990) found that the local equilibrium assumption may be used to describe the dissolution of toluene NAPLs in glass beads over a wide range of NAPL saturation and groundwater flow. Powers et al. (1992, 1994) reported that NAPLs dissolution rates for steady state conditions were dependent on the distribution pattern of the NAPLs as well as the aqueous phase velocity. For the transient conditions, Powers and coworkers found that mass transfer was related to the porous media properties, aqueous phase Reynolds number, and volumetric fraction of the NAPL.

In summary, the fate and transport of NAPLs in the saturated zone is a complex issue. Mass removal of NAPLs using air sparging may be affected by the dissolution characteristics of the NAPL and by the diffusivity of the dissolved product in the aqueous phase. Research on the behavior of NAPLs under air sparging conditions is fairly scarce in the literature. The objective of this study was to improve our conceptual understanding of the behavior of NAPLs under air sparging conditions by qualitatively investigate the dissolution, diffusion, and volatilization behavior of LNAPLs and DNAPLs by using a single-air channel setup. Experiments were designed to show the impact of air flow rate, type of porous media, and chemical type on the removal and control of plume spreading during air sparging.

Materials and Methods

The dissolution and volatilization patterns of NAPLs under air sparging conditions were investigated using a single-air channel setup (Braida and Ong, 1997a, 1997b). The experimental setup consisted of a box made of thick Plexiglas ™ in which air was circulated in a single air channel, 1.58 mm thick, over saturated porous media. A sketch of the experimental setup is shown in Figure 1. Even though the air flow was directed horizontally over the porous media, the experimental setup was designed to reproduce the air flow in air channels. The experimental setup allowed a 2-D visualization of NAPL dissolution and spreading in porous media under air sparging conditions. The VOCs concentrations in water were measured by using 15 sampling points placed across the experimental setup as shown.

A sampling point to measure the VOC concentration in the exhaust line of the experimental setup was also included.

In-house compressed air was filtered and then humidified before being used as sparging gas. Air flow was measured using a Gilmont Model 11 flowmeter (Barrington, IL). The porous media used were sand 30/50 and sand 70/100 from U.S. Silica Company (Ottawa, IL) with mean particle size of 0.305 mm and 0.168 mm, and uniformity coefficients of 1.41 and 1.64, respectively. Organic carbon contents were determined using the Walkley-Black procedure (Nelson and Sommers, 1982) and were found to be less than 0.007% for both porous media.

In a typical experiment, the porous media were mixed with distilled water and the slurry was then carefully packed layer by layer into the reactor to minimize the formation of air pockets. The resulting porosity of the packed media was 0.37 for the sand 30/50 and 0.4 for the sand 70/100. The top cover was then secured to provide an air gap of 1.58 mm above the porous media. The air gap was within the size of air channels (10-20 pore sizes) observed by others (Ji et al., 1993)

Two organic compounds were used. They were benzene for LNAPL and chlorobenzene for DNAPL. Both chemicals were of HPLC grade purchased from Sigma-Aldrich Chemical Company Inc. (Milwaukee, WI). NAPLs were created by injecting 60 μL of the chemical into the reactor. This represents a total mass of 52 mg for benzene and 66 mg for chlorobenzene. The NAPL was placed at approximately 19 mm below the air-water interface, 88.9 mm from the air inlet, and 25 mm from the front and back side walls. Experiments were conducted with no aeration, and with air flow rates of 27.5 and 68 mL/min. The experimental setup was kept a constant temperature of $21 \pm 2^{\circ}C$. A summary of the experimental matrix is shown in Table 1.

The VOC concentration in the air phase and in the liquid phase were measured with a Hewlett-Packard 5890 Series II gas chromatograph (Avondale, PA) equipped with a HP-5 capillary column and a flame ionization detector. Air phase concentration was determined by direct injection of 1 mL sample of exhaust air while the liquid phase concentration was measured using the head-space technique. For the head-space technique, 25 μL of an aqueous sample was placed in a 1.8 mL aluminum crimp cap vial. After equilibrium was

reached, the head-space concentration was measured and the aqueous concentration was estimated from the measured head space concentration. Aqueous phase samples were collected at the start of the experimental run, 24 hours, 48 hours, and 72 hours.

Results and Discussion

Based on the measured aqueous concentrations, two dimensional isoconcentration lines for the porous media were drawn by kriging using the Surfer 5.03 software package (Golden Software Inc., Golden, CO). Figure 2 shows two examples of isoconcentration lines and the measured concentrations. In this chapter, isoconcentration lines will be used to provide a qualitative assessment of the behavior of NAPLs under different air sparging conditions. The isoconcentration lines at various times throughout the experimental run are presented in Figures 3 to 8. An infinite point source with a concentration equal to the VOC solubility was assumed for the computations.

Stagnant air conditions

Figures 3a, 3b, and 3c show the changes in the dissolved benzene concentrations for sand 30/50 and zero air flow for 0, 24 and 48 hours, respectively. Figures 4a, 4b, 4c, and 4d show the results for chlorobenzene under the same conditions. For benzene, an almost symmetrical diffusion of benzene from the NAPL was seen after 24 hours. However, after 48 hours, an asymmetric distribution was evident. The vertical spreading was found to be less than the lateral spreading. Benzene concentrations at the air-water interface was between 100 to 500 mg/L directly above the location of the NAPL. At 48 hours, the lower isoconcentration line (1 mg/L) of the plume did not extend any further and was similar to that at 24 hours. Lateral diffusion clearly dominated over the downward vertical movement of benzene. This may indicate that volatilization at the air-water interface and, to certain extent, the buoyancy characteristics of the NAPL had an influence on the diffusion of the dissolved benzene in saturated porous media. On the other hand, chlorobenzene, a DNAPL, under the same experimental conditions, seemed to show a different behavior (see Figures 4a, 4b, 4c, and 4d). Chlorobenzene, with a solubility three times lower than benzene and a diffusivity 12% lower than benzene, seemed to diffuse further and more uniformly than benzene. Figure

4b shows that after 24 hours, the isoconcentration lines were fairly symmetrical around the point source. The 1 mg/L isoconcentration line covered more than 85 % of the experimental setup volume after 24 hours but unlike benzene NAPL, the maximum concentration at the air-water interface was not greater than 50 mg/L (compare Figure 3c with Figure 4c). The 25 mg/L isoconcentration line were located further laterally but the downward spreading seemed to be less extensive which may be due to the bottom wall of the reactor. After 72 hours (see Figure 4d), the 25 mg/L isoconcentration line covered approximately 65% of the experimental setup. The heavier density but less volatile nature of chlorobenzene appeared to have an influence on the diffusion of the dissolved product resulting in a more symmetrical diffusion around the point source.

Influence of air flow rate

The impact of air flow rate on the distribution of benzene and chlorobenzene is presented in Figure 5 and Figure 7, respectively. The isoconcentration line without air flow and with an air flow rate of 27.5 mL/min were fairly similar (compare Figures 3b and 5b). However, with an air flow rate, the plume did not change much with time and diffusion of benzene was limited to the upper central part of the experimental setup (see Figure 5b and Figure 5c). The influence of air flow at the air-water interface was evident and can be seen to be controlling the migration of the LNAPL plumes. Even after 72 hours, the plume remained the same, indicating that a quasi steady-state condition was reached whereby a balance was achieved between the dissolution and diffusion of benzene and the volatilization at the air-water interface.

With a higher flow rate (68 mL/min) the distribution of benzene isoconcentration lines was similar to that for an air flow rate of 27.5 mL/min (compare Figure 5b with Figure 6b). This shows that air flow rate had negligible influence on the distribution and dissolution of the NAPL. This may be due to the lack of physical contact between the NAPL and the advective air stream. Because of the lack of physical contact with the LNAPL, volatilization of benzene would be controlled by the diffusion of benzene. Therefore, as seen in Figures 6c and 6d, the distribution of the isoconcentration lines was similar to that of Figures 5c and 5d. The above results showed that when a LNAPL is located several centimeters from the air

channel, LNAPL volatilization was independent of the air flow rate. This behavior seemed to be in agreement with the work done by Johnson et al. (1997). Further evidence supporting this observation will be presented later.

Similarly, as for benzene, air sparging seemed to control the spreading of chlorobenzene NAPL. Examination of the isoconcentration lines for 1 mg/L and 25 mg/L in Figures 4b (no air flow) and Figure 7b (with an air flow rate of 27.5 mL/min) showed that chlorobenzene diffused farther from the point source in the absence of air flow. Figures 7c and 7d showed that the 50 mg/L isoconcentration line for chlorobenzene remained fairly the same. At the air-water interface the concentration of chlorobenzene was lower with air flow. This is due to volatilization at the air-water interface.

Influence of porous media

The influence of porous media on the distribution of benzene can be seen by comparing Figure 5 and Figure 8. Figure 8 presents the result for sparging benzene NAPL at a flow rate of 27.5 mL/min with sand 70/100 as a porous media. Sand 70/100 has a smaller mean particle size (0.168 mm) as compared to sand 30/50 (0.305 mm) but with a higher porosity (0.4 as compared to 0.37 for sand 30/50). In general, the experimental results showed that benzene tend to diffuse further laterally and vertically downward from the air-water interface in sand 70/100 (Figures 8b and 8c) as compared with sand 30/50. Figure 8 clearly showed that the size of the porous media affected the diffusion of the benzene to the air-water interface and therefore resulted in less volatilization at the air-water interface. This situation resulted in more spreading of the dissolved phase away from the air-water interface. Further evidence in terms of mass removed, supporting this observation will be presented later in Figure 9.

VOC removal efficiency

Figures 9a and 9b present the concentration of benzene and chlorobenzene in the exhaust air for the experimental conditions tested. The influence of a porous media particle size on the volatilization is evident in Figure 9a. For sand 30/50, the peak benzene concentration appeared approximately 60 hours after air sparging started. In contrast, the peak benzene

concentration for the sand 70/100 was attained only after 90 hours of sparging. In addition, the peak concentration for sand 30/50 was almost 3 times larger than the sand 70/100. The peak concentration for an air flow rate of 68 mL/min was 3 times smaller than for an air flow rate of 27.5 mL/min. The chlorobenzene concentration in the exhaust air was lower than that for benzene even though the porous media and air flow rate were the same (see Figure 9b). The concentration of chlorobenzene in the exhaust air ranged between 0.08 mg/L and 0.12 mg/L after 30 hours of sparging. The lower chlorobenzene concentrations may be related to four possible factors: (i) the higher density of chlorobenzene, (ii) a lower solubility compared with benzene (515 mg/L against 1780 mg/L), (iii) a lower Henry's law constant (0.137 against 0.197), and (iv) a lower diffusion coefficient (8.52×10^{-6} cm^2s^{-1} against 9.59×10^{-6} cm^2s^{-1})

Mass removal efficiency over time for the different experiments are shown in Figure 9c. For sand 30/50 with an air flow rate of 27.5 mL/min, mass removal efficiency after 120 hours was approximately 82%. With a higher air flow rate of 68 mL/min, an initial higher removal efficiency was obtained but after 144 hours the mass removal efficiencies for both air flow rates were similar. This result clearly shows that mass removal for NAPL located close to an air channel was independent of the air flow rate but depends on the liquid diffusion of the dissolved phase. For a finer porous media (sand 70/100), the mass removed was only 34%. The increase in the diffusion pathway for benzene in a porous media with a smaller mean particle size may be a reason for the lower removal efficiency. For chlorobenzene the removal efficiency after 120 hours of sparging was found to be just 29%. These results along with the isoconcentration plots suggest that the solubility of the compound may also have an influence on the effectiveness of air sparging of NAPLs. The visualization study showed that LNAPLs and DNAPLs behave differently under air sparging conditions. The spreading of LNAPLs, in this case benzene, seemed to be better controlled by air sparging than DNAPL, in this case chlorobenzene. This behavior may be due to the differences in solubility and diffusivity between benzene and chlorobenzene rather than the differences in density. Results from this study seemed to indicate that air flow may enhance diffusion and therefore indirectly affect NAPL dissolution but increasing the air flow rate did not increase the overall mass removal.

Conclusions

The fate of NAPLs under air sparging conditions was investigated using a laboratory-scale single-air channel setup. The study showed that the presence of advective air flow in air channels during air sparging has an effect and may control the spreading of the dissolved phase of NAPLs. The control of the spreading and remediation of the contaminant plume seemed to be more effective for NAPLs with higher solubilities and diffusivities. Removal efficiency was seriously impacted by the grain size of the porous media. More than 50% reduction in the removal of benzene was found when the mean particle size for the porous media was reduced from 0.305 mm to 0.168 mm. Removal efficiency was found to be independent of air flow rate. This suggests that for a NAPL located several centimeters away from the air-water interface, diffusion of VOC will control the volatilization and remediation of the NAPL.

In summary, this study showed that if a NAPL is not in direct contact with the air channel but several centimeters away from the air channel, air sparging may be an effective remedial tool in controlling the size of the dissolved phase around the NAPL.

References

Braida, W.J., and S.K. Ong, Air sparging effectiveness: the air channel mass transfer zone, submitted to *Water Resources Research*, 1997a.

Braida, W.J., and S.K. Ong, Air sparging: air-water mass transfer coefficients, submitted to *Water Resources Research*, 1997b.

Conrad, S.H., J.L. Wilson, W.R. Mason, and W.J. Peplinski, Visualization of residual organic trapped in aquifers, *Water Resources Research*, vol. 28(2), pp. 467-478, 1992.

Ji, W., A. Dahmani, D.P. Ahlfeld, J.D. Lin, and E. Hill, Laboratory study of air sparging: Air flow visualization, *GWMR*, vol. 13(4), pp. 115-126, 1993.

Johnson, P.C., A. Das, R.L. Johnson, A. Leeson, D. McWhorter, and R. Hinchee, Effects of IAS process changes on the removal of immiscible-phase hydrocarbons, in *Proceedings of the Four International In Situ and On-Site Bioremediation Symposium*, vol. 1, pp. 135-140, New Orleans, LA, April 28-May 1st, 1997.

Kennedy, A.C., and W. Lennox, A pore-scale investigation of mass transport from dissolving DNPL droplets, *Journal of Contaminant Hydrology*, vol. 24, pp. 221-246, 1997.

McCray, J.E., and R.W. Falta, Numerical simulation of air sparging for remediation of NAPL contamination, *Ground Water*, vol. 35(1), pp. 99-110, 1997.

Miller, C.T., M.M. Poirier-McNeil, and A.S. Mayer, Dissolution of trapped nonaqueous phase liquids: mass transfer characteristics, *Water Resources Research*, vol. 26(11), pp. 2783-2796, 1990.

Nelson, D.W., and L.E. Sommers, Total carbon, organic carbon, and organic matter, in *Methods of Soil Analysis, Part 2, Chemical and Microbiological Properties*, Second Edition, edited by A. L. Page, pp. 570-571, American Society of Agronomy, Inc., Soil Science Society of America, Inc., Madison, WI, 1982.

Powers, S.E., L.M. Abriola, and W.J. Weber Jr., An experimental investigation of nonaqueous phase liquid dissolution in saturated subsurface systems: steady state mass transfer rates, *Water Resources Research*, vol. 28(10), pp. 2691-2705, 1992.

Powers, S.E., L.M. Abriola, and W.J. Weber Jr., An experimental investigation of nonaqueous phase liquid dissolution in saturated subsurface systems: transient mass transfer rates, *Water Resources Research*, vol. 30(2), pp. 321-332, 1994.

Schroth, M.H., J.D. Istok, S.J. Ahearn, and J.S. Selker, Geometry and position of light nonaqueous-phase liquid lenses in water-wetted porous media, *Journal of Contaminant Hydrology*, vol. 19, pp. 269-287, 1995.

Wilkins, M.D., L.M. Abriola, and K.D. Pennel, An experimental investigation of rate-limited nonaqueous volatilization in unsaturated porous media: steady state mass transfer, *Water Resources Research*, vol. 31(9), pp. 2159-2172, 1995.

Zhou, D., and M. Blunt, Effect of spreading coefficient on the distribution of light non-aqueous phase liquid in the subsurface, *Journal of Contaminant Hydrology*, vol. 25, pp. 1-19, 1997.

Table 1. Experimental matrix

Experiment Number	NAPL	Aeration Rate (mL/min)	Porous Media
1	Benzene	Stagnant	30/50
2	Benzene	27.5	30/50
3	Benzene	27.5	70/100
4	Benzene	68	30/50
5	Chlorobenzene	Stagnant	30/50
6	Chlorobenzene	27.5	30/50

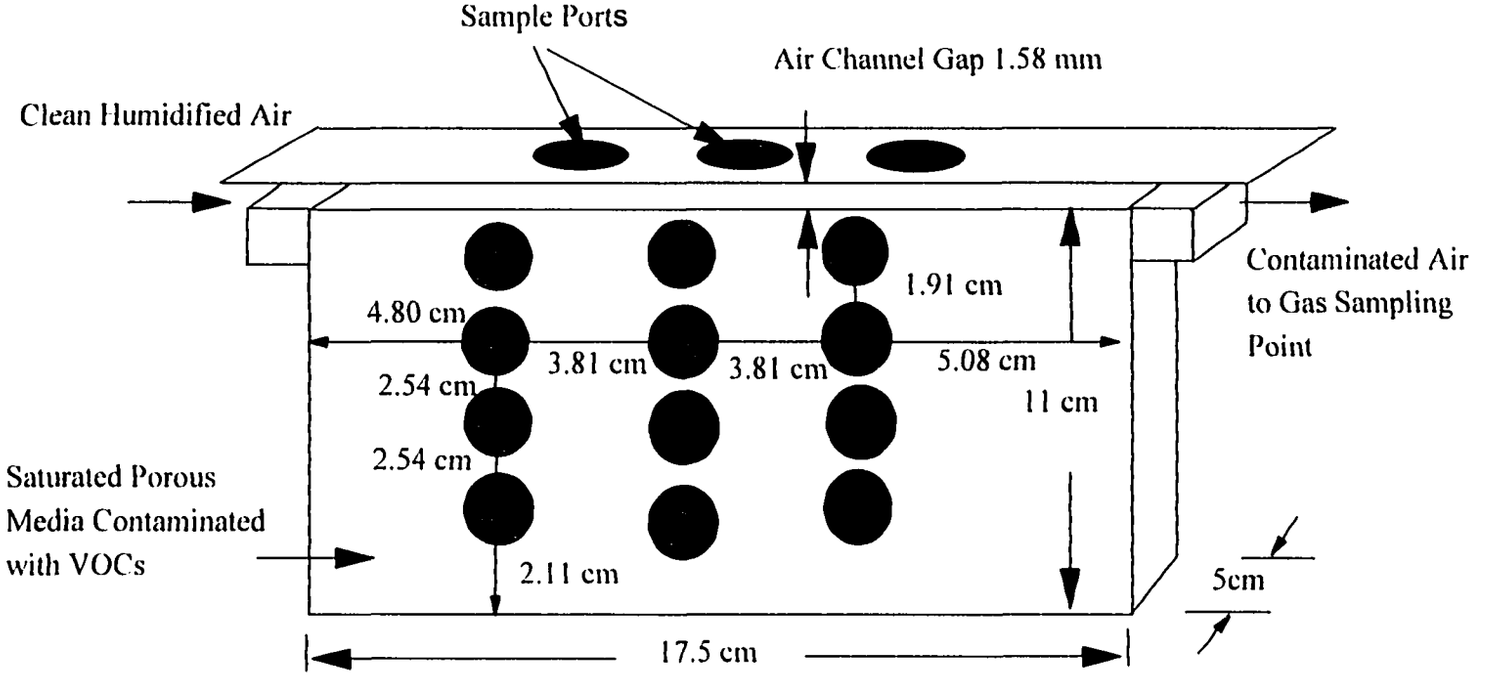

Figure 1. Single-air channel apparatus

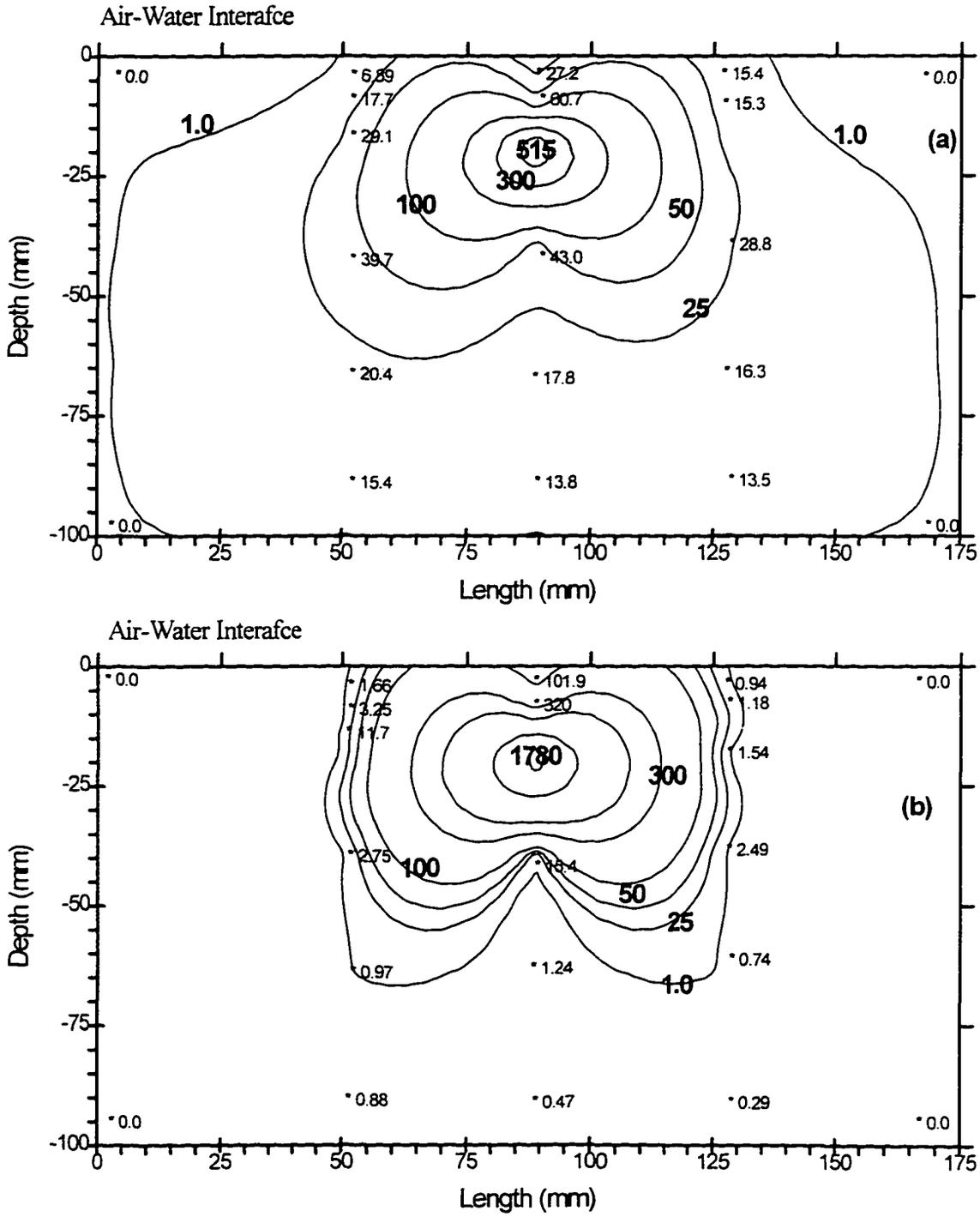

Figure 2. Isoconcentration lines (mg/L) and actual VOC concentrations, (a) chlorobenzene NAPL in sand 30/50 after 24 hours with no air flow, (b) benzene NAPL in sand 30/50 after 24 hours with an air flow rate of 68 mL/min

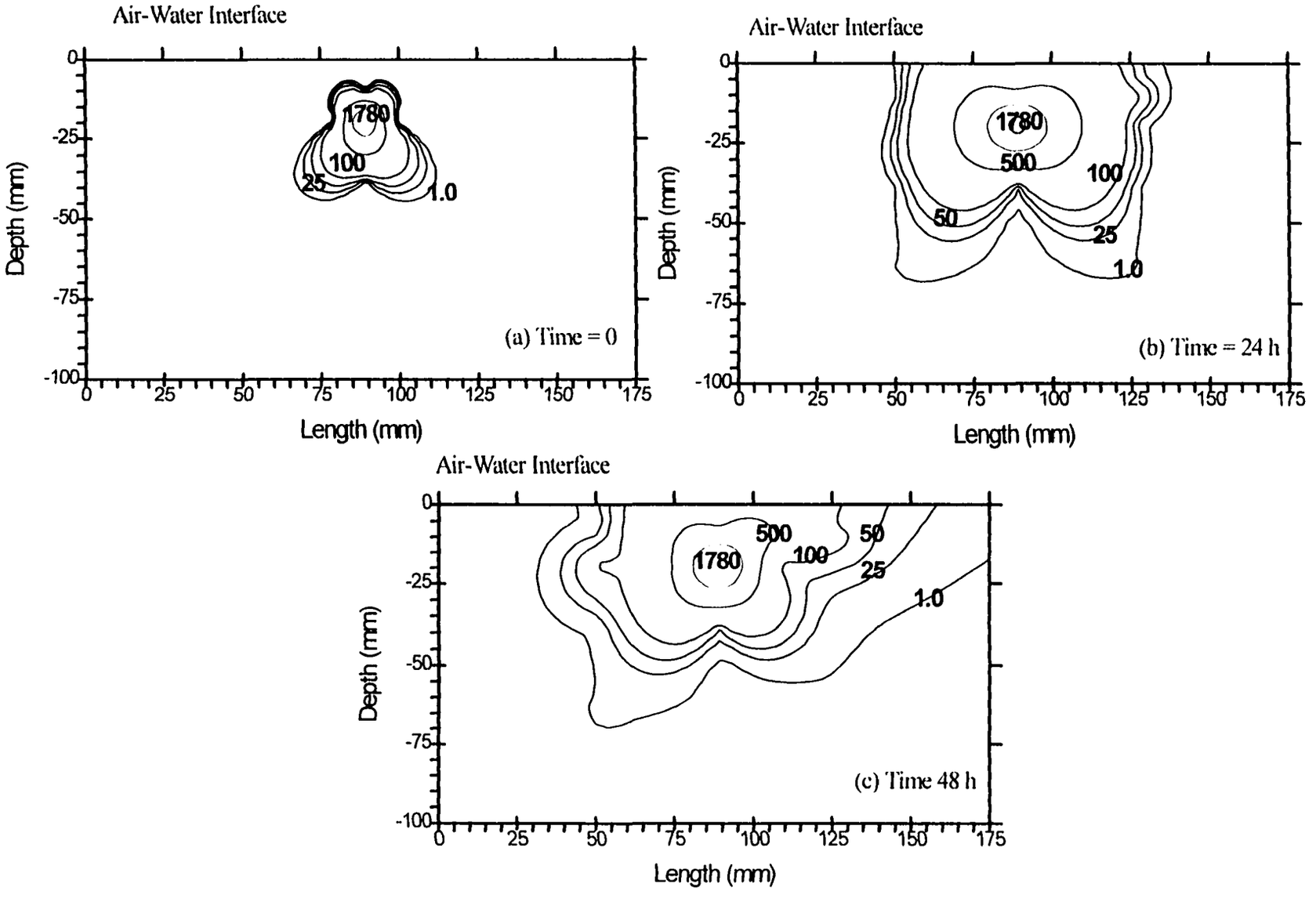

Figure 3. Isoconcentration lines (mg/L) for benzene NAPL in sand 30/50 and zero air flow.

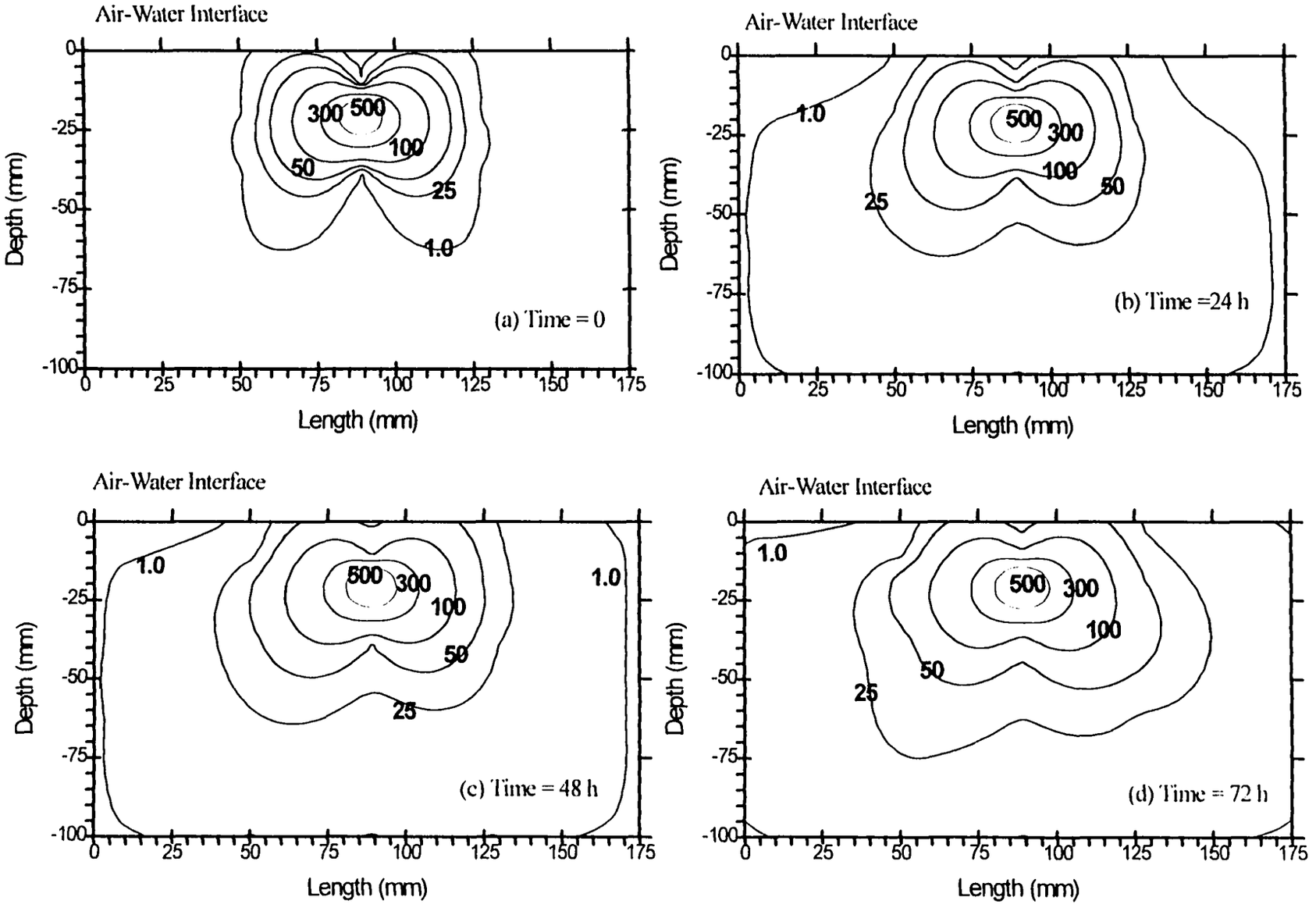

Figure 4. Isoconcentration lines (mg/L) for chlorobenzene NAPL in sand 30/50 and zero air flow.

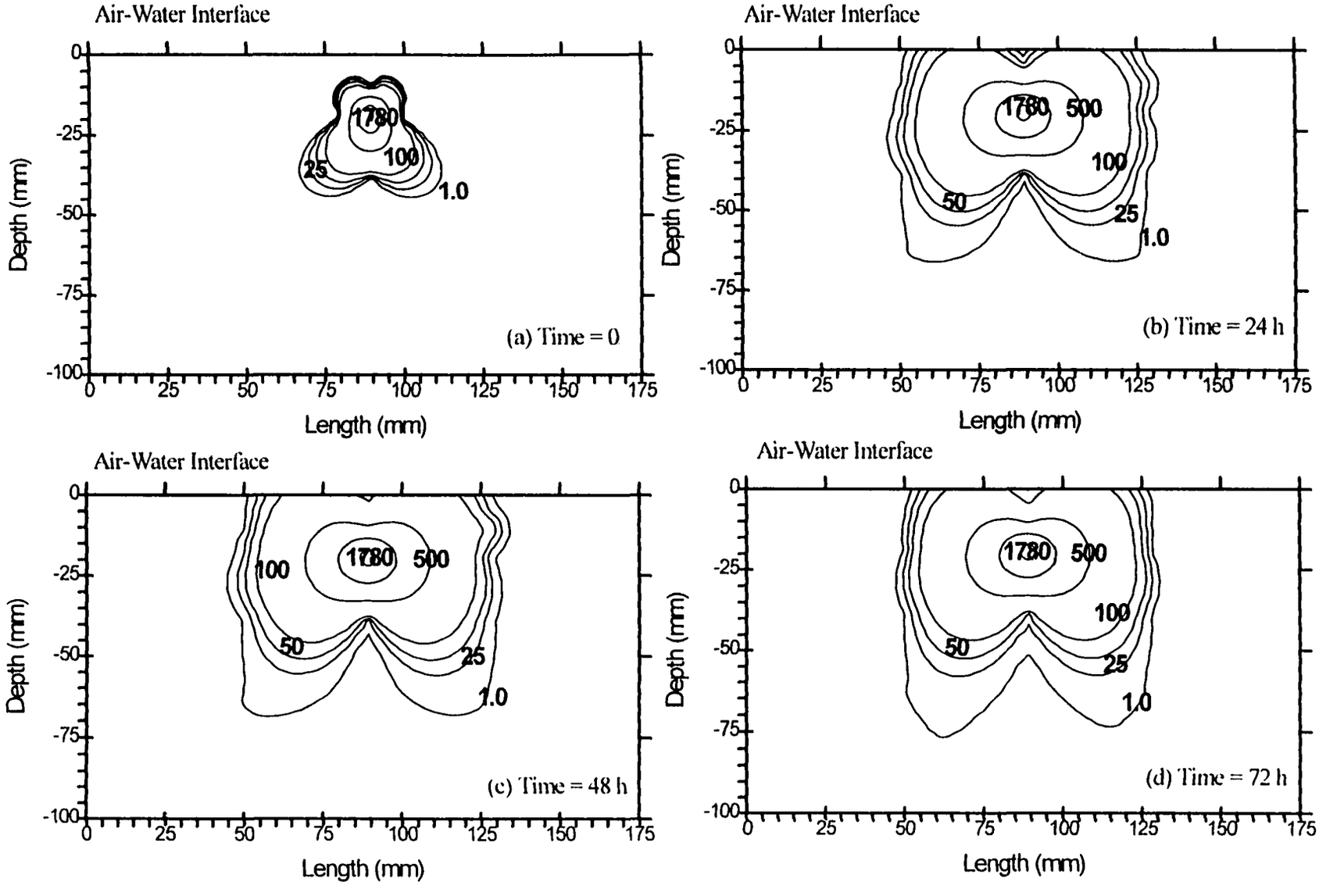

Figure 5. Isoconcentration lines for benzene NAPL in sand 30/50 and for an air flow rate of 27.5 ml /min.

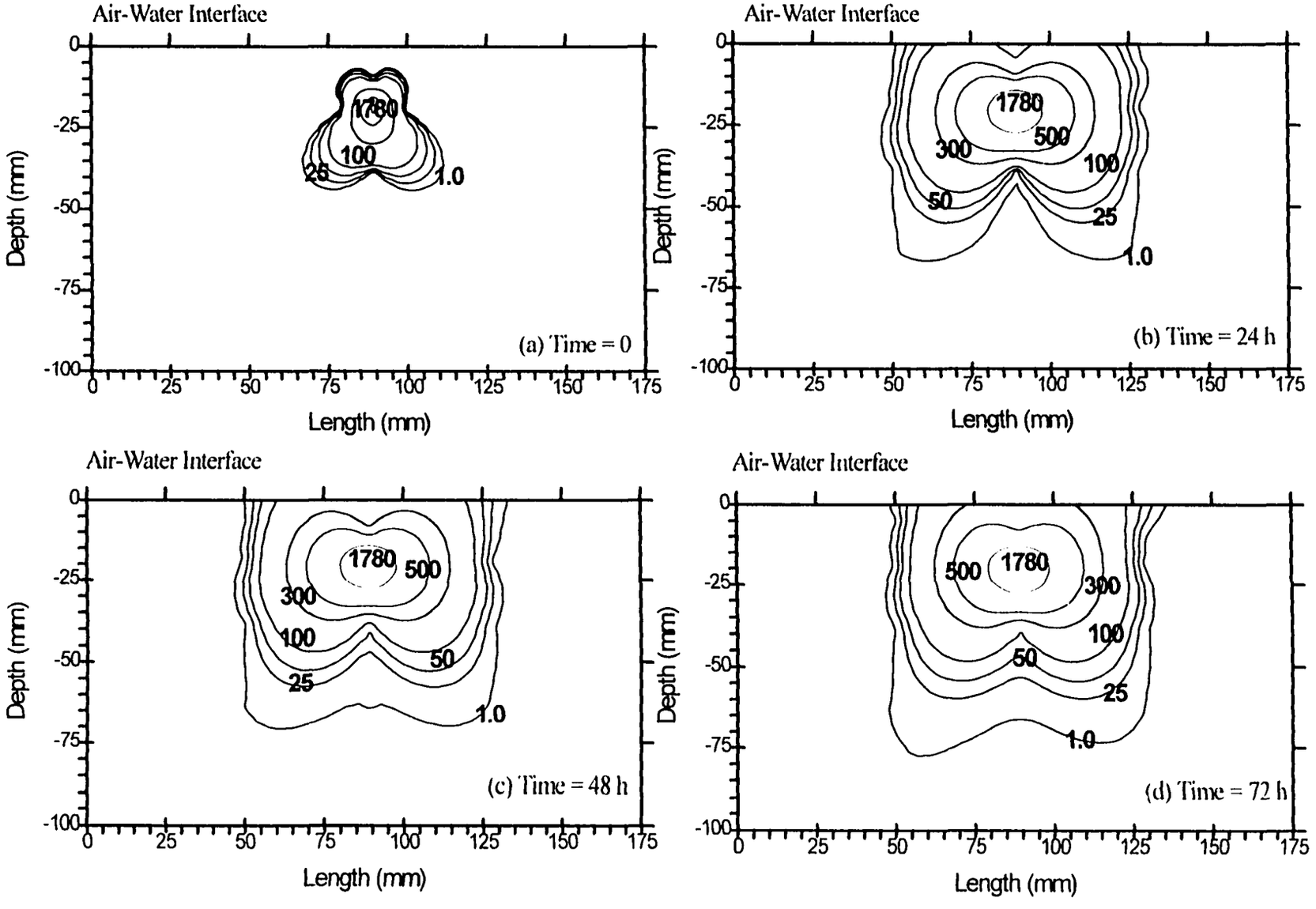

Figure 6. Isoconcentration lines for benzene NAPL in sand 30/50 for an air flow rate of 68 ml/min.

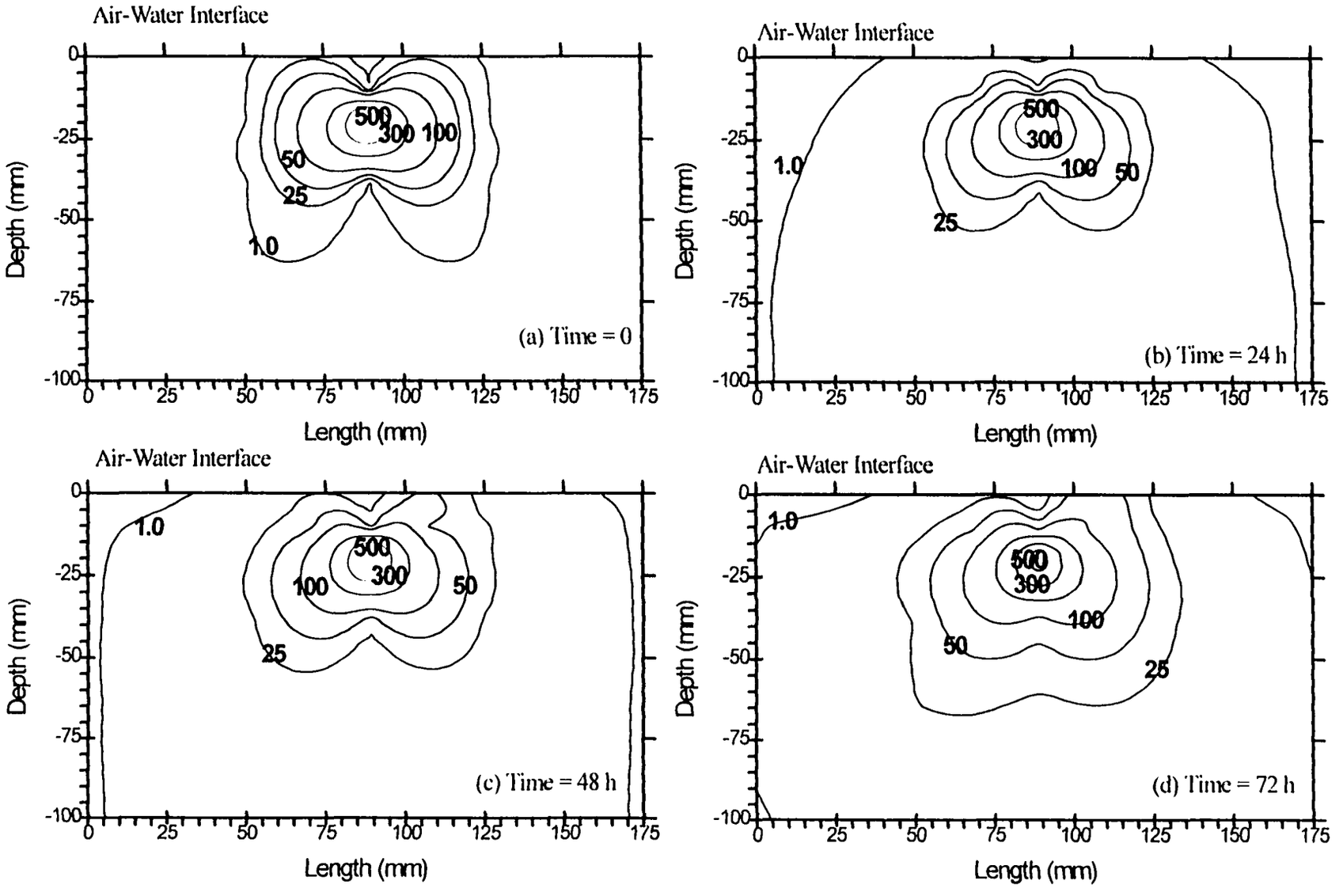

Figure 7. Isoconcentration lines (mg/L) for chlorobenzene NAPL in sand 30/50 and for an air flow rate of 27.5 ml /min.

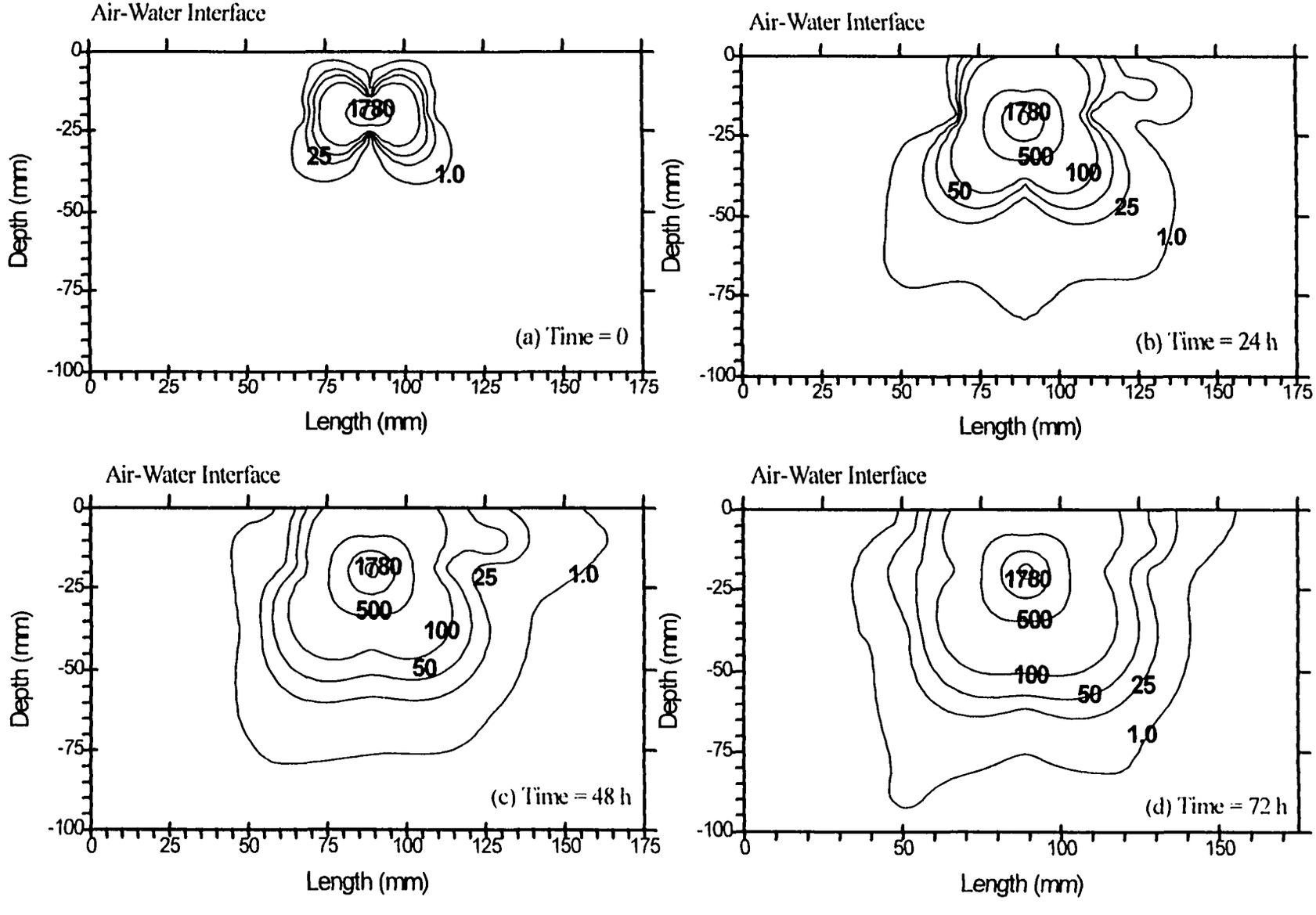

Figure 8. Isoconcentration lines for benzene NAPL in sand 70/100 and for an air flow rate of 27.5 ml /min.

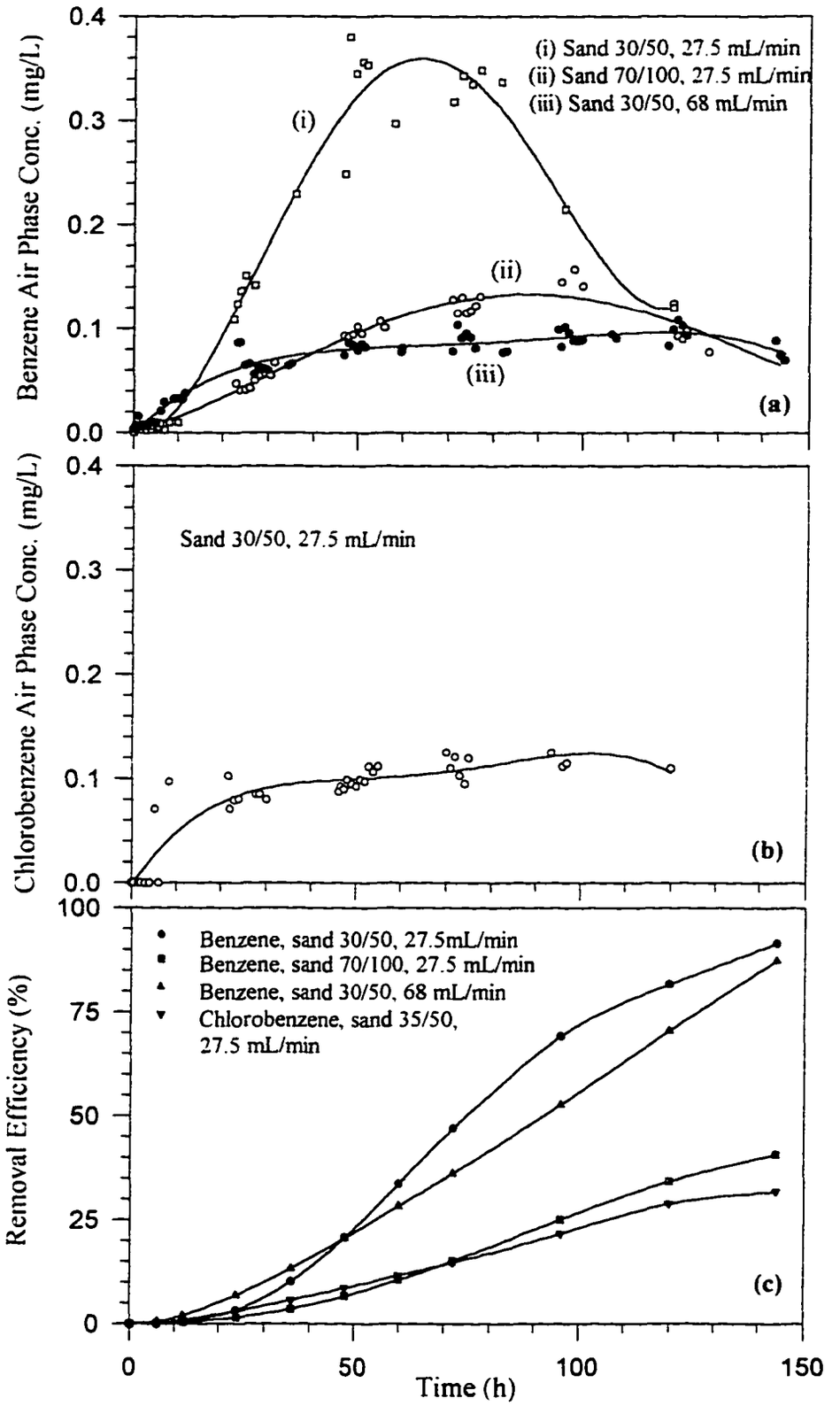

Figure 9. VOC concentration in the exhaust gas and VOC removal efficiency

CHAPTER SEVEN. INFLUENCE OF SORPTION-DESORPTION PROCESSES ON AIR SPARGING EFFECTIVENESS

A paper to be submitted to Journal of Contaminant Hydrology

Washington J. Braida, and Say Kee Ong

Abstract

Air sparging is a remediation technology which has been used for more than 10 years for the remediation of VOC-contaminated aquifers. Although it has been applied extensively in the field, an understanding of the controlling processes during air sparging is lacking. Using a single-air channel apparatus, the size of the air channel mass transfer zone (*MTZ*) was found to decrease with increasing organic carbon content of the porous media. This effect was larger for VOCs with low solubilities and high partition coefficients. A one-dimensional diffusion model, modified to include the retardation in the VOC transport as a result of partitioning between the liquid and solid phases, was found to predict the concentration curves for the liquid phase and the exhaust air fairly well. Experimental evidence suggest that sorbed VOCs were not substantially remediated using air sparging.

Introduction

Air sparging is a remediation technique which is potentially applicable for the remediation of aquifers contaminated with volatile organic compounds (VOCs). Air sparging involves the injection of air under pressure into the saturated zone to volatilize VOCs and at the same time, promote the biodegradation of contaminants present beneath the water table and in the unsaturated zone.

Much of the information on the volatilization of VOCs from bulk water may be applicable for air sparging systems. However, the presence of porous media introduces several barriers which may affect the volatilization of VOCs. These barriers include the extra distance VOCs must travel to reach the air-water interface, and the sorption-desorption of the VOCs onto the soil matrix. Braida and Ong (1997a) showed experimentally that mass transfer under air

sparging conditions was diffusion limited and that after a certain period of time, a mass transfer zone (*MTZ*) with a steep concentration gradient developed around the air channels. Beyond the *MTZ*, the VOC concentration was almost unaffected by the air flow. For soil media with high VOC affinity, sorption-desorption of VOCs onto the soil particles may also play a role in controlling the rate of mass transfer.

Sorption of VOCs onto soil may be modeled using a linear equilibrium isotherm:

$$C_S = K_d C_w \tag{1}$$

where C_S represents the concentration of the VOCs sorbed onto the soil matrix (MM^{-1}), C_w is the concentration of VOC in the liquid phase (ML^{-3}), and K_d is the linear partition coefficient (L^3M^{-1}). The linear isotherm has been widely used to describe the sorption of VOCs in the subsurface (Gierke et al., 1990, Ong and Lion, 1991). Karickhoff (1984) suggested that use of linear isotherms is a reasonable assumption for contaminant concentrations less than 10^{-5} M or less than half the water solubility of the organic contaminant.

Sorption of VOC onto soils has been related with the organic matter content of the porous media as follows (Karickhoff, 1984):

$$K_d = f_{oc} K_{oc} \tag{2}$$

where f_{oc} is the mass fraction of organic carbon in the soil and K_{oc} is the organic carbon partition coefficient (L^3M^{-1}). Equation 1 is valid for $f_{oc} > 0.001$.

Most organic contaminants are rapidly sorbed onto soils but desorption can be very slow. Batch desorption experiments by Pavlostathis and Mathavan (1992) showed that a substantial fraction of sorbed contaminant resisted desorption in deionized water-soil mixtures for more than 7 days.

The sorption-desorption phenomenon tends to reduce the overall removal efficiency of remediation technologies such as air sparging. Air sparging studies by Chao (1997) using bench-scale soil columns showed that after the VOC concentration in the exhaust gas fall below detection limits, a large fraction of initial mass of VOCs remained sorbed to the

porous media. In an air sparging study at a site contaminated with ethylbenzene and xylenes. Kraus et al. (1997) reported that even though the aqueous phase VOC concentration in monitoring wells was reduced by four orders of magnitude, analysis of the soils indicated that there was no statistically significant reduction of ethylbenzene and xylenes.

The objective of this study was to assess the influence of the sorption phenomenon on the performance of air sparging systems. A single-air channel experimental setup was used to study the influence of the organic carbon content of the porous media on the effectiveness of air sparging by evaluating changes in size of the *MTZ* and mass transfer parameters.

Materials and Methods

To investigate the influence of the sorption-desorption phenomenon under air sparging conditions, a single air channel setup was used (Braida and Ong, 1997a, 1997b, and 1997c). The experimental setup consisted of a box made of thick Plexiglas ™ sheets in which air was circulated in a single air channel over saturated porous media. The size of the air channel was fixed at 1.58 mm. The experimental setup reproduced the physical nature of the air flow in saturated porous media and allowed a visualization of the VOC concentration profiles near the air channel. In order to monitor the aqueous phase concentration of the VOCs in the porous media, 15 sampling points across the porous media were included. A sampling point to measure the VOC concentration in the exhaust gas was also included. A sketch of the experimental setup is shown in Figure 1.

In-house compressed air was filtered and then humidified before being used as sparging gas. Air flow was measured using a Gilmont Model 11 flowmeter (Barrington, IL). The experiments were conducted using three VOCs, and type of porous media with three different organic carbon contents. The VOCs used were benzene, ethylbenzene, and n-propylbenzene. Ottawa sand (U.S. Silica Company, Ottawa, IL) was used as porous media with an organic carbon content of less than 0.01%. The mean particle size of the Ottawa sand was 0.190 mm with an uniformity coefficient of 2.16. Using Ottawa sand, two other organic contents were prepared by coating the Ottawa sand with humic acid (Sigma-Aldrich Chemical Co, Inc., Milwaukee, WI). The organic carbon contents of the porous media were 0.04%a and 0.45%. The coating procedure followed that of Garbarini and Lion (1985). Eleven grams of humic

acid were dissolved in one liter of Nanopure™ water at a pH of 10. The pH was raised with a 0.25M NaOH solution. About 950 grams of Ottawa sand was added and the mixture was stirred continuously with the pH of the mixture gradually lowered to 4.0 with 0.25 M nitric acid. The suspension was allowed to stand for 48 hours after which the supernatant was decanted and the porous media rinsed several times with Nanopure™ adjusted to pH 4. The porous media was then air dried. Organic carbon content of the sand was determined using the Walkley-Black procedure (Nelson and Sommers, 1982).

Partition coefficients of the three VOCs for the three porous media were determined using the head-space technique described by Garbarini and Lion (1985). Linear partition coefficients ranged between 0.025 mL/g and 1.00 mL/g and are presented in Table 1.

Aqueous solutions containing the three VOCs were prepared using HPLC grade chemicals and their concentrations ranged between 4 mg/L and 76 mg/L. All chemicals were purchased from Sigma-Aldrich Chemical Company Inc. (Milwaukee, WI). A slurry was made by carefully mixing the porous media with the aqueous VOC solution and allowed to equilibrate for 16 hours. After the equilibration time, the slurry was transferred to the reactor and was rapidly packed layer by layer to avoid entrapment of air bubbles. The reactor was sealed immediately to minimize VOCs losses. A small quantity of the slurry was retained and analyzed for VOCs. The resulting porosity of the packed media was 0.377. Aqueous samples were then taken from the various sampling points to determine the initial aqueous phase concentrations in the porous media. Air was then circulated through the air channel. The air velocity used was 1.1 cm/s. The temperature of the experimental setup was maintained at $(21 \pm 2)^{\circ}C$.

The VOC concentrations in the air phase and in the liquid phase were measured with a Hewlett-Packard 5890 Series II gas chromatograph (Avondale, PA) equipped with a HP-5 capillary column and a flame ionization detector. Air phase concentration was determined by direct injection of a 1 mL sample while liquid phase concentration was measured using the head-space technique. For the head space technique, 25 µL of an aqueous sample was placed in a 1.8 mL aluminum crimp cap vial and the aqueous concentration estimated from the measured head space concentration after equilibrium was reached.

At the end of the experiments, samples of the porous media samples were collected from

different depths in the reactor and analyzed for sorbed VOC concentration. VOCs in the porous media was extracted using hexane. A 1:3 (w/w) mixture of hexane and wet soil was used with an extraction time of 12 hours. An aliquot of the supernatant was placed in a 1.8 mL glass vial capped with PTFE-faced silicone septa. VOCs in the sample were quantified by direct injection of the supernatant into the gas chromatograph. Mass of VOC sorbed on the porous media was estimated by subtracting the mass in the aqueous phase remaining in the wet soil from the mass extracted from the wet soil.

Results and Discussion

Figure 2 shows the change in the relative concentration of benzene, ethylbenzene, and n-propylbenzene in the exhaust air for the three porous media. The relative air phase concentration of benzene were not significantly affected by the presence of organic matter in the porous media. However, the different air phase concentration profiles for ethylbenzene and n-propylbenzene indicated that volatilization of these compounds were affected by the organic carbon content in the porous media. N-propylbenzene which has the lowest solubility and the highest water-solid partition coefficient of the three VOCs showed the most variation in the exhaust air concentration.

Table 2 presents the concentration of VOCs sorbed initially and after air sparging. As seen in Table 2, the concentration of VOCs sorbed to the porous media remained fairly constant even after 10 hours of sparging and that the mass sorbed were fairly the same throughout the depth of the porous media. This observation seemed to suggest that desorption was negligible over the experimental period. However, desorption kinetics may play an important role in the remediation of VOC contaminated aquifers once the dissolved VOCs are removed. This behavior seemed to reflect the work reported by Kraus et al. (1997) where the soil concentrations before and after air sparging were the same even though the VOC concentrations in the groundwater were reduced by 3 to 4 orders of magnitude. Rebound in the aqueous concentration of VOCs after the air sparging system is turned off may be due to the slow desorption of VOCs.

Concentration profiles in the aqueous phase for each VOC are presented in Figures 3 to 5. Measurement of initial aqueous concentrations indicated that at the start of the experiment

there was a concentration gradient near the air-water interface as a result of losses of VOCs during the packing of the reactor. Separate experiments indicated that when the experimental setup was left alone for 18 hours without any air flow, VOC losses, other than losses due to the initial packing were found to be less than 2%. When air was passed through the reactor. the VOC aqueous concentration near the air-water interface was rapidly depleted. This depletion was confined to a thin layer of porous media near the air-water interface. The rapid depletion is associated with a faster volatilization of VOC at the air-water interface as compared to the diffusive transport of VOCs to the air-water interface. After four hours of sparging the concentration gradient of the VOCs in the liquid phase became fairly constant suggesting that a quasi-steady state condition for the diffusion of the VOCs was reached. The distinctive zone with a steep concentration gradient may be defined as the mass transfer zone (*MTZ*) (Braida and Ong, 1997a). Beyond the *MTZ*, the impact of the air channels was strongly limited. For convenience, the size of the *MTZ* was taken as the distance from the air-water interface to where the VOC concentration was equal to 90% of the bulk concentration.

Figures 3, 4 and 5 showed the influence of the organic carbon content on the size of the *MTZ* for benzene, ethylbenzene, and n-propylbenzene, respectively. Benzene, the most soluble and least sorbable of the three VOCs studied, showed the smallest change in the size of the *MTZ* (see Figure 3). The size of the *MTZ* for benzene varied from approximately 35 mm to 26 mm when the organic carbon content increased from 0.01% to 0.45%. The size of the *MTZ* for ethylbenzene ranged from approximately 38 mm for organic carbon content less than 0.01% to 28 mm for an organic carbon content of 0.45% (see Figure 4). The size of the *MTZ* for n-propylbenzene showed the largest variation with the organic carbon content. For this VOC, the size of the *MTZ* ranged from approximately 37 mm for the sand with less than 0.01% organic carbon content to approximately 17 mm for a sand with an organic carbon content of 0.45% (see Figure 5). Based on Figures 3 to 5, the size of the *MTZ* was most affected for the VOC with the lowest solubility and the highest liquid-solid partition coefficient.

Transport of VOCs to the air-water interface is retarded by the partitioning of the VOC between the liquid phase and the solid phase. This retardation is given by the retardation

factor R :

$$R = 1 + \frac{\text{Adsorbed concentration}}{\text{Dissolved concentration}} \tag{3}$$

Equation 3 may be written in terms of the linear partition coefficient K_d (L^3M^{-1}), the bulk density of the porous media ρ_b (ML^{-3}), and the porosity of the porous media ε (dimensionless) as follows:

$$R = 1 + K_d \frac{\rho_b}{\varepsilon} \tag{4}$$

Using the equilibrium partition coefficients determined earlier, the retardation factor, R, for the experimental conditions tested may be computed as presented in Table 3.

Transport of VOCs from the liquid phase to the air-water interface may be described using a one-dimensional diffusion model (Braida and Ong, 1997c). The model is as follows:

$$\varepsilon \frac{\partial C_w}{\partial t} = \tau D_w \frac{\partial^2 C_w}{\partial z^2} \tag{5}$$

where z (L) is the depth of the porous media with the air-water interface located at $z = 0$ and the bottom of the reactor at $z = L$, C_w is the aqueous concentration of the VOC (ML^{-3}), D_w is the aqueous diffusivity of the VOC (L^2T^{-1}), ε is the porosity of the porous media (dimensionless), and τ is the tortuosity factor (dimensionless) which accounts for the change in the length of the diffusion path of the VOCs in the porous media. In the presence of partitioning, this model may be modified by including the retardation factor as shown in equation 6.

$$\varepsilon R \frac{\partial C_w}{\partial t} = \tau D_w \frac{\partial^2 C_w}{\partial z^2} \tag{6}$$

The initial condition (IC) and the boundary conditions (BC) are given by:

IC C_w is known for all z at time zero (experimental data)

BC $$\frac{\tau D_w}{R}\frac{\partial C_w}{\partial z} = -K_G(K_H\overline{C}_w - C_a) \qquad \text{at } z = 0 \text{ for all t} \qquad (7)$$

$$\frac{\partial C_w}{\partial z} = 0 \qquad \text{at } z = \text{L for all t} \qquad (8)$$

where $\overline{C}_w$ is the volumetric weighted average VOC concentration, of the mass transfer zone (*MTZ*). The volumetric average concentration, $\overline{C}_w$, was computed as follows:

$$\overline{C}_w = \frac{\sum V_n C_{wn}}{\sum V_n} \qquad (9)$$

where V_n is the volume of the n layer (L^3), C_n (ML^{-3}) is the aqueous concentration of VOC in the n layer, and the summation extends to all the layers included in the *MTZ*. C_a is the air phase concentration close to the air-water interface and was assumed to be zero.

The air phase concentration, $\overline{C}_a$, in the exhaust air (outlet of the reactor) was computed using the transport equation for the VOCs in the air phase:

$$V_a\frac{d\overline{C}_a}{dt} = -Q_a\overline{C}_a + K_G A K_H \overline{C}_w \qquad (10)$$

where $\overline{C}_a$ is the measured VOC concentration in the effluent air (ML^{-3}), V_a represents the air volume (L^3), Q_a represents the air flow (L^3T^{-1}), A is the air-water interfacial area (L^2) of the experimental setup (87.5 cm^2). Equation 6 and equation 10 were solved numerically using the Continuous System Modeling Program (CSMP) software (IBM, 1972). The porous media profile was divided into 26 horizontal layers of variable thickness (thinner layers were used closer to the air-water interface to compute more accurately the VOC concentrations in the region where the largest changes in the concentration occurred). To solve the equations,

used closer to the air-water interface to compute more accurately the VOC concentrations in the region where the largest changes in the concentration occurred). To solve the equations, the value for the mass transfer coefficient (K_G) and the tortuosity factor (τ) were taken from Braida and Ong (1997c) while the retardation factor used are presented were in Table 3. Table 4 lists the values of the parameters used in the model for the estimation of the aqueous phase concentration and the air phase concentration.

Figure 6a and Figure 6b showed the experimental and predicted liquid phase concentrations for the three VOCs in the same porous media with different organic carbon contents. The inclusion of the retardation factor in the diffusion model seemed to predict fairly well the concentration profiles after 10 hours of sparging.

The experimental and predicted exhaust air concentrations for benzene are presented in Figures 7a and 7b. As seen in Figures 7a and 7b, the model slightly overpredicted the air phase concentration. The model can be assessed further by comparing the actual mass volatilized and the predicted mass volatilized. Depending on the VOC, the predicted total mass volatilized was approximately 25 to 35% larger than the actual mass volatilized. It must be pointed out that the predictions were made based on mass transfer coefficients determined for a porous medium with less than 0.01% organic carbon and by assuming equilibrium partitioning. The discrepancy in the predictions of the model and the actual values may be due to the above two assumptions. If the mass transfer coefficients were assumed to be constant for a given porous medium but regardless of the organic carbon present, then the overprediction of the mass volatilized may be due to the equilibrium assumption of VOC partitioning. However, by assuming equilibrium partitioning, sorption would be maximized and therefore mass volatilized would be minimized. It is therefore possible that the overprediction may be due to the selection of the mass transfer coefficients. Instead of using the mass transfer coefficients for porous medium with less than 0.01% organic carbon, the model may be used to determine the mass transfer coefficients by curve fitting the model predictions with the actual aqueous phase and air phase concentrations and the total mass volatilized (Braida and Ong, 1997b). If this approach was taken, the estimated mass transfer coefficients were found to be approximately 30-35% smaller than the mass transfer coefficients for porous medium with less than 0.01% organic carbon. Possible

to the presence of the organic matter. In addition to the above possible reasons, the tortuosity factor used could be different due to the higher organic matter present.

Conclusions

The effects of the adsorption of VOCs on the performance of air sparging systems were studied using a single-air-channel experimental setup. The size of the *MTZ* was found to be affected by the amount of organic carbon present in the porous media. The increase in the organic carbon content of the soil resulted in a decrease in the size of the *MTZ*. This effect is larger for VOCs such as n-propylbenzene with low solubilities and high partition coefficients. The decrease in the size of the *MTZ* may be due to the retardation in the diffusion of the VOCs to the air-water interface as a result of aqueous-solid partitioning. Sorbed VOC concentration remained fairly constant along the soil profile during the sparging process. This finding seems to indicate that slowly desorption kinetics may seriously limit the remediation of contaminated aquifers.

A one-dimensional diffusion model that included the retardation factor (R) was found to predict fairly well the liquid and air phase concentrations. This show that equilibrium partitioning and a first order volatilization term at the air water interface may be used to predict concentrations and mass changes during air sparging.

Notation

C_a C_w	VOC concentration in the air and aqueous phases, ML^{-3}
$\overline{C}_w$	VOC weighted concentration average in the *MTZ*, ML^{-3}
$\overline{C}_a$	VOC measured concentration in the air phase
C_S	VOC concentration sorbed onto soil matrix, MM^{-1}
D_w	VOC aqueous diffusivity, L^2T^{-1}
D_a	VOC air diffusivity, L^2T^{-1}
f_{oc}	organic carbon fraction, dimensionless
ε	porous media porosity, dimensionless
τ	tortuosity coefficient, dimensionless
K_{oc}	organic carbon partition coefficient, L^3M^{-1}

K_d	linear partition coefficient, L^3M^{-1}
K_H	Henry's law constant, dimensionless
MTZ	width of the mass transfer zone, L
Q_a	air flow rate, L^3T^{-1}
V_a	air volume, L^3
R	retardation factor, dimensionless
K_G	overall air side mass transfer coefficient, LT^{-1}

References

Braida, W.J., and S.K. Ong, Air sparging effectiveness: the air channel mass transfer zone, submitted to *Water Resources Research*, 1997a.

Braida, W.J., and S.K. Ong, Nonaqueous liquid phase fate under air sparging conditions, submitted to *Journal of Contaminant Hydrology*, 1997b.

Braida, W.J., and S.K. Ong, Air sparging: air phase-liquid phase mass transfer coefficients, submitted to *Water Resources Research*, 1997c.

Chao, K.P., Aqueous-vapor mass transfer of VOCs in saturated porous media under air sparging conditions, Ph.D. Dissertation, 176 pp., Polytechnic University, Brooklyn, NY, 1997.

Garbarini, D.G., and L.W. Lion, Evaluation of sorptive partitioning of nonionic pollutants in closed systems by headspace analysis, *Environ. Sci. Technol.*, vol. 19(1), pp. 1122-1129, 1985.

Gierke, J.S., N.J. Hutzler, and J.C. Crittenden, Modeling the movement of volatile organic chemicals in columns of unsaturated soil, *Water Resources Research*, vol. 26(7), pp. 1529-1547, 1990,

IBM, System/360 Continuous System Modeling Program user's manual, Program Number 360A-CX, 5th ed., IBM Corp., Technical Publ. Dept., White Plains, New York, 1972.

Karickhoff, S.W., Organic pollutant sorption in aquatic systems, *J. Hydraulic Eng., ASCE*, vol. 110, pp. 707-735, 1984.

Kraus, J., S. Nelson, P. Boersma, and A. Maciey, Comparison of pre-/post-sparging VOC concentration in soil and groundwater, *In Situ and On-Site Bioremediation: Volume 1*, B. Alleman and A. Leeson (eds.), Battelle Press, Columbus, OH, 1997.

Nelson, D.W., and L.E. Sommers, Total carbon, organic carbon, and organic matter, in *Methods of Soil Analysis, Part 2, Chemical and Microbiological Properties*, Second Edition, edited by A. L. Page, pp. 570-571, American Society of Agronomy, Inc., Soil Science Society of America, Inc., Madison, WI, 1982.

Ong, S.K., and L.W. Lion, Effects of soil properties and moisture on the sorption of TCE vapor, *Water Research*, vol. 25(1), pp. 29-36, 1991.

Pavlostathis, S.G., and G.M. Mathavan, Desorption kinetics of selected organic compounds from field contaminated soils, *Environ. Sci. and Tech.*, vol. (26), pp.532-538, 1992.

Table 1. Linear partition coefficients (K_d) in mL/g for different VOCs into Ottawa sand as a function of organic carbon content.

VOC	Organic Carbon <0.01%	Organic Carbon 0.04%	Organic Carbon 0.45%
Benzene	0.054	0.226	0.228
Ethylbenzene	0.029	0.464	0.877
n-Propylbenzene	0.023	0.474	1.001

Table 2. Sorbed VOC concentrations (mg/Kg) ± standard deviation

Organic Carbon Content	Sample Description	Benzene	Ethylbenzene	n-Propylbenzene
0.04%	Initial Average	2.9 ± 0.1	1.0± 0.1	0.5± 0.1
	Final, Surface	2.9± 0.1	1.0± 0.1	0.4± 0.1
	Final, Depth 38.1 mm	3.0± 0.1	1.0± 0.1	0.5± 0.1
	Final, Depth 63.5 mm	2.9± 0.1	1.0± 0.1	0.5± 0.1
	Final, Depth 88.9 mm	3.0± 0.1	1.0± 0.1	0.5± 0.1
0.45%	Initial Average	3.7 ± 0.1	1.3 ± 0.1	0.3 ±0.1
	Final, Surface	3.6 ± 0.2	1.3 ± 0.1	0.3 ±0.1
	Final, Depth 19.1 mm	3.7 ±0.1	1.4 ± 0.1	0.3 ±0.1
	Final, Depth 38.1 mm	3.7 ±0.1	1.3 ± 0.1	0.3 ± 0.1
	Final, Depth 63.5 mm	3.7 ± 0.1	1.3 ± 0.1	0.3 ± 0.1
	Final, Depth 88.9 mm	3.7 ± 0.1	1.3 ± 0.1	0.3 ± 0.1

Computations:

$$\text{C (sorbed)} = \frac{C(\textit{measured in hexane})(\textit{Vol. of hexane}) - C(\textit{water})(\textit{Vol. of water in sample})}{\textit{Dry Mass (sorbent)}}$$

Table 3. Retardation factors (R) for different VOCs on Ottawa sand as a function of organic carbon content.

VOC	Organic Carbon <0.01%	Organic Carbon 0.04%	Organic Carbon 0.45%
Benzene	1.24	1.99	2.00
Ethylbenzene	1.13	3.03	4.84
n-Propylbenzene	1.10	3.07	5.38

Table 4. Parameters used in the model

Parameter	benzene	ethylbenzene	propylbenzene
Porosity (ε)	0.377	0.377	0.377
Tortuosity (τ)	0.52	0.52	0.52
K_G (cm/min)	0.00486	0.00436	0.00463
D_w (cm^2/min)	0.0005754	0.0004578	0.0004194
Q_a (mL/min)	55	55	55
K_H	0.197	0.294	0.369
R (OC < 0.01%)	1.24	1.13	1.10
R (OC = 0.04%)	1.99	3.03	3.07
R (OC = 0.45%)	2.00	4.84	5.38

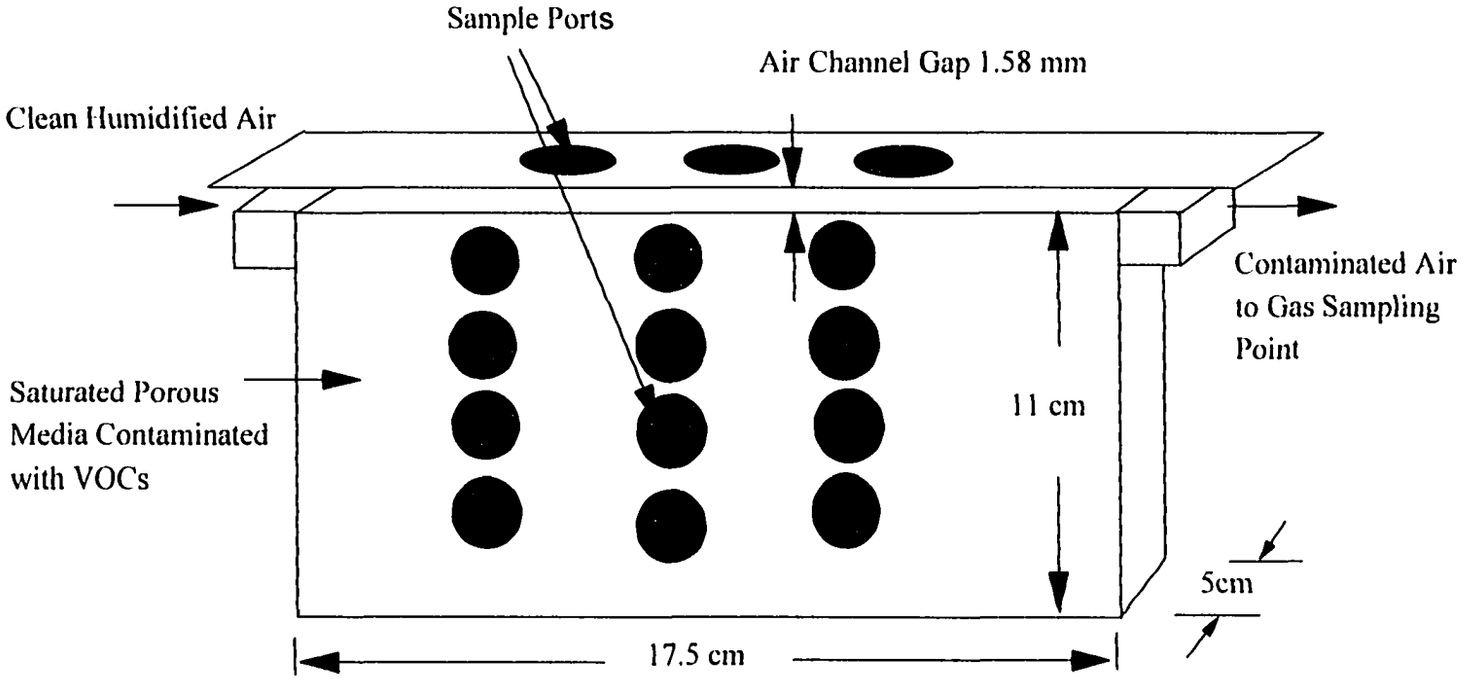

Figure 1. Single-air channel apparatus

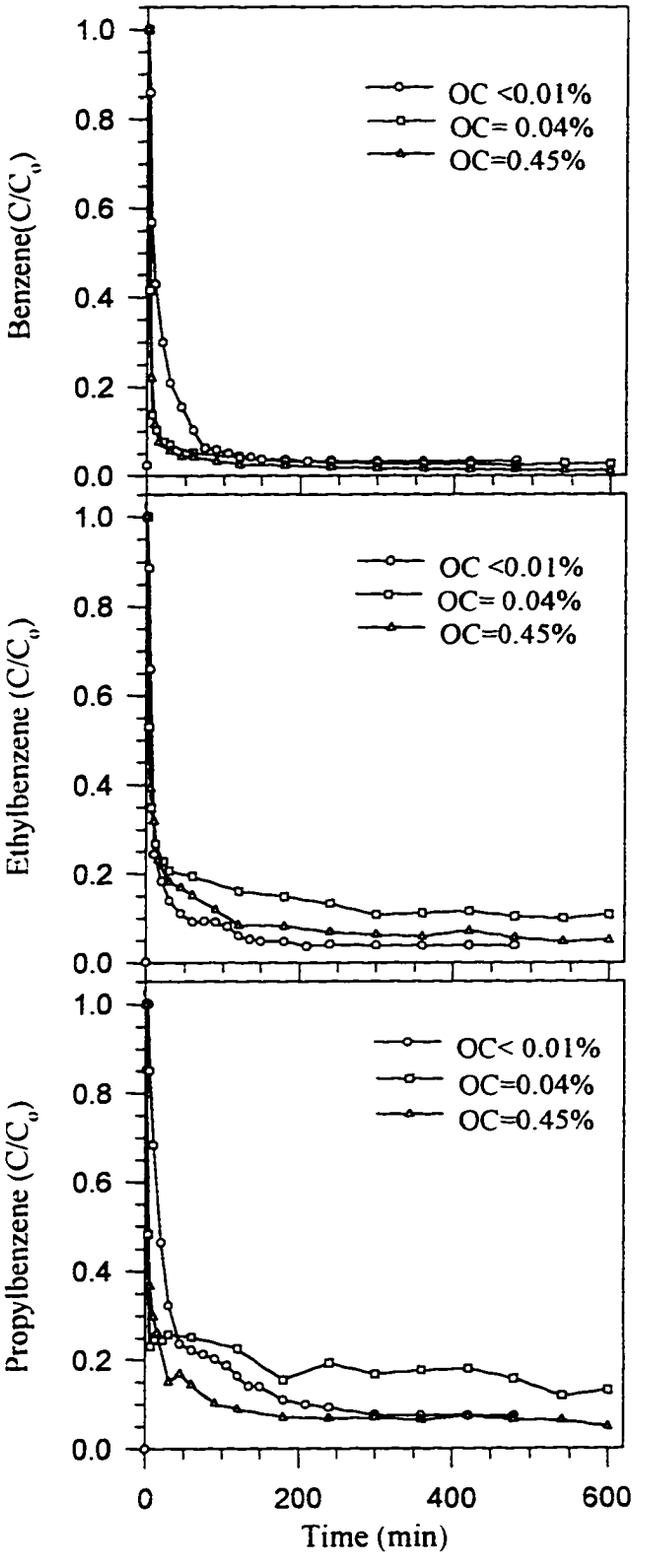

Figure 2. Relative VOC concentrations in the exhaust air for different organic carbon contents

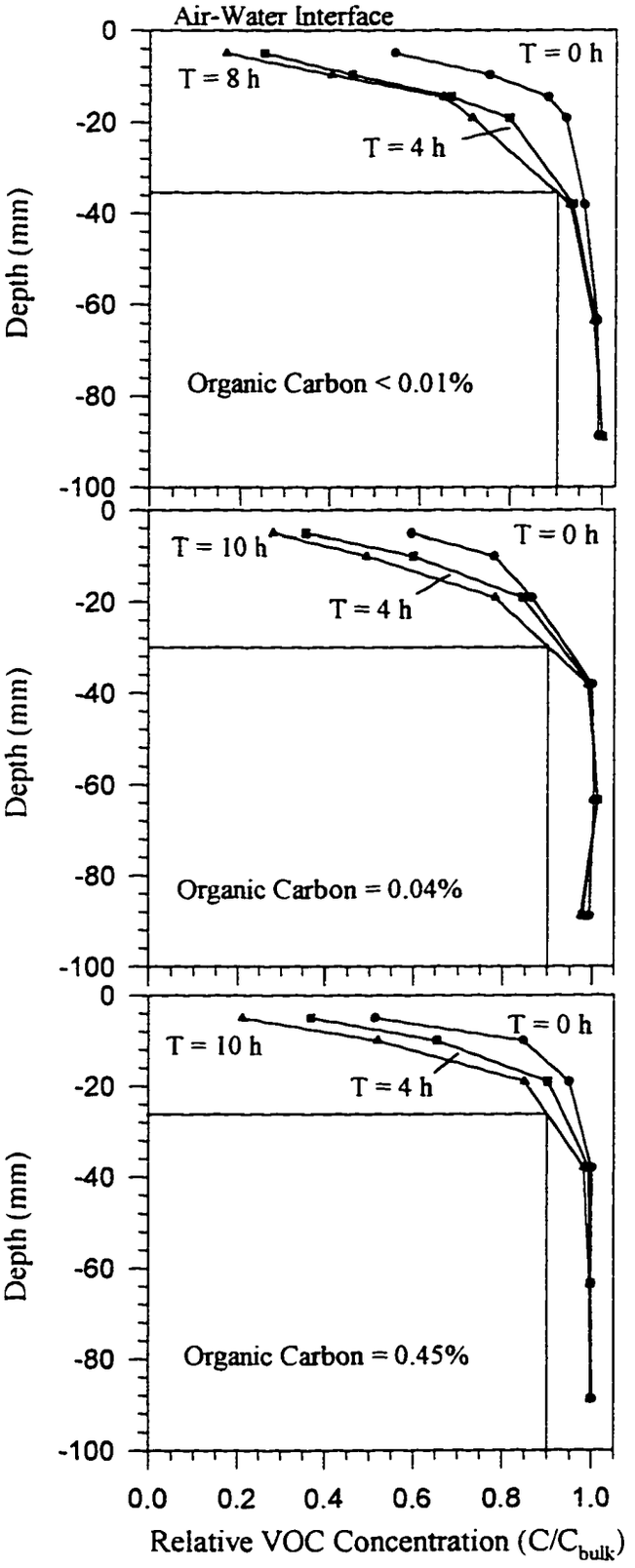

Figure 3. Benzene concentration profiles for different organic carbon contents

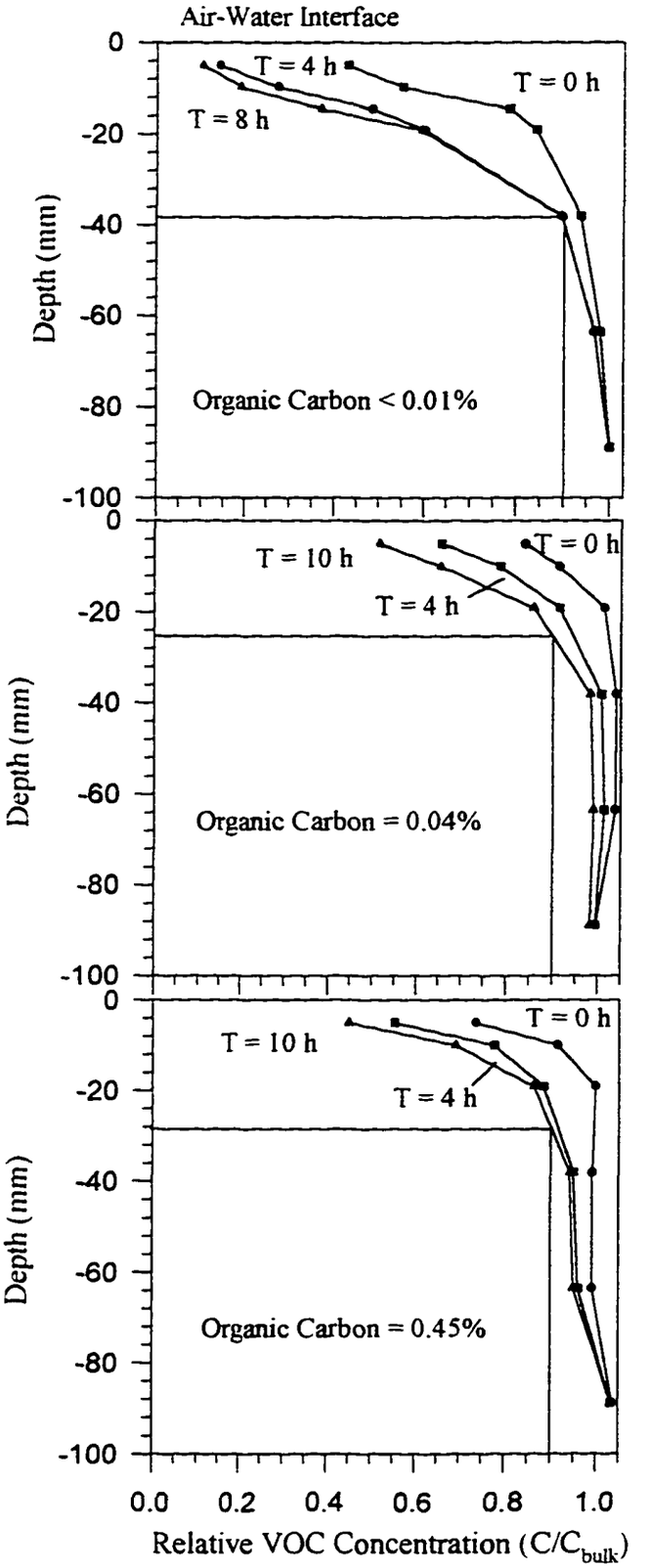

Figure 4. Ethylbenzene concentration profiles for different organic carbon contents

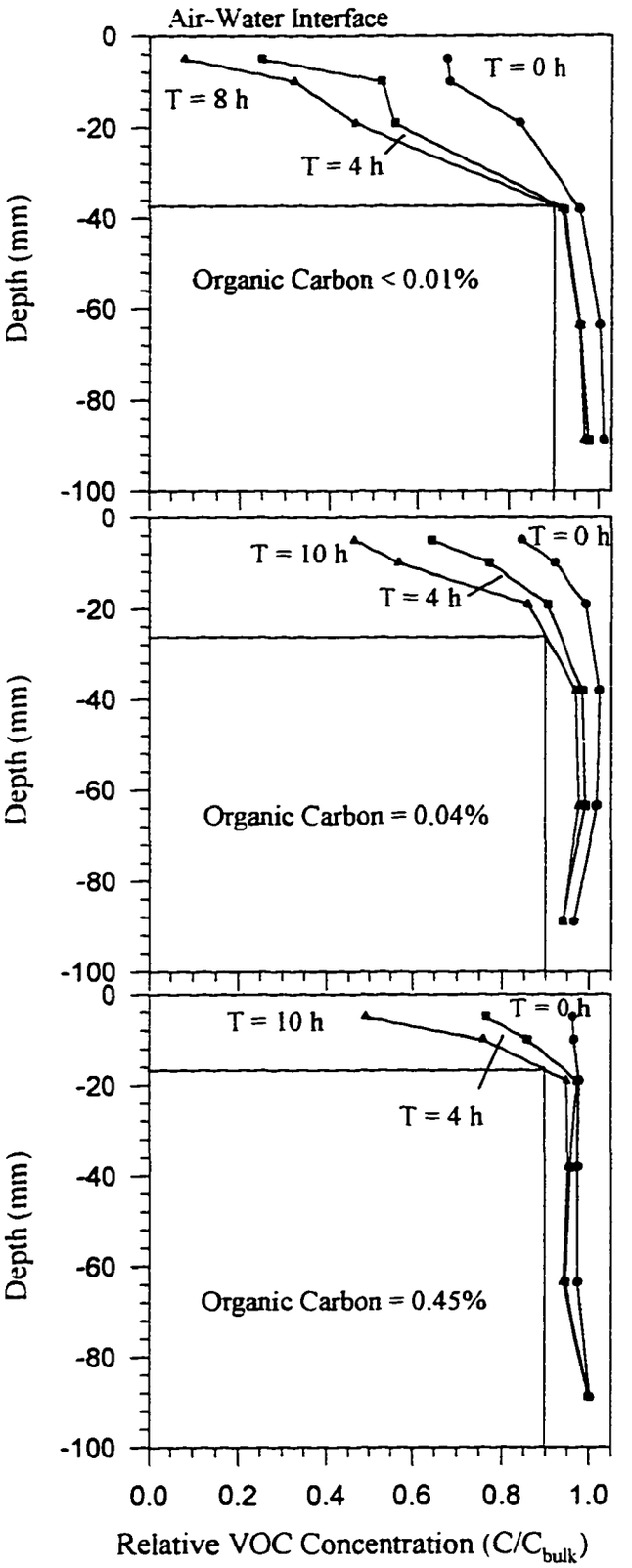

Figure 5. n-Propylbenzene concentration profiles for different organic carbon contents

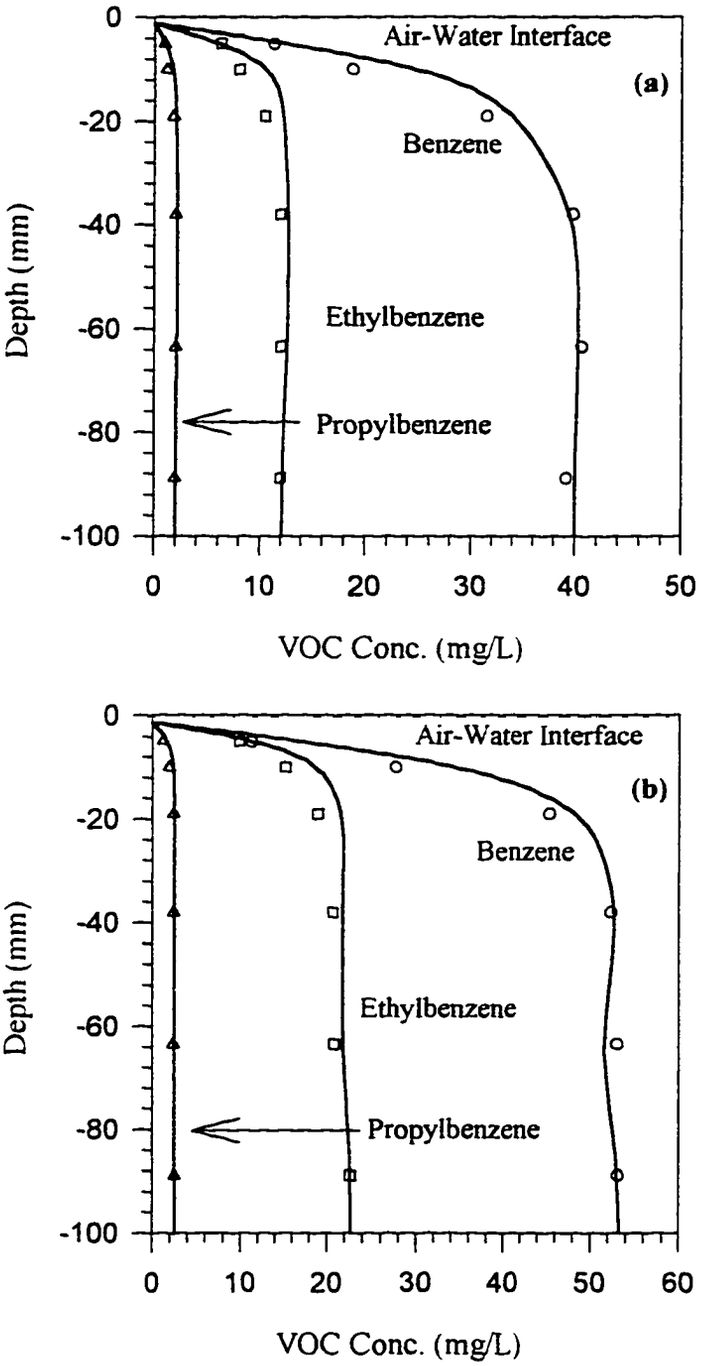

Figure 6. Experimental and modeled VOCs concentration profiles in the water phase; (a) organic carbon content 0.04%, (b) organic carbon content 0.45%

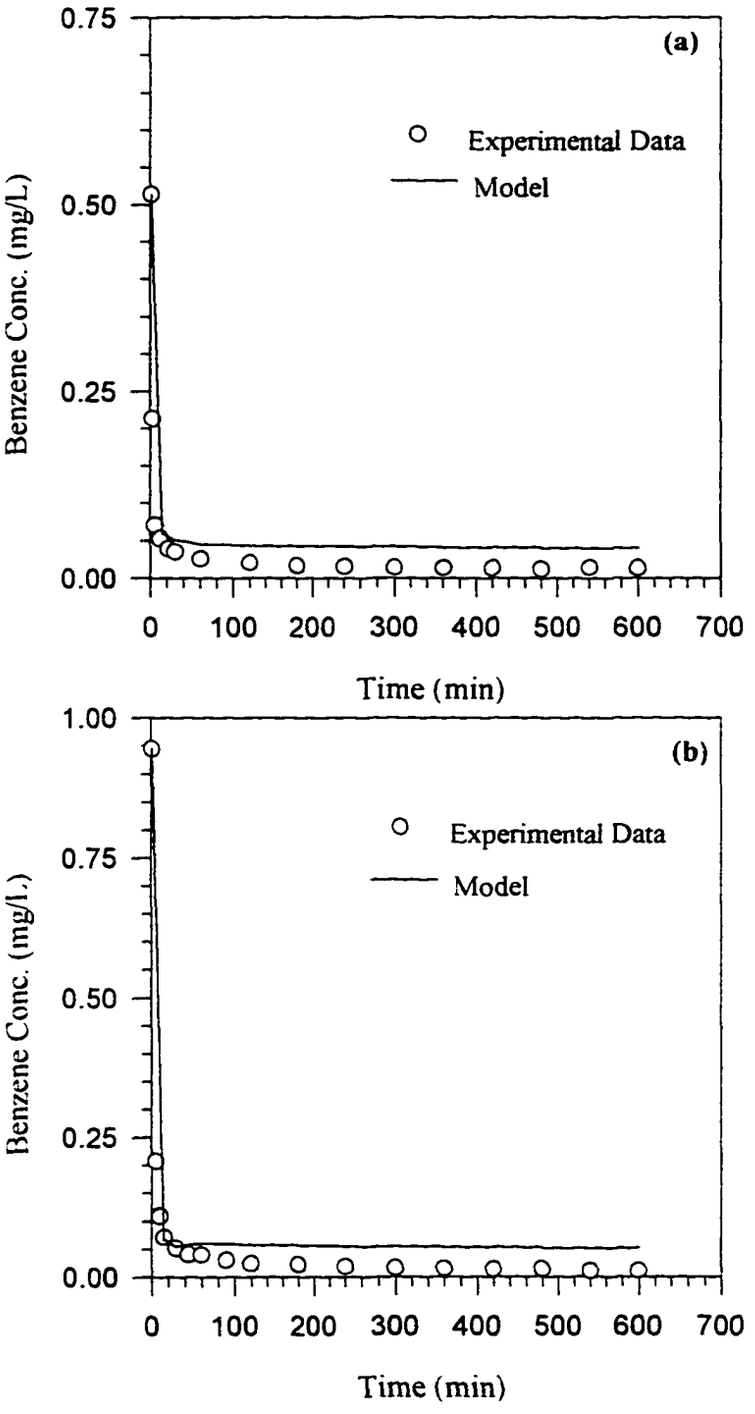

Figure 7. Benzene concentration in the exhaust air, (a) organic carbon content 0.04%, (b) organic carbon content 0.45%

CHAPTER EIGHT. MODELING AIR SPARGED SOIL COLUMNS

Introduction

Several researchers have attempted to model air sparging operations by using different mathematical modeling approaches. Of particular interest are the models which assumed air flow in the form of finger-like air channels (Hein, 1996; Ji, 1994; Drucker and Di Julio, 1996). Most of the models are limited in their application since they were optimized by curve fitting with the experimental results. However, application of a model would require "a priori" selection of appropriate model parameters and this had been the hardest task faced by modelers.

Volatilization of VOCs under air sparging conditions occurs at the air-water interface located at the air channels wall. Using a single-air channel experimental setup, Braida and Ong (1997a, 1997b) showed that, at the air channel level, the volatilization of VOCs during air sparging was controlled by the aqueous diffusion of the VOCs through a mass transfer zone adjacent to the air channels. In Chapter 3, a one-dimensional diffusion model was used to estimate the tortuosity and the mass transfer coefficients for the volatilization of VOCs at the air-water interface during air sparging operations.

In this chapter, the one-dimensional diffusion model developed in Chapter 3 for a single air-channel was modified from Cartesian to radial coordinates and applied for air sparged soil columns. The objective of this study was to assess whether the various parameters determined by using a single air-channel may be applied to a more complex system with many air channels such as air sparging of a soil column. Successful application of the model and the correlations developed in Chapter 3 will strongly suggest that the various physical-chemical phenomena observed at the air channel level or "microscale" level may be used to explain and predict the performance of large scale air sparging systems.

Materials and Methods

A Plexiglass™ column, 13.97 cm (5 1/2 inches) in diameter and 55.88 cm (22 inches) in length, was used for the soil column (see Figure 1). The column contained approximately 35

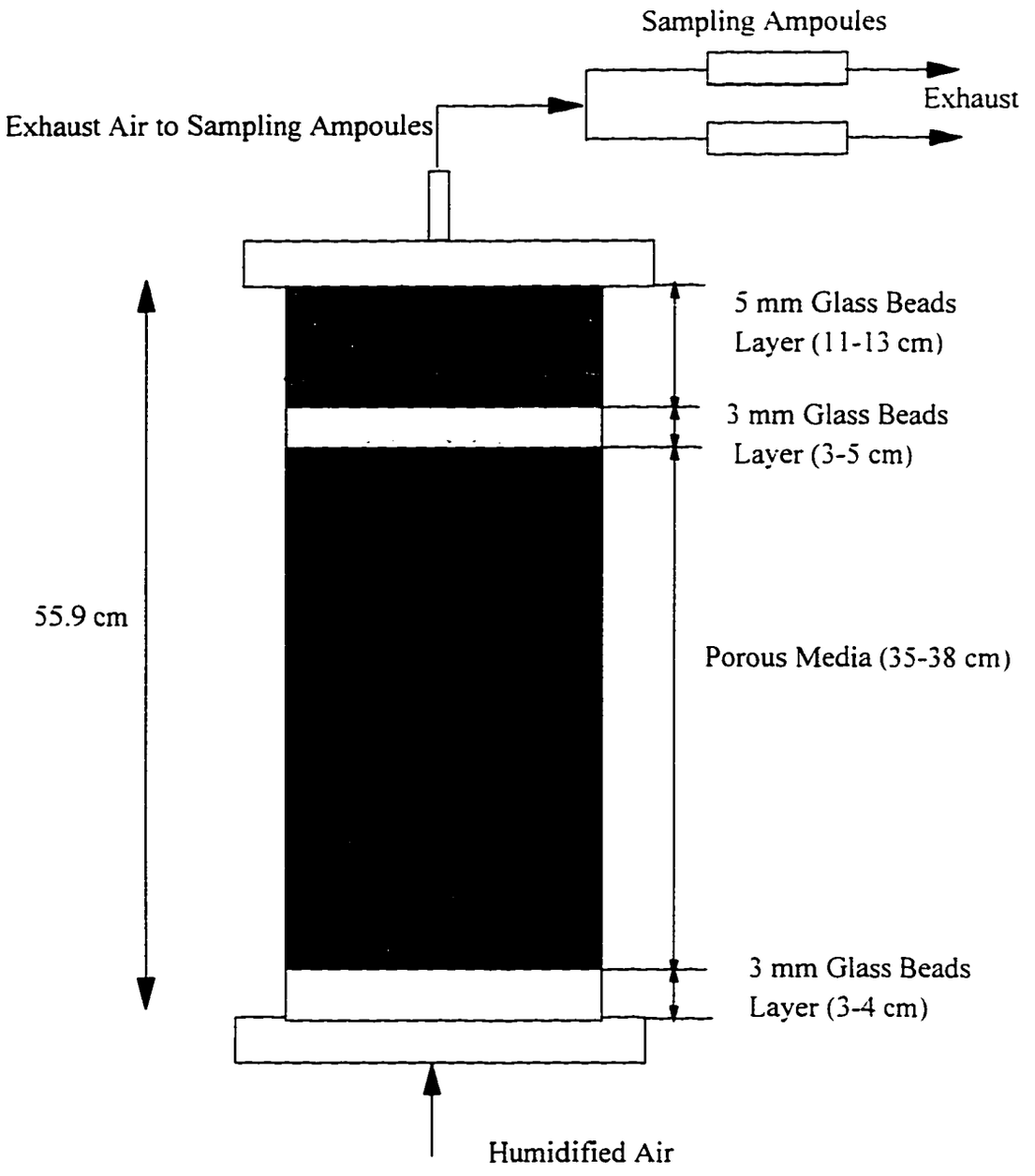

Figure 1. Sketch of soil column

cm of porous media sandwiched between layers of glass beads. The bottom layer was 3 - 5 cm deep and contained 3 mm diameter glass beads. Air was introduced into the column through a 1.1 cm diameter cylindrical air stone (Nature's Playland Co., Hicksville, NY) located at the base of the column. The bottom layer of glass beads provided an even distribution of air across the soil column. The top layer of glass beads consisted of a 3 - 5 cm lower layer of 3 mm diameter glass beads and a upper layer of 12 - 14 cm of 5 mm diameter glass beads. The upper layer provided an overburden pressure onto the porous media and minimized the fluidization of the porous media during sparging. The porosity of the glass beads were 0.40 and 0.42 for the 3 mm and 5 mm diameter glass beads, respectively. The exhaust air line was a PTFE hose with a pair of 125 mL gas sampling ampoules (Alltech, Deerfield, IL). In-house humidified air was used as the sparging air. Air flow was measured using a Gilmont Model 13 flowmeter (Barrington, IL).

Three sets of experiments with three different porous media were conducted. The porous media used were: (a) sand 30/50 with a porosity of 0.377, (b) sand 70/100 with a porosity of 0.40, and (c) Ottawa sand with a porosity of 0.37 (U.S. Silica Company, Ottawa, IL). The VOCs used were benzene, ethylbenzene, n-propylbenzene with sand 30/50 and sand 70/100, while toluene, chlorobenzene, styrene, and 1,2 dichlorobenzene were used with Ottawa sand. Concentrations ranging between 0.7 and 100 mg/L. All chemicals were HPLC grade and were purchased from Sigma-Aldrich Chemical Company Inc. (Milwaukee, WI). To pack the column with porous media, the 3 mm glass beads bottom layer, saturated with contaminated water, was first put in place. A slurry was made by carefully mixing the porous media with the aqueous solution of the VOCs. The column was then rapidly packed layer by layer with the slurry to avoid entrapment of air bubbles. Aqueous samples were taken from various depths along the packing to determine the initial aqueous phase concentration in the porous media. Slurry samples were also taken during packing to determine the mass sorbed onto the porous media. The composite top layer of glass beads was put in place and the column was immediately sealed to minimize VOCs losses. The column was allowed to equilibrate for 16 hours before being sparged.

The air flow rates were 0.8, 0.7, and 1.1 L/min for sand 30/50, sand 70/100, and Ottawa sand, respectively. The air saturation in the soil was estimated by measuring the volume of

water displaced into the top layer of glass beads. For the above air flow rates, the air saturation were 10%, 6.3%, and 8.1% for sand 30/50, sand 70/100, and Ottawa sand, respectively. The average air pore velocities may be estimated from the air flow rate divided by the cross sectional area of the column and the air saturation factor. The estimated air pore velocities were 0.86 cm/s for sand 30/50, 1.21 cm/s for sand 70/100, and 1.34 cm/s for Ottawa sand. This range of velocities was within the range of velocities for which the mass transfer zone and mass transfer coefficient correlations were determined and was similar to air velocities reported by others (Hein, 1996). Stagnant water conditions were assumed and the water temperature was maintained at 21 $\pm$ 1 °C. At the end of the experimental run, both aqueous and wet porous media samples were taken and analyzed for the VOCs remaining. A total of 16 samples were taken at depths of 0, 10, 20, and 30 cm from the top of the porous media (2 aqueous and two wet porous media samples per depth).

VOC concentrations in the exhaust air were measured by withdrawing air samples from the ampoules. The initial and final VOC concentrations in liquid phase were measured with a Hewlett-Packard 5890 Series II gas chromatograph (Avondale, PA) equipped with a HP-5 capillary column and a flame ionization detector. Air phase concentration was determined by direct injection of a 1 mL sample into the gas chromatograph. The liquid phase concentration was determined using the head space technique where 25 µL of an aqueous sample was placed in a 1.8 mL aluminum crimp cap vial. After equilibrium was reached, the head space concentration was measured by direct injection into the gas chromatograph. The aqueous concentration was then estimated from the measured head space concentration.

To perform a mass balance, VOCs sorbed to the porous media were determined using a hexane extraction procedure at the end of each experimental run. A 1:3 ratio (w/w) of hexane and wet soil was mixed for 12 hours in a wrist shaker (Burrell Scientific, Pittsburgh, PA). The solids were then allowed to settle. A portion of the clean supernatant was placed in a 1.8 mL glass vial capped with PTFE-faced silicone septa. VOCs in the sample were quantified by direct injection of the supernatant into the gas chromatograph. The mass of sorbed VOC was estimated by subtracting the mass of VOC present in the liquid phase remaining in the wet soil from the mass of VOC present in the hexane extract.

Description of Model

Under air sparging conditions, the air channels in the soil column may be represented by a composite of evenly spaced cylindrical air channels surrounded with a nonadvective water saturated region as seen in Figure 2 (Hein, 1996; Ji, 1994; Drucker and Di Julio, 1996). For convenience, the circumference of the nonadvective region for each air channel was assumed to touch the circumference of the adjacent nonadvective regions. As presented in Chapter 2 the air channel was found to be surrounded by a mass transfer zone (*MTZ*) where air flow has an impact on the mass transfer within the zone. The nonadvective region may be bigger or smaller than the *MTZ* depending on the number and diameter of the air channels present in the system. Using this idealized picture of air channels in a soil column, a one-dimensional diffusion model with cylindrical coordinates was used to model the air sparging of the soil column. The diffusion equation for each channel was given by:

$$\varepsilon \frac{\partial C_w}{\partial t} = \frac{\tau D_w}{r} \frac{\partial}{\partial r}\left(r \frac{\partial C_w}{\partial r} \right) \qquad \text{for } R \le r < c \qquad (1)$$

were C_w is the concentration of VOC in the water phase (ML^{-1}), r (L) is the radial distance from the center of the air channel, R is the air channel radius (L), c is the radius of the non advective saturated porous media region surrounding the air channel (L), ε is the water filled porosity of the porous media (dimensionless), D_w is the water diffusivity of the VOC (L^2T^{-1}), and τ is the tortuosity factor (dimensionless).

To determine the number of channels an estimation of the air filled porosity (air saturation) and the diameter and length of the air channels was needed. The air saturation was estimated from the volume of water displaced into the top layer of glass beads after air was turned on. The average air channel diameter was estimated by direct visual inspection of several air channels close to the column wall. The average air channel diameters were estimated to be 0.2 cm, 0.35 cm, and 0.30 cm for sand 30/50, sand 70/100, and Ottawa sand, respectively. The length (L_o) of the air channels was assumed to be equal to the depth of the bottom glass beads layer and the depth of the porous media. Under these conditions, the number of air channels may be estimated as follows:

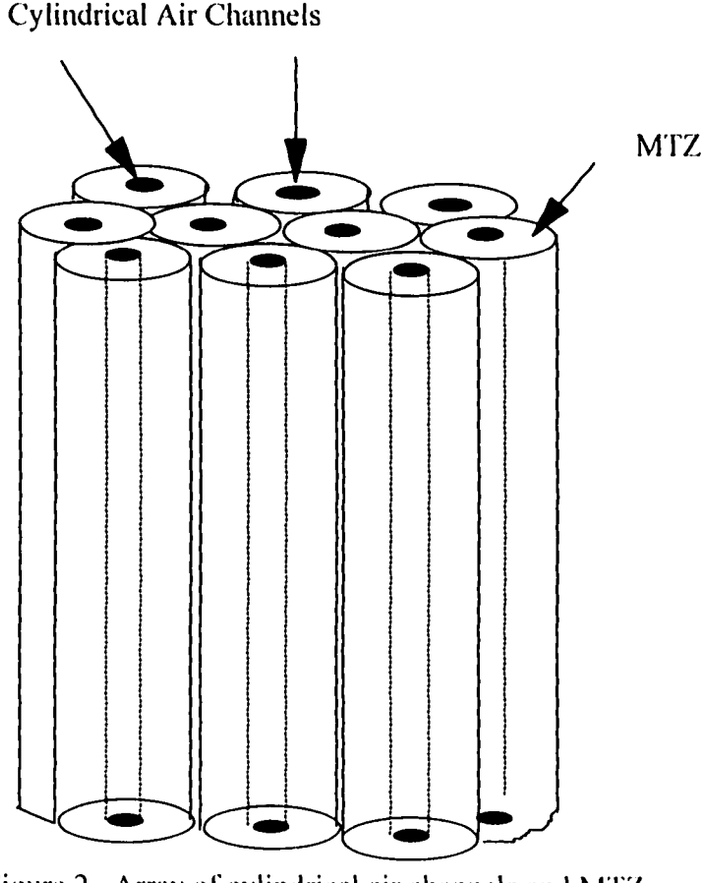

Figure 2. Array of cylindrical air channels and MTZ

$$\#\ \text{of air channels} = \frac{volume\ of\ water\ displaced}{\pi\ R^2 L_0} \tag{2}$$

and the total interfacial area may be estimated as follows:

$$A = (\#\ of\ air\ channels)\ 2\pi\ R\ L_o \tag{3}$$

The radius of the nonadvective saturated region, c, was estimated as follow:

$$c = \left(\frac{Cross\ sectional\ area\ of\ the\ column}{\pi\ (\#\ of\ air\ channels)} \right)^{0.5} \tag{4}$$

Based on the air saturation in the column for the air sparging experiments, the value of c was always smaller than the size of the *MTZ*. As explained later, to run the model, the nonadvective saturated zone or the *MTZ* was subdivided in several concentric rings. The number of rings was dependent on the value of c. The initial and boundary conditions for equation 1 are as follows (see Chapter 4):

C_w is known for all r at time zero (experimental data)

$$\tau D_W \frac{\partial C_W}{\partial r} = -K_G K_H \overline{C}_w \qquad \text{at } r = R \text{ for } t > 0 \tag{5}$$

VOC flux = zero at $r = c$ for $t > 0$

The volumetric average concentration, $\overline{C}_w$, was computed as follows:

$$\overline{C}_w = \frac{\sum V_n C_{wn}}{\sum V_n} \tag{6}$$

where V_n is the volume of the n concentric ring (L^3), C_{wn} (ML^{-3}) is the aqueous concentration of VOC in the n ring, and the summation extends to all the rings with $r<c$.

The air phase concentration was computed using the transport equation for the VOCs in the air phase as follows:

$$V_a \frac{d\overline{C}_a}{dt} = -Q_a \overline{C}_a + K_G A K_H \overline{C}_w \qquad (7)$$

where $\overline{C}_a$ is the measured VOC concentration in the effluent air (ML^{-3}), V_a represents the air volume (L^3), Q_a represents the air flow (L^3T^{-1}), A is the total air-water interfacial area (L^2) of the experimental setup.

Equation 1 and equation 7 were solved numerically by using the Continuous System Modeling Program (CSMP) software (IBM, 1972). The VOC concentration profile was divided into several concentric layers of equal thickness as seen in Figure 3. The number of concentric layers was chosen depending on the value of c. In general, the larger the value of c, the larger the number of layers were used. In this study, four layers with a thickness of 0.05 cm were used for sand 30/50 (c = 0.3 cm, R = 0.10 cm), six layers with a thickness of 0.08725 cm were used for sand 70/100 (c = 0.7 cm, R = 0.175 cm), and seven layers with a thickness 0.05 cm were used for Ottawa sand (c = 0.5 cm, R = 0.15 cm). K_G values were estimated using equation 11 in Chapter 4. Table 1 lists the values of all the parameters used in the model.

Results and Discussion

Examples of the modeling results are shown in Figures 4 to 7. Figure 4 shows the measured and the predicted vapor concentrations and the total mass removed over time for benzene. In Figure 4, sand 30/50 was used as the porous medium and the estimated air pore velocity was 0.86 cm/s. The average diameter of the air channels was visually estimated to be approximately 2 mm and the air saturation was estimated to be 10%. As seen in Figure 4, the predicted air phase concentrations of benzene by the model were approximately close to the experimental values. Similar predictions were obtained for the other two VOCs, ethylbenzene and n-propylbenzene, using sand 30/50 as the porous media. A summary of the modeling results is presented in Table 2. The mass of sorbed VOC at the end of the experimental run was found to be negligible. The predicted final masses of VOCs remaining in the soil column after sparging were close to the experimental values. The data presented in Table 2 showed that after 10 hours of sparging the difference between predicted and

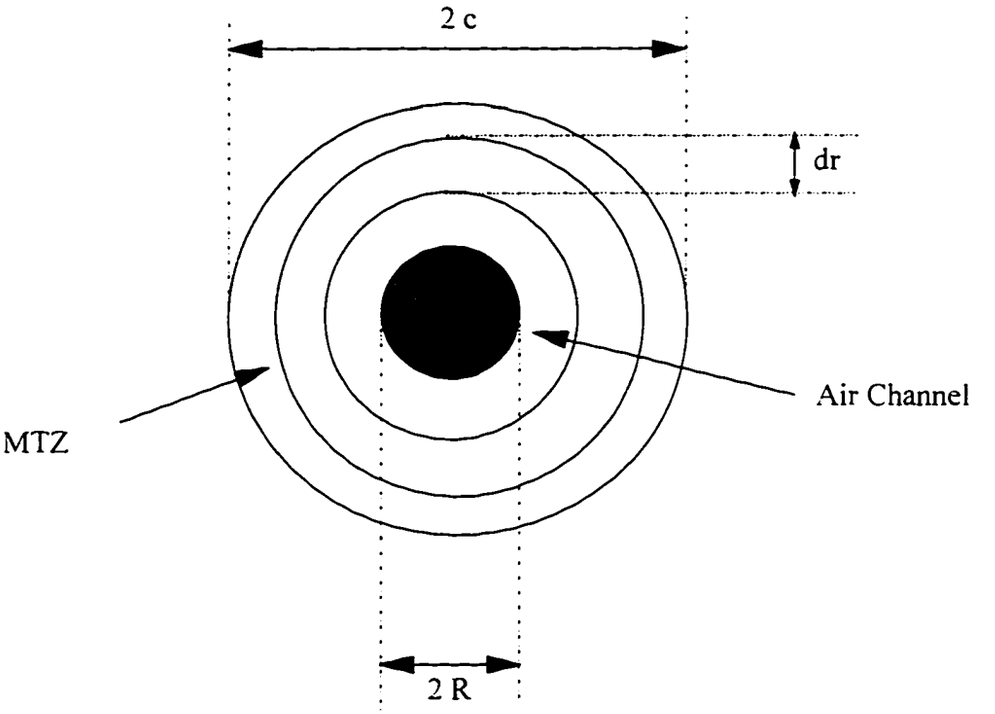

Figure 3. Cross section of air channel and MTZ

Table 1. Parameters used in the model

Porous Media	Air Flow Rate (L/min)	Air Channel Radius (cm)	Tortuosity	K_{Gi} (cm/min)						
				benzene	ethylbenzene	n-propyl-benzene	toluene	chlorobenzene	styrene	1,2 dichloro-benzene
Sand 30/50	0.8	0.100	0.51	0.00664	0.00393	0.00253	N/A	N/A	N/A	N/A
Sand 70/100	0.7	0.175	0.47	0.00774	0.00457	0.00295	N/A	N/A	N/A	N/A
Ottawa Sand	1.1	0.150	0.52	N/A	N/A	N/A	0.00612	0.00849	0.01173	0.01086

Henry's law constant and liquid phase diffusivities were taken from Table2 in Chapter 2

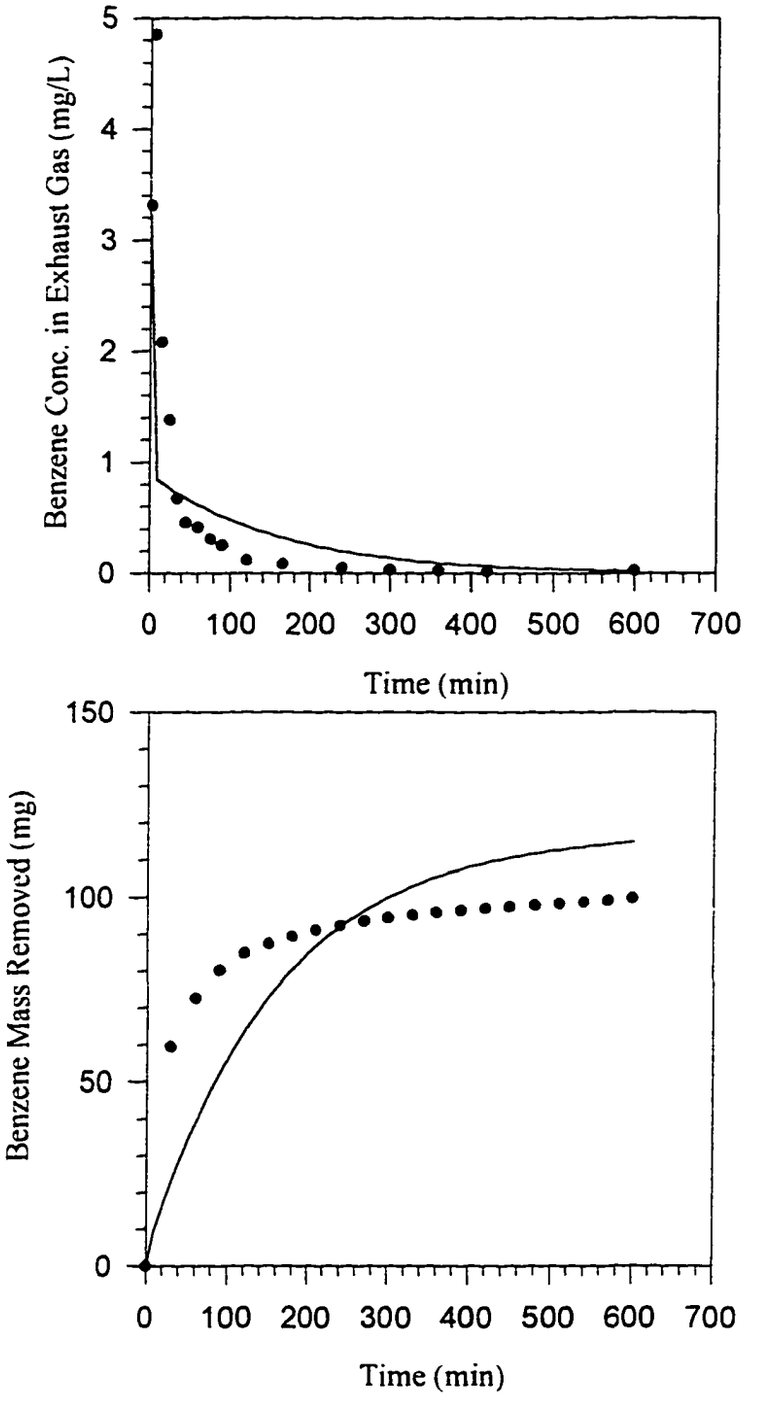

Figure 4. (a) Benzene concentrations in the exhaust air, (b) benzene mass removal for sand 30/50 at an air velocity of 0.86 cm/s

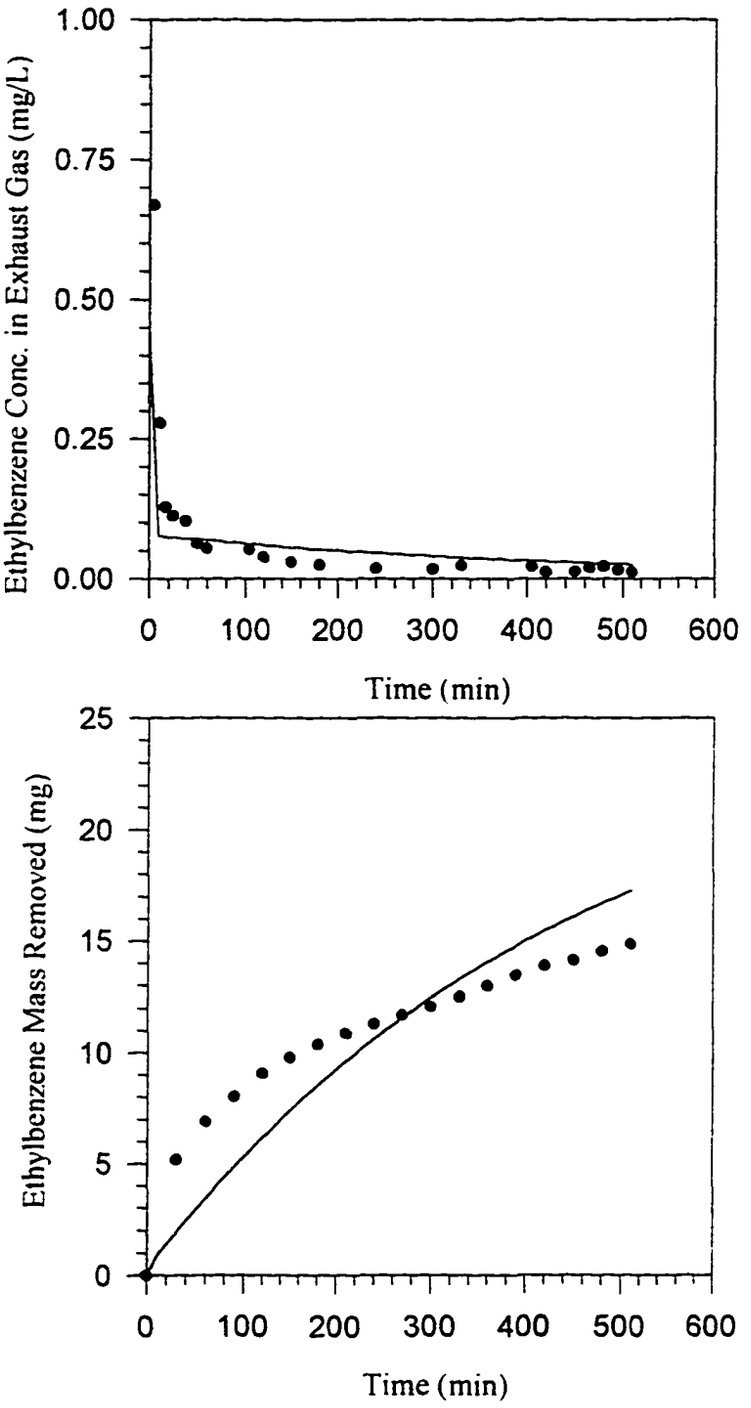

Figure 5. (a) Ethylbenzene concentrations in the exhaust air, (b) ethylbenzene mass removal for sand 30/50 at an air velocity of 1.21 cm/s

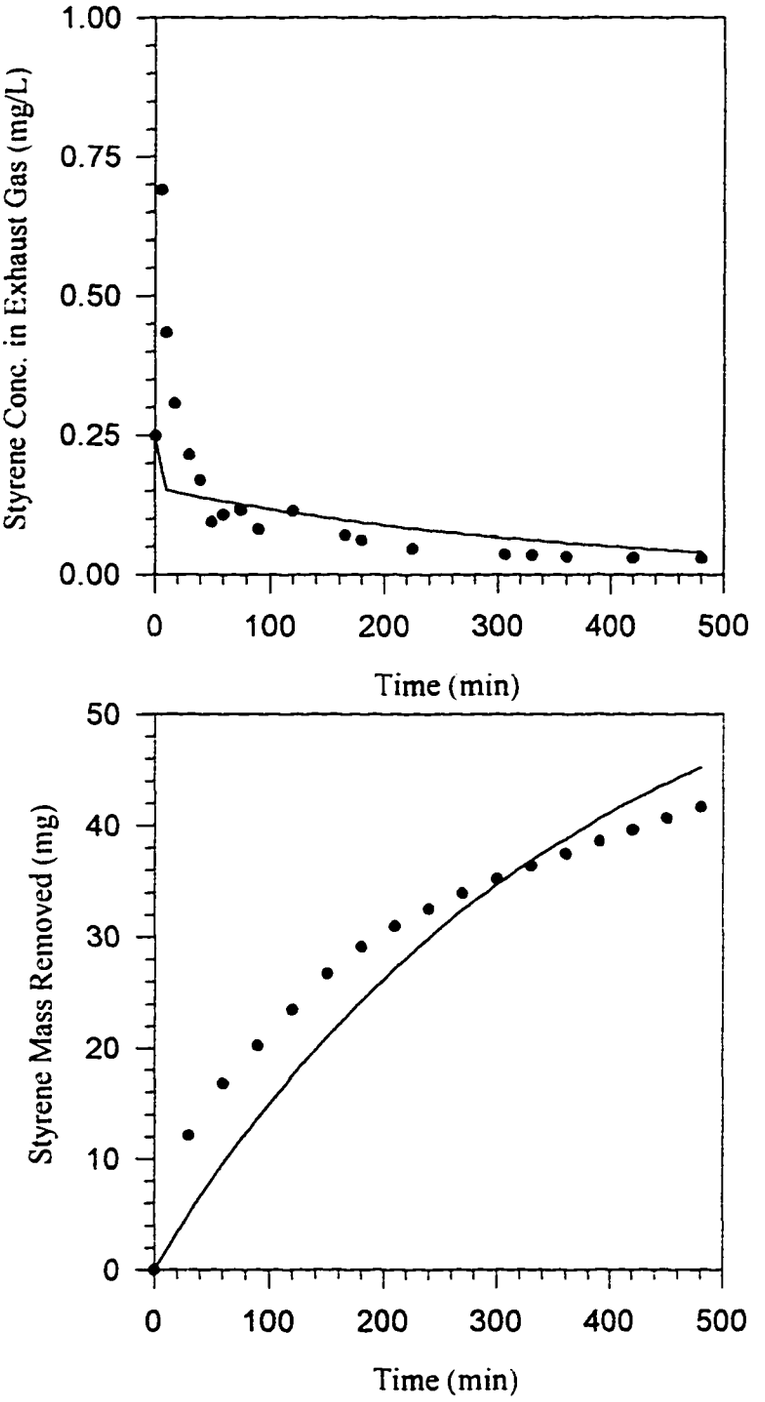

Figure 6. (a) Styrene concentrations in the exhaust air, (b) styrene mass removal for Ottawa sand and air velocity of 1.34 cm/s

Table 2. Summary of modeling results

Porous Media	Air Velocity (cm/s)	VOC	Experimental Initial Mass (mg)*	Experimental Mass Removed (mg)	Predicted Mass Removed (mg)	Experimental Final Average Aqueous Concentration (mg/L)*	Predicted Final Average Aqueous Concentration (mg/L)	Experimental Final Average Mass Remaining (mg) *	Predicted Final Average Mass Remaining (mg)
Sand 30/50	0.86	Benzene	118.7 ± 1.02	99.67	114.83	0.7 ± 0.7	1.15	1.51 ± 1.54	2.62
Sand 30/50	0.86	Ethylbenzene	96.98 ± 0.83	91.69	92.69	1.6 ± 0.4	1.47	3.63 ± 0.92	3.34
Sand 30/50	0.86	n-Propylbenzene	15.62 ± 0.44	11.74	14.45	0.2 ± 0.1	0.45	0.49 ± 0.22	1.02
Sand 70/100	1.21	Benzene	36.32 ± 1.92	23.56	26.22	5.43 ± 1.02	3.95	13.85± 2.60	10.22
Sand 70/100	1.21	Ethylbenzene	25.40 ± 1.23	14.87	17.17	4.42 ± 0.42	3.17	11.27 ± 1.07	8.20
Sand 70/100	1.21	n-Propylbenzene	1.88 ± 0.01	1.39	1.13	0.30 ± 0.01	0.29	0.77 ± 0.02	0.76
Ottawa Sand	1.34	Toluene	69.58 ± 2.75	39.96	55.86	14.3 ± 1.1	5.64	34.33 ± 2.53	13.62
Ottawa Sand	1.34	Chlorobenzene	239.9 ± 19.7	148.43	179.84	28.8 ± 8.6	24.56	69.04 ± 19.8	59.24
Ottawa Sand	1.34	Styrene	61.18 ± 3.25	41.66	45.21	10.6 ± 1.6	6.61	25.24 ± 3.68	15.95
Ottawa Sand	1.34	1,2-Dichlorobenzene	45.72 ± 1.79	37.97	35.66	4.9 ± 1.7	4.14	11.81 ± 3.91	10.00

* including standard deviation

experimental mass removed for sand 30/50 was 15 mg for benzene (13% of the total mass of benzene), 1 mg for ethylbenzene (1% of the total mass of ethylbenzene), and 2.7 mg for n-propylbenzene (17% of the total mass of n-propylbenzene). For the three VOCs, the model overpredicted the mass removed. For this experiment, the difference between the experimental and modeled final VOC concentrations in the liquid phase ranged between 0.3 mg/L and 1.1 mg/L.

Figure 5 shows the experimental and predicted ethylbenzene vapor concentrations and the cumulative mass removed using sand 70/100 as porous medium and an estimated average air pore velocity equal to 1.21 cm/s. The average air channel diameters were visually estimated to be 3.5 mm, and air saturation was estimated to be 6.3%. Just as in Figure 4, Figure 5 shows that for early sparging times, the predicted cumulative mass removed was lower than the experimental mass removed. This may be due to the initial volatilization of VOCs from the displaced water located at the top of the sparged porous media and the VOCs in the headspace of the soil column which were not considered in the formulation of the model. The difference between predicted and experimental mass removed may be estimated from Table 2. For sand 70/100, the difference between predicted and experimental mass removal was 2.7 mg for benzene (7.6% of the total mass of benzene), 2.3 mg for ethylbenzene (9% of the total mass of ethylbenzene), and 0.26 mg for n-propylbenzene (14% of the total mass of n-propylbenzene).

The sensitivity of the model can be seen by comparing the results for the sand 30/50 and the sand 70/100. For sand 30/50, the initial VOCs concentrations (benzene, ethylbenzene, and n-propylbenzene) were about four times higher than the initial concentrations used in the experiment for sand 70/100. On the other hand, the average air pore velocity for sand 70/100 was approximately 1.5 times higher than the average air pore velocity used for sand 30/50. If the mass removed or the mass remained were compared, it can be seen that despite the low concentration of the VOCs present in sand 70/100, the mass remaining was higher than of sand 30/50. This implies that the porous media had a strong effect on the mass volatilized by air sparging independent of the air flow rate once a quasi steady-state of aqueous VOC diffusion was established. The ability of the model to predict the experimental results for different porous media and air velocities indicates that the model was sensitive to the various

experimental conditions. In addition, the model also provides validation to the concept of the mass transfer zone (*MTZ*) surrounding the air channels.

Figure 6 presents the measured and predicted styrene concentrations and the cumulative mass removed using Ottawa sand as porous medium and an estimated air pore velocity of 1.34 cm/s. For this experimental run, the diameter of the air channels was approximately 3 mm and the air saturation was estimated to be 8.1%. The model predicted fairly well the measured experimental vapor concentrations for styrene. Table 2 presents the modeling results for the other three VOCs. The model predicted very well the final mass of chlorobenzene and 1,2 dichlorobenzene but the prediction was poor for toluene. After 8 hours of sparging the mass removed, experimentally and modeled, were fairly similar for styrene and 1,2 dichlorobenzene (less than 10% difference). For chlorobenzene, the difference was 30 mg or 20%. Even though this value seemed high it represented just 12.5% of the total initial mass of chlorobenzene present in the reactor. For toluene, the predicted average aqueous concentration was 5.64 mg/L while the experimentally determined aqueous concentration was 14.3 mg/L. A probable reason for the less than desirable prediction may be due to the cosolvent interactions between toluene and other VOCs. For this experimental run, the model over predicted the mass of VOC removed after 8 hours for all VOCs except for 1,2 dichlorobenzene. From Table 2, the difference between experimental and predicted mass of VOC remaining in the column after 8 hours was estimated to be 30% of the total mass for toluene, 4% of the total mass for chlorobenzene, 15% of the total mass for styrene, and 4% of the total mass for 1,2 dichlorobenzene.

For early sparging times, Figure 6 shows a similar behavior as seen in the two previous experimental runs with respect to the cumulative mass removal. The mass removed experimentally was higher than the predicted mass removal for early sparging times but the situation was reversed after 300 minutes of sparging. For all three experimental runs using different porous media, the model underpredicted the vapor concentrations for early sparging times but after 100 minutes of sparging the model slightly overpredicted the vapor concentration. As explained earlier, this behavior may be due to the initial displacement of head space above the saturated porous media and the volatilization of VOCs from the initial air-displaced water in the top layer of glass beads. These two processes were not considered

in the formulation of the model.

Given the experimental errors associated with the measurement of the VOC concentrations in the different phases, experimental mass balances were conducted and the differences were found to range from 1% of the total mass for ethylbenzene to 20% of the total mass for n-propylbenzene (sand 30/50). The experimental mass balance difference was computed for each VOC as follows:

$$\text{Experimental VOC Mass Balance Difference} = (X_o + S_o) - (Y + X_f + S_f) \quad (8)$$

where Y is the experimentally measured total mass of VOC removed (mg), X is the experimentally determined mass of VOC present in the aqueous phase (mg), S is the experimentally determined mass of VOC sorbed onto the solid phase (mg), and the subscripts o and f represent initial and final conditions, respectively. X was determined by multiplying the average value of the VOC aqueous concentration along the column depth times the volume of water present in the column. The average difference between initial and final mass for all VOCs tested was 10%. The measured mass of VOC remaining in the liquid phase and the experimentally determined mass of VOC removed were plotted and compared with the predicted values as shown in Figures 7 to 9 for the three experimental runs. Also plotted in the figures was the experimental VOC mass balance difference as defined in equation 8. Figures 7 to 9 showed that when the experimental mass balance differences were taken into account the results of the model, which conserved all the mass of the VOCs, compared fairly well with the experimental results and were within 5% of the initial mass present.

Of all the different parameters used in the model, the radius of the air channels was the most difficult parameter to be estimated. To assess the influence of the air channel radius on the overall benzene mass removal for sand 30/50, simulations were conducted by using air channel radius of 1.25 mm and 0.0875 mm. The results of the simulations are presented in Figure 10. Figure 10 shows that mass removal was inversely related to the radius of the air channel. When the radius of the air channel was smaller, the overall mass of benzene removed was larger due to an increase in the air-water interfacial area of the system. The

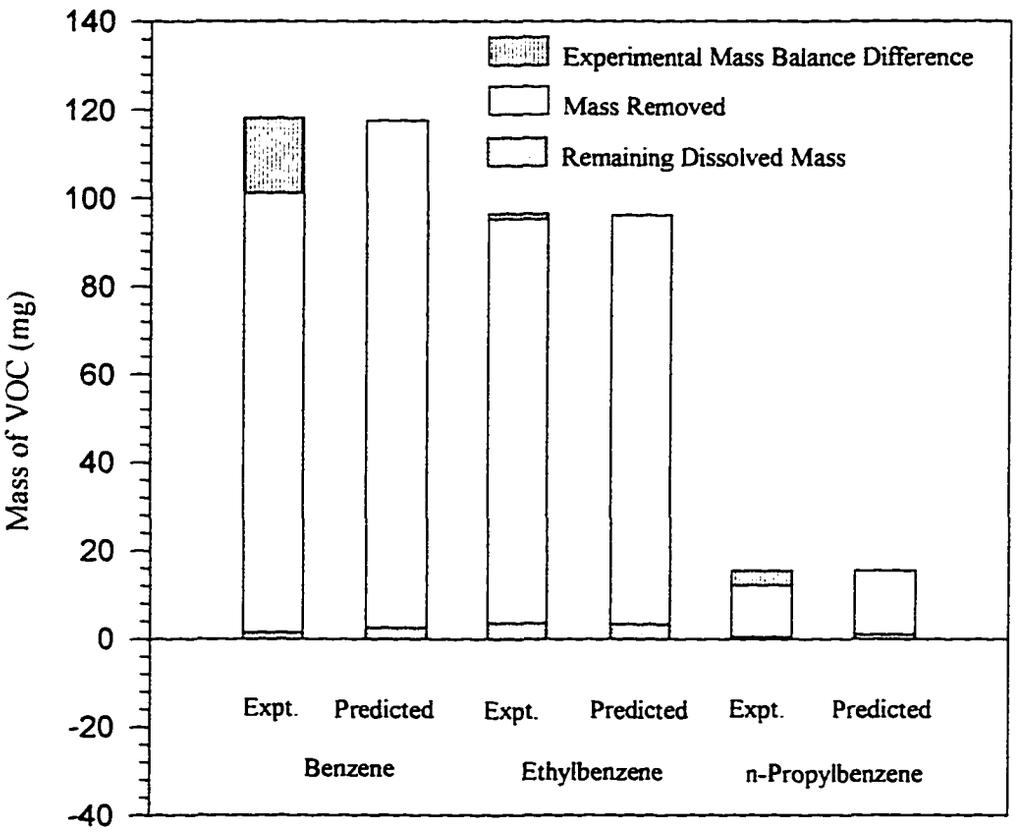

Figure 7. Comparison of experimental and predicted mass distribution after sparging for sand 30/50 and air velocity of 0.86 cm/s (Experimental mass balance difference = initial (sorbed + dissolved) VOC mass in the column - mass of VOC volatilized - final (dissolved + sorbed) mass of VOC in the column)

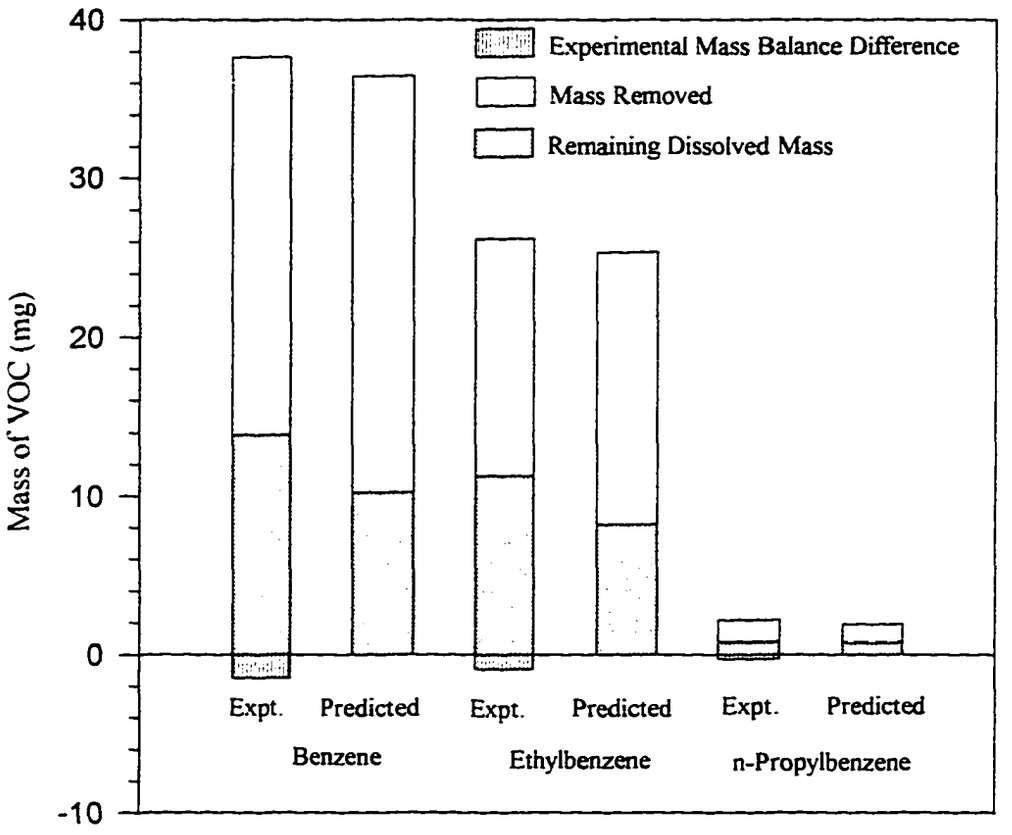

Figure 8. Comparison of experimental and predicted mass distribution after sparging for sand 70/100 and air velocity of 1.21 cm/s (Experimental mass balance difference = initial (sorbed + dissolved) VOC mass in the column - mass of VOC volatilized - final (sorbed + dissolved) mass of VOC in the column)

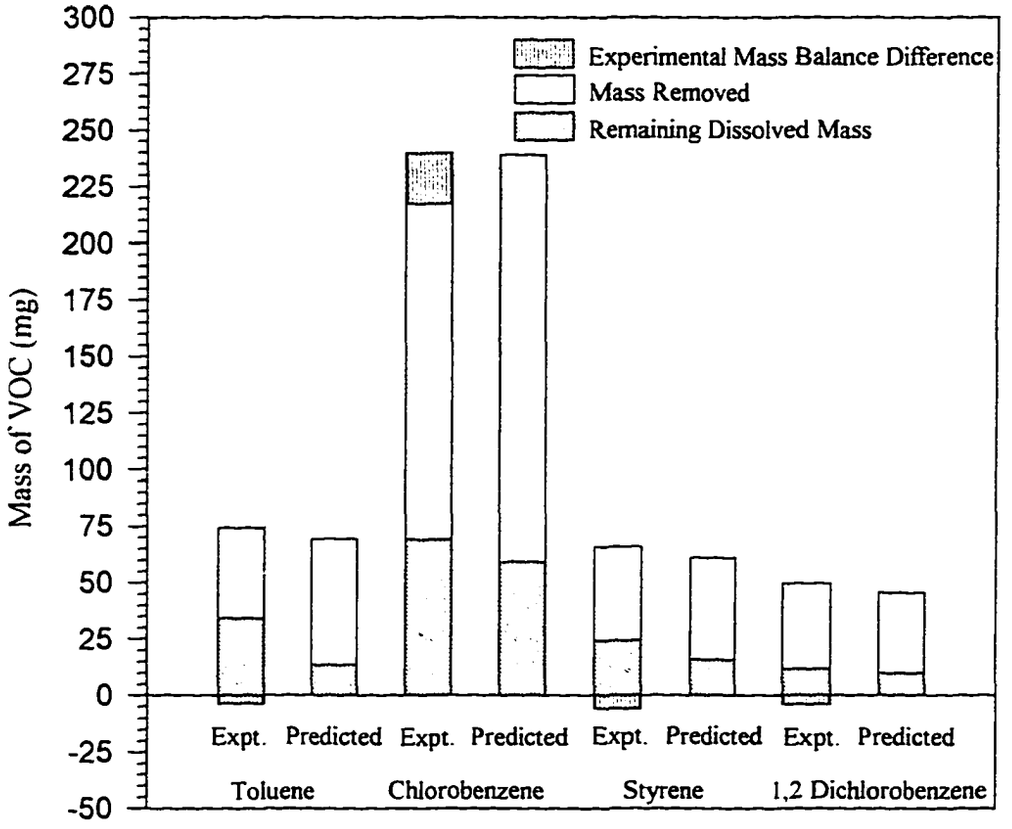

Figure 9. Comparison of experimental and predicted mass distribution after sparging for Ottawa sand and air velocity of 1.34 cm/s (Experimental mass balance difference = initial (sorbed + dissolved) VOC mass in the column - mass of VOC volatilized - final (sorbed + dissolved) mass of VOC in the column)

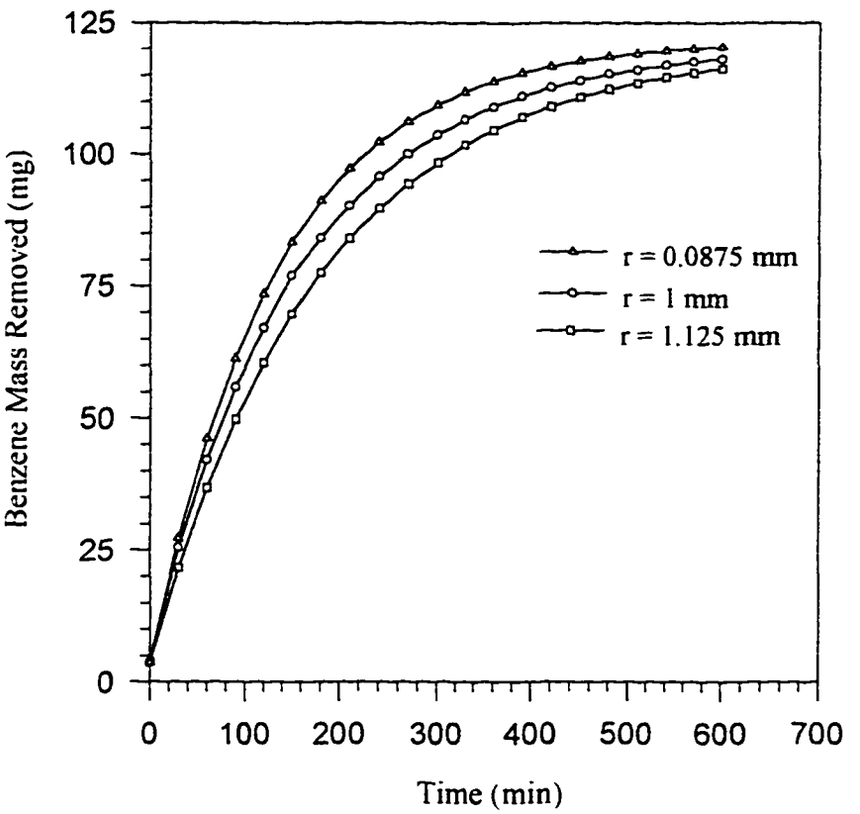

Figure 10. Influence of air channel radius on benzene mass removal

predicted mass of benzene remaining in the system after 10 hours of sparging was 1.36 mg for an air channel radius of 0.0875 mm and 4.11 mg for an air channel radius of 1.125 mm, respectively. When compared with the measured mass remaining (1.51 $\pm$ 1.54) mg it can be seen that model predictions were within the actual mass remaining in the soil column.

The predictions of the one-dimensional diffusion model which incorporated the independently determined mass transfer coefficients and mass transfer zone concept as determined in the single-air channel studies, showed that the model was capable of describing fairly well the VOC concentrations in the exhaust air, and final VOC concentrations in the liquid phase. It is possible that the successful application of the results from a single-air channel apparatus to a complex system such as a soil column may be extended by scaling up the model for the prediction of air sparging on a field scale. Further testing using saturated soil tanks, simulating field-scale sparging process, should be conducted to test and improve the model.

Conclusions

A one-dimensional diffusion model was used to model the air sparging of soil columns contaminated with VOCs. The tortuosity factor and mass transfer coefficients determined by single-air channel studies were used as input parameters for the model. In addition, the concept of mass transfer zone (*MTZ*) was incorporated into the model. The model predicted fairly well the VOC concentrations in the exhaust air and the total mass removed for nine out of the ten cases tested. Except for toluene, the predictions for mass removal were ranged from 1% to 17% of the initial VOC mass present in the column.

The results of the model seemed to suggest that air sparged soil columns may be represented by a composite of individual air channels surrounded by a nonadvective region of porous media or *MTZ*. The extent of the nonadvective region will depend on the air saturation and the physical-chemical properties of the air sparging system. Under these conditions, the closer the air channels, the better is the removal of VOCs.

Application of the model to predict field-scale air sparging operations may yield similar results. However, more laboratory testing is needed to verify the model and the validity of the mass transfer correlations for different air sparging conditions.

References

Braida, W.J., and S.K. Ong, Air sparging effectiveness: the air channel mass transfer zone, submitted to *Water Resources Research,* 1997a.

Braida, W.J., and S.K. Ong, Air sparging: air -water mass transfer coefficients, submitted to *Water Resources Research*, 1997b.

Drucker , A.S., and S.S. Di Julio, Groundwater clean up by *In situ* air sparging: Development of a model and application to saturated soil column experiments, in *Proceedings of the Water Environmental Federation 69 th Annual Conference and Exposition,* Dallas, Texas, October 5-9, 1996.

Hein, G.L., Air Sparging as a remediation technique: modeling and experimental analysis, Ph.D. Dissertation, 177 pp., Michigan Technological University, Houghton, MI, 1996.

Ji, W., Air Sparging: Experimental and theoretical analysis of flow and numerical modeling of mass transfer, Ph.D. Dissertation, 155 pp., The University of Connecticut, Storrs, CN, 1994.

CHAPTER NINE. GENERAL CONCLUSIONS AND FUTURE WORK

Conclusions

This chapter summarizes the conclusions presented in the preceding chapters. A single-air channel experimental setup was used to study the controlling mechanisms in the volatilization of VOCs during air sparging. Correlations between estimated mass transfer parameters and the physical-chemical properties of the system were developed. Once the controlling mechanisms for the volatilization of VOCs during air sparging were established, a one-dimensional diffusion model was developed. The model using the information determined by the single air channel setup was then used to predict the VOC concentrations in the exhaust air and in the liquid phase for the air sparging of soil columns. The conclusions of this study are as follows:

(i) According to the results of the single-air channel setup, mass transfer of VOCs during air sparging was found to be a diffusion-limited process. A steep concentration gradient zone was shown to exist in the saturated porous media next to the air channels during air sparging operations. The steep concentration zone was named as the mass transfer zone (*MTZ*). Depending on the VOC and the porous media used, the size of the *MTZ* ranged between 17 mm and 41 mm or between 70 and 215 dp_{50}.

(ii) A correlation was developed to predict the size of the *MTZ*. The correlation incorporated the Pore Diffusion Modulus, the air phase Peclet number, the uniformity coefficient and the dimensionless mean particle size of the porous media. The size of the *MTZ*, was found to be proportional to the aqueous diffusivity of the VOC, the uniformity coefficient, and the mean particle size of the porous media. Air velocity was found to have marginal effect on the size of the *MTZ*.

(iii) The size of the *MTZ* was found to be affected by the amount of organic carbon present in the porous media. An increase in the organic carbon content of the soil resulted in a decrease in the size of the *MTZ*. The effect was larger for VOCs with low solubilities and high partition coefficients (such as n-propylbenzene). The decrease in the size of the *MTZ* may be due to sorption onto the solid phase which retarded the diffusion of the VOCs to the air-water interface.

(iv) The overall gas phase mass transfer coefficients (K_G) for the volatilization of VOCs were found to be between 1.79 x 10^{-3} cm/min and 3.85 x 10^{-2} cm/min. Two correlations incorporating the modified Sherwood number and Damkohler number with Peclet number, dimensionless mean particle size, and dimensionless Henry's law constant were developed. K_G was found to be proportional to the gas phase diffusivity of the VOC but inversely proportional to the Henry's law constant of the VOC. The dominant and controlling factor in the determination of the overall mass transfer coefficients was the diffusivity of the VOC in the air phase.

(v) The two-resistance model of Whitman may be used to describe the controlling resistance for the volatilization of VOCs during air sparging. For VOCs with large values of the dimensionless Henry's law constant, the liquid side layer controlled the volatilization of VOCs at the air-water interface. For VOCs with low values of the Henry's law constant, air velocity and the mean particle size of the porous media seemed to have an effect on the relative magnitude of the liquid or gas resistance to mass transfer.

(vi) For a NAPL located several centimeters away from the air-water interface, air sparging has a positive effect on controlling the spreading of the NAPL. The effect was larger for compounds with high water solubilities and high diffusivity. An increase in the air flow rate did not produce any improvement in the removal efficiency of the VOCs. Porous media with larger particle size than fine sand ($\approx$ 0.2 mm) showed higher removal rates. This suggests that removal rate was controlled by the diffusion of the dissolved VOCs to the air-water interface.

(vii) A modification of the one-dimensional diffusion model which included a retardation factor (R) was found to predict fairly well the concentration curves for the liquid and air phases by using the mass transfer coefficients from the correlations developed in Chapter 4. Experimental results showed that the sorbed concentration in the porous media did not change after sparging for 8 hours. This indicates that sorption plays a significant role in retarding the VOCs and much of the VOCs volatilized were from the aqueous phase.

(viii) A one-dimensional diffusion model using cylindrical coordinates and the mass transfer coefficients estimated using the single air channel setup was found to predict fairly well the VOC concentrations in the exhaust air and the final VOC concentrations in the

liquid phase for air sparged soil columns.

Recommended Future Work

Even though the results of this research have answered some questions about the controlling mechanisms in the volatilization of VOCs during air sparging operations, some questions still remain unanswered. The following recommendations are provided for further research of this technology:

(i) Understand the exact nature of the air flow within sparged aquifers. Predict the size and number of channels within the sparged aquifer as a function of physical properties and air saturation.

(ii) Study the influence of organic carbon content of the soil and the water-solid partition coefficient of the VOCs on the size of the *MTZ*.

(iii) Study the rate of dissolution of NAPLs during air sparging operations and determine how the location of the NAPL with respect to the *MTZ* affects mass transfer.

(iv) Investigate the mass transfer of oxygen from the sparged air into the groundwater and assess the role of bioremediation in the cleanup of contaminated aquifers during air sparging operations.

(vi) Apply the one-dimensional diffusion model for the prediction of the volatilization of VOCs in air sparged soil columns containing different organic carbon contents.

(vii) Apply the diffusion model and the *MTZ* and K_G empirical correlations for the prediction of the volatilization of VOCs during air sparging in actual field conditions.

APPENDIX A. NOTATION

Dimensionless Numbers Definition and Parameters Nomenclature

Sh_i, overall i phase Sherwood number, $\frac{K_i d_p}{D_i}$, where d_p is the geometric mean particle diameter.

Sh_i', overall i phase modified Sherwood number, $\frac{K_i a_{ij} d_p^2}{D_i}$, where d_p is the geometric mean particle diameter.

a_{aw}, specific interfacial area (L^{-1}).

Re_i, i phase Reynolds number, $\frac{d_p v_i \rho_i}{\mu_i}$.

Sc_i, i phase Schmidt number, $\frac{\mu_i}{\rho_i D_i}$.

Nu_i, i phase Nusselt number, $\frac{K_i d_p}{D_i}$.

ε, porosity.

μ_l, i phase viscosity ($MT^{-1}L^{-1}$).

ρ_i, i phase density (ML^{-3}).

$D_{i,j}$, for $i = a,w$ and $j = x,z,r$, VOC's diffusion coefficient in liquid and air phase in the x z and r directions, respectively (L^2T^{-1}).

S_a, air saturation, dimensionless.

K_H, dimensionless Henry's law constant, dimensionless.

Pe, air phase Peclet number, $\frac{G L}{\rho_a A_p D_a}$, where G is the air mass flow rate, L is the length of sparging regime and A_P is the pore area.

St, Stanton number, $\frac{K_{L a_{aw}} L \rho_a A_p}{2 K_H G}$, where $K_L a_{aw}$ is the lumped mass transfer coefficient.

Ed, pore diffusion module, $\frac{\rho_a A_p D_w L}{G R_{oi}^2}$, where R_{oi} is the influence radius.

ϖ; Damkholer number, $\frac{K_{L a_{aw}} L}{v}$, where L is the air flowpath length, and v is the specific air discharge.

k_i, for i a and w, liquid and gas side mass transfer coefficients (L/T).

K_L, overall liquid side mass transfer coefficient between liquid and air phases (L/T).

K_G, overall air side mass transfer coefficient between liquid and air phases (L/T).

K_{ow}, octanol water partition coefficient, dimensionless.

k_{ws}, mass transfer coefficient between adsorbed and dissolved VOCs (T^{-1}).

V_i, *for* $i=a,s,w$ is the volume of the cited phase (air, solid, or liquid, respectively, L^3).

K_d, partition coefficient (adsorbed-dissolved, L^3/M).

K_{dis}, mass transfer coefficient between NAPL and dissolved VOC (T^{-1}).

C_a, VOC air-phase concentration (M/L^3).

C_w, VOC liquid-phase concentration (M/L^3).

C_s, VOC sorbed-phase concentration (M/M).

Q_a, air flow rate (L^3/T).

APPENDIX B. RAW DATA AND MASS BALANCES

Single-Air Channel Experiments
Gas Phase and Aqueous Phase VOC Concentrations

Ottawa Sand, Air Flow Rate 10 mL/min, Temperature 21°C
Air Phase Concentrations (mg/L)

Time (min)	Benzene	Ethylbenzene	m,p-Xylene	o-Xylene
1	0.039	0.006	0.002	0.000
3	0.068	0.051	0.001	0.000
5	0.116	0.102	0.026	0.053
10	1.583	0.190	0.194	0.140
20	2.135	0.299	0.329	0.197
30	1.855	0.389	0.388	0.153
45	1.881	0.431	0.462	0.278
60	1.815	0.433	0.485	0.368
75	1.614	0.371	0.410	0.254
90	1.563	0.408	0.427	0.262
105	1.442	0.389	0.446	0.276
120	1.387	0.433	0.428	0.248
150	1.020	0.324	0.349	0.189
180	0.890	0.324	0.304	0.190
210	0.649	0.236	0.270	0.161
240	0.548	0.212	0.221	0.145
270	0.508	0.236	0.253	0.125
300	0.487	0.160	0.185	0.103
360	0.487	0.157	0.154	0.101
420	0.485	0.154	0.152	0.100
480	0.483	0.154	0.151	0.100

Liquid Phase Concentrations (mg/L)

Depth (mm)	Benzene (0 h)	Benzene (8 h)	o-Xylene (0 h)	o-Xylene (8 h)
5.0	67.056	21.659	21.719	9.774
10.0	88.793	30.522	25.054	11.868
19.1	121.049	59.135	29.864	23.581
38.1	120.818	118.747	28.118	24.968
63.5	115.037	115.033	32.431	32.215
88.9	121.550	120.786	32.340	32.046

Liquid Phase Concentrations (mg/L)

Depth (mm)	Ethylbenzene (0 h)	Ethylbenzene (8 h)	m,p-Xylene (0 h)	m,p-Xylene (8 h)
5.0	24.394	9.916	26.575	10.288
10.0	28.767	15.835	32.642	17.312
19.1	38.230	30.690	43.925	36.256
38.1	37.816	35.327	46.013	45.291
63.5	39.965	38.916	46.202	46.408
88.9	38.597	38.200	48.025	47.091

Ottawa Sand, Air Flow Rate 10 mL/min, Temperature 21°C
Air Phase Concentrations (mg/L)

Time (min)	Toluene	Chlorobenzene	Styrene	Propylbenzene	1,2 DCB	1,2,4 TCB
0	0.000	0.000	0.000	0.000	0.000	0.000
1	0.000	0.000	0.000	0.000	0.000	0.000
3	0.000	0.000	0.000	0.000	0.000	0.000
5	0.095	0.000	0.000	0.000	0.000	0.000
10	0.411	0.227	0.143	0.095	0.046	0.000
20	0.583	0.357	0.197	0.170	0.086	0.027
30	0.587	0.434	0.221	0.195	0.132	0.027
45	0.590	0.442	0.259	0.214	0.248	0.042
60	0.552	0.468	0.337	0.293	0.271	0.056
75	0.538	0.462	0.252	0.329	0.285	0.131
90	0.514	0.446	0.255	0.336	0.376	0.160
105	0.481	0.420	0.248	0.337	0.334	0.125
120	0.446	0.410	0.240	0.344	0.268	0.103
135	0.423	0.406	0.220	0.284	0.219	0.108
150	0.400	0.362	0.218	0.279	0.209	0.093
180	0.392	0.358	0.209	0.274	0.202	0.089
210	0.367	0.347	0.210	0.224	0.180	0.067
240	0.331	0.346	0.200	0.219	0.200	0.060
300	0.321	0.309	0.200	0.137	0.185	0.063
360	0.307	0.263	0.189	0.126	0.190	0.051
420	0.293	0.245	0.179	0.084	0.188	0.041
480	0.292	0.232	0.165	0.085	0.178	0.029

Liquid Phase Concentrations (mg/L)
t = 0 h

Depth (mm)	Toluene	Chlorobenzene	Styrene	n-propylbenzene	1,2 DCB	1,2,4 DCB
5.0	49.132	48.614	34.501	13.896	39.824	6.548
10.0	65.001	66.051	38.865	18.005	42.882	7.329
19.1	64.244	70.247	42.924	19.649	45.456	9.879
38.1	68.205	70.302	44.370	22.712	46.019	9.750
63.5	69.887	71.313	43.981	25.846	46.160	10.420
88.9	69.883	71.313	44.370	25.775	46.600	10.831

Liquid Phase Concentrations (mg/L)
t = 4 h

Depth (mm)	Toluene	Chlorobenzene	Styrene	n-propylbenzene	1,2 DCB	1,2,4 DCB
5.0	40.281	42.521	27.644	11.279	26.261	5.534
10.0	46.397	46.579	29.743	15.379	41.948	7.067
19.1	57.070	63.117	41.130	18.978	40.957	9.804
38.1	63.923	69.312	41.889	20.974	43.392	9.357
63.5	68.995	70.228	43.497	24.650	45.297	10.179
88.9	69.435	70.234	44.245	24.905	46.511	10.733

Liquid Phase Concentrations (mg/L)
t = 8 h

Depth (mm)	Toluene	Chlorobenzene	Styrene	n-propylbenzene	1,2 DCB	1,2,4 DCB
5.0	26.778	34.022	19.844	7.368	23.861	4.534
10.0	44.097	41.759	31.043	15.166	36.928	7.067
19.1	56.870	58.527	37.630	17.902	40.937	9.004
38.1	62.823	68.210	41.881	20.196	43.388	9.250
63.5	68.856	70.224	43.500	23.655	45.097	9.879
88.9	69.430	70.224	44.235	24.035	46.501	10.723

Ottawa Sand, Air Flow Rate 25 mL/min, Temperature 21°C
Air Phase Concentrations (mg/L)

Time (min)	Benzene	Ethylbenzene	m,p-Xylene	o-Xylene
0	0.1600	0.0054	0.0043	0.0045
1	1.0325	0.0718	0.0735	0.0513
2	1.2897	0.3525	0.3530	0.2968
4	1.1155	0..3330	0.3350	0.2228
11	0.8325	0..1718	0.2965	0.1475
20	0.6653	0.1225	0.2260	0.1298
30	0.4858	0.0830	0.1250	0.1088
45	0.2395	0.0750	0.0972	0.0828
60	0.2028	0.0635	0.0790	0.0790
75	0.1793	0.0605	0.0744	0.0728
90	0.1623	0.0503	0.0694	0.0637
105	0.1533	0.0508	0.0585	0.0528
120	0.1485	0.0550	0.0565	0.0480
150	0.1493	0.0465	0.0510	0.0406
180	0.1473	0.0430	0.0378	0.0345
240	0.1178	0.0468	0.0329	0.0237
300	0.1145	0.0410	0.0272	0.0174
360	0.1087	0.0311	0.0269	0.0193
420	0.1078	0.0275	0.0215	0.0198
480	0.1098	0.0247	0.151	0.0100

Liquid Phase Concentrations (mg/L)

Depth (mm)	Benzene (0 h)	Benzene (4 h)	Benzene (8 h)	o-Xylene (0 h)	o-Xylene (4 h)	o-Xylene (8 h)
5.0	42.342	16.289	15.357	13.963	5.472	1.427
15.0	83.513	67.357	56.196	17.066	15.119	13.089
19.1	103.258	93.125	86.765	23.366	23.315	20.116
38.1	106.840	100.183	96.951	23.396	23.311	22.194
63.5	108.484	108.694	108.691	23.517	23.457	23.298
88.9	109.387	109.301	109.294	23.467	23.368	23.366

Liquid Phase Concentrations (mg/L)

Depth (mm)	Ethylbenzene (0 h)	Ethylbenzene (4 h)	Ethylbenzene (8 h)	m,p-Xylene (0 h)	m,p-Xylene (4 h)	m,p-Xylene (8 h)
5.0	9.264	3.217	1.065	10.592	3.978	2.858
15.0	26.843	18.713	13.170	25.682	14.012	13.845
19.1	30.252	23.561	22.044	30.010	26.117	23.336
38.1	31.385	30.613	30.549	30.307	30.105	27.140
63.5	31.225	31.224	31.165	31.434	31.569	31.723
88.9	31.589	31.580	31.563	31.492	31.489	31.468

Ottawa Sand, Air Flow Rate 25 mL/min, Temperature 21°C
Air Phase Concentrations (mg/L)

Time (min)	Toluene	Chlorobenzene	Styrene	Propylbenzene	1,2 DCB	1,2,4 TCB
1	0.0235	0.0161	0.0865	0.0469	0.0115	0.0006
5	0.7210	0.4415	0.2195	0.2425	0.0157	0.0006
10	0.6550	0.5400	0.2610	0.2875	0.0253	0.0008
20	0.6275	0.5535	0.2865	0.3345	0.0288	0.0148
30	0.5495	0.5335	0.2505	0.3580	0.0344	0.0138
45	0.5145	0.4550	0.2310	0.3690	0.0413	0.0128
60	0.4630	0.3750	0.1755	0.3720	0.0407	0.0118
75	0.3915	0.3600	0.1715	0.2310	0.0620	0.0118
90	0.3600	0.3270	0.1595	0.2130	0.0530	0.0142
105	0.2775	0.3160	0.1335	0.1835	0.0580	0.0171
120	0.2476	0.2950	0.1238	0.1045	0.0440	0.0167
150	0.2260	0.2334	0.1245	0.1055	0.0447	0.0166
180	0.1880	0.2070	0.1105	0.0925	0.0407	0.0160
210	0.1487	0.1410	0.0978	0.0752	0.0332	0.0138
240	0.1207	0.1201	0.0975	0.0745	0.0287	0.0109
300	0.1015	0.1082	0.0875	0.0742	0.0219	0.0093
360	0.1006	0.1058	0.0825	0.0742	0.0189	0.0093
420	0.1016	0.1024	0.0823	0.0739	0.0161	0.0095

Liquid Phase Concentrations (mg/L)
t = 0 h

Depth (mm)	Toluene	Chlorobenzene	Styrene	n-propylbenzene	1,2 DCB	1,2,4 DCB
5.0	29.908	22.958	14.439	18.063	5.672	1.682
10.0	30.255	31.582	20.503	23.339	7.080	2.127
19.1	32.687	34.547	22.603	25.731	7.402	4.756
38.1	35.357	35.013	22.767	28.390	9.961	4.902
63.5	35.417	35.550	24.114	28.614	9.746	4.904
88.9	35.521	35.709	24.579	29.333	9.915	4.999

Liquid Phase Concentrations (mg/L)
t = 4 h

Depth (mm)	Toluene	Chlorobenzene	Styrene	n-propylbenzene	1,2 DCB	1,2,4 DCB
5.0	9.581	10.114	6.918	6.195	3.012	1.091
10.0	19.639	19.157	13.071	11.917	3.231	2.034
19.1	32.552	29.541	21.123	23.983	7.302	4.658
38.1	34.971	34.816	21.727	26.464	9.098	4.813
63.5	34.918	34.176	23.238	27.318	9.819	4.968
88.9	35.209	34.830	24.049	28.798	9.939	4.969

Liquid Phase Concentrations (mg/L)
t = 8 h

Depth (mm)	Toluene	Chlorobenzene	Styrene	n-propylbenzene	1,2 DCB	1,2,4 DCB
5.0	3.773	2.794	4.711	1.595	0.495	0.991
10.0	10.108	10.072	7.081	7.919	3.170	1.635
19.1	28.522	27.392	20.034	19.853	6.517	4.458
38.1	32.412	31.966	21.121	25.986	8.998	4.804
63.5	32.532	33.776	22.038	26.448	9.839	4.868
88.9	32.565	33.901	24.079	28.392	9.959	4.959

Ottawa Sand, Air Flow Rate 55 mL/min, Temperature 21°C
Air Phase Concentrations (mg/L)

Time (min)	Benzene	Ethylbenzene	m,p-Xylene	o-Xylene
0	0.0370	0.0087	0.0000	0.0097
1	1.5383	0.4210	0.4110	0.3870
2	1.3205	0.3730	0.3870	0.2216
4	0.8738	0..2775	0.1960	0.1943
11	0.6600	0..1026	0.0895	0.0883
20	0.4620	0.0775	0.0750	0.0672
30	0.3200	0.0585	0.0598	0.0494
45	0.2390	0.0467	0.0390	0.0345
60	0.1578	0.0383	0.0353	0.0274
75	0.0953	0.0393	0.0303	0.0137
90	0.0895	0.0385	0.0273	0.0109
120	0.0758	0.0343	0.0272	0.0112
150	0.0695	0.0258	0.0274	0.0106
180	0.0635	0.0219	0.0225	0.0123
240	0.0570	0.0204	0.0215	0.0112
310	0.0557	0.0203	0.0127	0.0107
360	0.0503	0.0157	0.0123	0.0097
420	0.0518	0.0172	0.0164	0.0103
480	0.0505	0.0164	0.0122	0.0108

Liquid Phase Concentrations (mg/L)

Depth (mm)	Ben zene (0 h)	Benzene (3 h)	Benzene (8 h)	o-Xylene (0 h)	o-Xylene (3 h)	o-Xylene (8 h)
5.0	65.650	28.174	20.160	10.519	3.272	2.959
10.0	90.846	57.257	48.654	16.963	5.421	3.503
15.0	106.150	78.967	78.645	21.216	18.997	18.732
19.1	110.095	87.625	86.197	21.981	21.495	20.595
38.1	116.000	112.483	109.627	26.619	26.317	24.786
63.5	119.274	119.974	118.826	28.145	28.007	27.868
88.9	119.557	119.978	120.603	28.674	28.668	28.786

Liquid Phase Concentrations (mg/L)

Depth (mm)	Ethylbenzene (0 h)	Ethylbenzene (3 h)	Ethylbenzene (8 h)	m,p-Xylene (0 h)	m,p-Xylene (3 h)	m,p-Xylene (8 h)
5.0	13.917	4.987	3.345	12.888	5.912	3.642
10.0	17.840	8.543	6.193	17.416	7.644	6.105
15.0	25.406	16.121	12.047	24.709	14.323	12.243
19.1	27.228	19.345	19.251	29.466	26.917	19.602
38.1	29.920	28.737	26.918	32.281	30.005	29.831
63.5	31.084	31.074	30.988	32.405	32.369	32.338
88.9	32.392	32.380	32.376	33.566	33.489	33.500

Ottawa Sand, Air Flow Rate 55 mL/min, Temperature 21°C
Air Phase Concentrations (mg/L)

Time (min)	Toluene	Chlorobenzene	Styrene	Propylbenzene	1,2 DCB	1,2,4 TCB
0	0.0000	0.0000	0.0000	0.0000	0.0000	0.0000
1	0.7355	0.5900	0.3180	0.4855	0.2893	0.0000
3	0.5915	0.6035	0.3405	0.5690	0.2475	0.2473
5	0.4915	0.5485	0.2840	0.4835	0.3603	0.2620
10	0.4000	0.5305	0.2360	0.3885	0.2180	0.2578
20	0.3275	0.3720	0.2385	0.2645	0.1915	0.1608
30	0.2650	0.4115	0.2275	0.1835	0.1880	0.1148
45	0.2550	0.3810	0.2225	0.1345	0.1468	0.0823
60	0.2175	0.2975	0.2180	0.1258	0.1155	0.0716
75	0.1840	0.3005	0.2030	0.1208	0.1048	0.0656
90	0.1880	0.2400	0.1910	0.1145	0.1105	0.0558
105	0.1720	0.2450	0.1560	0.1065	0.0838	0.0543
120	0.1730	0.2320	0.1285	0.0932	0.0718	0.0504
135	0.1525	0.2140	0.1160	0.0800	0.0628	0.0402
150	0.1590	0.1945	0.1195	0.0794	0.0553	0.0304
180	0.1485	0.1790	0.1190	0.0564	0.0538	0.0184
210	0.1285	0.1620	0.1085	0.0524	0.0498	0.0074
240	0.1235	0.1365	0.1028	0.0528	0.0373	0.0052
300	0.1231	0.1250	0.1105	0.0435	0.0160	0.0044
360	0.1138	0.1270	0.0920	0.0425	0.0153	0.0039
420	0.1225	0.1280	0.0940	0.0422	0.0157	0.0039
480	0.1210	0.1310	0.0955	0.0418	0.0150	0.0039

Liquid Phase Concentrations (mg/L)
t = 0 h

Depth (mm)	Toluene	Chlorobenzene	Styrene	n-propylbenzene	1,2 DCB	1,2,4 DCB
5.0	48.903	52.262	40.630	26.579	44.258	12.085
10.0	61.568	63.761	48.288	26.821	46.028	15.446
19.1	76.063	88.107	53.193	32.948	55.237	17.378
38.1	82.243	92.469	56.098	34.442	55.593	18.332
63.5	84.006	94.421	59.857	40.097	59.214	18.988
88.9	85.218	95.562	60.627	40.505	59.053	19.171

Liquid Phase Concentrations (mg/L)
t = 4 h

Depth (mm)	Toluene	Chlorobenzene	Styrene	n-propylbenzene	1,2 DCB	1,2,4 DCB
5.0	18.437	25.218	25.119	11.843	27.127	7.328
10.0	46.037	50.873	31.846	22.567	42.149	9.996
19.1	62.317	66.127	42.321	23.019	43.327	12.174
38.1	76.591	87.128	56.119	34.409	50.911	17.296
63.5	81.126	92.123	56.320	38.453	59.157	18.947
88.9	83.379	93.834	59.176	39.665	58.971	19.069

Liquid Phase Concentrations (mg/L)
t = 8 h

Depth (mm)	Toluene	Chlorobenzene	Styrene	n-propylbenzene	1,2 DCB	1,2,4 DCB
5.0	16.937	18.399	11.563	3.189	24.505	2.356
10.0	34.637	38.621	21.820	12.810	35.820	4.610
19.1	46.080	53.689	34.254	18.304	38.230	9.480
38.1	76.460	84.898	52.806	34.362	50.867	17.074
63.5	80.720	89.216	56.209	38.350	58.757	18.752
88.9	82.079	92.088	57.713	38.816	58.870	18.969

Ottawa Sand, Air Flow Rate 120 mL/min, Temperature 21°C
Air Phase Concentrations (mg/L)

Time (min)	Benzene	Ethylbenzene	m,p-Xylene	o-Xylene
0	0.0000	0.0000	0.0000	0.0045
1	0.9450	0.3260	0.3348	0.1755
3	0.3705	0.1978	0.1803	0.1790
5	0.3327	0.1915	0.1915	0.1658
10	0.2003	0.1163	0.1275	0.0770
20	0.1583	0.1005	0.1100	0.0778
30	0.1332	0.0835	0.0750	0.0690
45	0.1300	0.0785	0.0778	0.0513
60	0.1055	0.0615	0.0515	0.0375
75	0.0868	0.0645	0.0585	0.0338
90	0.0793	0.0490	0.0440	0.0305
105	0.0703	0.0440	0.0393	0.0283
120	0.0558	0.0370	0.0393	0.0280
150	0.0630	0.0333	0.0323	0.0269
180	0.0530	0.0395	0.0285	0.0249
240	0.0425	0.0231	0.0265	0.0249
300	0.0428	0.0147	0.0185	0.0209
360	0.0413	0.0200	0.0139	0.0098
420	0.0425	0.0174	0.0149	0.0078
480	0.041	0.0124	0.0129	0.0075

Liquid Phase Concentrations (mg/L)

Depth (mm)	Ben zene (0 h)	Benzene (4 h)	Benzene (8 h)	o-Xylene (0 h)	o-Xylene (4 h)	o-Xylene (8 h)
5.0	64.359	29.974	15.454	19.541	17.292	10.937
10.0	99.622	61.257	48.905	39.637	23.021	18.655
19.1	122.978	116.625	104.015	39.792	35.012	30.019
38.1	127.000	124.483	116.270	39.055	36.977	32.226
63.5	128.643	126.974	124.183	41.421	41.237	40.870
88.9	134.025	132.978	130.018	42.222	42.221	42.141

Liquid Phase Concentrations (mg/L)

Depth (mm)	Ethylbenzene (0 h)	Ethylbenzene (4 h)	Ethylbenzene (8 h)	m,p-Xylene (0 h)	m,p-Xylene (4 h)	m,p-Xylene (8 h)
5.0	20.171	12.287	9.424	33.484	23.012	12.642
15.0	29.747	25.001	18.424	56.263	33.644	29.043
19.1	52.143	41.023	30.652	66.020	69.523	54.858
38.1	58.401	55.876	52.633	70.424	68.917	63.450
63.5	61.267	57.567	57.422	70.518	70.105	69.095
88.9	63.942	63.645	62.891	70.654	70.489	70.490

Ottawa Sand, Air Flow Rate 120 mL/min, Temperature 21°C
Air Phase Concentrations (mg/L)

Time (min)	Toluene	Chlorobenzene	Styrene	Propylbenzene	1,2 DCB	1,2,4 TCB
0	0.0000	0.0000	0.0000	0.0000	0.0000	0.0000
1	0.2923	0.2773	0.1605	0.3510	0.2805	0.1080
3	0.1665	0.1843	0.0900	0.1350	0.2145	0.0960
5	0.1393	0.1550	0.0810	0.1255	0.1540	0.0910
10	0.1043	0.1208	0.0813	0.1220	0.1445	0.0720
20	0.0930	0.1178	0.0833	0.1005	0.1015	0.0650
30	0.0843	0.0995	0.0593	0.0790	0.0970	0.0590
45	0.0813	0.0875	0.0538	0.0780	0.0730	0.0675
60	0.0675	0.0805	0.0456	0.0775	0.0610	0.0449
75	0.0645	0.0698	0.0448	0.0535	0.0540	0.0412
90	0.0622	0.0738	0.0415	0.0493	0.0340	0.0321
105	0.0600	0.0705	0.0438	0.0444	0.0171	0.0301
120	0.0550	0.0705	0.0343	0.0303	0.0152	0.0301
150	0.0550	0.0623	0.0313	0.0288	0.0121	0.0262
180	0.0538	0.0510	0.0340	0.0241	0.0045	0.0144
210	0.0560	0.0515	0.0310	0.0210	0.0036	0.0110
240	0.0530	0.0510	0.0335	0.0205	0.0025	0.0107
300	0.0453	0.0510	0.0330	0.0203	0.0025	0.0108
360	0.0454	0.0510	0.0313	0.0208	0.0025	0.0090
420	0.0448	0.0496	0.0315	0.0186	0.0023	0.0057
480	0.0446	0.0448	0.0312	0.0167	0.0022	0.0024

Liquid Phase Concentrations (mg/L)
t = 0 h

Depth (mm)	Toluene	Chlorobenzene	Styrene	n-propylbenzene	1,2 DCB	1,2,4 DCB
5.0	23.114	32.518	19.856	11.543	14.281	7.479
10.0	25.402	32.518	19.856	18.674	19.671	7.893
19.1	32.840	36.599	23.068	19.761	21.642	8.422
38.1	35.052	38.397	23.665	24.094	25.021	8.832
63.5	36.662	39.364	24.797	24.766	25.062	9.088
88.9	37.730	39.676	24.814	26.672	25.066	9.079

Liquid Phase Concentrations (mg/L)
t = 4 h

Depth (mm)	Toluene	Chlorobenzene	Styrene	n-propylbenzene	1,2 DCB	1,2,4 DCB
5.0	9.539	12.618	8.014	6.007	4.217	0.227
10.0	17.737	20.073	13.214	9.078	18.987	4.129
19.1	30.983	30.127	18.645	13.176	20.978	6.332
38.1	34.998	35.328	21.978	22.215	24.211	8.141
63.5	34.174	37.723	23.567	24.054	24.213	8.567
88.9	36.315	37.834	24.071	26.665	25.058	9.069

Liquid Phase Concentrations (mg/L)
t = 8 h

Depth (mm)	Toluene	Chlorobenzene	Styrene	n-propylbenzene	1,2 DCB	1,2,4 DCB
5.0	9.040	9.715	6.958	3.922	0.696	0.216
10.0	10.565	10.825	7.493	4.997	2.970	0.216
19.1	25.669	25.060	15.645	13.149	18.390	4.211
38.1	30.310	34.643	21.067	22.109	22.513	7.999
63.5	33.832	37.576	22.968	23.109	23.821	8.269
88.9	34.891	38.015	22.974	24.889	25.956	8.379

Sand 30-50, Air Flow Rate 10mL/min, Temperature 21°C
Air Phase Concentrations (mg/L)

Time (min)	Benzene	Ethylbenzene	m,p-Xylene	o-Xylene
0	0.0000	0.0000	0.0000	0.0000
1	0.0750	0.0123	0.0004	0.0000
3	0.1397	0.0620	0.0124	0.0113
5	0.3114	0.0620	0.0713	0.0207
10	0.7298	0.1503	0.0672	0.0273
20	0.6555	0.0823	0.0680	0.1063
30	0.6610	0.0900	0.0635	0.0570
45	0.5950	0.0812	0.0670	0.0513
60	0.5265	0.0090	0.0573	0.0460
75	0.4973	0.0795	0.0558	0.0438
90	0.4715	0.0763	0.0608	0.0460
105	0.4015	0.0695	0.0578	0.0360
120	0.3545	0.0645	0.0560	0.0343
150	0.3358	0.0563	0.0533	0.0360
180	0.3015	0.0538	0.0568	0.0370
210	0.2815	0.0535	0.0448	0.0295
240	0.2553	0.0555	0.0540	0.0285
300	0.2307	0.0490	0.0528	0.0305
330	0.2173	0.0463	0.0500	0.0283
360	0.2183	0.0495	0.0423	0.0226
420	0.1970	0.0455	0.0410	0.0216
480	0.2005	0.0475	0.0405	0.0214

Liquid Phase Concentrations (mg/L)

Depth (mm)	Ben zene (0 h)	Benzene (4 h)	Benzene (8 h)	o-Xylene (0 h)	o-Xylene (4 h)	o-Xylene (8 h)
5.0	39.918	14.324	8.401	3.1842	1.223	0.3673
10.0	44.897	28.332	23.971	4.5377	3.987	1.462
19.1	54.339	53.123	48.951	8.998	8.926	8.011
38.1	57.000	56.013	53.568	9.257	9.079	8.988
63.5	57.422	57.212	56.266	9.657	9.607	9.565
88.9	59.097	58.356	57.962	10.876	10.678	10.545

Liquid Phase Concentrations (mg/L)

Depth (mm)	Ethylbenzene (0 h)	Ethylbenzene (4 h)	Ethylbenzene (8 h)	m,p-Xylene (0 h)	m,p-Xylene (4 h)	m,p-Xylene (8 h)
5.0	5.420	3.331	2.920	6.492	2.914	1.496
10.0	6.636	4.765	3.022	7.859	5.015	3.364
19.1	9.086	7.863	7.354	9.453	9.321	8.108
38.1	9.953	9.356	9.144	10.061	9.865	9.301
63.5	10.821	10.317	9.956	11.655	11.567	11.496
88.9	11.302	11.105	10.988	12.000	11.508	11.919

Sand 30-50, Air Flow Rate 10 mL/min, Temperature 21°C
Air Phase Concentrations (mg/L)

Time (min)	Toluene	Chlorobenzene	Styrene	Propylbenzene	1,2 DCB	1,2,4 TCB
0	0.0000	0.0000	0.0000	0.0000	0.0000	0.0000
1	0.1035	0.1405	0.0000	0.0000	0.0077	0.0000
3	0.1885	0.3730	0.1235	0.0053	0.0098	0.0000
6	0.2180	0.5460	0.2175	0.0830	0.0128	0.0000
10	0.2915	0.7130	0.2230	0.0970	0.0657	0.0166
30	0.2950	0.7825	0.2375	0.1115	0.0914	0.0178
40	0.3225	0.9185	0.3855	0.3260	0.1925	0.0370
60	0.3405	1.1420	0.4620	0.4555	0.1115	0.0665
75	0.3010	1.0360	0.4230	0.3305	0.0962	0.0189
90	0.2865	0.9690	0.4015	0.2225	0.0566	0.0188
120	0.2765	0.8825	0.3470	0.2180	0.0326	0.0090
150	0.2640	0.8605	0.3110	0.1870	0.0254	0.0061
180	0.2520	0.8005	0.3035	0.1650	0.0189	0.0060
240	0.2135	0.6595	0.2825	0.1305	0.0138	0.0057
360	0.1865	0.6250	0.2815	0.1205	0.0129	0.0058
420	0.1770	0.6050	0.2815	0.1198	0.0127	0.0059
480	0.1745	0.6130	0.2835	0.1197	0.0130	0.0057

Liquid Phase Concentrations (mg/L)
t = 0 h

Depth (mm)	Toluene	Chlorobenzene	Styrene	n-propylbenzene	1,2 DCB	1,2,4 DCB
5.0	30.135	104.761	46.052	18.643	27.733	7.604
10.0	31.595	119.591	52.016	25.120	35.594	9.425
19.1	32.958	122.043	56.733	29.584	43.865	10.450
38.1	34.723	123.049	58.051	30.306	50.475	11.069
63.5	33.721	123.264	60.521	30.580	50.559	12.390
88.9	34.915	123.480	62.250	30.841	50.604	13.354

Liquid Phase Concentrations (mg/L)
t = 4 h

Depth (mm)	Toluene	Chlorobenzene	Styrene	n-propylbenzene	1,2 DCB	1,2,4 DCB
5.0	20.068	49.671	26.015	9.211	21.813	5.217
10.0	21.215	56.174	38.756	17.011	30.712	7.771
19.1	32.176	113.238	51.176	25.613	43.117	9.627
38.1	34.645	122.568	56.343	29.753	50.475	10.987
63.5	33.718	123.189	60.489	30.537	50.551	12.382
88.9	34.584	123.419	62.212	30.840	50.599	13.451

Liquid Phase Concentrations (mg/L)
t = 8 h

Depth (mm)	Toluene	Chlorobenzene	Styrene	n-propylbenzene	1,2 DCB	1,2,4 DCB
5.0	16.021	45.045	18.939	5.305	14.725	3.013
10.0	17.623	53.689	30.079	14.034	29.340	6.023
19.1	28.593	104.547	44.955	23.356	40.287	8.949
38.1	33.364	116.895	54.369	27.564	50.468	10.895
63.5	33.644	123.242	60.451	30.528	50.369	12.268
88.9	34.284	123.388	62.221	30.823	50.588	13.265

Sand 30-50, Air Flow Rate 25mL/min, Temperature 21°C
Air Phase Concentrations (mg/L)

Time (min)	Benzene	Ethylbenzene	m,p-Xylene	o-Xylene
0	0.0000	0.0000	0.0000	0.0000
1	0.0239	0.0000	0.0000	0.0106
3	0.9818	0.1718	0.1577	0.0735
5	2.4120	0.7103	0.6670	0.3295
10	1.9175	0.5315	0.5265	0.4820
20	1.2842	0.4890	0.4340	0.3090
30	1.0733	0.4928	0.3998	0.2860
45	0.8923	0.4110	0.3773	0.2918
60	0.6950	0.3598	0.3340	0.1783
75	0.6873	0.3433	0.2925	0.1675
90	0.6190	0.3420	0.2878	0.1570
105	0.5828	0.3168	0.2615	0.1525
120	0.5435	0.3083	0.2585	0.1475
150	0.4670	0.2630	0.2413	0.1410
180	0.4405	0.2233	0.1913	0.1320
240	0.3678	0.1803	0.1748	0.1023
300	0.3178	0.1505	0.1328	0.0983
360	0.3023	0.1238	0.1015	0.0895
420	0.2653	0.1138	0.1058	0.0853
480	0.2572	0.1168	0.1042	0.0863

Liquid Phase Concentrations (mg/L)

Depth (mm)	Ben zene (0 h)	Benzene (4 h)	Benzene (8 h)	o-Xylene (0 h)	o-Xylene (4 h)	o-Xylene (8 h)
5.0	120.818	77.815	42.889	23.060	18.117	12.885
10.0	123.091	94.114	75.727	30.872	24.315	16.622
19.1	129.990	123.259	116.541	32.074	28.274	22.218
38.1	131.000	130.134	124.901	34.074	31.973	31.911
63.5	131.799	129.431	126.911	35.448	35.121	34.244
88.9	132.456	130.123	128.795	35.684	235.069	34.360

Liquid Phase Concentrations (mg/L)

Depth (mm)	Ethylbenzene (0 h)	Ethylbenzene (4 h)	Ethylbenzene (8 h)	m,p-Xylene (0 h)	m,p-Xylene (4 h)	m,p-Xylene (8 h)
5.0	40.667	27.511	14.056	47.444	37.174	19.474
10.0	43.923	39.347	24.686	51.973	44.384	33.837
19.1	49.867	46.640	43.300	55.200	52.615	48.366
38.1	52.696	48.014	47.998	57.187	55.973	55.946
63.5	53.847	51.996	51.838	59.199	58.763	56.351
88.9	54.103	51.976	51.853	59.160	59.012	56.977

Sand 30-50, Air Flow Rate 25 mL/min, Temperature 21°C
Air Phase Concentrations (mg/L)

Time (min)	Toluene	Chlorobenzene	Styrene	Propylbenzene	1,2 DCB	1,2,4 TCB
0	0.0000	0.0000	0.0000	0.0000	0.0000	0.0000
1	0.2560	0.4731	0.1530	0.0535	0.0000	0.0000
3	0.2485	0.5201	0.1975	0.1915	0.0000	0.0000
5	0.3135	0.6425	0.4405	0.3705	0.0083	0.0000
10	0.6510	1.0975	0.3385	0.2495	0.0211	0.0147
20	0.3340	0.8745	0.3115	0.1845	0.1483	0.0174
30	0.3230	0.8611	0.3015	0.1386	0.0905	0.0184
40	0.2950	0.7670	0.3025	0.1025	0.0790	0.0302
60	0.2840	0.7230	0.3002	0.0805	0.0655	0.0215
75	0.2800	0.7025	0.2750	0.0774	0.0547	0.0072
90	0.2780	0.7245	0.2570	0.0745	0.0344	0.0062
120	0.2570	0.7335	0.2761	0.0725	0.0188	0.0000
180	0.2210	0.7015	0.2885	0.0736	0.0114	0.0000
240	0.2100	0.7315	0.2685	0.0743	0.0080	0.0000
300	0.2050	0.7150	0.2700	0.0725	0.0081	0.0000
360	0.2051	0.7101	0.2570	0.0715	0.0085	0.0000
420	0.2015	0.7065	0.2270	0.0728	0.0083	0.0000
480	0.2023	0.7059	0.2287	0.0721	0.0082	0.0000

Liquid Phase Concentrations (mg/L)
t = 0 h

Depth (mm)	Toluene	Chlorobenzene	Styrene	n-propylbenzene	1,2 DCB	1,2,4 DCB
5.0	41.884	157.68	60.649	32.457	38.457	5.379
10.0	46.462	181.05	78.554	44.745	48.755	8.985
19.1	50.582	198.66	85.423	48.410	51.410	9.068
38.1	50.810	200.40	90.081	53.823	53.023	10.363
63.5	51.568	200.29	90.054	54.306	54.306	10.334
88.9	51.718	200.59	90.010	54.030	55.030	10.527

Liquid Phase Concentrations (mg/L)
t = 4 h

Depth (mm)	Toluene	Chlorobenzene	Styrene	n-propylbenzene	1,2 DCB	1,2,4 DCB
5.0	18.412	76.58	24.821	5.018	25.917	2.501
10.0	28.128	131.11	49.123	39.021	46.181	6.153
19.1	41.374	154.81	72.066	46.039	49.871	8.415
38.1	47.728	190.45	86.474	50.075	53.001	10.327
63.5	51.501	199.12	90.023	54.296	55.309	10.298
88.9	51.691	200.11	90.001	54.018	55.028	10.513

Liquid Phase Concentrations (mg/L)
t = 8 h

Depth (mm)	Toluene	Chlorobenzene	Styrene	n-propylbenzene	1,2 DCB	1,2,4 DCB
5.0	12.708	32.04	16.962	3.987	22.263	0.212
10.0	24.490	98.73	32.443	38.534	45.160	6.535
19.1	38.451	143.30	69.121	44.905	49.630	8.303
38.1	45.844	188.60	80.998	48.346	52.905	10.312
63.5	50.988	198.52	89.848	54.305	54.305	10.285
88.9	51.571	198.96	89.982	54.029	55.029	10.509

Sand 30-50, Air Flow Rate 55 mL/min, Temperature 21°C
Air Phase Concentrations (mg/L)

Time (min)	Benzene	Ethylbenzene	m,p-Xylene	o-Xylene
0	0.0000	0.0000	0.0000	0.0000
1	2.8318	1.5158	0.9168	0.5070
3	0.9700	0.4053	0.4383	0.3585
5	0.6410	0.3345	0.3515	0.2185
10	0.3928	0.1933	0.2145	0.1100
20	0.3340	0.1830	0.2048	0.1075
30	0.2458	0.1413	0.1288	0.0973
45	0.1858	0.1388	0.1355	0.0978
60	0.1637	0.1318	0.0973	0.0613
75	0.1413	0.1265	0.0858	0.0595
90	0.1360	0.1088	0.0858	0.0565
105	0.1218	0.1058	0.0778	0.0525
120	0.1160	0.0798	0.0665	0.0500
150	0.1103	0.0785	0.0590	0.0453
180	0.0905	0.0613	0.0475	0.0390
240	0.0818	0.0525	0.0355	0.0378
300	0.0790	0.0375	0.0325	0.0223
360	0.0705	0.0363	0.0320	0.0209
420	0.0650	0.0293	0.0275	0.0172
480	0.0630	0.0253	0.0258	0.0159

Liquid Phase Concentrations (mg/L)

Depth (mm)	Ben zene (0 h)	Benzene (4 h)	Benzene (8 h)	o-Xylene (0 h)	o-Xylene (4 h)	o-Xylene (8 h)
5.0	86.173	51.876	32.257	20.445	17.713	11.885
10.0	111.203	74.212	73.300	31.548	23.271	17.622
19.1	134.683	130.123	128.880	40.770	37.613	28.212
38.1	146.000	135.127	130.959	42.640	42.512	40.110
63.5	147.062	146.567	145.541	43.338	42.918	42.624
88.9	147.531	147.012	146.831	43.610	43.599	43.595

Liquid Phase Concentrations (mg/L)

Depth (mm)	Ethylbenzene (0 h)	Ethylbenzene (4 h)	Ethylbenzene (8 h)	m,p-Xylene (0 h)	m,p-Xylene (4 h)	m,p-Xylene (8 h)
5.0	38.100	32.712	16.174	45.037	40.118	29.210
10.0	60.475	41.477	28.692	58.553	48.023	37.750
19.1	65.602	58.456	50.936	66.095	62.215	51.091
38.1	66.750	62.631	62.476	72.445	72.234	67.046
63.5	68.504	68.312	68.022	74.409	74.401	74.327
88.9	68.629	68.218	68.547	75.762	75.567	75.726

Sand 30-50, Air Flow Rate 55 mL/min, Temperature 21°C
Air Phase Concentrations (mg/L)

Time (min)	Toluene	Chlorobenzene	Styrene	Propylbenzene	1,2 DCB	1,2,4 TCB
0	0.0000	0.0000	0.0000	0.0000	0.0000	0.0000
1	0.4455	1.0545	0.4280	0.2471	0.0000	0.0000
3	0.2120	0.6745	0.2500	0.1285	0.0000	0.0000
5	0.2085	0.5515	0.2270	0.1250	0.0000	0.0000
10	0.1815	0.4900	0.2145	0.1220	0.0000	0.0000
20	0.1715	0.4315	0.2015	0.1151	0.0000	0.0000
30	0.1545	0.4255	0.1805	0.1045	0.0000	0.0000
40	0.1315	0.4095	0.1770	0.1000	0.0000	0.0000
60	0.1085	0.3650	0.1690	0.0930	0.0000	0.0000
90	0.0975	0.3075	0.1370	0.0885	0.0000	0.0000
120	0.0845	0.2865	0.1045	0.0730	0.0000	0.0000
180	0.0790	0.2125	0.0895	0.0530	0.0000	0.0000
240	0.0650	0.1804	0.0735	0.0404	0.0000	0.0000
300	0.0635	0.1785	0.0695	0.0435	0.0000	0.0000
360	0.0630	0.1675	0.0687	0.0425	0.0000	0.0000
420	0.0632	0.1675	0.0685	0.0425	0.0000	0.0000

Liquid Phase Concentrations (mg/L)
t = 0 h

Depth (mm)	Toluene	Chlorobenzene	Styrene	n-propylbenzene	1,2 DCB	1,2,4 DCB
5.0	33.187	108.49	45.288	11.207	6.308	4.472
10.0	37.917	119.35	57.228	18.977	7.345	4.756
19.1	45.394	133.79	58.627	21.068	7.826	5.266
38.1	45.775	148.76	66.038	21.442	8.448	8.639
63.5	45.928	147.90	66.954	23.982	9.052	9.204
88.9	45.978	148.38	66.901	23.630	9.083	9.230

Liquid Phase Concentrations (mg/L)
t = 4 h

Depth (mm)	Toluene	Chlorobenzene	Styrene	n-propylbenzene	1,2 DCB	1,2,4 DCB
5.0	22.619	60.07	31.854	5.861	2.137	3.012
10.0	31.143	92.54	42.073	8.012	5.989	3.251
19.1	39.497	127.48	57.096	15.324	6.979	4.267
38.1	42.467	146.98	66.012	21.021	8.127	8.529
63.5	45.512	147.52	66.871	23.137	9.038	9.003
88.9	45.513	148.12	66.902	23.571	9.003	8.998

Liquid Phase Concentrations (mg/L)
t = 7 h

Depth (mm)	Toluene	Chlorobenzene	Styrene	n-propylbenzene	1,2 DCB	1,2,4 DCB
5.0	18.095	49.96	24.785	3.130	0.113	1.764
10.0	26.016	80.60	38.206	7.770	2.180	2.214
19.1	38.451	114.27	50.852	14.195	6.771	4.038
38.1	41.732	131.89	59.074	19.188	7.895	8.445
63.5	44.500	147.29	65.320	22.518	8.991	8.897
88.9	44.878	147.60	65.685	23.266	8.993	8.918

Sand 30-50, Air Flow Rate 120 mL/min, Temperature 21°C
Air Phase Concentrations (mg/L)

Time (min)	Benzene	Ethylbenzene	m,p-Xylene	o-Xylene
0	0.0000	0.0000	0.0000	0.0000
1	0.6123	0.2460	0.2268	0.1493
3	0.2485	0.1265	0.0928	0.1193
5	0.1620	0.0973	0.0743	0.0863
10	0.1245	0.0773	0.0625	0.0653
20	0.1100	0.0723	0.0490	0.0640
30	0.1008	0.0715	0.0480	0.0440
45	0.0840	0.0658	0.0385	0.0425
60	0.0802	0.0465	0.0278	0.0363
75	0.0758	0.0448	0.0244	0.0370
90	0.0747	0.0390	0.0242	0.0315
105	0.0718	0.0363	0.0216	0.0197
120	0.0698	0.0338	0.0188	0.0225
150	0.0660	0.0290	0.0183	0.0180
180	0.0535	0.0283	0.0173	0.0118
240	0.0410	0.0260	0.0157	0.0046
300	0.0408	0.0227	0.0123	0.0030
360	0.0408	0.0243	0.0121	0.0025
420	0.0403	0.0213	0.0105	0.0023
480	0.0383	0.0223	0.0102	0.0019

Liquid Phase Concentrations (mg/L)

Depth (mm)	Ben zene (0 h)	Benzene (4 h)	Benzene (8 h)	o-Xylene (0 h)	o-Xylene (4 h)	o-Xylene (8 h)
5.0	72.067	49.761	25.196	14.195	9.812	5.416
10.0	72.911	61.451	51.834	15.126	13.117	10.527
19.1	89.908	83.079	77.154	20.982	18.879	17.569
38.1	90.000	89.071	81.507	23.301	21.978	21.952
63.5	91.286	90.123	89.840	24.240	24.102	23.319
88.9	91.616	91.134	90.253	24.553	23.068	23.517

Liquid Phase Concentrations (mg/L)

Depth (mm)	Ethylbenzene (0 h)	Ethylbenzene (4 h)	Ethylbenzene (8 h)	m,p-Xylene (0 h)	m,p-Xylene (4 h)	m,p-Xylene (8 h)
5.0	20.153	12.612	5.391	18.614	15.237	4.935
10.0	28.771	23.107	16.681	26.613	20.071	12.226
19.1	37.345	33.211	28.616	39.635	33.203	25.246
38.1	39.645	35.749	35.758	40.181	40.054	38.258
63.5	40.354	39.714	38.345	42.951	42.911	42.866
88.9	40.643	39.898	39.130	43.190	40.175	43.103

Sand 30-50. Air Flow Rate 120 mL/min, Temperature 21°C
Air Phase Concentrations (mg/L)

Time (min)	Toluene	Chlorobenzene	Styrene	Propylbenzene	1,2 DCB	1,2,4 TCB
0	0.0000	0.0000	0.0000	0.0000	0.0000	0.0000
1	0.2163	0.8205	0.3463	0.2685	0.3120	0.0000
3	0.1093	0.3268	0.1295	0.2435	0.2015	0.0373
5	0.0908	0.2933	0.1145	0.2270	0.1185	0.0805
10	0.0773	0.2330	0.1108	0.0915	0.0693	0.0642
20	0.0675	0.2290	0.0990	0.0670	0.0421	0.-327
30	0.0633	0.1945	0.0930	0.0660	0.0335	0.0171
40	0.0568	0.1760	0.0938	0.0650	0.0286	0.0126
60	0.0543	0.1950	0.0823	0.0484	0.0184	0.0084
75	0.0473	0.1553	0.0785	0.0381	0.0152	0.0064
120	0.0463	0.1243	0.0655	0.0279	0.0142	0.0025
180	0.0457	0.1170	0.0655	0.0343	0.0102	0.0000
240	0.0452	0.0935	0.0538	0.0275	0.0096	0.0000
300	0.0468	0.0920	0.0528	0.0221	0.0095	0.0000
360	0.0478	0.0913	0.0490	0.0212	0.0094	0.0000
480	0.0416	0.0720	0.0490	0.0209	0.0089	0.0000

Liquid Phase Concentrations (mg/L)
t = 0 h

Depth (mm)	Toluene	Chlorobenzene	Styrene	n-propylbenzene	1,2 DCB	1,2,4 DCB
5.0	42.892	132.84	60.768	28.764	33.147	10.057
10.0	47.436	183.43	84.400	37.355	40.939	17.986
19.1	54.505	197.07	87.035	41.838	46.582	19.718
38.1	55.998	211.58	89.622	44.154	49.478	21.004
63.5	56.451	217.06	92.657	44.575	50.033	21.445
88.9	56.456	219.59	92.774	45.034	51.899	21.904

Liquid Phase Concentrations (mg/L)
t = 4 h

Depth (mm)	Toluene	Chlorobenzene	Styrene	n-propylbenzene	1,2 DCB	1,2,4 DCB
5.0	20.064	59.89	28.117	6.879	4.023	5.067
10.0	37.147	130.39	57.234	22.321	36.683	15.214
19.1	48.794	192.56	83.274	32.641	39.241	17.251
38.1	54.617	207.31	86.129	41.503	49.471	20.996
63.5	54.856	216.39	91.993	44.901	50.029	21.405
88.9	56.123	218.15	92.435	44.987	51.798	21.876

Liquid Phase Concentrations (mg/L)
t = 7 h

Depth (mm)	Toluene	Chlorobenzene	Styrene	n-propylbenzene	1,2 DCB	1,2,4 DCB
5.0	9.929	54.32	22.479	5.872	3.725	2.034
10.0	33.034	95.56	46.441	12.626	35.600	14.037
19.1	48.522	178.72	79.494	30.856	38.802	17.945
38.1	52.489	201.12	85.493	40.018	49.000	20.993
63.5	54.015	215.35	91.069	44.626	49.983	21.435
88.9	55.898	215.43	91.551	44.597	51.883	21.900

Sand 70-100, Air Flow Rate 10 mL/min, Temperature 21°C
Air Phase Concentrations (mg/L)

Time (min)	Benzene	Ethylbenzene	m,p-Xylene	o-Xylene
0	0.0000	0.0000	0.0000	0.0000
1	0.1700	0.0007	0.0007	0.0001
3	0.6633	0.0443	0.0425	0.0227
5	1.0665	0.0983	0.0958	0.0440
11	1.5525	0.1838	0.2005	0.0980
20	1.6368	0.1938	0.2165	0.1058
30	1.2728	0.1923	0.2140	0.1058
45	1.1580	0.1855	0.1993	0.0935
60	1.0565	0.1873	0.1955	0.0090
80	0.9275	0.1855	0.1873	0.0920
90	0.8948	0.1848	0.1928	0.0945
120	0.8333	0.1820	0.1960	0.0930
150	0.7250	0.1790	0.1990	0.0943
180	0.7080	0.1728	0.1980	0.0943
240	0.6168	0.1718	0.1835	0.0915
300	0.5667	0.1685	0.1723	0.0883
360	0.5387	0.1270	0.1450	0.0790
420	0.5368	0..1353	0.1558	0.0608
480	0.5240	0.1225	0.1432	0.0654

Liquid Phase Concentrations (mg/L)

Depth (mm)	Ben zene (0 h)	Benzene (4 h)	Benzene (8 h)	o-Xylene (0 h)	o-Xylene (4 h)	o-Xylene (8 h)
5.0	81.586	52.871	31.062	12.566	8.727	5.895
10.0	82.511	78.341	34.496	14.156	11.613	8.330
15.0	84.322	81.269	77.616	15.009	14.174	13.079
19.1	91.220	89.614	82.026	16.716	16.112	15.512
38.1	92.261	91.897	89.480	17.918	17.645	16.949
63.5	95.729	95.613	94.644	17.849	17.843	17.841
88.9	95.699	95.456	95.114	17.938	17.932	17.927

Liquid Phase Concentrations (mg/L)

Depth (mm)	Ethylbenzene (0 h)	Ethylbenzene (4 h)	Ethylbenzene (8 h)	m,p-Xylene (0 h)	m,p-Xylene (4 h)	m,p-Xylene (8 h)
5.0	18.512	12.217	7.126	23.006	15.126	10.288
10.0	19.304	15.217	10.068	24.601	22.147	16.300
15.0	20.171	20.007	16.137	26.157	25.789	24.056
19.1	22.735	21.329	21.264	27.106	26.692	26.195
38.1	26.279	25.714	23.866	33.333	31.879	30.010
63.5	26.731	25.929	25.846	33.446	32.862	32.812
88.9	26.616	26.501	26.411	33.255	32.989	32.890

Sand 70-100. Air Flow Rate 10 mL/min, Temperature 21°C
Air Phase Concentrations (mg/L)

Time (min)	Toluene	Chlorobenzene	Styrene	Propylbenzene	1,2 DCB	1,2,4 TCB
0	0.0000	0.0000	0.0000	0.0000	0.0000	0.0000
1	0.1078	0.1280	0.0760	0.0166	0..0000	0.0000
3	0.1162	0.1195	0.0765	0.0244	0.0000	0.0000
5	0.1200	0.1610	0.0820	0.0266	0.0000	0.0000
10	0.1615	0.1620	0.0875	0.0369	0.0212	0.0000
20	0.1560	0.2880	0.1235	0.0396	0.0212	0.0000
30	0.2650	0.3085	0.1275	0.0540	0.0267	0.0000
40	0.2845	0.4735	0.1365	0.0845	0.0419	0.0000
60	0.3035	0.4965	0.1920	0.1200	0.0425	0.0000
90	0.3780	0.5205	0.2190	0.1330	0.0447	0.0000
105	0.3740	0.4088	0.2360	0.1485	0.0425	0.0042
120	0.3605	0.4075	0.2020	0.1417	0.0402	0.0089
150	0.3015	0.4075	0.1885	0.1367	0.0390	0.0142
180	0.2810	0.3965	0.1860	0.1315	0.0373	0.0118
240	0.2795	0.3659	0.1985	0.1285	0.0339	0.0036
300	02780	0.3364	0.1775	0.1040	0.0287	0.0000
360	0.2600	0.2995	0.1675	0.0925	0.0281	0.0000
420	0.2470	0.2745	0.1654	0.0875	0.0127	0.0000
480	0.2435	0.2237	0.1570	0.0798	0.0097	0.0000

Liquid Phase Concentrations (mg/L)
t = 0 h

Depth (mm)	Toluene	Chlorobenzene	Styrene	n-propylbenzene	1,2 DCB	1,2,4 DCB
5.0	37.534	59.558	36.971	23.206	22.849	14.610
10.0	37.534	65.902	39.030	25.327	22.909	15.447
15.0	38.070	68.043	40.831	31.154	22.949	16.741
19.1	41.579	68.995	44.629	31.154	27.937	21.111
38.1	41.860	70.185	49.569	31.522	28.492	22.269
63.5	41.809	72.643	50.085	33.597	28.733	22.218
88.9	41.148	72.722	50.149	33.692	28.894	22.201

Liquid Phase Concentrations (mg/L)
t = 4 h

Depth (mm)	Toluene	Chlorobenzene	Styrene	n-propylbenzene	1,2 DCB	1,2,4 DCB
5.0	30.008	44.917	29.972	18.013	13.281	10.211
10.0	34.834	58.012	34.127	24.274	18.129	14.689
	37.962	67.249	38.861	25.318	21.873	15.417
19.1	40.867	68.331	40.173	29.213	26.317	20.128
38.1	40.656	70.021	48.911	31.139	28.328	21.818
63.5	40.718	71.871	49.912	33.415	28.339	22.150
88.9	40.079	72.678	50.121	33.716	28.792	22.161

Liquid Phase Concentrations (mg/L)
t = 8 h

Depth (mm)	Toluene	Chlorobenzene	Styrene	n-propylbenzene	1,2 DCB	1,2,4 DCB
5.0	18.558	30.807	25.149	14.195	10.585	9456
10.0	27.007	45.045	28.490	17.4823	13.953	14.579
	31.356	61.039	32.937	24.459	21.722	15.376
19.1	37.532	66.299	37.242	27.269	25.196	19.702
38.1	40.305	69.809	48.253	30.781	28.182	21.798
63.5	40.509	71.020	49.418	33.407	28.320	22.147
88.9	40.947	72.556	49.956	33.645	28.818	22.165

Sand 70-100, Air Flow Rate 25 mL/min, Temperature 21°C
Air Phase Concentrations (mg/L)

Time (min)	Benzene	Ethylbenzene	m,p-Xylene	o-Xylene
0	0.0000	0.0000	0.0000	0.0000
1	0.7748	0.0685	0.0625	0.0189
3	1.0095	0.1218	0.1020	0.0613
5	1.1685	0.1345	0.1440	0.0845
11	1.0182	0.1560	0.1460	0.0978
20	0.9460	0.1938	0.1923	0.1255
30	0.8040	0.1898	0.1943	0.1615
40	0.6930	0.1788	0.1923	0.1603
60	0.6162	0.1705	0.1925	0.1190
75	0.5537	0.1548	0.1673	0.1014
90	0.4555	0.1370	0.1550	0.1045
120	0.4058	0.1130	0.1183	0.0858
150	0.3180	0.1003	0.1077	0.0743
180	0.2120	0.0927	0.1016	0.0625
240	0.1475	0.0912	0.0921	0.0490
300	0.1375	0.0906	0.0871	0.0483
360	0.1341	0.0880	0.0851	0.0458
420	0.1335	0.0825	0.0798	0.0365

Liquid Phase Concentrations (mg/L)

Depth (mm)	Ben zene (0 h)	Benzene (4 h)	Benzene (7 h)	o-Xylene (0 h)	o-Xylene (4 h)	o-Xylene (7 h)
5.0	48.924	28.791	6.257	9.851	4.561	1.372
10.0	50.398	44.819	18.218	9.925	7.373	4.904
15.0	60.603	50.816	46.443	10.029	9.913	8.425
19.1	63.426	60.039	53.428	10.833	10.476	9.525
38.1	65.743	63.211	63.049	11.460	10.984	10.782
63.5	66.517	65.198	63.361	11.699	11.012	10.937
88.9	67.255	67.021	66.890	11.937	11.871	11.458

Liquid Phase Concentrations (mg/L)

Depth (mm)	Ethylbenzene (0 h)	Ethylbenzene (4 h)	Ethylbenzene (7 h)	m,p-Xylene (0 h)	m,p-Xylene (4 h)	m,p-Xylene (7 h)
5.0	13.450	6.256	2.635	14.857	7.778	2.138
10.0	14.214	12.961	5.500	15.175	12.496	7.465
15.0	15.948	14.003	8.632	20.097	14.691	11.870
19.1	17.089	16.511	15.545	21.950	21.687	19.985
38.1	17.735	17.129	16.763	22.551	22.098	21.640
63.5	17.946	17.728	17.650	22.803	22.758	22.665
88.9	17.933	17.471	17.305	23.158	23.123	23.081

Sand 70-100, Air Flow Rate 25 mL/min, Temperature 21°C
Air Phase Concentrations (mg/L)

Time (min)	Toluene	Chlorobenzene	Styrene	Propylbenzene	1,2 DCB	1,2,4 TCB
0	0.0000	0.0000	0.0000	0.0000	0.0000	0.0000
1	0.3235	0.1280	0.0750	0.0450	0.0436	0.0000
3	0.3555	0.3705	0.1585	0.0820	0.0447	0.0000
5	0.3395	0.4555	0.2035	0.1230	0.0476	0.0600
12	0.2980	0.5340	0.22130	0.1270	0.0487	0.1533
21	0.2685	0.4375	0.2090	0.1190	0.0453	0.0142
30	0.2520	0.4295	0.1955	0.1185	0.0419	0.0136
45	0.2340	0.3905	0.1935	0.1010	0.0402	0.0112
60	0.2125	0.3760	0.1930	0.0995	0.0367	0.0107
90	0.1880	0.3740	0.1705	0.0965	0.0321	0.0107
120	0.1765	0.3215	0.1540	0.0935	0.0333	0.0081
150	0.1645	0.2930	0.1345	0.0705	0.0321	0.0089
180	0.1525	0.2560	0.1315	0.0675	0.0203	0.0042
210	0.1445	0.2355	0.1150	0.0655	0.0150	0.0000
300	0.1165	0.2025	0.1014	0.0615	0.0127	0.0000
360	0.1145	0.1895	0.1001	0.0595	0.0120	0.0000
420	0.1107	0.1765	0.0954	0.0475	0.0114	0.0000
480	0.1105	0.1734	0.0875	0.0456	0.0123	0.0000

Liquid Phase Concentrations (mg/L)
t = 0 h

Depth (mm)	Toluene	Chlorobenzene	Styrene	n-propylbenzene	1,2 DCB	1,2,4 DCB
5.0	37.536	59.559	36.971	25.925	25.159	17.554
10.0	39.061	68.123	38.063	26.821	28.239	17.943
15.0	39.290	69.233	39.783	29.660	29.446	18.029
19.1	39.748	70.264	40.924	29.959	30.814	18.419
38.1	41.503	70.264	41.418	34.890	31.457	18.764
63.5	41.732	70.310	41.476	35.131	31.593	19.055
88.9	41.642	70.666	41.556	35.029	31.652	19.004

Liquid Phase Concentrations (mg/L)
t = 4 h

Depth (mm)	Toluene	Chlorobenzene	Styrene	n-propylbenzene	1,2 DCB	1,2,4 DCB
5.0	17.839	38.271	21.756	20.023	15.793	10.134
10.0	33.219	62.311	33.214	25.275	22.769	16.758
15.0	36.114	70.003	35.105	29.295	26.054	17.673
19.1	38.093	64.617	37.586	29.839	29.347	18.312
38.1	40.713	67.121	40.002	32.073	30.684	18.761
63.5	40.825	70.128	41.419	33.991	31.491	19.038
88.9	40.914	70.617	41.512	35.017	31.562	19.001

Liquid Phase Concentrations (mg/L)
t = 8 h

Depth (mm)	Toluene	Chlorobenzene	Styrene	n-propylbenzene	1,2 DCB	1,2,4 DCB
5.0	8.9392	28.111	16.855	14.195	10.459	6.826
10.0	28.838	41.063	25.596	17.109	18.562	8.389
15.0	32.119	50.028	27.984	23.011	25.297	16.133
19.1	35.010	60.531	35.242	27.143	27.113	17.238
38.1	39.290	63.109	39.753	31.614	30.320	18.651
63.5	40.214	69.568	41.206	33.792	31.592	19.043
88.9	40.596	69.809	41.272	34.913	31.630	19.985

Sand 70-100, Air Flow Rate 55 mL/min, Temperature 21°C
Air Phase Concentrations (mg/L)

Time (min)	Benzene	Ethylbenzene	m,p-Xylene	o-Xylene
0	0.0000	0.0000	0.0000	0.0000
1	1.4158	0.2078	0.2288	0.0820
3	0.7283	0.1655	0.1485	0.1245
5	0.5193	0.0933	0.0998	0.0640
13	0.3468	0.0893	0.0960	0.0540
23	0.2528	0.0703	0.0835	0.0595
32	0.2233	0.0610	0.0578	0.0535
45	0.1718	0.0485	0.0523	0.0428
60	0.1248	0.0435	0.0473	0.0380
75	0.1165	0.0423	0.0465	0.0373
90	0.1170	0.0363	0.0418	0.0370
120	0.0878	0.0325	0.0327	0.0318
180	0.0900	0.0325	0.0280	0.0313
240	0.0665	0.0278	0.0265	0.0258
300	0.0678	0.0248	0.0183	0.0155
360	0.0600	0.0195	0.0171	0.0042
420	0.0515	0.0152	0.0169	0.0040
480	0.0424	0.0131	0.0144	0.0035

Liquid Phase Concentrations (mg/L)

Depth (mm)	Ben zene (0 h)	Benzene (4 h)	Benzene (8 h)	o-Xylene (0 h)	o-Xylene (4 h)	o-Xylene (8 h)
5.0	45.540	13.147	9.981	7.693	2.247	1.559
10.0	69.099	42.182	41.776	10.735	6.147	5.973
15.0	73.878	73.213	65.130	12.915	11.675	9.703
19.1	79.963	76.021	69.716	16.691	15.204	14.604
38.1	82.279	78.763	77.748	17.328	15.906	15.991
63.5	82.819	81.027	80.813	17.314	17.098	16.871
88.9	83.050	82.917	81.778	17.315	17.101	17.003

Liquid Phase Concentrations (mg/L)

Depth (mm)	Ethylbenzene (0 h)	Ethylbenzene (4 h)	Ethylbenzene (8 h)	m,p-Xylene (0 h)	m,p-Xylene (4 h)	m,p-Xylene (8 h)
5.0	8.521	4.766	1.109	9.643	3.231	1.298
10.0	19.455	11.319	8.370	21.412	11.412	11.313
15.0	20.736	19.073	12.970	24.069	19.746	17.198
19.1	20.759	20.341	18.323	25.170	23.011	22.513
38.1	20.887	20.779	20.508	25.321	24.812	24.158
63.5	21.264	21.931	20.736	25.511	24.915	24.247
88.9	21.312	21.012	20.736	25.967	25.786	25.260

Sand 70-100, Air Flow Rate 55 mL/min, Temperature 21°C
Air Phase Concentrations (mg/L)

Time (min)	Toluene	Chlorobenzene	Styrene	Propylbenzene	1,2 DCB	1,2,4 TCB
0	0.0000	0.0000	0.0000	0.0000	0.0000	0.0000
1	0.3250	0.2198	0.1790	0.0630	0.0228	0.0000
3	0.2220	0.1589	0.1235	0.0525	0.2150	0.0000
5	0.2085	0.1583	0.1150	0.0478	0.0228	0.0600
12	0.1760	0.1215	0.1140	0.0378	0.0168	0.0010
21	0.1690	0.1060	0.1075	0.0374	0.0159	0.0009
30	0.1430	0.0990	0.0980	0.0279	0.0141	0.0007
40	0.1320	0.0970	0.0955	0.0218	0.0128	0.0006
60	0.1320	0.0956	0.0895	0.0190	0.0018	0.0005
120	0.1285	0.0873	0.0875	0.0108	0.0000	0.0004
180	0.1115	0.0848	0.0770	0.0097	0.0000	0.0003
240	0.1025	0.0838	0.0765	0.0047	0.0000	0.0003
300	0.1017	0 0798.	0.0730	0.0046	0.0000	0.0003
360	0.1010	0.0745	0.0725	0.0041	0.0000	0.0000
420	0.0901	0.0695	0.0721	0.0040	0.0000	0.0000
480	0.0906	0.0671	0.0700	0.0040	0.0000	0.0000

Liquid Phase Concentrations (mg/L)
t = 0 h

Depth (mm)	Toluene	Chlorobenzene	Styrene	n-propylbenzene	1,2 DCB	1,2,4 DCB
5.0	33.113	42.269	28.891	7.787	5.294	4.696
10.0	35.449	46.869	30.196	9.792	6.026	10.636
15.0	37.399	59.320	33.366	16.959	8.045	13.317
19.1	39.162	60.113	33.678	18.454	12.631	15.095
38.1	40.664	63.920	35.007	20.023	12.953	16.689
63.5	41.411	63.753	34.977	20.741	13.275	17.467
88.9	41.563	63.777	35.029	20.965	13.619	17.445

Liquid Phase Concentrations (mg/L)
t = 4 h

Depth (mm)	Toluene	Chlorobenzene	Styrene	n-propylbenzene	1,2 DCB	1,2,4 DCB
5.0	19.934	27.713	22.619	6.313	3.475	3.569
10.0	24.117	32.219	25.117	8.813	5.001	8.545
15.0	28.412	39.782	27.431	12.747	7.096	11.832
19.1	33.789	57.890	32.129	18.407	10.819	15.602
38.1	38.234	63.713	34.349	18.399	13.009	15.978
63.5	41.119	63.561	34.458	20.713	13.198	17.418
88.9	41.321	63.681	34.992	20.899	13.602	17.431

Liquid Phase Concentrations (mg/L)
t = 8 h

Depth (mm)	Toluene	Chlorobenzene	Styrene	n-propylbenzene	1,2 DCB	1,2,4 DCB
5.0	9.174	12,223	10.681	2.090	0.291	0.147
10.0	15.844	20.426	17.233	3.736	2.711	8.007
15.0	20.888	27.374	20.115	12.439	5.524	9.858
19.1	28.865	53.482	26.808	17.643	10.659	15.457
38.1	37.705	63.444	30.408	18.408	12.913	15.985
63.5	40.901	63.709	33.995	20.686	13.172	17.394
88.9	41.029	63.057	37.747	20.950	13.599	17.421

Sand 70-100, Air Flow Rate 120 mL/min, Temperature 21°C
Air Phase Concentrations (mg/L)

Time (min)	Benzene	Ethylbenzene	m,p-Xylene	o-Xylene
0	0.0000	0.0000	0.0000	0.0000
1	0.7180	0.1143	0.1318	0.0923
2	0.4368	0.0735	0.0743	0.1173
5	0.2555	0.0680	0.0660	0.0950
11	0.2003	0.0490	0.0388	0.0698
23	0.1113	0.0453	0.0235	0.0550
30	0.1030	0.0218	0.0236	0.0345
40	0.0665	0.0170	0.0260	0.0328
60	0.0588	0.0174	0.0201	0.0304
90	0.0580	0.0137	0.0157	0.0278
120	0.0480	0.0122	0.0107	0.0237
180	0.0373	0.0115	0.0076	0.0109
240	0.0368	0.0111	0.0071	0.0087
300	0.0373	0.0105	0.0633	0.0071
360	0.0308	0.0100	0.0058	0.0069
420	0.0308	0.0099	0.0057	0.0065
480	0.0301	0.0091	0.0047	0.0067

Liquid Phase Concentrations (mg/L)

Depth (mm)	Ben zene (0 h)	Benzene (4 h)	Benzene (8 h)	o-Xylene (0 h)	o-Xylene (4 h)	o-Xylene (8 h)
5.0	56.728	27.091	12.178	8.555	2.137	1.757
10.0	61.469	46.371	18.344	9.375	4.891	3.176
15.0	81.933	63.761	40.273	10.693	5.991	4.227
19.1	84.052	82.189	78.368	12.131	10.914	10.455
38.1	85.478	84.319	83.819	12.533	11.812	11.403
63.5	86.437	84.231	84.091	12.793	12.217	12.156
88.9	88.368	88.127	87.983	12.909	12.605	12.600

Liquid Phase Concentrations (mg/L)

Depth (mm)	Ethylbenzene (0 h)	Ethylbenzene (4 h)	Ethylbenzene (8 h)	m,p-Xylene (0 h)	m,p-Xylene (4 h)	m,p-Xylene (8 h)
5.0	12.442	3.291	0.600	9.339	4.197	0.203
10.0	14.855	6.871	3.576	12.225	7.813	3.731
15.0	15.647	10.237	6.542	17.719	12.625	7.492
19.1	18.925	18.734	18.632	18.906	17.831	16.490
38.1	19.304	19.297	19.117	18.902	18.321	17.937
63.5	21.754	21.553	21.057	18.906	18.607	18.467
88.9	22.525	22.386	22.079	18.817	18.819	18.782

Sand 70/100, Air Flow Rate 120 mL/min, Temperature 21°C
Air Phase Concentrations (mg/L)

Time (min)	Toluene	Chlorobenzene	Styrene	Propylbenzene	1,2 DCB	1,2,4 TCB
0	0.0000	0.0000	0.0000	0.0000	0.0000	0.0000
1	0.1165	0.1578	0.1690	0.0965	0.0000	0.0000
3	0.0795	0.1103	0.1170	0.0615	0.0230	0.0100
5	0.0713	0.0953	0.1025	0.0456	0.0235	0.0292
12	0.0643	0.0970	0.1005	0.0423	0.0213	0.0142
21	0.0625	0.0900	0.0960	0.0495	0.0189	0.0000
31	0.0563	0.0880	0.0885	0.0364	0.0109	0.0000
45	0.0555	0.0820	0.0855	0.0260	0.0115	0.0000
60	0.0548	0.0800	0.0855	0.0259	0.0067	0.0000
90	0.0530	0.0735	0.0830	0.0141	0.0058	0.0000
120	0.0503	0.0700	0.0875	0.0135	0.0038	0.0000
180	0.0468	0.0598	0.0685	0.0116	0.0000	0.0000
210	0.0468	0.0598	0.0575	0.0091	0.0000	0.0000
300	0.0453	0.0573	0.0405	0.0088	0.0000	0.0000
360	0.0448	0.0503	0.0385	0.0081	0.0000	0.0000
420	0.0437	0.0456	0.0276	0.0079	0.0000	0.0000
480	0.0384	0.0416	0.0274	0.0079	0.0000	0.0000

Liquid Phase Concentrations (mg/L)
t = 0 h

Depth (mm)	Toluene	Chlorobenzene	Styrene	n-propylbenzene	1,2 DCB	1,2,4 DCB
5.0	32.119	47.662	33.878	18.229	19.309	12.452
10.0	32.424	52.500	36.866	23.534	25.182	14.398
15.0	44.179	70.958	38.678	25.665	25.665	14.830
19.1	47.148	72.333	41.253	29.286	28.883	14.700
38.1	47.612	75.156	46.688	30.974	30.374	14.916
63.5	47.835	75.314	47.305	31.457	30.457	15.511
88.9	47.971	75.574	47.482	32.262	30.462	15.560

Liquid Phase Concentrations (mg/L)
t = 4 h

Depth (mm)	Toluene	Chlorobenzene	Styrene	n-propylbenzene	1,2 DCB	1,2,4 DCB
5.0	19.918	29.471	18.071	9.012	5.671	6.251
10.0	28.224	45.014	24.997	18.789	17.761	8.721
15.0	33.719	64.032	32.003	20.178	22.043	12.155
19.1	47.023	70.271	32.997	28.347	27.567	14.121
38.1	47.412	72.693	43.627	30.931	30.298	14.909
63.5	46.917	74.876	47.291	31.358	30.312	15.413
88.9	47.018	75.108	47.397	32.213	30.315	15.467

Liquid Phase Concentrations (mg/L)
t = 8 h

Depth (mm)	Toluene	Chlorobenzene	Styrene	n-propylbenzene	1,2 DCB	1,2,4 DCB
5.0	8.692	8.884	5.962	4.776	2.896	2.361
10.0	15.964	29.546	10.091	10.609	10.316	6.485
15.0	21.593	54.218	18.067	18.761	20.574	11.745
19.1	41.075	63.200	24.172	26.408	26.688	13.360
38.1	44.735	72.444	43.589	30.861	30.297	14.843
63.5	46.053	74.516	46.998	31.395	30.259	15.473
88.9	46.835	74.960	47.180	32.199	30.455	15.459

Mass Balance Calculations

Initial mass of VOC

$$X_o = \varepsilon\, L\, W \sum C^o_{wn} \Delta Z_n$$

Final mass of VOC

$$X_f = \varepsilon\, L\, W \sum C^f_{wn} \Delta Z_n$$

VOC mass removed

$$Y = Q_a \sum C_{an} \Delta t_n$$

Mass balance difference

$$P = X_0 - X_f - Y$$

Where C^i_{wn} for ($i = o$ or f) is the average concentration of VOC in the aqueous phase in the layer of thickness ΔZ_n, L is the length of the single-air channel setup (17.5 cm), W is the width of the single-air setup (5 cm), ε is the porosity of the porous media, Q_a is the air flow rate (L/min), and Δt_n is the time interval elapsed between two consecutive air phase samples.

Ottawa Sand, Air Flow Rate 10 mL/min

VOC	X_0 (mg)	X_f (mg)	Y (mg)	P (mg)
Benzene	41.38	35.80	4.99	0.59
Ethylbenzene	13.47	12.15	1.45	-0.13
m,p-Xylenes	16.05	14.80	1.51	-0.25
o-Xylene	10.89	9.81	0.92	0.16
Toluene	24.35	22.31	1.80	0.24
Chlorobenzene	25.12	23.32	1.60	0.20
Styrene	15.48	14.60	0.98	-0.10
n-Propylbenzene	8.38	7.48	0.91	-0.01
1,2-Dichlorobenzene	16.52	15.57	0.97	-0.02
1,2,4-trichlorobenzene	3.58	3.36	0.31	-0.09

Ottawa Sand, Air Flow Rate 25 mL/min

VOC	X_0 (mg)	X_f (mg)	Y (mg)	P (mg)
Benzene	36.39	33.71	2.15	0.53
Ethylbenzene	10.42	9.71	0.61	0.10
m,p-Xylenes	10.38	9.43	0.64	0.31
o-Xylene	8.04	7.41	0.50	0.13
Toluene	12.45	10.38	2.36	-0.29
Chlorobenzene	12.43	10.53	2.28	-0.38
Styrene	8.34	7.29	1.30	-0.25
n-Propylbenzene	9.93	8.43	1.42	0.08
1,2-Dichlorobenzene	3.30	2.98	0.34	0.06
1,2,4-trichlorobenzene	1.64	1.58	0.13	-0.07

Ottawa Sand, Air Flow Rate 55 mL/min

VOC	X_0 (mg)	X_f (mg)	Y (mg)	P (mg)
Benzene	40.75	37.25	2.87	0.63
Ethylbenzene	10.41	9.23	0.82	0.36
m,p-Xylenes	10.94	9.77	0.72	0.45
o-Xylene	9.21	8.58	0.49	0.14
Toluene	28.73	24.80	4.20	-0.27
Chlorobenzene	32.20	27.81	5.11	-0.72
Styrene	20.48	17.40	3.44	-0.36
n-Propylbenzene	13.20	11.29	2.17	-0.26
1,2-Dichlorobenzene	20.34	18.25	1.53	0.56
1,2,4-trichlorobenzene	6.55	5.53	0.92	0.10

Ottawa Sand, Air Flow Rate 120 mL/min

VOC	X_0 (mg)	X_f (mg)	Y (mg)	P (mg)
Benzene	44.67	39.91	3.78	0.98
Ethylbenzene	20.15	17.80	2.06	0.29
m,p-Xylenes	24.14	21.84	1.95	0.35
o-Xylene	14.29	12.80	1.24	0.25
Toluene	12.53	10.60	2.84	-0.91
Chlorobenzene	13.79	11.58	3.11	-0.90
Styrene	8.60	7.10	1.91	-0.41
n-Propylbenzene	8.46	7.16	1.74	-0.44
1,2-Dichlorobenzene	8.65	7.48	1.00	-0.13
1,2,4-trichlorobenzene	3.18	2.42	1.04	-0.28

Sand 30-50, Air Flow Rate 10 mL/min

VOC	X_0 (mg)	X_f (mg)	Y (mg)	P (mg)
Benzene	19.95	18.03	1.81	0.11
Ethylbenzene	3.54	3.15	0.34	0.05
m,p-Xylenes	3.76	3.40	0.29	0.07
o-Xylene	3.24	2.99	0.19	0.06
Toluene	12.04	11.00	0.99	0.05
Chlorobenzene	43.32	39.12	3.18	1.02
Styrene	20.85	18.88	1.32	0.65
n-Propylbenzene	10.44	9.38	0.71	0.35
1,2-Dichlorobenzene	16.81	16.17	0.14	0.50
1,2,4-trichlorobenzene	4.16	3.86	0.05	0.25

Sand 30-50, Air Flow Rate 25 mL/min

VOC	X_0 (mg)	X_f (mg)	Y (mg)	P (mg)
Benzene	46.40	41.58	5.80	-0.98
Ethylbenzene	18.39	16.25	2.67	-0.53
m,p-Xylenes	20.30	18.34	2.37	-0.41
o-Xylene	11.99	10.58	1.61	-0.20
Toluene	17.93	15.75	2.72	-0.54
Chlorobenzene	69.82	61.21	8.37	0.24
Styrene	30.88	27.36	3.08	0.44
n-Propylbenzene	18.26	16.87	0.96	0.43
1,2-Dichlorobenzene	18.68	18.14	0.25	0.29
1,2,4-trichlorobenzene	3.49	3.27	0.03	0.19

Sand 30-50, Air Flow Rate 55 mL/min

VOC	X_0 (mg)	X_f (mg)	Y (mg)	P (mg)
Benzene	49.49	45.77	3.23	0.49
Ethylbenzene	23.23	20.95	1.95	0.33
m,p-Xylenes	25.05	23.11	1.64	0.30
o-Xylene	14.47	13.13	1.15	0.19
Toluene	15.83	14.35	1.98	-0.50
Chlorobenzene	50.54	45.84	5.71	-1.01
Styrene	22.65	20.56	2.38	-0.29
n-Propylbenzene	7.76	6.66	1.43	-0.33
1,2-Dichlorobenzene	3.02	2.65	0.00	0.37
1,2,4-trichlorobenzene	2.84	2.58	0.00	0.26

Ottawa Sand, Air Flow Rate 120 mL/min

VOC	X_0 (mg)	X_f (mg)	Y (mg)	P (mg)
Benzene	31.54	28.43	3.35	-0.24
Ethylbenzene	13.46	11.82	1.91	-0.27
m,p-Xylenes	14.00	12.54	1.14	0.32
o-Xylene	8.00	7.24	0.88	-0.12
Toluene	19.45	17.53	2.40	-0.48
Chlorobenzene	73.46	67.37	6.04	0.05
Styrene	31.57	28.88	3.14	-0.45
n-Propylbenzene	15.22	13.26	1.73	0.23
1,2-Dichlorobenzene	17.21	16.01	0.82	0.39
1,2,4-trichlorobenzene	7.22	7.19	0.23	-0.19

Sand 70-100, Air Flow Rate 10 mL/min

VOC	X_0 (mg)	X_f (mg)	Y (mg)	P (mg)
Benzene	37.67	34.67	3.12	-0.12
Ethylbenzene	9.63	8.76	0.69	0.18
m,p-Xylenes	12.04	11.14	0.76	0.14
o-Xylene	6.60	6.16	0.37	0.07
Toluene	15.77	14.55	1.33	-0.11
Chlorobenzene	27.10	25.57	1.68	-0.15
Styrene	18.34	17.24	0.85	0.25
n-Propylbenzene	12.23	11.51	0.51	0.22
1,2-Dichlorobenzene	10.68	10.00	0.14	0.54
1,2,4-trichlorobenzene	8.11	7.83	0.02	0.26

Sand 70-100, Air Flow Rate 25 mL/min

VOC	X_0 (mg)	X_f (mg)	Y (mg)	P (mg)
Benzene	24.67	22.01	3.32	-0.66
Ethylbenzene	6.65	5.85	1.15	-0.35
m,p-Xylenes	8.38	7.61	1.19	-0.42
o-Xylene	4.37	3.81	0.74	-0.18
Toluene	15.76	14.10	2.06	0.40
Chlorobenzene	26.77	24.05	3.49	-0.77
Styrene	15.75	14.40	1.71	-0.36
n-Propylbenzene	12.81	11.73	0.96	0.12
1,2-Dichlorobenzene	11.86	11.00	0.29	0.57
1,2,4-trichlorobenzene	7.21	6.67	0.09	0.44

Sand 70-100, Air Flow Rate 55 mL/min

VOC	X_0 (mg)	X_f (mg)	Y (mg)	P (mg)
Benzene	30.40.	27.75	2.89	-0.24
Ethylbenzene	7.77	7.01	0.90	-0.14
m,p-Xylenes	9.34	8.44	0.90	0.00
o-Xylene	6.20	5.64	0.67	-0.11
Toluene	15.43	13.44	2.69	-0.70
Chlorobenzene	23.48	21.33	2.09	0.06
Styrene	13.15	11.48	2.00	-0.33
n-Propylbenzene	7.27	6.78	0.25	0.24
1,2-Dichlorobenzene	4.68	4.36	0.06	0.26
1,2,4-trichlorobenzene	6.00	5.78	0.02	0.20

Sand 70-100, Air Flow Rate 120 mL/min

VOC	X_0 (mg)	X_f (mg)	Y (mg)	P (mg)
Benzene	32.05	28.85	2.77	0.43
Ethylbenzene	7.70	6.91	0.77	0.02
m,p-Xylenes	6.88	6.12	0.61	0.15
o-Xylene	4.69	4.05	0.91	-0.23
Toluene	17.65	15.62	2.49	-0.16
Chlorobenzene	27.70	25.30	3.18	-0.78
Styrene	17.27	14.75	3.06	-0.54
n-Propylbenzene	11.50	10.68	0.71	0.11
1,2-Dichlorobenzene	11.20	10.31	0.14	0.75
1,2,4-trichlorobenzene	5.79	5.26	0.03	0.50

APPENDIX C. ONE-D DIFFUSION MODEL. COMPUTER CODES

Computer Code for Ethylbenzene, Single Air Channel Setup

```
 TITLE THIS PROGRAM COMPUTES THE CONCENTRATION
 TITLE PROFILE OF VOCs IN THE SOIL MATRIX FOR
 TITLE A SINGLE AIR CHANNEL SETUP ASSUMING
 TITLE 1D MOVEMENT OF THE CHEMICALS FROM THE SOIL MATRIX
 TITLE TO THE AIR CHANNEL, WHERE D REPRESENTS THE MOLECULAR
 TITLE DIFFUSION COEFFICIENT, ALPHA THE TORTUOSITY FACTOR,
 TITLE K REPRESENTS THE MASS TRANSFER
 TITLE COEFFICIENT BETWEEN LIQUID AND AIR PHASES, PORO REPRESENTS
 TITLE THE POROSITY AND KH REPRESENTS THE DIMENSIONLESS
 TITLE HENRY'S LAW CONSTANT FOR THE VOC
 TITLE THE SOIL MATRIX HAS BEEN DIVIDED IN 26 LAYERS
 TITLE OF VARIABLE THICKNESS DZ
 PARAMETER D=0.0004578,K=0.00514, AREA=87.5, PORO=.4, KH=.294
 PARAMETER ALPHA=.47, Q=115.0, V=13.825
      STORAGE FLUX(27), DZ(26), C(26), Z(26)
/     DIMENSION FNET(26), MCON(26), IMCON(26)
/     EQUIVALENCE (FNET1,FNET(1)), (MCON1,MCON(1)), (IMCON1, IMCON(1))
      TABLE DZ(1-18)=18*.25, DZ(19-21)=3*.50,DZ(22-26)=5*1.
 INITIAL
   NOSORT
   FUNCTION CURVE1=0,.00001,1,.1143,2,.0735,5,.068,11,.049,...
   23,.0453,30,.0218,40,.017,60,.0174,90,.0137,...
   120,.0122,180,.0115,240,.0111,300,.0105,360,.01,...
   420,.00987,480,.00908
   FUNCTION CURVE2=0,.009953,.5,0.012442,1.0,.014855,1.5,.015647,...
   1.905,.018925,3.81,.019304,6.35,.021754,8.89,.022525,11.0,.022525
   R(1)=.5*DZ(1)
   DO 2 I=1,26
    Z(I+1)=Z(I)+.5*(DZ(I+1)+DZ(I))
2   C(I)=AFGEN(CURVE2,R(I))
    C(26)=0.022525
   DO 5 I=1,26
5   IMCON(I)=PORO*C(I)*D(Z)*AREA
    DYNAMIC
    NOSORT
    CAVE=(C(1)+C(2)+C(3)+C(4)+C(5)+C(6)+C(7)+C(8)+C(9))/9
    CAIR=AFGEN(CURVE1,TIME)
    FLUX(1)=-K*(((CAVE)*KH))*AREA
    CC=((.1143/1000)+FLUX(1)/Q)*(EXP(-Q*(TIME-.5)/V))-FLUX(1)/Q
    FIXED I
    NOSORT
    DO 10 I=2,26
10  FLUX(I)=(C(I-1)-C(I))*D*ALPHA*AREA/(Z(I)-Z(I-1))
    FLUX(27)=0
    FIXED I
    NOSORT
    DO 20 I=1,26
20  FNET(I)=FLUX(I)-FLUX(I+1)
    MCON1=INTGRL(IMCON1,FNET1,26)
    FIXED I
    NOSORT
    DO 30 I=1,26
30  C(I)=MCON(I)/(PORO*DZ(I)*AREA)
    FLIX1=FLUX(1)
    MTRANS=-INTGRL(0.0,FLUX1)
    AIRPH=Q*INTGRL(0.0,CC)
    AIRPH1=(Q/1000)*INTGRL(0.0,CAIR)
    TIMER FINTIM=480, PRDEL=60, DELT=1.0
    METHOD SIMP
    DO 31 I=1,26
```

```
31  IF(C(I) .LT. 0.0) GO TO 35
    GO TO 40
35  C(I)=0.0
40  CONTINUE
    C1=C(1)*1000
    C2=C(2)*1000
    C3=C(3)*1000
    C4=C(4)*1000
    C5=C(5)*1000
    C6=C(6)*1000
    C7=C(7)*1000
    C8=C(8)*1000
    C9=C(9)*1000
    C10=C(10)*1000
    C11=C(11)*1000
    C12=C(12)*1000
    C13=C(13)*1000
    C14=C(14)*1000
    C15=C(15)*1000
    C16=C(16)*1000
    C17=C(17)*1000
    C18=C(18)*1000
    C19=C(19)*1000
    C20=C(20)*1000
    C21=C(21)*1000
    C22=C(22)*1000
    C23=C(23)*1000
    C24=C(24)*1000
    C25=C(25)*1000
    C26=C(26)*1000
    FLUX1=FLUX(1)
    PRINT C1,C2,C3,C4,C5,C6,C7,C8,C9,C10,C11,C12,C13,C14,C15,C16,...
    C17,C18,C19,C20,C21,C22,C23,C24,C25,C26,CAVE,FLUX1,CC,...
    MTRANS,AIRPH,AIRPH1
    END
    STOP
```

Computer Code for Ethylbenzene, Single Air Channel Setup, Adsorption

```
TITLE THIS PROGRAM COMPUTES THE CONCENTRATION
TITLE PROFILE OF VOCs IN THE SOIL MATRIX FOR
TITLE A SINGLE AIR CHANNEL SETUP ASSUMING
TITLE 1D MOVEMENT OF THE CHEMICALS FROM THE SOIL MATRIX
TITLE TO THE AIR CHANNEL, WHERE D REPRESENTS THE MOLECULAR
TITLE DIFFUSION COEFFICIENT, ALPHA THE TORTUOSITY FACTOR,
TITLE K REPRESENTS THE MASS TRANSFER
TITLE COEFFICIENT BETWEEN LIQUID AND AIR PHASES, PORO REPRESENTS
TITLE THE POROSITY AND KH REPRESENTS THE DIMENSIONLESS
TITLE HENRY'S LAW CONSTANT FOR THE VOC
TITLE THE SOIL MATRIX HAS BEEN DIVIDED IN 26 LAYERS
TITLE OF VARIABLE THICKNESS DZ
PARAMETER D=0.0004578,K=0.00199, AREA=87.5, PORO=.377, KH=.294
PARAMETER ALPHA=.52, Q=55.0, V=13.825, R=4.8405
      STORAGE FLUX(27), DZ(26), C(26), Z(26)
/     DIMENSION FNET(26), MCON(26), IMCON(26)
/     EQUIVALENCE (FNET1,FNET(1)), (MCON1,MCON(1)), (IMCON1, IMCON(1))
      TABLE DZ(1-18)=18*.25, DZ(19-21)=3*.50,DZ(22-26)=5*1.
INITIAL
  NOSORT
  FUNCTION CURVE1=0,.00001,1,.2465,5,.0965,10,.00785,15,.057,...
  30,.04455,45,.04165,60,.03725,90,.0293,120,.02085,...
  180,.0202,240,.0169,300,.01545,360,.0145,420,.01765,...
  480,.01375,540,.01115,600,.01245
  FUNCTION CURVE2=0,.012909,.5,0.0161359,1.0,.0200568,...
  1.905,.0218664,3.81,.0217156,6.35,.0217156,8.89,.0226958,11.0,.022696
  Z(1)=.5*DZ(1)
  DO 2 I=1,26
   Z(I+1)=Z(I)+.5*(DZ(I+1)+DZ(I))
2  C(I)=AFGEN(CURVE2,Z(I))
   C(26)=0.0226958
  DO 5 I=1,26
5  IMCON(I)=PORO*C(I)*DZ(I)*AREA
   DYNAMIC
   NOSORT
   CAVE=(C(1)+C(2)+C(3)+C(4)+C(5)+C(6)+C(7)+C(8)+C(9)+C(10)+C(11)...
   )/11
   CAIR=AFGEN(CURVE1,TIME)
   FLUX(1)=-K*(((CAVE)*KH))*AREA
   CC=((.2465/1000)+FLUX(1)/Q)*(EXP(-Q*(TIME-1)/V))-FLUX(1)/Q
   FIXED I
   NOSORT
   DO 10 I=2,26
10 FLUX(I)=(C(I-1)-C(I))*(D/R)*ALPHA*AREA/(Z(I)-Z(I-1))
   FLUX(27)=0
   FIXED I
   NOSORT
   DO 20 I=1,26
20 FNET(I)=FLUX(I)-FLUX(I+1)
   MCON1=INTGRL(IMCON1,FNET1,26)
   FIXED I
   NOSORT
   DO 30 I=1,26
30 C(I)=MCON(I)/(PORO*DZ(I)*AREA)
   FLIX1=FLUX(1)
   MTRANS=-INTGRL(0.0,FLUX1)
   AIRPH=Q*INTGRL(0.0,CC)
   AIRPH1=(Q/1000)*INTGRL(0.0,CAIR)
   TIMER FINTIM=600, PRDEL=120, DELT=1.0
   METHOD SIMP
```

```
      DO 31 I=1,26
31    IF(C(I) .LT. 0.0) GO TO 35
      GO TO 40
35    C(I)=0.0
40    CONTINUE
      C1=C(1)*1000
      C2=C(2)*1000
      C3=C(3)*1000
      C4=C(4)*1000
      C5=C(5)*1000
      C6=C(6)*1000
      C7=C(7)*1000
      C8=C(8)*1000
      C9=C(9)*1000
      C10=C(10)*1000
      C11=C(11)*1000
      C12=C(12)*1000
      C13=C(13)*1000
      C14=C(14)*1000
      C15=C(15)*1000
      C16=C(16)*1000
      C17=C(17)*1000
      C18=C(18)*1000
      C19=C(19)*1000
      C20=C(20)*1000
      C21=C(21)*1000
      C22=C(22)*1000
      C23=C(23)*1000
      C24=C(24)*1000
      C25=C(25)*1000
      C26=C(26)*1000
      FLUX1=FLUX(1)
      PRINT C1,C2,C3,C4,C5,C6,C7,C8,C9,C10,C11,C12,C13,C14,C15,C16,...
      C17,C18,C19,C20,C21,C22,C23,C24,C25,C26,CAVE,FLUX1,CC,...
      MTRANS,AIRPH,AIRPH1
      END
      STOP
```

Computer Code for Styrene, Soil Column

```
 TITLE THIS PROGRAM COMPUTES THE FINAL CONCENTRATION
 TITLE PROFILE OF VOCs IN THE SOIL MATRIX FOR A COLUMN MODEL AS
 TITLE AN ARRAY OF AIR CHANNELS OF LENGTH L ASSUMING RADIAL
 TITLE 1D MOVEMENT OF THE CHEMICALS FROM THE SOIL MATRIX
 TITLE TO THE AIR CHANNEL, WHERE D REPRESENTS THE MOLECULAR
 TITLE DIFFUSION COEFFICIENT(cm^2/min), ALPHA THE TORTUOSITY FACTOR,
 TITLE AREA IS THE AREA OF THE AIR CHANNEL AIR-WATER INTEFACE (cm^2)
 TITLE K REPRESENTS THE MASS TRANSFER (cm/min)
 TITLE COEFFICIENT BETWEEN LIQUID AND AIR PHASES, PORO REPRESENTS
 TITLE THE POROSITY, KH REPRESENTS THE DIMENSIONLESS
 TITLE HENRY'S LAW CONSTANT FOR THE VOC, Q (cm^3/min) IS THE AIR FLOW
 TITLE RATE, X IS THE NUMBER OF CHANNELS, AND S IS THE EMPTY REACTOR
 TITLE VOLUMEN (cm^3)
 TITLE THE SOIL MATRIX SURROUNDING THE AIR CHANNEL
 TITLE HAS BEEN DIVIDED IN 7 CONCENTRIC LAYERS
 TITLE OF THICKNESS DR
 TITLE MASS TRANSFER COEFFICIENTS WERE DETERMINED USING CORRELATIONS
 TITLE DEVELOPED IN CHAPTER IV AND RCH AND AREA ARE EXPERIMENTAL
 PARAMETER D=0.0004734,K=0.01173, AREA=33.9, PORO=.379, KH=.0967
 PARAMETER ALPHA=.52, Q=1100, L=49, RCH=0.15, X=175, S=1150
      STORAGE FLUX(8), DR(7), C(7), R(7), V(7), IA(7)
/     DIMENSION FNET(7), MCON(7), IMCON(7)
/     EQUIVALENCE (FNET1,FNET(1)), (MCON1,MCON(1)), (IMCON1, IMCON(1))
      TABLE DR(1-7)=7*0.05
 INITIAL
   NOSORT
   FUNCTION CURVE1=0.1,0.025498,.2,0.025498,.3,.025498,.4,.025498
   FUNCTION CURVE2=0,.0001,1,.249,3,.69,10,.434,17,.3075,30,...
   .2145,40,.169,50,.0945,60,.1075,75,.1155,90,.0815,120,.1135,...
   165,.071,180,.0615,225,.046,306,.0365,330,.035,...
   360, .032,420,.0325,480,.0295
   R(1)=RCH + 0.5*DR(1)
   DO 2 I=1,7
    R(I+1)=R(I)+.5*(DR(I+1)+DR(I))
2   C(I)=AFGEN(CURVE1,R(I))-(.119/1000)
    C(7)=0.025498-(.119/1000)
   DO 5 I=1,7
    V(I)=3.1416*L*(((0.5*DR(I)+R(I))**2)-((R(I)-0.5*DR(I))**2))
    IA(I+1)=3.1416*(L-13)*2*(R(I)+0.5*DR(I))
5   IMCON(I)=PORO*C(I)*V(I)
    VOL= (V(1)+V(2)+V(3)+V(4)+V(5)+V(6)+V(7))
    TVOL=X*VOL*PORO
    VAIRE= 3.1416*(L-9)*(RCH**2)
    IMCONA=1150*.249/1000
    DYNAMIC
    NOSORT
    CAVE=(C(1)*V(1)+C(2)*V(2)+C(3)*V(3)+C(4)*V(4)+C(5)*V(5)+...
    C(6)*V(6)+C(7)*V(7))/VOL
    TMASS=X*CAVE*VOL*PORO
    CAIR=AFGEN(CURVE2,TIME)
    FLUX(1)=-K*(((CAVE)*KH))*AREA
    FIXED I
    NOSORT
    DO 10 I=2,7
10  FLUX(I)=(C(I-1)-C(I))*D*ALPHA*IA(I)/(DR(I))
    FLUX(8)=0
    FNETA=(-FLUX(1)-(Q/X)*CC)*X
    MCONA=INTGRL(IMCONA,FNETA)
    CC=MCONA/( S + X*VAIRE)
    FIXED I
```

```
      NOSORT
      DO 20 I=1,7
20    FNET(I)=FLUX(I)-FLUX(I+1)
      MCON1=INTGRL(IMCON1,FNET1,7)
      FIXED I
      NOSORT
      DO 30 I=1,7
30    C(I)=MCON(I)/(PORO*V(I))
      FLUX1=FLUX(1)
      MTRANS=-X*INTGRL(0.0,FLUX1)+IMCONA
      AIRPH=Q*INTGRL(0.0,CC)+IMCONA
      AIRPH1=(Q/1000)*INTGRL(0.0,CAIR)
      TIMER FINTIM=480, PRDEL=30, DELT=1.0
      METHOD SIMP
      FIXED I
      NOSORT
      DO 32 I=1,7
32    IF(C(I) .LT. 0.0) GO TO 35
35    C(I)=0
40    CONTINUE
      C1=C(1)*1000
      C2=C(2)*1000
      C3=C(3)*1000
      C4=C(4)*1000
      C5=C(5)*1000
      C6=C(6)*1000
      C7=C(7)*1000
      FLUX1=FLUX(1)
      FLUX2=FLUX(2)
      FLUX3=FLUX(3)
      FLUX4=FLUX(4)
      FLUX5=FLUX(5)
      FLUX6=FLUX(6)
      FLUX7=FLUX(7)
      PRINT C1,C2,C3,C4,C5,C6,C7,CAVE,FLUX1,FLUX2,FLUX3,FLUX4,FLUX5,...
      FLUX6,FLUX7,CC,TVOL,MTRANS,AIRPH,AIRPH1,TMASS
      END
      STOP
```

BIOGRAPHICAL SKETCH

Washington J. Braida was born on December 18, 1956 in Montevideo, Uruguay. He received his Bachelor of Science degree in Chemistry and a Master of Science degree in Chemical Engineering from Universidad de la Republica (Uruguay) in 1978 and 1982, respectively. After 10 years of working in the pharmaceutical industries, he was admitted into the graduate program of environmental engineering at Polytechnic University, Brooklyn. New York. He received his Master of Science degree in Environmental Engineering in June 1994. Since August 1994, he has been working towards his Ph.D. degree at Iowa State University. During his studies at Iowa State, he was awarded the Society of Hispanics Professional Engineers (SHPE) Region VI Graduate Scholarship in 1995 and the Merwin Dougal Award/Scholarship (Best Graduate Student in the Environmental Engineering Program) in 1997. He has served as a Research and Teaching Assistant in the Department of Civil and Construction Engineering at Iowa State University. He is married with Gaye Goker and has two daughters, Maria Eugenia and Constanza.